Neural Computations
in
Spatial Orientation

Een wetenschappelijke proeve op het gebied van de
Sociale Wetenschappen

Proefschrift

ter verkrijging van de graad van doctor
aan de Radboud Universiteit Nijmegen,
op gezag van de rector magnificus prof. mr. S.C.J.J. Kortmann,
volgens besluit van het College van Decanen
in het openbaar te verdedigen op woensdag 27 augustus 2008
om 15.30 uur precies

door

Rens Adriaan Anton Vingerhoets

geboren op 23 december 1979 te Tilburg

Promotores	:	Prof. dr. C.C.A.M. Gielen Prof. dr. H. Bekkering
Co-promotores	:	Dr. J.A.M. Van Gisbergen Dr. W.P. Medendorp
Manuscriptcommissie	:	Prof. dr. ir. D.F. Stegeman Prof. dr. M.A. Frens (EUR) Prof. dr. A.V. van den Berg (UU)

ISBN: 978-90-9023173-0

Originele foto omslag en boekenlegger: Dick van Aalst, FNWI
Gedrukt door PrintPartners Ipskamp, Enschede

Contents

Chapter 1

General introduction

Usually we are quite well aware of how our body is oriented in space and when we are moving about we can still keep track of the location and orientation of objects around us. Having and preserving this awareness is usually referred to as spatial orientation. The central topic of this thesis is how the brain is able to maintain spatial orientation. Which sensors and computations play a role in this process? In this chapter, we will begin by explaining the human vestibular system and then continue by discussing earlier experiments and modeling efforts concerning spatial orientation.

1.1 The human vestibular system

For spatial orientation the human brain relies mostly on two sensory systems. The eyes and the visual pathways for processing visual information and the vestibular system, which consists of the semicircular canals (which work as angular accelerometers) an the otoliths (which are essentially linear accelerometers).

1.1.1 The semicircular canals

The semicircular canals are embedded in the bone of the skull at both sides of the head (Figure 1.1). They consist of fluid filled rings that respond to angular accelerations around an axis with a component normal to the plane of the ring. As a result of their arrangement in three approximately orthogonal planes, the semicircular canals are able to detect and transduce angular accelerations about any axis in space. Because of their narrow lumen and the high viscosity of the fluid, they act

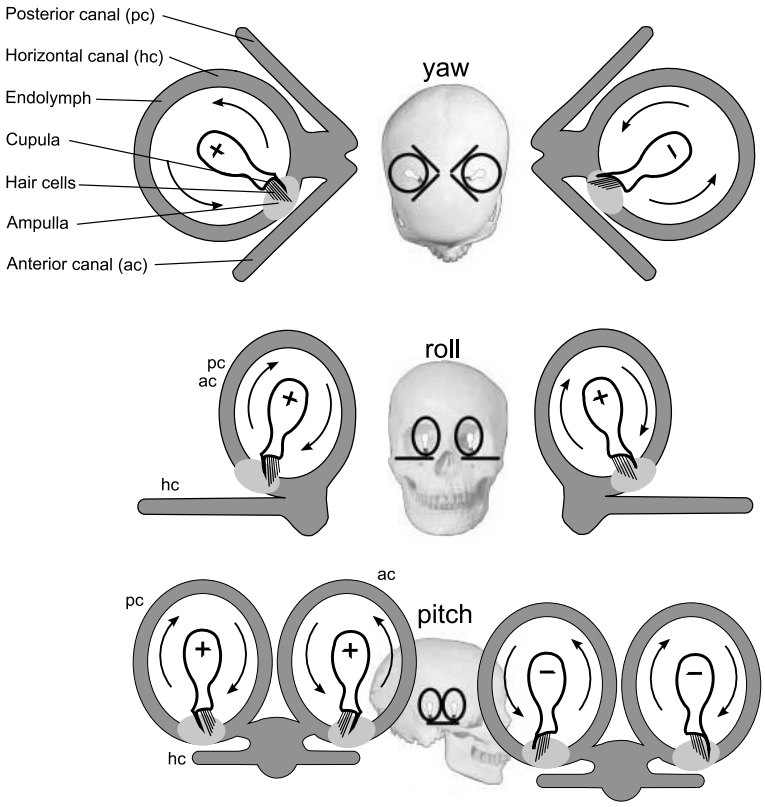

Figure 1.1 *Orientation and location of semicircular canals. Three semicircular canals on each side sense angular acceleration about any axis in space. Yaw rotation stimulates the horizontal canals. Anterior and posterior canals are stimulated by both pitch and roll. Adapted from Fitzpatrick and Day (2004).*

as approximate integrators and consequently their output reflects angular velocity rather than angular acceleration during fast rotations (Young, 1984).

The receptor cells of each canal are contained within an enlargement called the ampulla. The hairs of the hair cells are embedded in a gelatinous substance called the cupula (see Figure 1.1). When the head begins to rotate, the fluid within the canals resists the movement due to its inertia. As a result, the fluid pushes against the cupula, causing it to bend until it returns to its equilibrium position, due to its elasticity, after prolonged rotation. When the cupula is in equilibrium again, angular velocity is no longer detected although it may still be present. When head rotation is suddenly stopped, the fluid pushes the cupula in opposite direction and a counter rotation is perceived. Since the canals are not very sensitive to rotations below about 0.1 Hz (Young, 1984) and adapt to constant angular velocity, the sys-

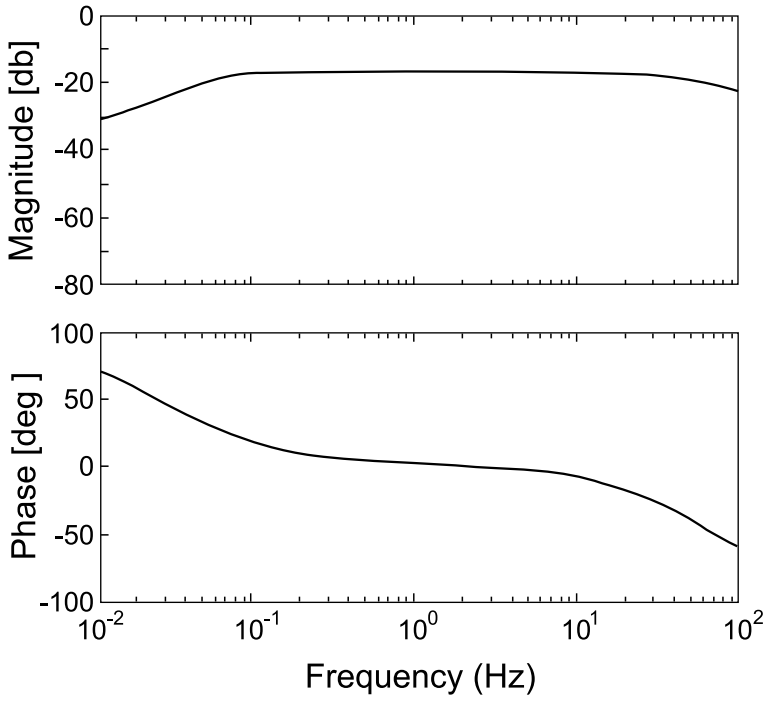

Figure 1.2 *Transfer function of the semicircular canals. In the frequency range of 0.1 Hz to 10 Hz the semicircular canals transduce head velocity. Parameters taken from Fernandez and Goldberg (1971).*

tem is often modeled by a first-order high-pass filter with a time constant of about 5 s (Goldberg and Fernandez, 1971). Yet, it should be noted that this is an approximation. Figure 1.2 provides a more correct account of the canal dynamics, showing that gain and phase behavior is best characterized by a band-pass filter. Due to a central mechanism denoted as velocity storage, the short time constant of the canal system of 5 s is lengthened up to about 20 s. It is also known that optokinetic stimulation during rotation in the light functions as a backup system for the canals to detect body rotation at low frequencies.

1.1.2 The otoliths

The otoliths consist of the utricule and the saccule, two small organs at both sides of the head. Linear acceleration and changes in orientation with respect to the gravity vector are measured by receptor cells that form the macula. On top of each receptor cell in the macula there are 50-100 small hairs, the stereocilia, and one large hair, the kinocilium (see Figure 1.3). The position of the kinocilium relative to the

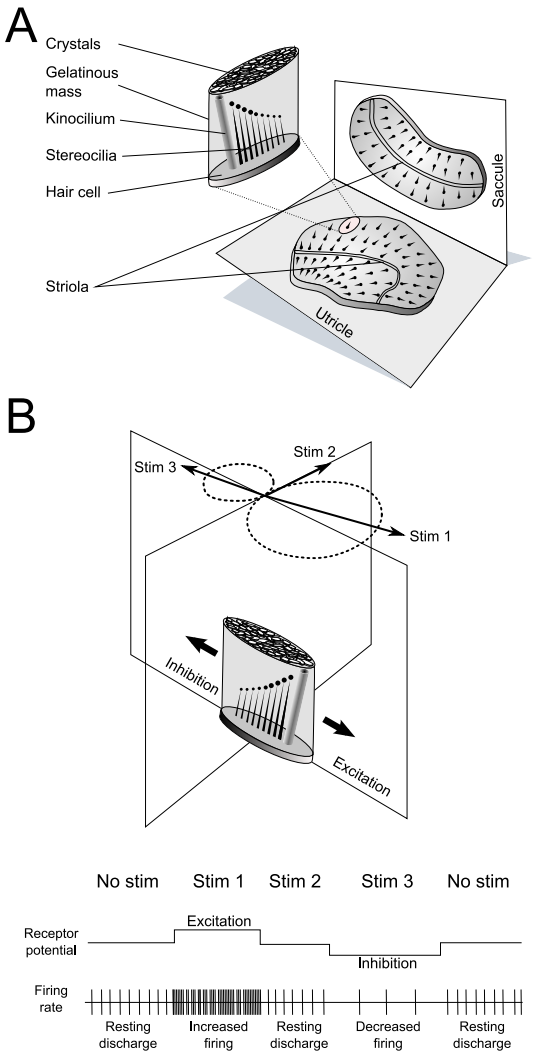

Figure 1.3 *Schematic representation of the otoliths. A: The utricle lies in a horizontal plane that is pitched up by about 30° when the head is upright. The saccule is approximately oriented in a vertical plane parallel to the midsagittal plane of the head. Alignment of hair cells on the macula surface is depicted by the kinocilia at the thick end and the stereocilia at the thin end. Adapted from Fitzpatrick and Day (2004). B: When the stereocilia are at rest, the cell is at its resting potential and the primary afferent (not shown) has a baseline firing rate. Deflection of the cilia towards the kinocilium depolarizes the cell and increases the firing rate of the afferent fiber. Deflection of the cilia away from the kinocilum hyperpolarizes the cell and decreases the firing rate.*

stereocilia determines the polarization direction of the cell. Information about the direction of the acceleration vector is available because of the approximate orthogonal orientation of the utricle and the saccule and due to the systematic variation in the polarization direction of hair cells in each macula. The membrane potential of the hair cell changes when the stereocilia are bent, which happens when the otolithic membrane in the utricle and the saccule, more dense than the surrounding endolymph fluid by the presence of numerous calcite crystals, slides downhill when the head is tilted or lags behind when the head is accelerated. As shown in Figure 1.3B, bending of the stereocilia towards the kinocilium depolarizes the cell and leads to an increased number of action potentials in the associated primary afferent, whereas bending of the stereocilia away from the kinocilium leads to hyperpolarization and a decreased firing rate in the afferent. Forces perpendicular to the polarization direction of the cell, leave the membrane potential unaffected. For other stimulations of the cell, the firing rates of the afferent lie in between these extreme values and together result in a cosine like tuning of the cell.

The deflection of the stereocilia and thus the afferent signals from the otoliths depend on the gravito-inertial force (GIF), which is the sum of gravitational and inertial acceleration. This dual sensitivity leads to the ambiguity problem, illustrated in Figure 1.4: based on the otolith signal alone the brain cannot distinguish between linear acceleration and a change of orientation with respect to gravity. In essence, this is simply a consequence of Einstein's equivalence principle stating that inertial accelerations and gravitational acceleration are physically indistinguishable.

1.2 Solving the ambiguity problem

While tilt and translation are physically indistinguishable at the level of a single otolith hair cell, the brain usually responds adequately to each movement. For example, even in darkness, we do not confuse leftward translation with right-ear-down tilt, although they may result in the same otolith stimulation. Apparently, the central nervous system uses some sort of disambiguation strategy to discriminate tilt and translation. We will now discuss two possible approaches to solve the ambiguity problem depicted in Figure 1.5.

1.2.1 Frequency-segregation

The frequency-segregation hypothesis proposes that the otolith ambiguity is resolved by filtering the otolith signal in two parallel pathways as shown in Figure 1.5A. The low-frequency component of the otolith signal is then linked to head tilt, whereas the signal that remains after high-pass filtering is ascribed to trans-

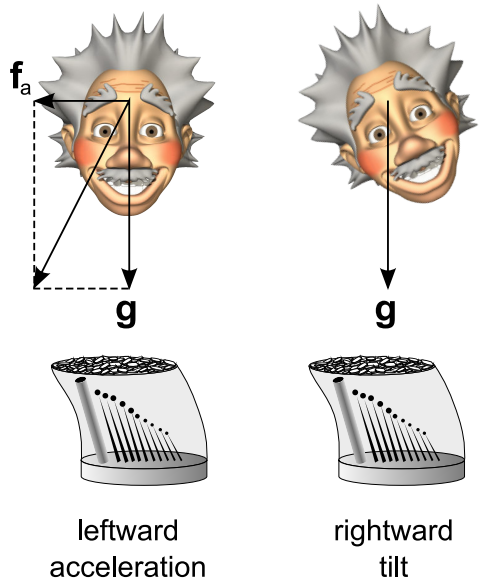

Figure 1.4 *Illustration of ambiguity problem. According to Einstein's "equivalence principle", gravitoinertial accelerations due to translation or gravity cannot be distinguished. Accordingly, otoliths (bottom row) respond identically to leftward acceleration and rightward tilt. Motion directions seen from the viewpoint of the subject.*

lation (Mayne, 1974; Paige and Seidman, 1999; Paige and Tomko, 1991; Seidman et al., 1998; Telford et al., 1997). The underlying idea is that gravity is generally constant in direction and magnitude and thus stimulates the otoliths in the low-frequency range. In contrast, translational motions are characterized by short-lasting and fast-changing signals, causing high-frequency stimulation of the otoliths. Paige and Tomko (1991) provided support for this hypothesis by studying eye movements in the squirrel monkey. They found that torsional eye-movements (reflecting tilt compensation) occurred mostly during low-frequent sinusoidal head translation, whereas horizontal eye movements (reflecting translation compensation) were elicited mainly during high-frequency stimulation. In humans, Seidman et al. (1998) found that the occurrence of tilt perception as a function of translation frequency can be described by a simple low-pass filter.

1.2.2 Canal-otolith interaction

The canal-otolith interaction hypothesis, presented in Figure 1.5B, suggests that the brain uses canal signals to solve the ambiguity problem(Angelaki et al., 1999;

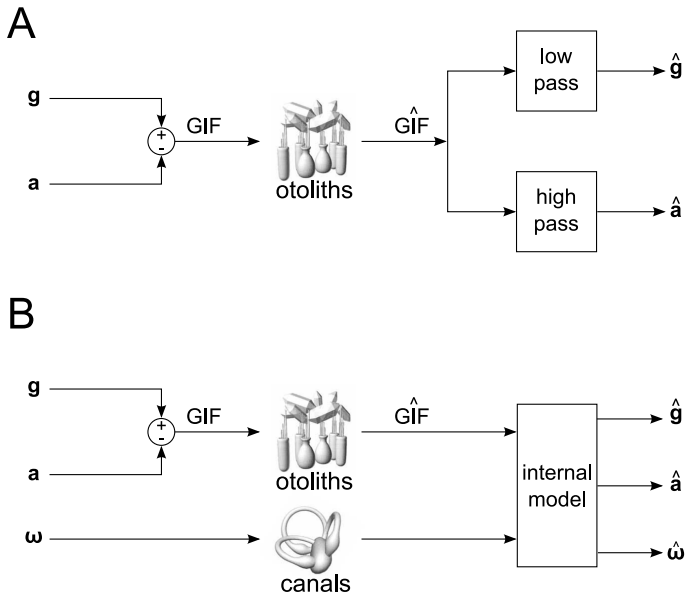

Figure 1.5 *Disambiguation strategies. Otoliths sense gravitoinertial force (GIF) which is the sum of gravitational and inertial acceleration. The brain needs a disambiguation strategy to solve the inverse problem: which combination of gravity and acceleration gave rise to the present GIF signal. A: Schematic illustration of frequency-segregation model. Decomposition of the otolith signal into tilt and translation related components is achieved by filtering in two parallel pathways. High-frequency input is interpreted as linear acceleration caused by translation and low-frequency input is seen as result of tilt. B: Canal-otolith interaction model. The brain uses canal signals and internal models to discriminate tilt and translation.*

Bos and Bles, 2002; Glasauer, 1992; Glasauer and Merfeld, 1997; Merfeld, 1995a; Merfeld et al., 1993; Merfeld and Zupan, 2002; Zupan et al., 2002). The basic idea behind this hypothesis is that when a change in the otolith signal is consistent with rotation signaled by the canals it should be ascribed to tilt, and is more likely to be due to translation otherwise. Data collected by Angelaki et al. (1999), schematically reproduced in Figure 1.6, show that semicircular canal signals are indeed essential for the correct discrimination between different sources of linear acceleration. The panels for a monkey with intact canals show that the slow phase eye velocity (torsional and horizontal components) is roughly compensatory for the imposed movement. Horizontal eye movements are made in response to translation and ocular counterroll occurs when the monkey is tilted. When the canals are plugged, oculomotor responses to tilt and translatinon are identical, suggesting that the brain is unable to discriminate between tilt and translation without rotational

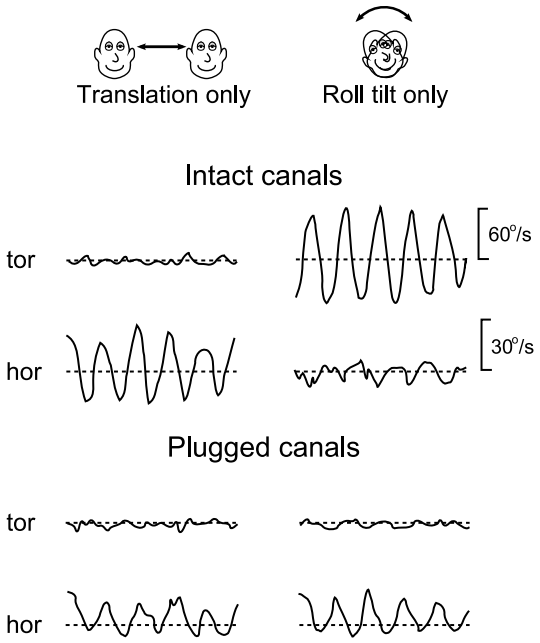

Figure 1.6 *Oculomotor responses to tilt and translation in monkeys with active and inactive semicircular canals. Solid lines: torsional (tor), and horizontal (hor) slow phase eye velocity. Dashed lines: zero eye velocity. Reponses are compensatory with intact canals. With plugged canals, the eyes do not compensate correctly for roll-tilt. Adapted from Angelaki et al. (1999).*

information from the canals.

This thesis focuses mainly on the canal-otolith interaction model proposed by Merfeld (Merfeld, 1995a,b; Merfeld et al., 1993; Merfeld and Zupan, 2002). In addition to the canal-otolith interaction hypothesis, this model also incorporates internal models, which mimic basic physical principles and sensory dynamics. Recently, Merfeld et al. (2005a,b) suggested that human oculomotor and perceptual responses depend on qualitatively different mechanisms in that egomotion perception is governed by canal-otolith interaction, while the frequency-segregation model governs the generation of movements.

The complete canal-otolith interaction model as suggested by Merfeld and Zupan (2002) is shown in Figure 1.7 and comprises the following main stages:

Body and sensor dynamics. The top left of the figure depicts the first stage, which represent the true dynamics of the body and the sensors. The block labeled as 'body dynamics' mimics the physical effect that a rotation of the head changes its orientation relative to gravity. In the sensors section, the model assumes that the otoliths

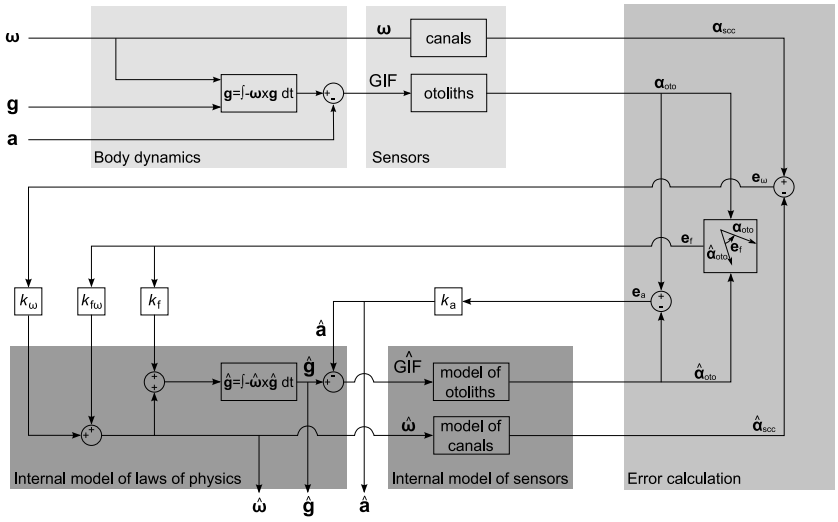

Figure 1.7 *Schematic illustration of canal-otolith interaction model (Merfeld and Zupan, 2002). Inputs are angular velocity (*$\boldsymbol{\omega}$*), gravity (*$\mathbf{g}$*) and linear acceleration (*$\mathbf{a}$*). Outputs are internal representations of these variables (*$\hat{\boldsymbol{\omega}}$*,* $\hat{\mathbf{g}}$*,* $\hat{\mathbf{a}}$*). Light shaded box represents how rotation affects the orientation of gravity in a head-fixed frame of reference and which signals are sensed by otoliths and canals. Intermediate shading represents the error calculations. Error vectors (*$\mathbf{e}_\omega$*,* $\mathbf{e}_f$*,* $\mathbf{e}_a$*) correspond to the difference between the sensory signal (*$\boldsymbol{\alpha}_{scc}$*,* $\boldsymbol{\alpha}_{oto}$*) and the estimated sensory signal (*$\hat{\boldsymbol{\alpha}}_{scc}$*,* $\hat{\boldsymbol{\alpha}}_{oto}$*). Error vectors are multiplied by feedback gains (*$k_\omega, k_{f\omega}, k_f, k_a$*) and fed into the internal model, indicated by the dark shading.*

measure the GIF correctly. For simplicity, it is also assumed that the semicircular canals are mutually orthogonal, dynamically identical and aligned with the *x*-, *y*- and *z*-axis of the head. Angular velocity is indicated by $\boldsymbol{\omega}$, which represents angular rotation about the yaw, pitch and roll axes as defined in Figure 1.1. GIF represents the sum of gravitational and linear acceleration along the *x*, *y* and *z*-axes.

Internal models. The bottom left section of the scheme depicts the internal models, which represent the assumption that the brain knows its own sensors, understands that a rotation can change the orientation of the head with respect to gravity and is aware that the internal estimates of gravity and acceleration must add up to the internal estimate of the GIF. Thus, the internal models of the laws of physics and the sensors are consistent with the actual dynamics. The internal model provides estimates of both the motion variables ($\hat{\boldsymbol{\omega}}$, $\hat{\mathbf{g}}$ and $\hat{\mathbf{a}}$) and the sensory signals ($\hat{\boldsymbol{\alpha}}_{\text{scc}}$ and $\hat{\boldsymbol{\alpha}}_{\text{oto}}$).

Error calculations. The estimated sensory signals provided by the internal model

($\hat{\boldsymbol{\alpha}}_{\text{scc}}$ and $\hat{\boldsymbol{\alpha}}_{\text{oto}}$) are compared to the real sensory signals ($\boldsymbol{\alpha}_{\text{scc}}$ and $\boldsymbol{\alpha}_{\text{oto}}$). Initial discrepancies between real and estimated signals give rise to a set of error vectors. The angular velocity error ($\mathbf{e}_\omega$) represents the difference between the actual semicircular canal signal and the expected canal signal. The linear acceleration error ($\mathbf{e}_a$) denotes the vector difference between the actual otolith signal and the expected otolith signal, whereas the GIF rotation error ($\mathbf{e}_f$) represents the angular difference between the estimated and the actual direction of the GIF vector.

In an iterative process, four feedback gains (k_ω, k_a, k_f and $k_{f\omega}$) are used to drive the estimates of the motion variables toward values that minimize the error vectors. The angular velocity error feedback gain (k_ω) determines how the semicircular canal error influences the central estimate of angular velocity. Likewise, the linear acceleration error gain (k_a) controls the central estimate of linear acceleration. A negative value for this parameter ensures that force detected by the otoliths is transformed into acceleration. The GIF feedback gain (k_f) determines how the GIF rotation error induces the internal sense of gravity to align with the gravito-inertial force measured by the otoliths. The remaining feedback gain ($k_{f\omega}$) determines how the GIF rotation error influences the central estimate of angular velocity. In essence, the path containing $k_{f\omega}$ monitors the angular difference between the measured GIF and the estimated GIF, and thus plays a critical role in keeping track of the direction of gravity and maintaining a central estimate of angular velocity. The complete iterative process finally leads to the estimates of angular velocity ($\hat{\boldsymbol{\omega}}$), gravity ($\hat{\mathbf{g}}$) and acceleration ($\hat{\mathbf{a}}$).

1.2.3 Bayesian processing of vestibular information

The disambiguation strategies described above are deterministic, which means that a given input to the model will always produce the same end result. However, it is known that neural signals are noisy which causes variations in the final percept. To account for this phenomenon, Laurens and Droulez (2007) reformulated the canal-otolith interaction model in terms of Bayesian probability theory, taking into account the uncertainty inherent in neural signals and providing a role for prior information on the probability of self-motion. The basic idea is that when there is no sensory signal, the brain makes a conservative a priori assumption based on prior knowledge. For example, when no canal signal is available, the best guess is that the head is not rotating, because this is the most commonly experienced situation in daily life. Usually, sensory signals are available and these provide the likelihood function which determines the probabilities of possible states, given the sensory signal. Bayes' rule then describes an optimal way to combine the a prior

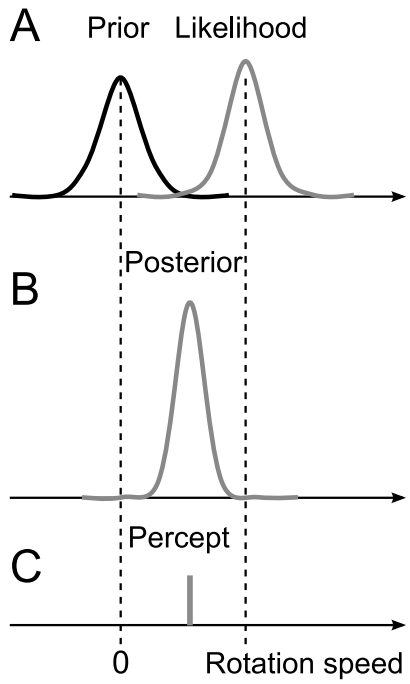

Figure 1.8 *Simple Bayesian model of rotation speed perception. A: Prior and likelihood distributions. B: Prior and likelihood are multiplied to obtain the posterior distribution. C: The final percept is taken as the maximum a posteriori (MAP) of the posterior distribution. Adapted from Carandini (2006).*

assumption with the likelihood:

$$\overbrace{P(\text{state}|\text{input})}^{\text{posterior}} = c \cdot \overbrace{P(\text{input}|\text{state})}^{\text{likelihood}} \overbrace{P(\text{state})}^{\text{prior}} \tag{1.1}$$

In this equation, the posterior distribution, representing the belief in a given state, based on a combination of sensory evidence and prior knowledge, is obtained by normalizing (c) the product of the likelihood and the prior. In the case of a rotation estimate, the prior peaks at zero speed and the likelihood peaks around the actual angular velocity. The Bayesian observer then decides that an intermediate speed is most likely, based on the speed at the peak of the posterior as shown in Figure 1.8. Based on this figure, one can see that the exact location of the posterior depends both on the width of the prior and the width of the likelihood. A smaller width means a more sharply peaked signal and thus a relatively larger weight. Consequently, when the sensory signal deteriorates, the width of the likelihood increases and the prior gains more weight, leading to a final estimate closer to the mean of the prior.

A schematic representation of the complete model by Laurens and Droulez (2007) is shown in Figure 1.9. The model has two inputs, representing the canal and otolith signals (**GIF**). Noise is added to the canal signal, yielding signal **V**, to model the stochastic fluctuations in neural processes. Based on these inputs, the

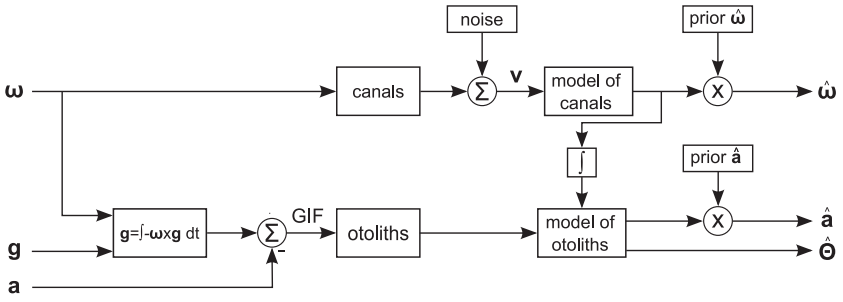

Figure 1.9 *Schematic representation of the Bayesian canal-otolith interaction model. The noisy canal signal (***V***) is processed in an internal model of canal dynamics, which leads to an estimate of angular velocity ($\hat{\boldsymbol{\omega}}$). The integrated angular velocity is used to disambiguate the otolith signal (**GIF**) into an estimate of body orientation ($\hat{\boldsymbol{\Theta}}$) and of linear acceleration ($\hat{\mathbf{a}}$). Priors on angular velocity and linear acceleration implement the default assumption of stationarity.*

model estimates the self-motion percept, which consists of rotational velocity ($\boldsymbol{\omega}$), linear acceleration (**a**), both defined as in the Merfeld model, and head orientation ($\hat{\boldsymbol{\Theta}}$). The scheme uses an internal model of the canal dynamics to estimate rotational velocity from the canal signal. Subsequently the estimated rotational velocity is integrated to calculate a new head orientation. The head orientation signal, in combination with the otolith signal, is then used by an internal model of the otoliths to calculate linear acceleration. These estimates are further influenced by priors on angular velocity and linear acceleration, which were chosen to be centered around zero, in line with the idea that we are mostly stationary.

If all sensory signals were free of noise and unambiguous, the model could calculate an exact and veridical spatial orientation percept. However, this is not the case and the purpose of the Bayesian model is to compute the probability of a certain self-motion percept given the input of the canals and the otoliths. Using Bayes' rule and some additional mathematical steps that go beyond the scope of this introduction (see Laurens and Droulez, 2007), it can be derived that this distribution depends only on the noise added to the canal signal, the prior on acceleration, the prior on rotation and the previous state.

To illustrate by example how the model works, we provide a model simulation that replicates the somatogravic illusion. This phenomenon refers to the percept of body-tilt that occurs during prolonged linear acceleration, such as when a pilot is catapulted from an aircraft carrier, which can be explained as follows. Due to the linear acceleration, the GIF vector, which is the sum of gravity and linear acceleration, is tilted relative to the head. When the acceleration is sustained long enough, the subject's internal estimate of gravity aligns with the orientation of the

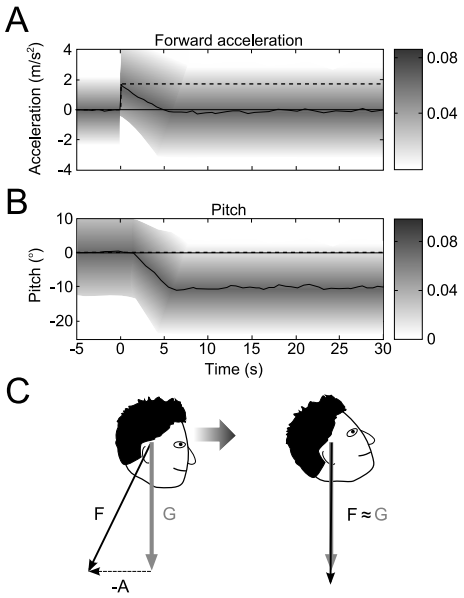

Figure 1.10 *Bayesian model simulation of somatogravic effect. During prolonged acceleration subjects report that they feel tilted. A: Estimate of forward acceleration decays due to prior on zero acceleration. B: Illusory percept of pitch tilt emerges due to decreased percept of acceleration. C: Schematic illustration of initial percept (acceleration) and final percept (tilt). Adapted from Laurens and Droulez (2007).*

GIF. Figure 1.10, showing a model simulation of a forward acceleration at 2 m/s^2, demonstrates that the model replicates the illusion. While the accurate percept of acceleration decays, a percept of backward tilt emerges simultaneously. This illusion clearly illustrates the effect of the prior on acceleration. When the subject starts to accelerate the otoliths suddenly sense a change in the GIF vector which is correctly interpreted as acceleration. However, when the acceleration continues the model uses prior information to interpret the ambiguous otolith signal. As the prior on acceleration states that it is more likely to be stationary, the brain starts to interpret the GIF signal as caused by tilt instead of translation, leading to the illusory tilt signal. In a similar fashion the model also replicates the decay of the rotation percept during yaw rotation and other motion percepts during centrifugation and off-vertical axis rotation.

1.2.4 Which disambiguation strategy is used?

Chapter 2 and 3 of this thesis report studies on translation and tilt perception during off-vertical axis rotation (OVAR). During OVAR, subjects are rotated about their long-body axis, while this axis is tilted relative to the direction of gravity (see Figure 1.11A). Denise et al. (1988) reported that during OVAR, subjects initially perceive rotation, but gradually develop an illusory percept of being translated along a cone (see figure 1.11B). In addition, they suggested that subjects overestimate their tilt angle during OVAR. In chapter 2 and 3 we quantify the translation and tilt percepts from human subjects and compare the results to predictions from

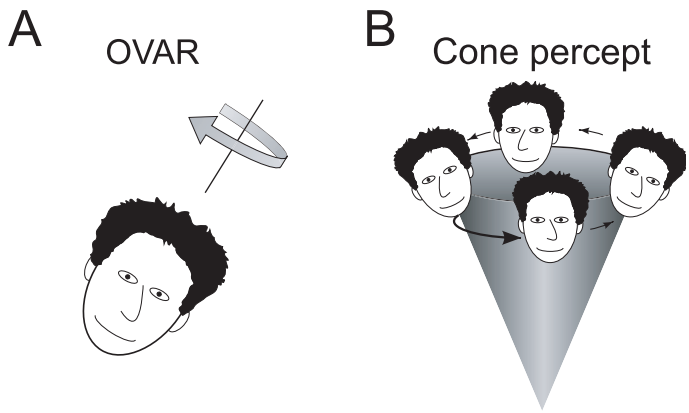

Figure 1.11 *Schematic summary of self-motion percept during OVAR. A: Subject is rotated clockwise in yaw, in darkness, about an axis that is tilted relative to gravity. B: Translational motion perceived by the subject after prolonged OVAR. Subjects feel their head describing a circular path while always facing the same direction in space. Together with the continuously changing perception of tilt, this induces a feeling of being translated along a cone, where the subject successively feels to be nose up, right ear down, nose down and left ear down etc.*

the frequency segregation model and the canal-otolith interaction model.

1.3 The perceived direction of gravity

In the previous section we described potential strategies for disambiguating the otolith signal into acceleration caused by translation or by gravity. Under normal conditions, gravity is constant, both in strength and direction. Thus, one would guess that knowing the direction of gravity suffices to form a correct percept about body-tilt and about the orientation of objects in space. However, Mittelstaedt (1983) revealed an intriguing paradox. He asked subjects on a tilt table to actively assume a 90° roll tilt position in total darkness, and then, in that actively chosen position, to set a luminous line parallel to gravity (subjective visual vertical, SVV task). The results showed that almost all subjects were able to roll themselves very close to the intended 90° position. Yet, surprisingly, the subsequently-obtained luminous line settings deviated up to 30° from true vertical. Van Beuzekom et al. (2001) found the same phenomenon even when the observer tilts himself actively. Recently, Kaptein and Van Gisbergen (2004, 2005) further established the dissociation between body tilt estimates and verticality perception across the whole 360° tilt range, as shown in Figure 1.12. The solid line denotes the errors in the SVV and shows clear A-effects (undercompensation for tilt), which are absent in the body tilt estimates

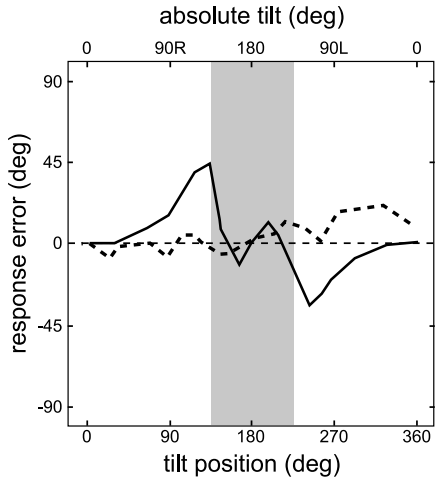

Figure 1.12 *Dissociation between errors in verticality perception and errors in body tilt estimates. Errors in visual verticality perception (solid line) show clear A-effects in the white zone and E-effects in the gray zone. Errors in body tilt perception (dashed line) are generally smaller and show a clearly different pattern. Adapted from Kaptein and Van Gisbergen (2004).*

(dashed line). In addition, Kaptein and Van Gisbergen revealed that at absolute tilts larger than 120°, the A-effect can suddenly collapse and become an E-effect (overcompensation for tilt), as indicated by the gray zone in Figure 1.12.

1.3.1 The Mittelstaedt model

To account for the errors in the SVV and their absence in body-tilt perception, Mittelstaedt (1983) proposed that an internal bias signal, the idiotropic vector, plays a crucial role in visual verticality perception, but not in the estimation of body tilt. The idiotropic vector represents a tendency to align the visual line with the long body axis, independent of the roll angle sensed by the vestibular system. According to Mittelstaedt, the fact that the saccule has fewer hair cells than the utricle, leads to a different gain of both otolith components. When the brain does not take this difference into account, it would cause errors in the estimation of the direction of gravity for small tilts, as illustrated by vector $\hat{\mathbf{g}}$ in Figure 1.13A. Mittelstaedt therefore proposed the existence of the idiotropic vector, which prevents these errors at small tilts (Figure 1.13A) at the expense of errors at large tilt angles (Figure 1.13B). According to Mittelstaedt, this is not a major problem as large tilts are rarely encountered in daily life.

1.3.2 The Bayesian SVV model

Recent studies have suggested an alternative modeling approach in which the idiotropic vector is reinterpreted in terms of a tilt prior in a Bayesian observer model (De Vrijer et al., 2008; Eggert, 1998; MacNeilage et al., 2007). As explained earlier in this introduction, a Bayesian model provides an optimal compromise based

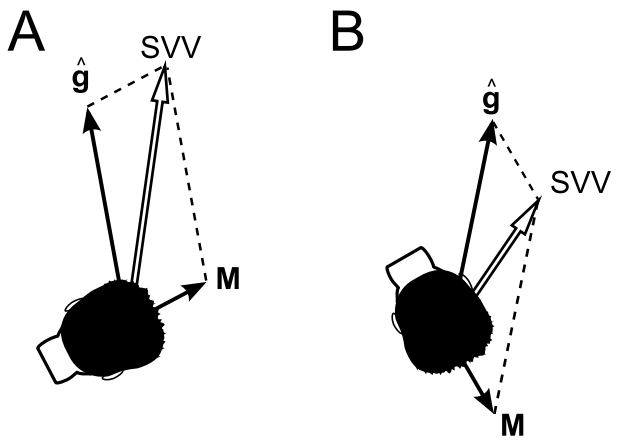

Figure 1.13 *Schematic illustration of Mittelstaedt's model. A: At moderate tilt angles the direction of gravity (***ĝ***) is misperceived due to unequal numbers of hair cells on the utricle and the saccule. The idiotropic vector,* ***M****, is added to reduce the error in the SVV. B: At large tilts, the idiotropic vector causes large errors.*

on prior knowledge and the statistical properties of the available signals. Figure 1.14 presents the model developed by De Vrijer et al. (2008). In this scheme, the computation of the SVV is based on the head tilt signal, which is assumed to be veridical but corrupted by noise, and an a prior assumption that the head is usually upright. The prior and the head tilt signal are combined as illustrated in Figure 1.8 to provide the posterior distribution. The location of the peak of the posterior distribution is denoted by β and lies in between the peaks of the prior and the vestibular tilt signal. Signal β represents the central tilt signal that ultimately transforms retinal signals to spatial coordinates. Due to the prior, the β estimate is biased toward smaller tilt angles, which mimics the effect of the idiotropic vector in the model proposed by Mittelstaedt (1983). While the predicted effects of both models are similar, the underlying assumptions are different. As explained earlier, Mittelstaedt proposed that the idiotropic vector is a computational strategy to mitigate the effect of putative systematic errors in the tilt signal caused by unequal numbers of hair cells in the saccule and the utricle. In the Bayesian scheme, the prior is part of a trade-off between accuracy and precision: combining the likelihood with the prior yields a more stable percept than when the final percept is based on the likelihood alone. In this way the prior could play a role in visual stability. While this strategy works out fine for tilt angles close to upright, it induces large errors for large tilt angles, which is acceptable as they occur only rarely.

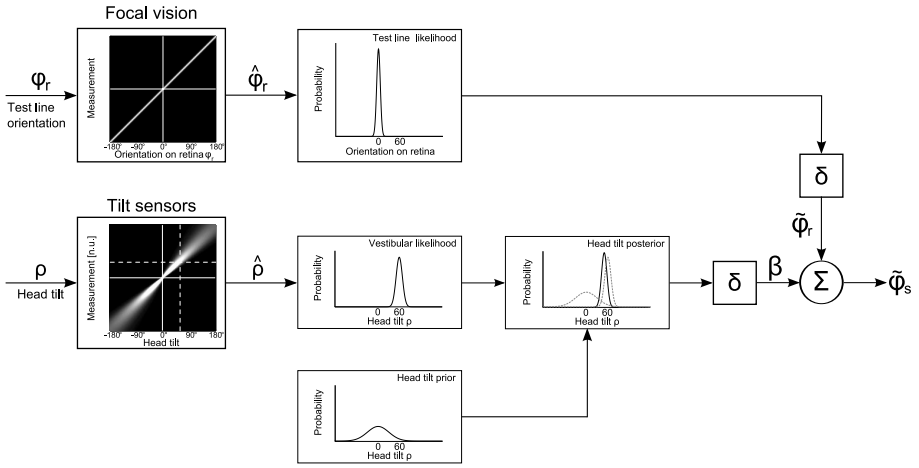

Figure 1.14 *Schematic presentation of the Bayesian SVV model. Inputs to the model: visual orientation of the stimulus on the retina ϕ_r and head tilt ρ. The sensory tilt signal $\hat{\rho}$ is assumed to be accurate but contaminated by noise, which increases linearly with tilt angle (lower left hand panel). In the indicated example, the tilted observer receives the neural signal corresponding to the horizontal dotted line and computes the likelihood of corresponding tilt angles. The likelihood is multiplied with the prior centered at zero tilt. The resulting optimal posterior probability distribution of tilt angles is biased with respect to the likelihood function. A decision rule δ is imposed to select the compensatory tilt angle β with maximum posterior probability (MAP). A similar decision rule is used to select $\tilde{\phi}_r$: the visual orientation on the retina with maximum probability. The world-centered orientation of the visual stimulus $\tilde{\phi}_s$ is then obtained by a linear combination of the compensatory tilt signal and the perceived visual orientation on the retina $\beta + \tilde{\phi}_r$. Adapted from De Vrijer et al. (2008).*

1.3.3 Effect of disambiguation errors on the perception of verticality

Both the Mittelstaedt and the Bayesian model describe how the subjective vertical is constructed when the brain has access to an estimate of the direction of gravity. However, both models sidestep the problem of how the brain obtains this estimate. As explained earlier, this is not trivial due to the ambiguity problem. Since the canal-otolith interaction model implies that canal signals are crucial to disambiguate the otolith signal, we explored the effect of dissipating canal cues on subjective body tilt (SBT) and SVV estimates in chapter 4. We investigated whether both the SVV and the SBT show errors caused by improper disambiguation of the otolith signal. In addition, we tested if the dissociation between the SVV and SBT found in static conditions (Mast and Jarchow, 1996; Mittelstaedt, 1983; Kaptein and Van Gisbergen, 2004) also holds up during dynamic conditions.

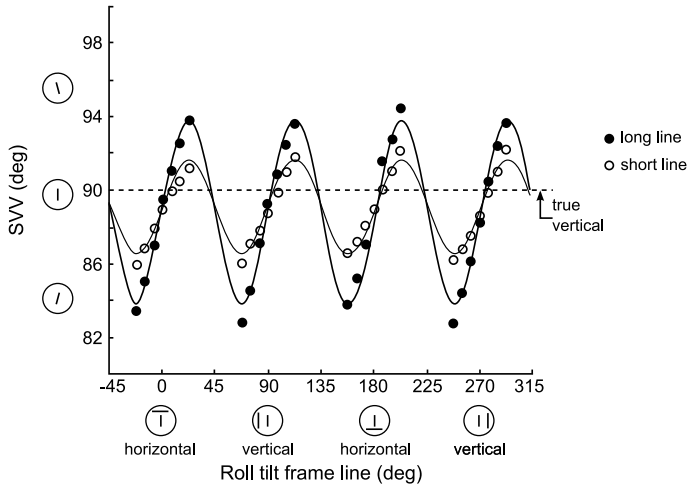

Figure 1.15 *SVV as a function of frame line orientation in space. Filled circles: 48° long lines. Open circles: 16° long lines. Measurements were taken at four different 45° segments within the 360° range. Data are fitted with a sinusoid with an almost 90° periodicity. Adapted from Li and Matin (2005a).*

1.3.4 Visual frame effects on judgments of the visual vertical

In daily life, we encounter visible objects and surfaces which usually maintain a constant orientation to the direction of gravity. Such objects and surfaces constitute the visual frame of reference for the vertical. For example, when viewing the room around us, we know that it is truly vertical and the task of adjusting a line parallel to the direction of gravity reduces to adjusting the line to the vertical indicated by the visual scene. However, if the visual framework is tilted though assumed to be vertical, orientation illusions can occur, as has been demonstrated clearly by Asch and Witkin (1948b). In their experiment, upright subjects viewed a room that was tilted 22°. When they were instructed to set a rod seen inside the tilted room parallel to the direction of the vertical, rod settings deviated up to 15° in the direction of the tilted room.

In a later experiment, Witkin and Asch (1948) investigated the well known rod-and-frame effect, by using a simple square frame instead of a rich visual scene. They showed that even such a stimulus without cues to the vertical attracts the rod settings in the direction of the tilted frame. Later, many others manipulated various parameters of the frame in an attempt to determine the basis of its influence on the SVV (Beh et al., 1971; Cian et al., 2001; DiLorenzo and Rock, 1982; Dyde and Milner, 2002; Ebenholtz, 1977; Ebenholtz and Benzschawel, 1977; Spinelli et al., 1991; Wenderoth and Beh, 1977; Zoccolotti et al., 1992). Recently, Li and Matin

(2005a,b) showed that the rod-and-frame effect does not depend on the presence of a square frame. Results from their experiments, presented in Figure 1.15, show that even a single line can attract the SVV in manner similar to the complete frame. The effect of the line was found to depend on the retinal length of the line, but was well-described by a fourfold sinusoidal periodicity (Figure 1.15).

In chapter 5 we investigated how the effects of body-tilt and a visual frame consisting of a single peripheral visual line influence the percept of verticality. We interpret the results in terms of predictions from the Mittelstaedt model and the Bayesian model, both extended with a stage to process visual frame cues.

Chapter 2

Time course and magnitude of illusory translation perception during off-vertical axis rotation

2.1 Introduction

During passive motion in darkness, egomotion perception depends heavily on how the brain interprets signals mediated by somatosensory cues and by the two types of specialized vestibular receptors: the semicircular canals and the otoliths. The semicircular canals convey information about the angular acceleration of the head, while the otoliths sense gravito-inertial force (GIF), which is the vector sum of gravitational force and inertial force due to linear acceleration. Thus, the otoliths produce ambiguous information: they cannot distinguish between head translation and a change in head orientation with respect to gravity.

Many studies have tested human egomotion perception in the sole presence of canal cues (for review see Guedry, 1974). A classical example is perception of egomotion in human subjects during constant-velocity yaw rotation about an earth-vertical axis in darkness (Brown, 1966; Young, 1984). In this case, the motion percept starts out veridically, but then vanishes following an exponential decay, with a time constant of about 15-20 s. This decline is generally attributed to the high-pass filter characteristics of the canals in combination with a mechanism that

Adapted from: Vingerhoets RAA, Medendorp WP, Van Gisbergen JAM (2006) *J. Neurophysiol.* 95: 1571-1587

extends the neural memory of head velocity, called velocity storage (Raphan and Cohen, 1985; Raphan et al., 1979).

By contrast, both the canals and the otoliths are stimulated when subjects are rotated in yaw at a constant angular velocity, about a rotation axis that is tilted relative to the direction of gravity. In such motion conditions, referred to as *off-vertical axis rotation* (OVAR), the canals will initially sense the rotation, but their activity will again die out following an exponential decay. The otoliths, however, will be stimulated continuously by a rotating gravity component in the transverse head plane, which induces a sinusoidally varying linear acceleration along the interaural and nasooccipital axes. The frequency of these sinusoidal variations in shearing force is proportional to the rotation velocity, while their amplitude is proportional to the tilt angle.

A well-known example of an OVAR paradigm is "barbecue spit rotation", where subjects are rotated in yaw about an earth-horizontal axis, i.e., OVAR with 90°tilt. When this occurs in darkness, subjects initially have a veridical rotation percept, but after a while they perceive an illusory translation along an orbital trajectory while facing a constant direction in space (Lackner and Graybiel, 1978a,b; Mittelstaedt et al., 1989). The perceived direction of translational selfmotion along the circular trajectory is opposite to the direction of the actual rotation. This illusion also occurs during rotation in roll or pitch at a constant velocity about an earth-horizontal axis (see Bos and Bles, 2002; Mayne, 1974)). Collectively, this type of illusion is often referred to as the Ferris wheel illusion, because subjects experience a circular path of body-motion without a sense of turning, just like in a gondola of a Ferris wheel.

Previous studies have also shown that, in darkness, subjects have an illusory percept of motion during OVAR even at small angles of tilt (for review see Guedry, 1974; Denise et al., 1988). While subjects are actually rotated in yaw about a tilted axis (Figure 2.1A), the perceived rotation velocity gradually decreases and a percept of head sway around a cone against the actual direction of movement emerges (Figure 2.1B-C). The decay of rotation sensation is generally attributed to the high-pass characteristics of the canals, but the explanation of the illusory translation percept is still an unresolved problem. It has been suggested that the illusory translation percept during prolonged OVAR may reflect improper interpretation of the ambiguous otolith signal (Denise et al., 1988).

It is generally agreed that disambiguation of the otolith signal takes place at a central level in the nervous system. Two neural strategies for solving the problem have been proposed. First, the canal-otolith interaction hypothesis (see Figure 2.2A) suggests that the brain uses an internal model, which combines information from canals and otoliths to differentiate translation from tilt (Angelaki et al., 1999; Bos and Bles, 2002; Droulez and Darlot, 1989; Glasauer, 1992; Glasauer and

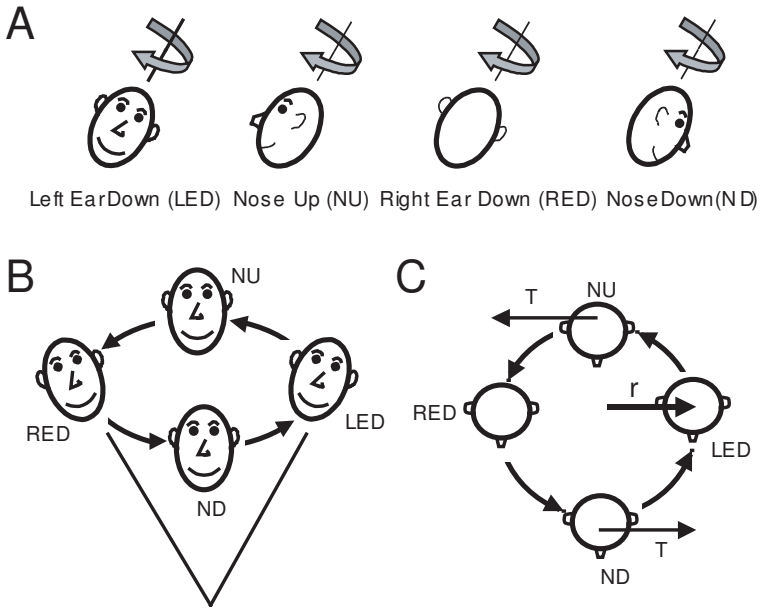

Figure 2.1 *Illustration of self-motion percept during prolonged OVAR. A: Actual stimulation. Subject is rotated clockwise in yaw about an axis that is tilted with respect to gravity. The successive head orientations are shown, starting from left ear down (LED). B: Movement perceived by the subject after prolonged rotation. Subjects feel their head describing a circle in the direction opposite to the actual rotation, i.e. leftward translation in the ND phase and backward translation in the LED phase. The perception of tilt in the absence of a rotation percept induces the feeling of being translated along a cone with the summit below the head, while always facing the same direction with respect to the laboratory. C: Perceived translation movement (cone illusion) seen from above the subject with r the radius of the perceived cone. The direction of perceived movement in the NU and ND phase is indicated by the linear velocity vector T.*

Merfeld, 1997; Merfeld, 1995a,b; Merfeld et al., 1993; Merfeld and Zupan, 2002; Zupan et al., 2002). In essence, this model exploits the canal signal to determine the changes in the otolith signal resulting from a reorientation of the head relative to gravity, and attributes the remaining part of the otolith signal to linear translation. Indeed, experiments on canal-plugged monkeys have suggested that semicircular canal signals are essential for the correct discrimination between different sources of linear acceleration needed to elicit appropriate oculomotor responses (Angelaki et al., 1999; Hess and Angelaki, 1999).

The second hypothesis, known as the frequency-segregation model (see Figure 2.2B), proposes that the ambiguity is resolved by filtering the otolith signal in two

parallel pathways, such that high-frequency otolith signals are linked to translation while low-frequency signals are ascribed to tilt (Mayne, 1974; Paige and Seidman, 1999; Paige and Tomko, 1991; Seidman et al., 1998; Telford et al., 1997). The rationale behind this model is that gravity is a constant factor, effectively stimulating the otoliths in the low-frequency range. In contrast, translational movements are mostly short-lasting, causing high-frequency changes in the otolith signal. Paige and Tomko (1991) provided support for this hypothesis on the basis of vestibulo-ocular reflex (VOR) responses in the squirrel monkey during sinusoidal head translation along the interaural axis. They found that torsional eye-movements (reflecting tilt compensation) occurred mostly during low-frequency translation along the interaural axis whereas horizontal eye-movements (reflecting translation compensation) were elicited mainly during high-frequency interaural stimulation.

While most efforts exploring the mechanisms of otolith disambiguation have concentrated on the oculomotor system (Angelaki et al., 2001; Haslwanter et al., 2000; Merfeld, 1995a; Paige and Seidman, 1999; Paige and Tomko, 1991), the question arises whether the same principles apply to the perception of egomotion (Glasauer, 1995; Merfeld et al., 2001; Mittelstaedt et al., 1989; Seidman et al., 1998). For example, the finding that subjects exposed to low-frequency linear acceleration on a sled have tilt percepts (Seidman et al., 1998), has been claimed as evidence for the frequency-segregation hypothesis. Recently, Merfeld et al. (2005b) reported different percepts for a given dynamic GIF stimulus, depending on whether it was imposed by tilt, translation or a combination. These perceptual responses were best explained by the canal-otolith interaction model. By contrast, the oculomotor responses recorded in the same motion paradigm, were much more consistent with the predictions of the frequency-segregation model. On this basis, Merfeld et al. (2005a; 2005b) concluded that human oculomotor and perceptual responses depend on qualitatively different mechanisms.

Until now, the applicability of the two models to self-motion perception during OVAR has not been studied. The qualitative descriptions provided by previous studies (Denise et al., 1988; Guedry, 1974) are insufficient to evaluate the two models in the perception domain. Our objective was to obtain quantitative measurements of self-motion percepts, both as a function of time and under conditions involving various degrees of otolith stimulation. For this purpose, we developed a novel method to assess psychophysical performance during OVAR at various tilt angles and velocities. Using these quantitative perceptual data, we tested whether the percept of translating along a cone (see Figure 2.1B) has a time course and a pattern of stimulus dependence that would favor one of the two major hypotheses for otolith disambiguation.

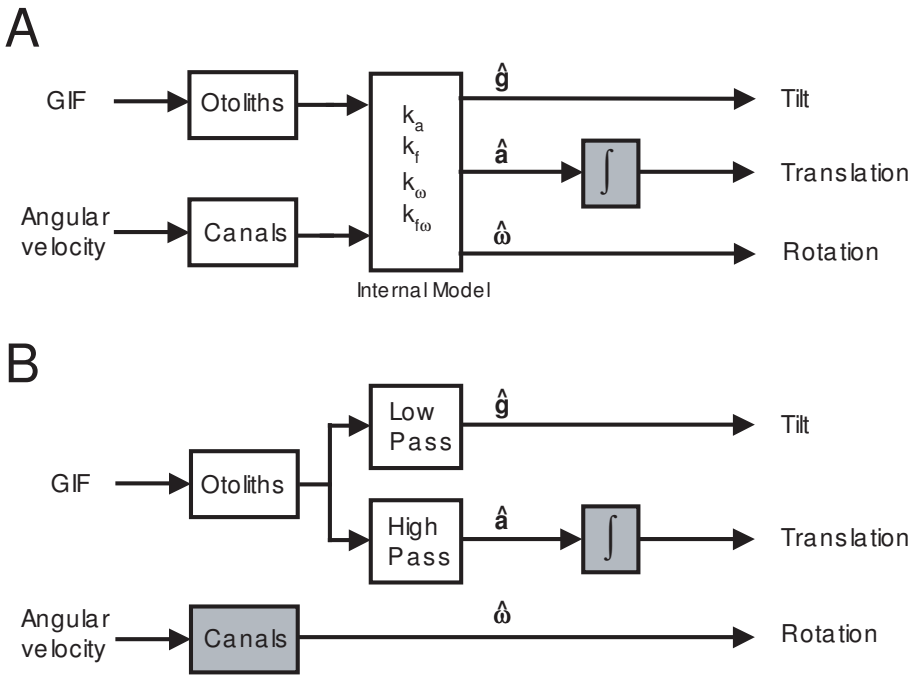

Figure 2.2 *Extended versions of the two otolith disambiguation models. Gray boxes denote the extensions to the original models. Integration stage ($\int$) is required to obtain an estimate of translation velocity measured in the experiments. A: Canal-otolith interaction model. The canals sense angular velocity and the otoliths sense gravito-inertial force (GIF), the sum of inertial acceleration and gravitational acceleration. The core of the scheme, the internal model with parameters k_a,k_f,k_ω and $k_{f\omega}$, uses canal signals to decompose GIF into components that originate either from tilt or translation. B: Frequency-segregation model. In this model, the decomposition of the otolith signal into tilt and translation related components is achieved by filtering in two parallel pathways. High-frequency input is interpreted as linear acceleration caused by translation and low-frequency input is seen as result of tilt. According to this scheme, the percept of rotation is derived from canal signals. The combination of canals and central velocity storage was modeled as a high-pass filter. Abbreviations:* $\hat{\mathbf{g}}$*, internal representation of gravity;* $\hat{\mathbf{a}}$*, internal representation of acceleration;* $\hat{\boldsymbol{\omega}}$*, internal representation of angular velocity.*

2.2 Methods

2.2.1 Subjects

Six males, aged between 24 and 60 years (mean ± SD: 33 ± 14), gave written informed consent to participate in the experiments. Three of them (MK, NK and SP) were totally naive regarding experimental goals. No systematic differences in

performance were found between naïve and nonnaïve subjects. All subjects were free of any known vestibular or ocular disorders.

2.2.2 Setup

Subjects were seated comfortably in a computer-controlled vestibular chair that could rotate about any axis orientation in space. Chair position was measured with an angular resolution of 0.04°. In the chair, subjects were secured with safety belts, hip and shoulder supports and Velcro straps around the feet. The head was firmly fixated in a natural upright position for looking straight ahead using a padded adjustable helmet. The rotation axis of the chair was aligned with the middle of the interaural axis, parallel to the long body axis. The right eye was patched to avoid double vision. A semi-translucent screen was attached to the chair at 0.27 m in front of the subject. A motor-controlled laser, on board of the vestibular chair, rear-projected a red dot with an angular subtense of 2° on the screen. The velocity of this dot was computer controlled with an accuracy of 1°/s. The dot was used to determine the subjects' perceived egomotion velocity in a psychophysical matching experiment (see Experiments).

2.2.3 Experiments

The experiments took place in complete darkness. Subjects were rotated clockwise (seen from above) about their yaw axis that was either vertical or tilted (15 or 30°) relative to the earth-vertical (i.e., off-vertical axis rotation, OVAR). Starting with the subject in left-ear down position, the constant velocity chosen for the experiment was reached within 3 seconds and then maintained for 3 minutes (see Figure 2.3). Subjects were instructed to keep looking straight ahead during the experiments. During the OVAR runs, all subjects reported that, initially, they felt themselves turning about their body axis. Later in the run, they perceived their head progressing counterclockwise along a conical path, at the frequency of rotation, while always facing the same direction in space (Figure 2.1B, C). All subjects felt the summit of the translation cone below the head. During each OVAR run, subjects indicated verbally when the cone illusion became first noticeable. In the case of vertical axis-rotation they signaled when their motion percept had disappeared. Furthermore, subjects gave an estimate of the radius, in cm, of the perceived circle described by their heads.

To quantify the self-motion percept, we used a two-alternative forced-choice task. During the run, at each nose-up and nose-down phase (see Figure 2.3), the laser rear-projected a dot moving from left-to-right or from right-to-left for 350 ms, starting from the center of the translucent screen in front of the subject. In runs

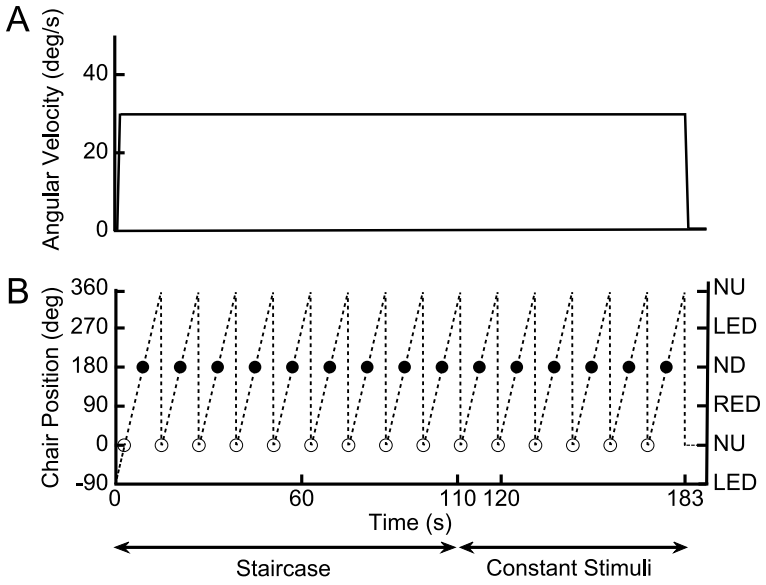

Figure 2.3 *Schematic description of an experimental run at 30°/s. A: Angular velocity of the chair. B: Chair position as a function of time (dashed line). Chair rotation starts at -90°(left ear down) and lasts for 183 seconds. Circles indicate when measurements were taken: open circles for the nose up position and filled circles for the nose down position. Staircase measurements: 0-110 s. Method of constant stimuli: 110-183 s.*

with vertical axis rotation, the laser dot was presented at the same points in time after rotation onset. Using a toggle switch, subjects indicated how the speed of the dot had to be adjusted (faster or slower) to be perceived as space-fixed. Since the laser and the screen were head-fixed, spatial stability was ensured only if the target moved away from the subject at the speed of perceived self-motion. An adaptive psychophysical procedure used the set of responses collected in a given run to update the speed of the dot to be presented at the same test points in the next run (see section Psychophysical procedures). The purpose of this procedure was to adjust the movement of the laser dot on the head-fixed screen so that it appeared fixed in space. In effect, the velocity of the dot will then reflect the velocity of perceived self-motion and hence will be referred to as the subject's matching velocity.

As noted before, the subjects' matching velocity could reflect a pure rotation percept, a pure translation percept, or a combination. Since rotational and translational velocities are expressed in units of deg/s and cm/s, respectively, we present the matching velocity data in both units, using doubly-labeled axes in the figures. In good approximation, the relationship between these units is given by $v = \pi/180 \cdot \alpha D$, with v laser dot speed in m/s, α laser dot speed in deg/s from the viewpoint of the

subject, and *D* screen distance in meters (Medendorp et al., 2002).

Subjects were tested in the NU and ND phase (see Figure 2.3) in which the perceived lateral translation is near its maximum (see Figure 2.1C). As a result, the interval between the stimuli, and thus the number of trials within a run, depended on the rotation speed. For example, at a chair velocity of 20°/s, a test trial occurred every 9 s. When using 50°/s, trials were performed every 3.6 s.

Between runs, there was a 90 s rest period during which the room lights were turned on in order to allow reorientation. In separate sessions, subjects were tested for different combinations of rotation velocity and tilt angle to be denoted as a speed series and a tilt series. The speed series comprised the speeds 20, 30, 40 and 50°/s and was performed at a fixed tilt angle of 15°. Effectively, this means that the otoliths were stimulated at frequencies of 0.056, 0.083, 0.11, and 0.14 Hz, respectively. The tilt series consisted of measurements at 0, 15 and 30° tilt at a fixed velocity of 30°/s. It took 2 to 3 sessions of about 40 minutes each to collect the data from the 18 to 20 runs comprising each experimental condition. Before measurements were taken, all subjects practised a few runs to get used to the vestibular stimulation, the motion percept and the task. The first experimental session of each subject was performed at a rotation speed of either 20 or 30°/s. In later sessions, the various conditions were tested in random order. Subjects never received feedback about their performance. All subjects performed the OVAR experiments at rotational velocities of 20 and 30°/s. Due to OVAR-related nausea, one subject did not complete the 40°/s runs and two subjects did not participate in the 50°/s OVAR experiments.

2.2.4 Psychophysical procedures

During the first 110 s of the run (see Figure 2.3), we used an adaptive staircase procedure (for details see Ehrenstein and Ehrenstein, 1999) to determine the velocity of the moving dot required for matching the subject's perceived egomotion, at regular intervals after rotation onset. Matching velocity was defined as the dot velocity at which the response in repeated trials fluctuated between 'faster' and 'slower'. The idea behind the adaptive staircase method is to present a series of ascending and descending dot speeds in order to find the stimulus level at which dot speed matches perceived egomotion. Since the percept of egomotion changed with time after rotation onset, it was necessary to perform this procedure for each and every trial within the entire sequence comprised in the first 110 s of a run. Based upon the collected series of responses ('faster' or 'slower') of a given run, the presentation in the forthcoming run was adjusted in the requested direction. Thus, if the subject's response to the first stimulus in trial n was 'slower', the next test stimulus would be presented at a slower speed, and so on, until the response to the same trial n

in a later run reversed from 'slower' to 'faster'. Such a response reversal started a staircase-type series of adjustments in opposite direction until the next response reversal occurred. In this fashion, alternations between ascending and descending staircases straddled the matching velocity where 'slower' and 'faster' responses are equally probable. In line with common practice, the step size in the adaptive staircase, which began at a course level of 6 ± 1 °/s in the first run, was reduced to a smaller value of 3 ± 1 °/s later on, once the first two response reversals had occurred.

To illustrate how the adaptive staircase procedure was applied in our experiments, Figure 2.4A shows the stimuli presented in the first and second run of an OVAR experimental session. For example, in trial # 4 of the first run, the stimulus moved at 15°/s and yielded a 'slower' response. Accordingly, the test stimulus of trial 4 in the second run was adjusted to a lower level of 9°/s. Figure 2.4B shows how stimulus levels later in the session bounced up and down between two limits marked by multiple response reversals. Note step size reduction after the second reversal which occurred in the sixth run. With rare exceptions (< 1%), the staircases from all subjects and all sessions yielded at least six reversals (typically eight to twelve). The matching velocity was computed as the mean across the last six reversals.

Not noticeable for the subject, the final part of the run (110 -183 s, see Figure 2.3), served a different purpose. At this time, perceived self-motion had reached a steady state. This allowed us to obtain a further benchmark of vestibular psychophysics: the steepness of the psychometric function which is a measure of noise in the egomotion signal (Green and Swets, 1966). To collect these data, it was necessary to present a fixed set of stimuli, following a procedure known as the method of constant stimuli. The method of constant stimuli involves multiple presentations, in random order, of test stimuli in a predetermined range above and below threshold (see Ehrenstein and Ehrenstein, 1999). This range was determined in earlier pilot experiments, and consisted of at least eleven different velocities at intervals of 2°/s (equivalent to 0.94 cm/s). By presenting each laser dot velocity multiple times (typically ten), we determined the probability of getting a 'slower' or 'faster' response for each velocity. These scores were used to construct a psychometric function, under the assumption that the distribution of 'faster' and 'slower' responses is binomial, with a probability of getting a 'slower' response given by p (see Equation 2.1) and the probability of a 'faster' response by $1 - p$. Using the method of maximum likelihood (Wichmann and Hill, 2001), we fitted a cumulative Gaussian curve to these data, given by:

$$P(x) = \lambda + (1 - 2\lambda)\frac{1}{\sigma\sqrt{2\pi}}\int_{-\infty}^{x} e^{-((x'-\mu))^2/2\sigma^2}\,\mathrm{d}x' \qquad (2.1)$$

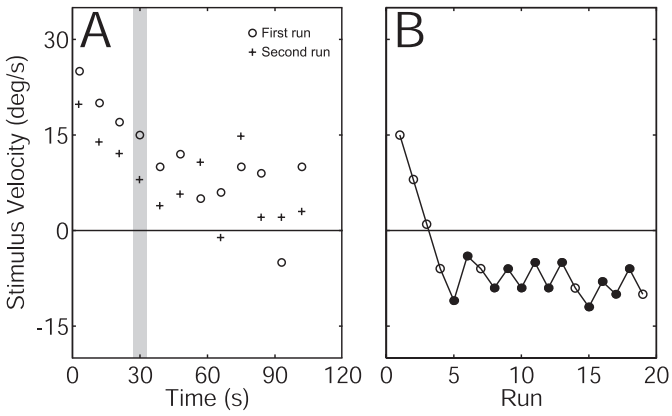

Figure 2.4 *Illustration of the adaptive-staircase procedure. A: Stimuli presented in subsequent trials in the course of the first and second run of a session. Open circles denote the stimuli that were presented during trials of the first run. For the second run, all stimuli were adapted in the desired direction indicated by the subject during first the run, as depicted by the crosses. In this example, the subject's response to the first six stimuli in the first run indicated that stimuli in the second run should be presented at reduced speed. The course of events in trial 7 of the first run was opposite: here the subject asked for a faster stimulus in the second run. B: Adaptive changes in stimulus velocity across runs for the fourth trial. The two stimuli in the gray bar in panel A correspond to the first two stimuli in panel B. Panel B further shows that this subject repeatedly responded 'slower' at the fourth trial in the first four runs but shifted to 'faster' response in the fifth. Runs with such a response change, known as a reversal, are marked by filled circles. In this example, 12 reversals can be observed. The matching velocity was calculated as the mean of the last six reversals.*

in which x is laser dot velocity, μ is the subject's matching velocity, σ is the standard deviation of the cumulative Gaussian, and λ a parameter ($0 < \lambda < 0.06$) that accounts for stimulus independent errors, i.e. errors caused by subject lapses. This latter term refers to errors caused by subject lapses or mistakes, for example a misjudgment of the stimulus due to a temporary lack of attention. These lapses are supposed to be task independent and can be excluded from the analysis by allowing $\lambda > 0$ (for details see Klein, 2001; Wichmann and Hill, 2001). The standard deviation (σ) can be interpreted as a measure of the subject's uncertainty about the perceived speed.

2.2.5 Data analysis

Data analysis was performed using programs written in MATLAB (MATLAB 6.0; The Mathworks). Unless otherwise specified, an ANOVA was used to determine whether differences in the results among various stimulus conditions were statisti-

cally significant ($P < 0.05$). As will become clear in the Results section, we fitted various types of analytical functions in order to describe the data in the most parsimonious fashion. We used the adjusted R^2 measure to evaluate and compare the goodness of fit. The adjusted R^2 is a correction on the normal R^2 statistic based on residual degrees of freedom. The notion of "residual degrees of freedom" is defined as the number of response values minus the number of fitted coefficients. The adjusted R^2 is then given by:

$$R^2_{\text{adj}} = 1 - \frac{\text{SSE} \cdot (n-1)}{\text{SST} \cdot \text{df}} \tag{2.2}$$

in which SSE is the sum of squared residuals, SST is the sum of squares about the mean, n is the number of responses and df represents the residual degrees of freedom.

2.2.6 Model simulations

We used Matlab 6.0 and Simulink 4.0 (The MathWorks) to simulate the models outlined in Figure 2.2. The predictions of these models will be discussed extensively in the Discussion. Comparing the model predictions to the collected data of translation and rotation perception proceeded as follows. First, the model predictions of linear acceleration (**a**) and angular velocity ($\boldsymbol{\omega}$) were obtained as time-dependent 3D vectors. The z-component of $\boldsymbol{\omega}$ was taken as the prediction of the model for the rotation component of our data. Since the illusory translation percept was quantified in the velocity domain, a transformation was needed to derive a velocity prediction from the acceleration output of the models. Therefore, we separately integrated the components of **a** and then computed the vector sum of the integrated x (naso-occipital) and y (inter-aural) components to obtain a model prediction for perceived translation velocity. In the Discussion we will address the question of whether the integration process is perfect or leaky to some extent. The best-fit time constant of the leaky integrator was obtained by minimizing the sum of squared errors between models and data using the Matlab routine fmincon.

The canal-otolith interaction model was implemented following Merfeld and Zupan (2002). This model has 4 free parameters: k_a, k_f, $k_{f\omega}$ and k_ω. In a first exploration of this model (Figure 2.2A), we used the parameter values that Merfeld et al. (2005a) found suitable for egomotion perception: $k_a = -2$ s^{-1}, $k_f = 1$ s^{-1}, $k_{f\omega} = 1$ and $k_\omega = 3$. In further examination of this model, we searched within a limited parameter space to find out whether a different set of values would provide a better match to our data. Due to computational limitations the search was limited to the values -0.5, -1, -2 ,-4 and -8 for k_a and 0.5, 1, 2 ,4 and 8 for the other three parameters, yielding a total of 625 combinations.

We implemented the frequency segregation model following Telford et al. (1997) using a high-pass filter in the translation pathway and a low-pass filter in the tilt-pathway (see Figure 2.2B). Since we did not measure tilt perception in these experiments, the tilt pathway played no role in simulations with this model. To obtain predictions for the rotation perception we added an independent path which consisted of a first order high-pass filter with a time constant of 23 s to approximate the combined effect of the canal dynamics and velocity storage cascade. This time constant yielded the smallest sum of squared errors for describing rotation perception. In the first series of simulations with this model, the high-pass filter in the translation pathway was modeled using a time constant of 0.05 s, as suggested by Telford et al. (1997), in combination with a perfect integrator. We also tested the predictions of this model in combination with a leaky integrator.

We used the root mean squared error (RMSE) as a measure for the goodness of fit to compare model predictions and data. The RMSE measure for the residuals is defined as the square root of the mean squared distance between the data points and the corresponding model prediction. Accordingly, RMSE values closer to 0 indicate a better fit. All model evaluations were based on the fit residuals from all conditions and subjects simultaneously. The set of parameters that yielded the minimal value for the sum of squared errors was defined as the best set.

2.3 Results

We used two different approaches to investigate the effects of pitch tilt and rotation speed on the perception of egomotion induced by OVAR. Verbal reports were obtained about both the onset of the cone illusion and the radius of the perceived circular head trajectory in the steady state. The main body of results was collected using an adaptive psychophysical procedure which adjusted the speed of a briefly presented moving dot in the frontal plane such that it matched the speed of perceived egomotion.

2.3.1 Verbal reports about the illusion

At some point in the OVAR run, all subjects developed a percept of being translated along a cone. Figure 2.5 shows a histogram of the verbally reported onsets of this illusion, pooled across testing conditions. As shown, for each subject separately, the cone illusion started between 18 and 75 s (mean ± SD: 39 ± 14 s) after rotation onset, with considerable scatter in latencies within and across subjects. For example, subject JG reported the illusion noticeably later than subject SP (Figure 2.5). There was no systematic effect of either tilt angle or rotation speed on the observed

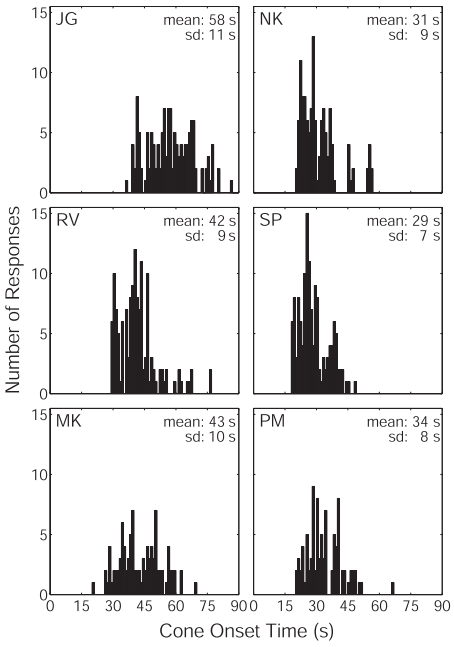

Figure 2.5 *Histograms of reported cone illusion latencies in seconds. Responses pooled across experimental conditions. Most latencies were between 25 and 45 seconds with only a few cone onset times above one minute. The subjects that completed all experimental conditions (JG, NK, RV and SP) contributed about 100 estimates, the other two about 60.*

latencies (tilt angle: $F(3,20) = 0.15,\ P = 0.93$, speed: $F(2,17) = 0.2,\ P = 0.82$). In the case of vertical-axis rotation, for which subjects reported when their sense of self-rotation had faded away, latencies ranged from 24 to 59 s (mean ± SD: 41 ± 12 s). These values were not significantly different from the illusion onset latencies obtained during the OVAR runs (t-test, $P = 0.28$).

After each OVAR experiment, subjects provided an estimate of the radius of the perceived head trajectory during the cone illusion. Figure 2.6 shows the results for different rotation speeds and tilt angles. Across all subjects, the estimated radius ranged from 15 to 60 cm (mean ± SD: 32 ± 13 cm). A larger tilt angle increases the component of gravity stimulating the otoliths in the transverse head plane. This implies a larger acceleration component that could potentially be interpreted as translation, which in turn could lead to a larger perceived radius. However, the verbal estimates provide no support for this idea: the differences between the estimated radii for the 15ř and 30ř tilt condition were not significant ($F(1,11) = 0.83,\ P = 0.38$). Likewise, there was no statistically significant effect of rotation speed on the estimated radii ($F(3,20) = 0.48,\ P = 0.70$).

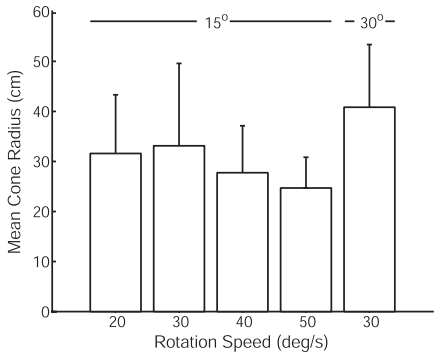

Figure 2.6 *Radii of the perceived head trajectory during the cone illusion. Mean estimates ranged from 25 to 41 cm. Differences across experimental conditions were not significant.*

2.3.2 Time course of self-motion percept

To assess the time course of the self-motion percept at various tilt angles and rotation speeds, we used an adaptive staircase procedure in the first 110 seconds of a run (see Figures 2.3 and 2.4). With this procedure we determined egomotion matching velocity as a function of time in the run. To introduce the description of these results, we start with the zero tilt condition: rotation about an earth-vertical axis at 30°/s. According to classical descriptions, the rotation sensations during earth-vertical rotations in darkness decay to negligible values in a time interval of 20 to 40 seconds (Brown, 1966; Guedry, 1974; Young, 1984). We found that the duration of the rotation sensation was approximately in this range, perhaps somewhat longer, as shown in the left-hand panels of Figure 2.7. These panels show the data from both test phases for all subjects (A) and the population average (D). In all subjects the matching velocity at the start of the run was near the actual value of 30°/s (Figure 2.7A). As time proceeded, the matching velocity decreased exponentially, with the fastest decay reaching zero at about 30 seconds after rotation onset and the slowest about 60 seconds after rotation onset.

What is the time course of the motion percept when the rotation axis is tilted? As Figures 2.7B and C show for all subjects separately, OVAR stimulation led to a different pattern of motion percepts in all subjects. In the initial part of the run, we observed no substantial differences: the matching velocity at the start of the run was perhaps somewhat larger than the actual value and then again followed an exponential decay. However, as can also be seen from the population averages (Figures 2.7E and F) clear differences between the NU phase and ND phase emerged after about 15 seconds. From this time onward, the self-motion percept bifurcated into two opposite velocity levels, instead of simply decaying to zero. These two opposite velocity levels reflect the subject's perception of moving rightward in the NU phase as opposed to moving leftward in the ND phase, as schematically indicated in Figure 2.1C. Noticeably, in the tilted-axis experiments there was more inter-subject vari-

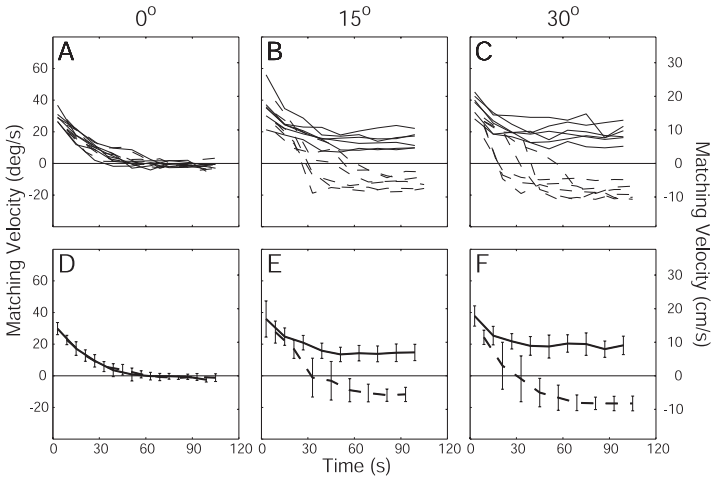

Figure 2.7 *Time course of matching velocity during the tilt series. A-C: Matching velocities from all individual subjects. D-F: Population average from all subjects. Error bars denote the standard deviations. The tilt series consisted of measurements at tilts 0, 15 and 30°and a rotation speed of 30°/s. Solid lines represent measurements from the nose up phase. Dashed lines: nose down phase. Vertical axes are doubly labeled, in deg/s and in cm/s. Panels A and D show that perceived ego-motion corresponds to classical descriptions of motion percepts during vertical axis yaw-rotation. When the rotation axis is tilted (B,C, E, F) there is initially little difference between vertical axis rotation and off-vertical axis rotation. However, after 15 to 45 seconds clear differences can be observed, with responses bifurcating into two different velocity levels.*

ability than in the earth-vertical axis experiment. All curves bifurcated at about 15 to 45 s after rotation onset and then approached an asymptotic value, that we quantified by taking the mean of the last three data points from each curve. Table 2.1, which shows the asymptotic values of the matching velocities obtained in this fashion, suggests that the magnitude of the bifurcation increases with tilt angle. Indeed, a two-way ANOVA, with tilt angle (0, 15 and 30°) and rotation phase (NU/ND) as factors, revealed a significant two-way interaction ($F(2,35) = 68.74,\ P < 0.0001$). This confirms that the asymptotic values depend on both rotation phase and tilt angle.

These results are in agreement with anecdotal reports about self-motion provided after the experiments. Initially, subjects felt themselves rotating clockwise about their body axis. Later in the run, they felt themselves pivoting about a point some distance below the head, thus tracing a conical trajectory with their body, always facing the same direction in space. In combination, the rotation and the

Experimental condition		Asymptotic Value, cm/s	
Tilt	Velocity	NU	ND
0°	30°/s	−0.5 ± 0.9	−0.5 ± 0.9
15°	30°/s	6.8 ± 2.3	−5.6 ± 1.9
30°	30°/s	8.8 ± 2.8	−8.2 ± 1.9
15°	20°/s	4.8 ± 1.6	−4.4 ± 1.3
15°	30°/s	6.8 ± 2.4	−5.6 ± 1.9
15°	40°/s	9.7 ± 2.6	−9.4 ± 2.7
15°	50°/s	12.7 ± 2.6	−11.0 ± 1.4

Table 2.1 *Asymptotic matching velocities. Values are means ± SD.*

translation percept produced the matching velocity results shown in Figure 2.7.

Figure 2.8 illustrates the matching velocities from all subjects separately (panel A-D) together with the population averages (panel E-H) in the speed series. In all conditions, after an initial exponential decay, the matching velocities for the NU and ND phase started bifurcating at some point between 15 and 45 s after rotation onset. Next, from 60 seconds after rotation onset onward, the matching velocities remained roughly constant in all subjects. Furthermore, it is evident from this figure that the magnitude of the bifurcation increased with rotation speed. The asymptotic values of the matching velocities are shown in Table 2.1. Again, the asymptotic values depended significantly on both rotation phase and rotation speed ($F(3,41) = 23.49,\ P < 0.0001$).

2.3.3 Decomposition of response curves

Anecdotal reports indicated that all subjects developed two distinct motion percepts in different phases of the experiment: an initial rotation percept, followed by a translation sensation. This suggests that there are contributions from two processes to egomotion perception during OVAR. In an attempt to separate these contributions, we decomposed the response curves to isolate the putative rotation component (R) and translation component (T). In this procedure, we assumed that R follows the same time course in both phases (NU and ND). The translation component, however, was supposed to have opposite signs because subjects sensed a rightward translation in the NU phase and a leftward motion in the ND phase (see Figure 2.1C). Based on these assumptions, the matching velocity (V) equals V_{NU} = R + T and V_{ND} = R - T in the NU and ND phase, respectively. Hence, the R and T components can easily be computed following R = (V_{NU} + V_{ND})/2 and T = (V_{NU} - V_{ND})/2 for each point in time along the response curve. In this analysis we used

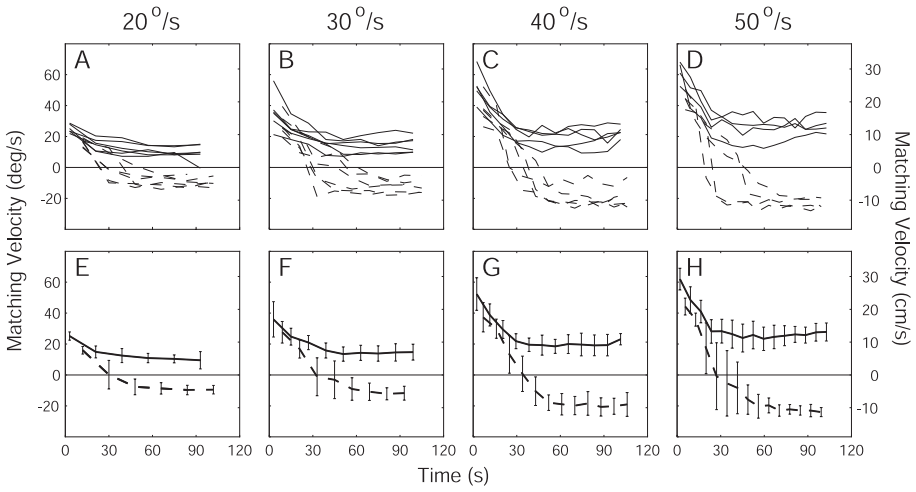

Figure 2.8 *Time course of matching velocity during the speed series. A-D: Matching velocities from all individual subjects. E-H: Mean matching velocity computed from pooled results of all subjects. The speed series consisted of measurements at rotation speeds of 20, 30, 40 and 50°/s at 15° tilt. Format as in Figure 2.7. Panel B and F are the same as B and E in Figure 2.7. At all rotation speeds the initial exponential decay bifurcates into two velocity levels after about 30 s. Bifurcation becomes more pronounced with higher speeds.*

linear interpolation to solve the problem that the matching velocities for the NU and ND phase were not determined at the same point in time. We also assumed that, at the very start of the run, subjects only sensed rotation and no translation, which implies that R = V_{NU} and T = 0 at the time of the first trial.

Effect of tilt angle

Figure 2.9 presents the result of the decomposition analysis for all subjects in the tilt series. The top row depicts the putative rotation component whereas the bottom row shows the reconstructed translation component. As the figure suggests, the decay of the R component showed a similar time course across tilt angles (see panels A, B, C). For all tilt conditions, the rotation component showed an exponential decay to negligible values. Thus, no evidence for a persistent rotation percept was found. The translation component, however, clearly depended on tilt angle. It equaled zero for the zero-tilt condition (panel D), in line with the fact that subjects did not perceive translational motion during this type of stimulation. For 15 and 30° tilts the translation component gradually climbed to an asymptotic level, in accordance with anecdotal reports. It is important to note that this increase did

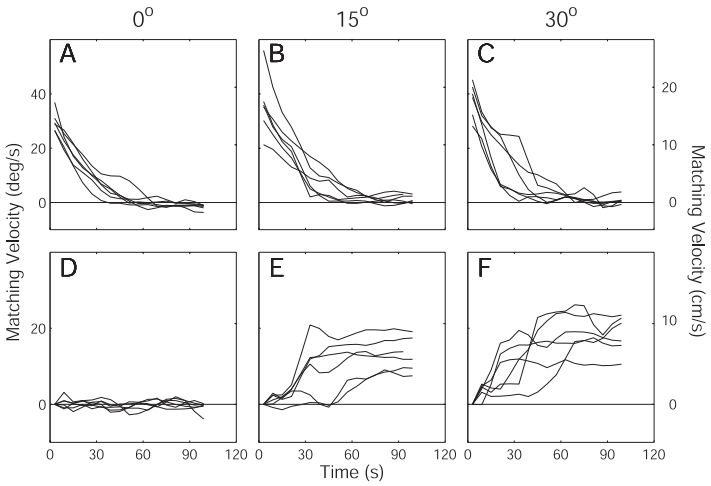

Figure 2.9 *Decomposition of response curves from the tilt series. A-C: Rotation component. D-F: Translation component. For zero tilt, the T component is always zero (D), while it reaches non-zero levels in tilt conditions (E, F). T shows considerable inter-subject variation and may be delayed by as much as 50 seconds in some subjects.*

not always start immediately at rotation onset. In some subjects the increase was delayed by as much as 50 s. Another noteworthy observation is that there was more inter-subject variability in the T components than in the R components at 15 and 30° tilt (compare panels B,C to E,F).

We quantified the asymptotic level of the R component by again taking the mean of the last three points of the curve. Only the zero tilt condition yielded a value (-1.22°/s, SD 1.04) that differed significantly from zero (t-test, $P = 0.035$).

Effect of rotation speed

Figure 2.10 shows the results of the decomposition analysis for the speed series. The top panels (A-D) illustrate that the R component followed a smooth stereotypic decay for all rotation speeds. As expected, there was a clear effect of rotation speed, because as rotation speed increased the initial matching velocities increased correspondingly. In addition, just as in the tilt series, the rotation component decayed to an asymptotic level near zero, indicating the absence of a persistent rotation component. Again we quantified the asymptotic level of the R component by taking the mean of the last three points of the curve. Averaged across subjects, we found small positive values for each condition in the speed series, but these values were not significantly different from zero (t-test, $P > 0.09$ for each condition).

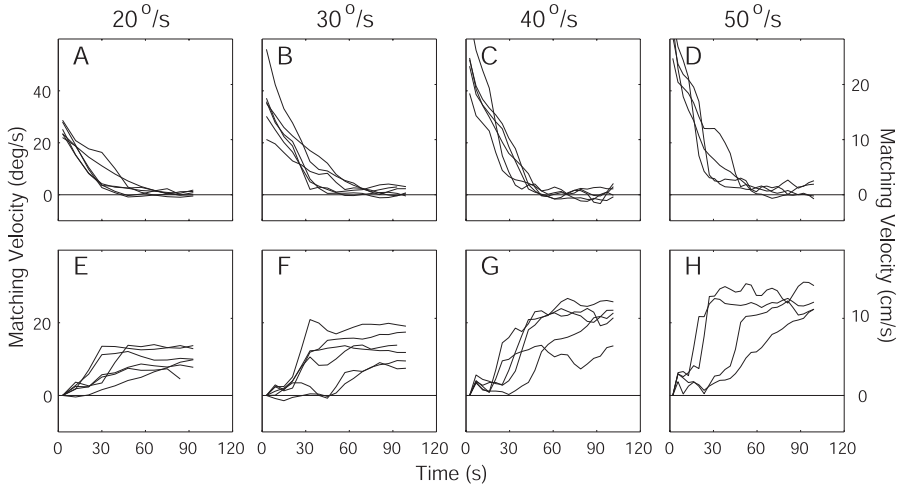

Figure 2.10 *Decomposition of the response curves from the speed series. A-D: Rotation component. E-H: Translation component. The final values of the translation component increase with increasing speed. There is more inter-subject variability in the translation component than in the rotation component. The decay in the rotation component is rather stereotyped, whereas the increase in the T component shows a more variable pattern. The increase can be delayed for about 50 seconds in some subjects.*

As in the tilt series (Figure 2.9), the T component (E-H) increased gradually with time. Again as in Figure 2.9, the time course was less stereotyped than the decay of the rotation component, with more inter-subject variability. Moreover, proper quantification of this response seemed to require inclusion of a pure time delay, because in some subjects the rise of the T component could be delayed by as much as 50 seconds.

Quantitative analysis of R and T components

Taken together, Figures 2.9 and 2.10, convey a strong suggestion that the rotation component follows an exponential decay to an asymptotic level near zero as the constant rotation continues. To quantify this temporal pattern, we fitted an exponential function to the data, expressed by:

$$R(t) = A \cdot e^{-t/\tau_R} \tag{2.3}$$

with A initial amplitude and τ_R the time constant of the decay. This is exemplified in Figure 2.11 for the experimental condition with tilt angle 15° and rotation

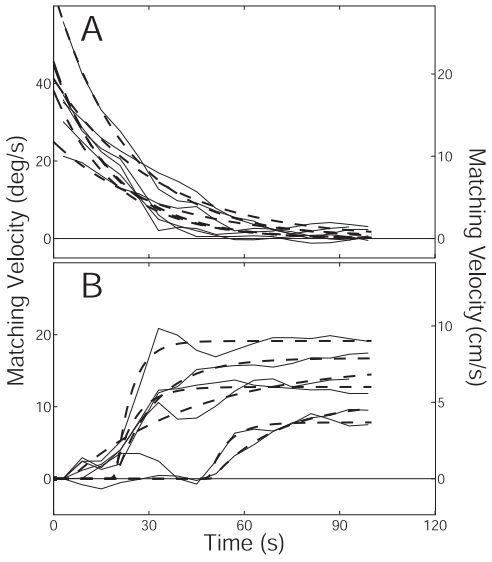

Figure 2.11 *Characterizing the translation and rotation components. Data and fits from all subjects for a rotation speed of 30°/s at 15° tilt. A: R component data and fitted R curves, following* $R(t) = A{\cdot}exp(-t/\tau_R)$ *(Equation 2.3). The fits describe the data quite well,* $R^2 > 0.93$. *B: T component data and fitted T curves, following* $T(t) = B \cdot (1-exp(-(t-\Delta t)/\tau_T)$ *if* $t > \Delta t$ *and* $T(t) = 0$ *when* $t < \Delta t$ *(Equation 2.4). The fits describe the data rather well,* $R^2 > 0.79$.

speed 30°/s, by showing the best-fit lines superimposed on the observed responses, for each subject. As shown, there is a close correspondence between the observed responses and the fitted curves. The fit parameters for all conditions are shown in Table 2.2. For all subjects and all conditions the fit results had goodness of fit values $R^2 > 0.93$. In all conditions, averaged across subjects, the fitted time constants (τ_R) ranged from 12 to 32 s (mean ± SD: 20 ± 6 s). There was no significant effect of either tilt angle or rotation speed on the fitted time constants ($F(5,32) = 0.58$, $P = 0.72$). Table 2.2 also reveals that the fitted initial amplitude (A) was on average always larger than the imposed rotation speed. However, there was no significant effect of tilt angle on the fitted initial amplitude values ($F(2,15) = 1.67$, $P = 0.22$). Not surprisingly, the effect of rotation speed on the initial amplitudes was significant ($F(3,20) = 13.9$, $P < 0.001$). In summary, the R component decayed from an initial value somewhat larger than the imposed rotation speed and followed a stereotyped exponential decline, that was independent of tilt angle and rotation speed. Potential factors that may have caused the initial overshoot, such as the proximity of the target and eye movements, will be evaluated in the Discussion.

From a modeling perspective, an important question is whether the decay in the rotation component and the rise in the translation component reflect a similar time course. To investigate this possibility, an exponential function should be fitted to the translation component as well. However, as described above, close scrutiny of the T component indicates that it did not always start immediately at $t = 0$. To account

Experimental Condition		R Component		T Component		
Tilt	Velocity	Amplitude A, °/s	Time Constant τ_R, s	Delay Δt, s	Asymptote B, cm/s	Time Constant τ_T, s
0°	30°/s	37.0 ± 4.0	18.7 ± 4.4	-	-	-
15°	30°/s	43.1 ± 12.7	23.9 ± 6.3	26.9 ± 18.2	6.5 ± 2.0	15.0 ± 13.3
30°	30°/s	45.9 ± 7.0	19.5 ± 7.5	17.8 ± 13.1	9.4 ± 2.8	14.8 ± 11.0
15°	20°/s	30.7 ± 3.7	20.9 ± 6.5	11.0 ± 4.8	5.1 ± 1.5	15.2 ± 5.9
15°	30°/s	43.1 ± 12.7	23.9 ± 6.3	26.9 ± 18.2	6.5 ± 2.0	15.0 ± 13.3
15°	40°/s	62.7 ± 14.7	19.7 ± 2.6	22.1 ± 11.7	10.1 ± 2.7	15.8 ± 7.4
15°	50°/s	71.7 ± 19.7	19.7 ± 6.2	16.5 ± 11.5	12.6 ± 1.1	12.0 ± 4.1

Table 2.2 *Best-fit parameters of decaying exponential fit to rotation component and of delayed exponential fit to translation component. Values are means ± SD. Outliers (time constants > 95 s) were excluded. The large SDs associated with the delay term are caused by large intersubject variability.*

for this fact, we included a delay as an additional fit parameter to characterize the T component. If the decay in the R component and the rise in T component reflect a common time course, this delay should not differ significantly from zero. Thus we analyzed the T component using the following fit function:

$$\begin{aligned} T(t) &= 0 && \text{if} \quad t < \Delta t \\ T(t) &= B \cdot (1 - e^{-(t-\Delta t)/\tau_T}) && \text{if} \quad t \geq \Delta t \end{aligned} \tag{2.4}$$

where Δt is the delay, B is the asymptotic value and τ_T is the time constant of the exponential increase.

Table 2.2 displays the best-fit parameters, and shows that the mean delays (Δt) ranged from 11 to 27 s across conditions. The individual delays ranged from 5 to 50 s (mean ± SD: 19 ± 13 s). The table also demonstrates that the asymptotic value (B) increased from about 5 cm/s at 20°/s to about 13 cm/s at 50°/s. For each condition, the averaged time constants (τ_T) were generally close to 15 s. Pooled across subjects and conditions they ranged from 5 to 40 s (mean ± SD: 15 ± 9 s). Figure 2.11B demonstrates the observed responses and their best-fit lines for the experimental condition with tilt angle 15° and rotation speed 30°/s. For all subjects and all conditions, Equation 2.4 described the data fairly well, $R^2 > 0.70$. Furthermore, we found positive values for the delay (Δt) for all conditions and subjects. This finding shows that the increase in the translation percept cannot be characterized by a simple exponential function with a single time constant, but that adding a delay, as in Equation 2.4, is necessary for an adequate description of the data. This conclusion held if we corrected the goodness of fit for the number

of parameters: the mean improvement in adjusted R^2 was 0.11 when the delay was included. Across individuals and conditions the increase in adjusted R^2 ranged from 0.005 to 0.284. An ANOVA revealed no effect of test condition on either the delay ($F(4,22) = 1.09$, $P = 0.38$) or on the fitted time constants ($F(4,20) = 0.08$, $P = 0.99$). But, consistent with our earlier observations, there was a significant effect of experimental condition on the asymptotic values of the T component ($F(4,20) = 7.6$, $P = 0.0007$).

For comparison, we tested whether a second-order linear model without delay, of the form $T(t) = B \cdot (1-\exp(t/\tau_1)(1-\exp(t/\tau_2))$ could describe the T component equally well as the delay model specified by Equation 2.4. The second order model also gave a fairly good description of the data, with $R^2 > 0.70$. However, it was rarely better than the delay model. In the total set of 27 T components the second order model was slightly better than the delay model in six cases, showing a mean improvement in R^2 of 0.009. In all other cases the delay model was better, with a mean increase in R^2 of 0.043. Thus overall, the combination of a pure time delay and a single exponential (Equation 2.4) provided a better description of the T component. For the remainder of this chapter, we therefore adhere to this description of the data when discussing our results.

Relation between verbal reports and T and R components

To investigate whether the decay in R component and the rise in T component reflect a shared mechanism, as implied by the canal-otolith interaction model, we looked for correlations between the coefficients that quantify these components. A strong correlation was found only between the time constant of the rotation component, τ_R, and the delay of the translation component, Δt ($r = 0.73$; $P < 0.001$; $n = 27$). This means that translation percepts were more delayed when rotation percepts persisted longer, as would be expected when canal cues play a role in the onset of translation perception. A just significant correlation was found between τ_R and τ_T ($r = 0.40$; $P = 0.049$; $n = 25$), suggesting that, despite the additional delays associated with translation, canal and otolith signals may share some extent of neural processing.

Is there any relationship between the fitted parameters and the verbal reports? Linear regression analysis revealed that the verbally reported cone illusion latencies correlated moderately with fit parameters,τ_R, τ_T and Δt, with correlation coefficients larger than 0.59. This suggests, at least, that the verbal and psychophysical results are descriptions of the same phenomenon. Notably though, the reported verbal latency was typically longer than the fitted delay, with a mean difference of 19.7 ± 11.2 s across conditions and subjects. In other words, a detectable T signal

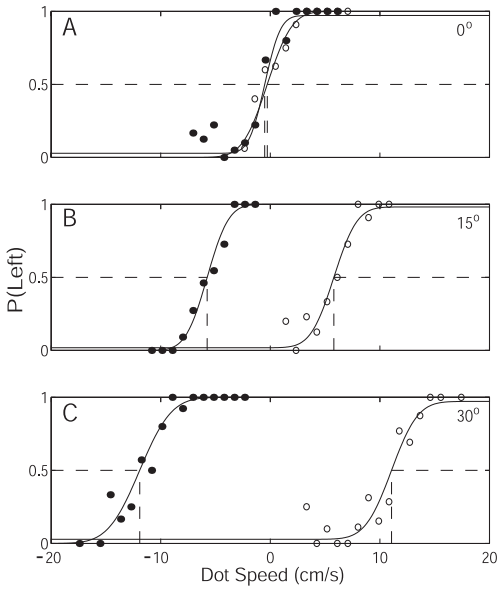

Figure 2.12 *Psychometric curves obtained with the method of constant stimuli for the tilt series. Filled circles: ND measurements. Open circles: NU measurements. Solid line: Fitted psychometric curve. Dotted line: 50 % point, taken as the matching velocity. Curves for the NU phase and the ND phase are symmetrically spaced around zero. Matching velocities (in cm/s) increase with tilt angle. Subject JG.*

had developed before subjects reported the cone illusion, indicating that the psychophysical method is more sensitive than the verbal reports.

2.3.4 Steady-state percept

The previous section described how the illusory motion percept develops over time during a constant velocity rotation about a tilted axis. Figures 2.7-2.11 show that at about 90 s after rotation onset the percept of translational motion had stabilized in all subjects. To obtain a sensitivity measure for this steady-state translation percept, based on a psychometric curve, we used the method of constant stimuli in the final part (110-183 s) of the run (see Figure 2.3 and Methods). The psychometric curve, constructed on the basis of the responses, was characterized by three parameters: threshold, standard deviation and lapse rate, a correction for stimulus-independent errors (see Equation 2.1). The threshold parameter can be regarded as the subject's matching velocity while the standard deviation can be seen as a measure of noise in the signal. A small standard deviation reflecting a steep curve, implies that the subject is relatively certain about the perceived velocity.

To illustrate the results obtained with the method of constant stimuli, we first present the data from the zero-tilt condition. In this condition, subjects perceive themselves to be stationary, which should correspond to a threshold close to zero. Figure 2.12A shows the psychometric curve fitted to the data from one subject in the 0° tilt experiment. Indeed, the thresholds for two test phases were very close to the expected value of 0 cm/s.

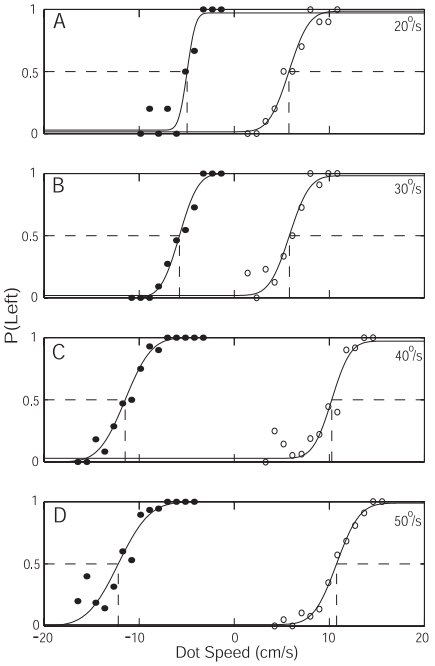

Figure 2.13 *Psychometric curves obtained with the method of constant stimuli for the speed series. Format as in Figure 2.12. Subject JG. Matching velocities increase with rotation speed; the curves become less steep when rotation speed increases.*

Figure 2.12B and C show that during OVAR at tilts of 15 and 30°, thresholds at NU and ND phase differed significantly and had opposite signs, consistent with the results from the first part of the run (staircase procedure, 0-110 seconds). Likewise, the magnitude of the matching velocity depended on tilt angle, with higher amplitudes for the 30° tilt angle. It also appears that the slope became less steep with increasing tilt angle, but this was not observed consistently in all subjects.

Earlier, we pointed out that the net difference between NU and ND asymptotical values in the first 110 seconds of a run increased with rotation speed. The same trend was seen in the psychometric curves constructed from the speed series. Figure 2.13 shows the psychometric-curve fits for the speed series from the same subject as in Figure 2.12. In all conditions, matching velocities were significantly different from zero, and their amplitudes increased with increasing speed. Note also that the curves became less steep when rotation speed increased, which implies a decrease in the sensitivity for estimating the speed of self-motion. Table 2.3 shows the population means for the threshold and the standard deviation in both the tilt series and the speed series. As shown, most trends observed in individual subjects in Figure 2.12 and 2.13 also emerged in the pooled data. The threshold increased significantly with both tilt angle ($F(2,35) = 78.58$, $P < 0.0001$) and rotation

Experimental condition		Threshold, cm/s		SD	
Tilt	Velocity	ND	NU	ND	NU
0°	30°/s	−1.0 ± 0.8	−0.7 ± 0.8	1.6 ± 1.0	1.7 ± 0.4
15°	30°/s	−6.2 ± 1.4	6.9 ± 1.8	1.3 ± 0.2	1.6 ± 0.8
30°	30°/s	−9.0 ± 2.4	9.8 ± 2.8	1.9 ± 0.7	1.9 ± 0.5
15°	20°/s	−5.1 ± 1.7	5.3 ± 1.4	1.3 ± 0.8	1.8 ± 0.2
15°	30°/s	−6.2 ± 1.4	6.9 ± 1.8	1.3 ± 0.2	1.6 ± 0.8
15°	40°/s	−9.7 ± 3.0	9.8 ± 2.6	2.2 ± 0.8	1.8 ± 0.8
15°	50°/s	−11.7 ± 1.4	12.7 ± 2.3	2.6 ± 0.7	2.5 ± 0.3

Table 2.3 *Population means for threshold and SD of the psychometric curves for the tilt series and the speed series. Thresholds increase with tilt angle and rotation speed. SD increases with rotation speed. Values are means ± SD.*

speed ($F(3,41) = 26.44$, $P < 0.0001$). There was no significant effect of tilt angle (0, 15, 30°) or rotation phase (NU/ND) on the standard deviation of the psychometric curves. By contrast, the standard deviation of the psychometric curve increased with rotation speed ($F(3,41) = 5.68$, $P = 0.0029$), indicating that the sensitivity for self-motion decreased with increasing rotation speed.

Finally, we compared the matching velocities obtained with the method of constant stimuli to the asymptotic values found with the staircase procedure (see section "Time course of self motion percept"). A two-way ANOVA, with method (staircase or constant stimuli) and test condition as factors, revealed no significant main effects (($F(1,131) = 0.04$, $P = 0.851$), ($F(5,131) = 0.07$, $P = 0.997$)) or interactions ($F(5,131) = 0$, $P = 1.0$), indicating that both methods yielded consistent results.

2.4 Discussion

Application of an adaptive psychophysical testing procedure allowed us to quantify time course and stimulus dependence of self-motion percepts during OVAR for the first time. The quantitative results were consistent with anecdotal reports from our subjects about their self-motion. All subjects sensed rotational motion during the initial part of the run, but then gradually developed an illusory percept of being translated about a cone in a direction opposite to the direction of rotation. We will first recapitulate our main experimental findings and compare them with previous reports. Then we will compare our results with predictions of the two contemporary models on otolith disambiguation, outlined in the Introduction.

2.4.1 Overview of main findings

Verbal reports

The verbal reports from our subjects (Figure 2.5 and 2.6) about the motion illusion are in quite good correspondence with earlier findings. The rotation percepts during vertical axis rotations lasted at least 24 and at most 59 seconds, somewhat longer than commonly reported in the literature (Brown, 1966; Guedry, 1974; Okada et al., 1999). A comparable range of values (18 to 75 s) was found for the onset of the translation percept during OVAR. Averaged across subjects and conditions we found a latency of 39 s. A similar latency was found by Guedry (1974), who reported values of about 45 s for 90° OVAR at 180°/s. Finally, the reported radii of the perceived cone during OVAR, ranging from 15 to 60 cm, are in the same range as reported for the perceived cylindrical orbits during "barbecue spit rotation" (Lackner and Graybiel, 1978a). Taken together, our verbal reports provide confidence that the type of stimulation during our experiments has been effective in eliciting illusory motion percepts.

Psychophysical results

To quantify the motion percept in more detail, psychophysical testing was performed at two phases during the rotation, the nose-up and nose-down phase. Using an adaptive staircase method in the beginning of the run and the method of constant stimuli in its final part, we obtained matching velocities at regular intervals. The matching velocities were used as a measure of the subjects' perceived egomotion. For the initial part of the run, the matching velocity reflected rotational motion, consistent with anecdotal reports. As time proceeded, the psychophysical results yielded two separate patterns for NU and ND, that bifurcated into two different velocity levels, consistent with how subjects described the translation percepts that occurred later in the run. More specifically, the translation was perceived as motion along an orbital path (leftward in the ND phase, rightward in the NU phase), without a sensation of turning. Which neural processes could have mediated the observed motion percepts?

As explained in the Introduction, OVAR stimulates both the semicircular canals and the otoliths. The semicircular canals gradually adapt, just as during vertical-axis yaw rotation, but the otoliths are modulated constantly because of the continuous reorientation of the head with respect to gravity. Do the time courses that we have observed reflect these processes? In an attempt to separate the putative contributions from the otoliths and the canals, we decomposed the responses from the NU and ND phase in terms of a rotation and a translation component. Basically, we followed an approach proven sound by others for separating the angular

and translation VOR in post-rotational tilt experiments (Merfeld et al., 1999; Zupan et al., 2000). Accordingly, subtraction of responses from both phases eliminated the rotation component and isolated the translation component. The mean of the two responses yielded the rotation component by removing the translation component.

R component. We found that the R component declined exponentially to zero in about 30 to 60 s after rotation began, which is again slightly longer than reported in previous studies (Brown, 1966; Okada et al., 1999). It is also noteworthy that the R component always decayed to zero, without a convincing sign of the residual rotation percept reported anecdotally by Denise et al. (1988). Since this R pattern was found irrespective of tilt angle or rotation speed, it seems reasonable to conclude that the R component stems mainly, if not exclusively, from the semicircular canals.

How can it be understood, that the rotation percepts in our study lasted longer than earlier reported? It is known that vision is dominant in motion perception, so that when a subject is rotated in a rich lighted environment the rotation percept will not decay, despite adaptation of the canals. In our experiments, subjects were exposed to a small visual stimulus that moved away from them as if it was a world-fixed point. This stimulus was presented twice in a cycle and may have prolonged the rotation percept.

We further found that the initial amplitude of the R component (see Table 2.2) was somewhat larger than the imposed rotation speed. What may have caused this phenomenon? One potential factor is eye movements. To determine the speed of the dot relative to the head, the brain needs to combine retinal motion and eye velocity. If eye velocity is only partly taken into account in this process, as suggested in literature (Freeman, 2001; Turano and Massof, 2001; Wertheim, 1994), this could explain why we found an overestimate of the initial speed. The spatial geometry of our set-up, in which stimuli were presented close to the subject and the eyes were off-centric from the rotation axis, may also have contributed to the effect. That is, rotations of the head cause the eyes to translate, so that a near target should move with a slightly greater angular velocity than that of the head in order to be perceived stationary in space. The relation between ideal gain (G), ocular eccentricity from the rotation axis (r) and fixation distance (D) can be approximated by $G = 1 + r/D$ (Telford et al., 1998; Medendorp et al., 2000). Applied to our situation, where r is about 8 cm and D is 27 cm, this predicts a gain of 1.3 which would largely explain the observed effects.

T component. Which sensory signals are reflected in the time course of the T component? As our results show, the envelope for the oscillatory translation perception gradually rose from zero levels to an asymptotical value, in both the speed and

tilt series. During vertical axis rotations (i.e. tilt angle zero), all T curves straddled the zero line, in accordance with the fact that subjects never perceived translation during earth-vertical axis rotation (see Figure 2.9D). These results suggest that the steady-state T component reflects the otolith contribution to self-motion perception, consistent with the present findings that the T component increased at larger tilt angles which involve stronger forces stimulating the utricles. The magnitude of perceived translation velocity during prolonged OVAR can be transformed into a corresponding radius of the perceived orbit, based on the fact that the angular velocity in circular motion equals linear velocity divided by the radius. Using this relation, the expected perceived radius can be calculated by dividing the matching velocity by the angular velocity of the vestibular chair in radians. Such computations show that the observed translational velocities (5-13 cm/s, see Table 2.2 and 2.3) correspond to perceptual radii of 6 to 23 cm, slightly smaller than the verbal reports (Figure 2.6). In this context, it should be noticed that the verbal radii were independent of tilt angle, but the translation velocity values clearly were not. This discrepancy may reflect a difference in sensitivity between the quantitative psychophysical method and the reports based on introspection.

Finally, in all subjects, we found that the T component did not start immediately after rotation onset but could be delayed by as much as 50 s. We fitted a delayed exponential (Equation 2.4) to capture this characteristic. Indeed, analysis showed that incorporating a delay significantly improved the fit. Another interesting finding in our experiments was that signs of an emerging translation signal could be detected well before a conscious awareness of head translation developed. This indicates that the translation signal may already have an effect at one level in the system (in this case, the detection of object motion) at a time when it has not yet penetrated the conscious percept of body motion in space.

2.4.2 Perception versus action

Many studies have been concerned with the eye movements elicited during OVAR in humans (Darlot et al., 1988; Furman et al., 1992; Haslwanter et al., 2000; Wood, 2002) and in monkeys (Angelaki and Hess, 1996a,b; Kushiro et al., 2002). Although these studies have used various techniques and paradigms, their results are generally fairly consistent.

To see how the perceptual findings in our study relate to the oculomotor results, let us first compare our perceptual τ_R values to the time constants found by Haslwanter et al. (2000). In the case of earth-vertical axis rotation they reported a time constant of about 17 s, close to the present value of 19 s. Haslwanter et al. (2000) further found that increasing the tilt angle shortens the time constant, but we did not see this reduction. Furthermore, human oculomotor studies have reported

a significant positive offset in horizontal eye velocity in the steady-state situation after prolonged OVAR, that increased with increasing tilt angle. Such positive offsets could reflect a persisting rotation percept, but the verbal reports and our psychophysical data provided no sign of such an effect.

Various oculomotor studies have reported a modulation in horizontal eye position that may represent a compensation for illusory head translation during OVAR (Angelaki and Hess, 1996a; Darlot et al., 1988; Haslwanter et al., 2000). For example, Darlot et al. (1988) found horizontal eye position modulations of about 4°. Under the assumption that the eyes were at the dark vergence position, say at about 0.8 m in depth (Fisher et al., 1988), this 4° modulation would reflect a 6 cm cone radius, slightly smaller than the radii reconstructed from the matching velocities in this study. Wood (2002) rotated subjects about a 30° off-vertical yaw-axis at various constant velocities. His results show a decrease in tilt-related and an increase in translation-compensatory eye movements as rotation speed increased. These findings are in line with the present results, showing that the magnitude of translation increased with rotation speed.

2.4.3 Modeling aspects

Why did subjects experience translation along a cone?

To better understand the translation illusion, it is helpful to consider the signals that would occur during actual motion along a cone. It can be shown that the type of conical motion perceived by our subjects would evoke the same pattern of otolith stimulation as evoked by OVAR. To illustrate this, we compared the motion signals during OVAR at 15° tilt and 30°/s (Figure 2.14A,C and E) with those expected when actually moving along a cone with a 25 cm radius and a height of 1 m (Figure 2.14B,D and F). Interestingly, to obtain the same otolith signals, with the interaural GIF component leading the naso-occipital component by 90°, the translation along a cone must proceed in a direction opposite to the OVAR rotation. Thus, due to the ambiguity of the otoliths, the two conditions can only be distinguished if additional motion signals are available. Therefore, a comparison of the rotation signals in the two situations is crucial. Panels 2.14C,D show that the rotations in the two simulated motion paradigms are very different. During OVAR, the subject is rotated only in yaw (Figure 2.14C). During the cone motion, the yaw component is lacking but there is alternating right-left and front-back tilt (Figure 2.14D). Finally, Figures 2.14E,F show the expected canal signals. The point to be taken is that the canals will adapt during OVAR but not during actual cone motion at the simulated rotation speed. Thus, these simulations illustrate the dilemma facing the brain when it has to interpret the otolith signal when the yaw rotation signal is weakening. The original

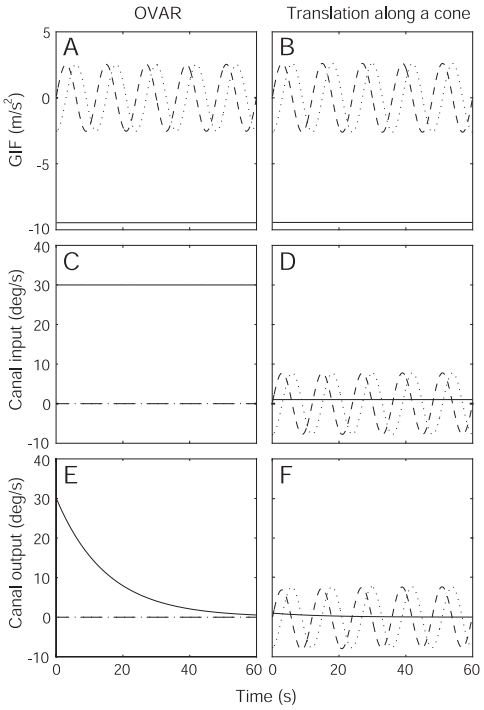

Figure 2.14 *Forces and rotations imposed on the otoliths and canals during OVAR and during actual motion along a cone with a radius of 25 cm and a height of 1 m. The dotted line denotes the naso-occipital (x) component, the dashed line indicates the interaural (y) component and the solid line represents the vertical (z) component. Simulations started in the NU position and were run for 15° tilt and a speed of 30°/s. The canals and the velocity-storage system were modeled by a high-pass filter with a time constant of 15 s. For simplicity, the canals were aligned with the midsagittal, frontal and horizontal plane of the head. A: GIF acting on the otoliths during clockwise OVAR (seen from above the subject). B: GIF acting on the otoliths during counterclockwise translation along a cone while always facing the same direction in space. The z-component is not modulated, because pitch tilt and roll tilt are 90° out of phase. C: Input to the canals during OVAR, which involves rotation about the z axis. D: Input to the canals during the cone movement. In this case there is no rotation about the z-axis. Instead there is rotation about the naso-occipital and the interaural axes, representing tilt from left to right and front to back, respectively. E: Output of the canals during OVAR. Canals adapt to constant velocity, therefore the output decays to zero. F: Output of the canals during the cone movement. There is a time varying input to the canals due to rotation about the naso-occipital and interaural axes, which passes through the high-pass filter.*

interpretation of rotation about a tilted axis is no longer tenable. The alternative, motion along a cone, although perfectly compatible with the otolith signals, is not straightforward either since the vertical canal signals expected in that situation are lacking. Thus the brain is faced with a sensory conflict, because as the canals have decayed out, the sensory signals are compatible with neither the actual motion nor the illusion.

In this vein, an interesting analogy can be seen in results from centrifuge experiments. For rotations with a fixed radius, subjects developed a tilt percept that considerably lagged behind the temporal change in GIF caused by the centrifugal force (Merfeld et al., 2001). In this situation, the canals and otoliths initially provide accurate information and the motion percept is veridical. As the canals gradually adapt a tilt percept appears, as if the brain reluctantly interprets the GIF as due to tilt although the subject is in fact upright. Our experiments, which provide the first quantitative assessment of illusory translation percepts during OVAR, also show that the central interpretation of the GIF signal, when canal cues are weakening, lags behind considerably, even with signs of a delay. Thus, the situation here has a striking similarity with the fixed-radius centrifuge experiment, except that now subjects develop an illusory translation percept. Again, we see that it takes considerable time before the brain reluctantly adopts a new interpretation of the time-varying GIF signal.

As can be seen in Figure 2.14F, during real cone motion vertical canal cues are present, but this is not the case during OVAR (Figure 2.14E). Still our subjects did have tilt sensations: i.e., they felt conical rather than cylindrical movement. Thus, these tilt sensations may reflect the interpretation of the ambiguous GIF signal which is partially assigned to translation and partially to tilt. The central interpretation of the GIF signal is the theme of the canal-otolith interaction model and the frequency-segregation model and will be discussed in the next paragraphs.

Neural strategies for otolith disambiguation

Denise et al. (1988) proposed a conceptual scheme to explain the illusory motion percepts during OVAR. According to their hypothesis, part of the GIF acting on the otoliths, actually caused by tilt, is incorrectly assigned to translation by the central nervous system. Various possible decompositions of the GIF into tilt and translation were considered but no specific model allowing quantitative predictions was specified . More recently, new quantitative models have been developed, such as the canal-otolith interaction model (Angelaki et al., 1999; Bos and Bles, 2002; Glasauer and Merfeld, 1997; Merfeld and Zupan, 2002; Zupan et al., 2002) and the frequency-segregation model (Mayne, 1974; Paige and Seidman, 1999; Paige and Tomko, 1991; Seidman et al., 1998; Telford et al., 1997), which make spe-

cific predictions about the disambiguation of the otolith signal. The final section of this chapter will compare these predictions to our data. However, as Figure 2.2 illustrates, making this comparison requires extension of these schemes, since both models predict perceived translation acceleration, whereas we measured translation velocity. Thus, for comparison with our velocity data, assumptions have to be made on how the brain integrates acceleration to yield velocity.

Canal-otolith interaction. As explained in Methods, we obtained predictions from the canal-otolith interaction model by simulating the model proposed by Merfeld et al. (2005a) for our stimulus conditions. As a first step we used the parameters as specified by Merfeld et al. (2005a) and further assumed the integration from acceleration to velocity (see integration stage in figure 2.2A) to be perfect, compatible with behavioral evidence that the nervous system can perform this integration accurately (Israel et al., 1993, 1997; Medendorp et al., 2003). We will refer to this first model version as model C1. To quantify how well model C1 predicts the data, we present the root mean squared error (RMSE, see Methods) for each subject in Table 2.4. The RMSE measure was based on the joint fit to T and R component, and was expressed in deg/s. As shown in the first row, the RMSE values for model C1 reveal a poor fit: there is a huge discrepancy between the model predictions and the data. This discrepancy mainly reflects the overestimation of translation velocities. Model C1 predicts translation velocities ranging from about 200 cm/s to 325 cm/s, whereas we found much smaller velocities ranging from 5 to 14 cm/s. It is interesting to note that simply changing the gain of the output, after the internal model and the perfect integrator, would yield a negative correlation between steady-state translation velocity and rotation speed, whereas we found the opposite result. An alternative explanation for the magnitude difference which can also account for the relation between translation velocity and rotation speed, is that subjects were not able to achieve perfect integration, as also suggested by Merfeld and Zupan (2002). To explore this, we simulated the same canal-otolith interaction model (fixed parameters), combined with a leaky integrator (model C2). We found that model C2, in combination with a leaky integrator having a time constant of 0.04 s, provided the best prediction of the asymptotic translation velocities. This value of the time constant is somewhat smaller than the 0.1 s suggested by Merfeld and Zupan (2002). As Table 2.4 demonstrates, model C2 was much better than model C1 by showing much smaller RMSE values. Figure 2.15 shows the predictions of model C2 for perceived angular yaw velocity (Figure 2.15A) and translation velocity (Figure 2.15B) at 20°/s and 15° tilt. As can be seen, the time course of the R component roughly follows the prediction of the model, but the predicted initial amplitude is clearly smaller and the decay is a little too fast. Another prediction of model C2 is that the R component reverses sign at a late stage, which was however not ob-

	Parameter values					Fit Residuals (RMSE)						
Model	k_a	k_f	$k_{f\omega}$	k_ω	τ_{leaky}	JG	MK	NK	PM	RV	SP	Pooled
C1	-2	1	1	3	∞	349	367	344	383	346	344	356
C2	-2	1	1	3	0.04	8.6	5.6	8.2	5.0	8.6	8.6	7.4
C3	-4	2	8	8	0.04	5.7	4.1	6.7	3.1	5.6	6.2	5.2

Table 2.4 *Performance of different versions of the canal-otolith intercation model. C1 as proposed by Merfeld et al. (2005a), combined with perfect integration. C2 is like C1 but combined with leaky integration. C3 is like C2 but with best-match parameters in internal model (see Figure 2.2A). Parameter values for C2 and C3 were determined using pooled data from all conditions and all subjects. Dimensions:* k_f *and* $k_{f\omega}$ s^{-1}; τ_{leaky}, *s; RMSE, deg/s*

served in the present study. With regard to translation perception (Figure 2.15B), model C2 predicts an exponential increase of the envelope of the oscillatory T component, which seems in line with the observations. On average, the magnitude of the T component is well predicted by model C2. Thus, it is clear that model C2 provides a better description of the data than model C1. It is important to point out that neither C1 nor C2, can account for the delay seen in the data of most of our subjects.

Finally, we tested a third version of the canal-otolith interaction model (model C3), in which we searched for parameters that would improve the time course predictions. Now the magnitude problem was solved, we kept the time constant of the leaky integrator fixed at 0.04 s (as in model C2), and searched for the optimal values of the parameters in the internal model as explained in the methods section. The best-match values were $k_a = -4$, $k_f = 2$, $k_{f\omega} = 8$ and $k_\omega = 8$ (Figure 2.2A). As shown in Table 2.4, model C3 yields the smallest RMSE values. Figure 2.15A,B illustrates the predictions of model C3. The prediction of the R-component has improved, i.e., model C3 predicts a slower time course than model C2. Model C3 also predicts a slower time course for the T component, providing a closer match to the data. However, as models C1 and C2, model C3 also failed in predicting the delay observed in most subjects.

To explain differences in model performance we have used a single condition for illustrative purposes, but our experiments comprised several speeds and tilt angles. The data showed an increase of steady-state matching velocity with rotation speed from 5.1 cm/s to 12.6 cm/s (see Table 2.2). Model C3 predicted a smaller increase from 4.4 to 7.1 cm/s for the speed series. With regard to the tilt series, model C3 predicts an increase with tilt angle (5.8 to 9.7 cm/s), capturing the main trend seen in the data.

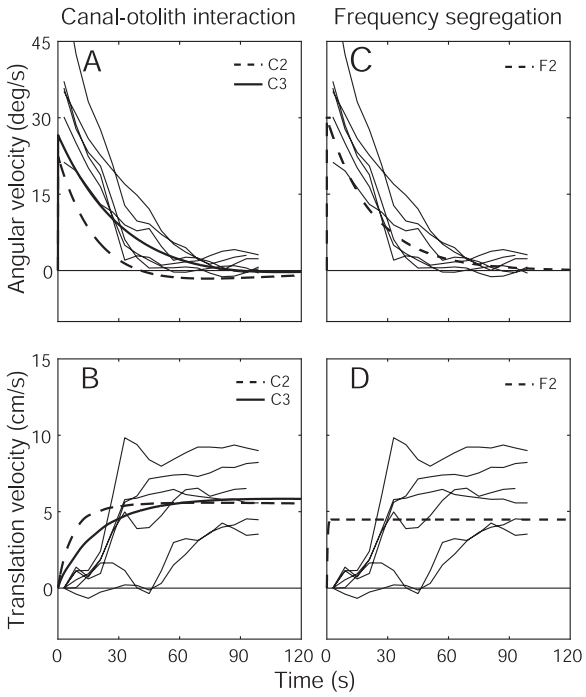

Figure 2.15 *Predictions for rotation and translation perception from both models. The plots show predictions for 30°/s at 15° tilt. A: Predicted angular velocity from the canal-otolith interaction model in combination with leaky integration using original parameters from Merfeld et al. (2005a) (C2, dashed line) and using best-match parameters (C3, solid line). The R component of all 6 subjects (thin lines) is also shown. The prediction for angular velocity shows an exponential decay to near zero values, just as in the data. Model C3 performs better than model C2. B: Predicted translation velocity from the canal-otolith interaction model with original (C2, dashed line) and adjusted parameters (C3, solid line), superimposed on the T component of all 6 subjects (thin lines). The predicted time course rises faster than the data. C: Predicted perceived angular velocity from the frequency-segregation model (F2). The canals and the velocity storage system are modeled by a high-pass filter with a time constant of 23 s. The prediction for angular velocity matches the data quite well. D: Predicted translation velocity from the frequency segregation model with high-pass filter from Telford et al. (1997) and leaky integration (F2) superimposed on the T components of all subjects (thin lines). The discrepancy between the time course of the T component in the data and the model predictions is even larger than for the canal-otolith interaction model. The frequency segregation model predicts an immediate onset of translation perception.*

Frequency segregation. The model structure of the frequency-segregation model is depicted in Figure 2.2B. We simulated various versions of this model, as outlined below. In model F1 we assumed perfect integration of linear acceleration to velocity. Incorporating perfect integration caused overestimation of the translation percept, but to a lesser extent than in model C1. This is indicated by the RMSE values in Table 2.5. In model F2 we incorporated a leaky integrator in the translation pathway. Basically, model F2 reflects a similar proposal by Telford et al. (1997) for the translation VOR. The best-fit time constant of 0.68 s for the leaky integrator in model F2 was slightly larger than the value of 0.25 s suggested by Telford et al. (1997). Model F2 was a substantial improvement compared to model F1, as shown by its smaller RMSE values. Yet, the time course of the predicted T component, shown in Figure 2.15D, was much faster than in the data, reaching its final value within a few seconds. To investigate how closely the model could match the observed data, we simulated model F3. Here, we searched for the best-match time constants of the leaky integrator and the high-pass filter. Yet, we were unable to find a combination of time constants that could produce a time to peak beyond about 6 seconds, whereas our data require a time to peak of roughly 30 s. This result can be understood in terms of systems theory, from the characteristics of a high-pass filter. Recall that the constant velocity stimulus during OVAR effectively stimulates the otoliths in a sinusoidal manner (Figure 2.14A). Therefore, an increase of this velocity would increase the frequency of the otolith input, without changing its amplitude. The time constant of the high-pass filter determines the extent of filtering at a given frequency. Thus, the time constant effectively regulates the range of rotation velocities which will result in a significant translation perception. However, this can never explain the long time constants and delays associated with the translation perception. Clearly, the slow time course must be strongly related to the decay of the canal signal. For this reason, model F3 did not provide a better fit than model F2 and was not incorporated in Table 2.5 and Figure 2.15. We conclude that, for fundamental reasons, the slow time course in our data can not be captured by any of the tested frequency-segregation models. This model version could, however, explain the increase of steady-state velocity with rotation speed. Model F2 actually predicted an increase from about 2.9 cm/s to about 6.4 cm/s. The increase with tilt angle was also captured by model F2, which predicts an increase from 4.3 cm/s to 8.2 cm/s when the tilt angle increases from 15 to 30°.

In conclusion, we have developed a method to quantify the motion percepts that occur during off-vertical axis rotation. Using this approach, we demonstrated the gradual emergence of an illusory translation percept. Simulations showed that current disambiguation models fail to account for the magnitude of this illusory translation percept, unless the assumption is made that the integration of accelera-

	Parameter values		Fit Residuals (RMSE)						
Model	$\tau_{\text{high-pass}}$	τ_{leaky}	JG	MK	NK	PM	RV	SP	Pooled
F1	0.05	∞	15.8	15.3	13.1	14.4	13.1	11.8	13.9
F2	0.05	0.68	6.1	3.8	6.9	3.4	6.5	7.2	5.7

Table 2.5 *Performance of two versions of the frequency-segregation model. Version F1 uses the high-pass filter time constant taken from Telford et al. (1997) and perfect integration. Version F2 uses the high-pass filter combined with leaky integration. The time constant of the leaky integrator for F2 was determined using pooled data from all conditions and all subjects. Dimensions:* $\tau_{high\text{-}pass}$*, s;* τ_{leaky}*, s; RMSE, deg/s*

tion signals during OVAR is imperfect. With this allowance and when tuned with an adapted parameter set that differed from the proposal by Merfeld et al. (2005a,b) for self-motion perception in a different stimulation paradigm, the canal-interaction model could approximate the slow time course of the translation percept but not its delay. Despite this restriction, our results clearly suggest a role of canal-otolith interaction in self-motion perception during OVAR. The fact that the model requires different parameter settings for different stimulus conditions points to an additional level of complexity in the system, hitherto not foreseen. The translation results appear to rule out the filter model which matched neither the slow time course nor the delay.

Acknowledgements We thank Hans Kleijnen, Ger van Lingen, Stijn Martens and Günter Windau for technical support and acknowledge Martijn Leisink for stimulating discussions and helpful suggestions. Tjeerd Dijkstra gave valuable advice on the psychophysical methods. This work was supported by Radboud University Nijmegen (NICI and FNWI) and the Netherlands Organization for Scientific Research.

Chapter 3

Verticality perception during off-vertical axis rotation

3.1 Introduction

To ensure perceptual stability and a veridical percept of verticality, we use information about self-orientation and self-motion from various sensory modalities, in particular the visual and vestibular system. The vestibular system has specialized organs for detecting rotational acceleration (the semicircular canals) and for sensing linear acceleration (the otoliths). Like any linear accelerometer, the otoliths sense both inertial and gravitational accelerations, so that their signal is ambiguous as to the source of the gravito-inertial force (GIF). For a correct interpretation, the brain has to solve the nontrivial inverse problem of determining whether the otolith signal was caused by tilt, by translation or by a combination of these motions.

Previously it was suggested that the brain resolves the ambiguity problem by using frequency filtering of the otolith signal. According to this account, low-frequency otolith components are interpreted as the result of gravitational acceleration (tilt) whereas high-frequency components are attributed to inertial accelerations (Mayne, 1974; Paige and Seidman, 1999; Paige and Tomko, 1991; Seidman et al., 1998; Telford et al., 1997). An alternative hypothesis proposes that the brain disambiguates otolith information by exploiting information from the canals (Angelaki et al., 1999; Droulez and Darlot, 1989; Glasauer, 1992; Glasauer and Merfeld, 1997; Merfeld et al., 1993; Merfeld and Zupan, 2002; Zupan et al., 2002). This

Adapted from: Vingerhoets RAA, Van Gisbergen JAM, Medendorp WP (2007) *J. Neurophysiol.*, 97: 3256-3268

so-called canal-otolith interaction model assumes that otolith signals accompanied by a canal signal are caused by head tilt, whereas otolith signals in the absence of rotational canal cues reflect inertial accelerations due to translations of the head. Merfeld et al. (2005a,b) found support for either hypothesis in different domains. The filtering hypothesis best explained otolith disambiguation in the action domain, i.c., the vestibulo-ocular reflex, whereas perception data appeared more compatible with a canal-otolith interaction model. Since the present study will focus on perception, the filtering model will not be considered further.

A schematic representation of the canal-otolith interaction model is shown in Figure 3.1A. The core of this scheme, the internal model, transforms inputs from the canals and the otoliths into three internal variables that play crucial roles in spatial orientation (Merfeld and Zupan, 2002). Variable $\hat{\mathbf{g}}$ is the internal representation of the direction of gravity relative to the head; $\hat{\mathbf{a}}$ is the internal representation of head acceleration assigned to translation and $\hat{\boldsymbol{\omega}}$ is the internal representation of head angular velocity. In line with Zupan et al. (2002), we extended the original model with a leaky integrator operating on the $\hat{\mathbf{a}}$ output signal to obtain an internal representation of head linear velocity $\hat{\mathbf{v}}$ (see also Vingerhoets et al., 2006) and a downward pointing head-fixed vector (idiotropic vector, $\mathbf{h}$) affecting the tilt signal. A similar combination of a canal-otolith interaction stage, followed by an idiotropic vector was proposed earlier by Mittelstaedt et al. (1989). As will be explained below, the present study was designed to test whether the combined effects of canal-otolith interaction and the idiotropic mechanism are necessary and sufficient to explain tilt perception under dynamic conditions.

So far, few studies have dealt with the issue of otolith disambiguation in verticality perception during motion, which is the main topic of the present investigation. Merfeld et al. (2001) tested the subjective visual horizontal in subjects who were seated upright while being subjected to fixed-radius yaw rotation in a centrifuge. As expected from earlier studies (Clark and Graybiel, 1966; Curthoys, 1996; Graybiel and Brown, 1951), these subjects experienced tilt but their horizontality settings clearly lagged behind the rotation of the GIF. Merfeld et al. (2001) also performed a variable-radius centrifuge experiment where subjects were first rotated on axis for several minutes. The radius was then varied to yield the same centrifugal force profile as in the fixed-radius trials. In contrast with the lag observed in the fixed-radius experiment, such a delay was no longer found. An important difference between the variable-radius and fixed-radius trials is the presence of canal cues in the latter, which were therefore held responsible for the lag observed in the fixed radius paradigm (Merfeld et al., 2001). In other words, Merfeld et al. (2001) interpreted the delay in terms of a gradually disappearing sensory conflict between the canal and otolith signals. The canal cues initially indicate yaw-rotation

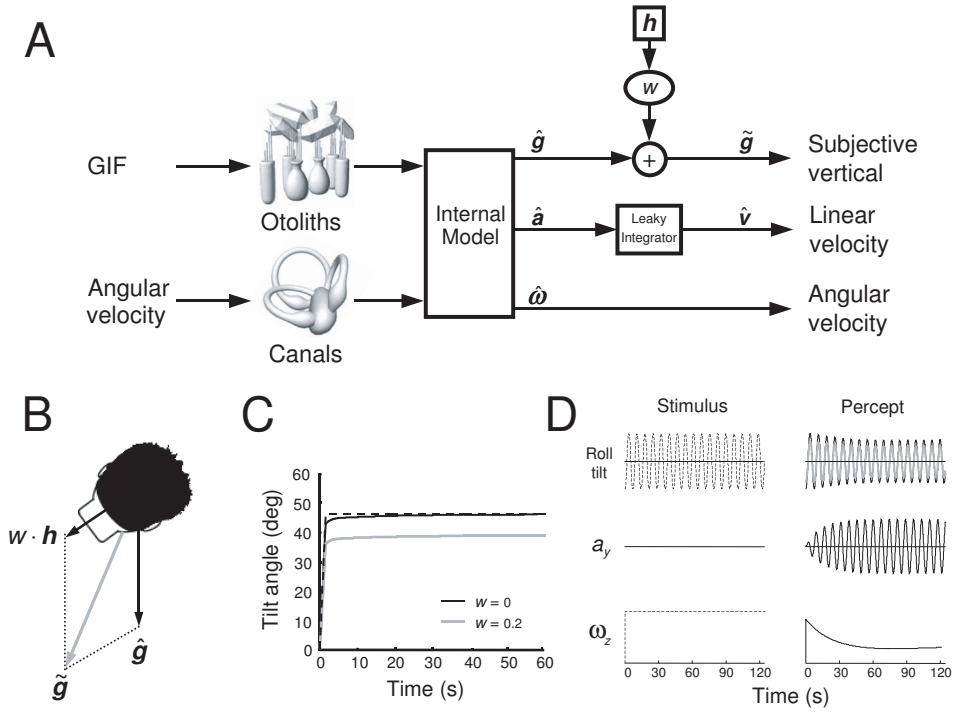

Figure 3.1 *A: Extended canal-otolith interaction model. Canals detect angular velocity and the otoliths sense gravito-inertial force (GIF), the sum of inertial acceleration and gravitational acceleration. Internal model uses canal signals to decompose GIF into tilt and translation related components. The model is an adapted version of the model proposed by Merfeld and Zupan (2002). Leaky integrator was added to obtain correct predictions of the magnitude of illusory translation during OVAR (see Vingerhoets et al., 2006). Head vector (***h***) biases the verticality percept toward the long-body axis, in line with the effect of static tilt on the sense of verticality. Symbols:* $\hat{\mathbf{g}}$*, internal representation of gravity;* $\hat{\mathbf{a}}$*, internal representation of linear acceleration;* $\hat{\boldsymbol{\omega}}$*, internal representation of angular velocity; w weight of the head vector;* $\tilde{\mathbf{g}}$*, internal representation of gravity after weighting with head vector;* $\hat{\mathbf{v}}$*, internal representation of linear translation velocity. All motion variables are 3D vectors. Illustrations of canals and otoliths were taken from Angelaki et al. (1999), with permission. (Copyright ©1999 by the Society for Neuroscience). B: Subjective visual vertical, corresponding to signal* $\tilde{\mathbf{g}}$*, is obtained as weighted vector sum of the sensed direction of gravity and a head vector, resulting in a bias toward the long-body axis. We followed Merfeld and Zupan (2002) who defined* $\hat{\mathbf{g}}$ *as pointing downward. For consistency,* **h** *also points downward, in contrast with Mittelstaedt (1983) who defined both vectors as pointing upward. C: Model predictions for the perception of roll tilt when a subject is rotated in roll toward a stationary tilt of 45° at 30°/s. Internal-model parameters:* $k_a = -4$, $k_f = 4\ s^{-1}$, $k_{f\omega} = 8\ s^{-1}$ *and* $k_\omega = 8$. *Dashed line shows actual tilt position. Black line denotes model*

prediction without effect of head vector (w = 0). Gray line represents model prediction for w = 0.2. When w = 0 the model predicts rapid convergence of the estimated tilt position to the real position. With the bias mechanism (w = 0.2), the tilt position is systematically underestimated, as commonly found in static experiments. D: Illustration of input signals (left) and perceptual signals (right) of the model during OVAR at 50°/s and 45° tilt. Internal-model parameters as in C. Left column: actual stimulation. Roll-tilt of the chair changes periodically from -45° in the LED position to +45° in the RED position; no physical interaural acceleration is present during OVAR as indicated by a_y; ω_z represents the constant velocity about the yaw axis. Right column: predicted percept. Top right: SVV in head coordinates: SVV = atan($\tilde{g}_y/\tilde{g}_z$) . Without head vector (w = 0, black line) the model predicts a gradually worsening underestimation of tilt for the SVV settings; when w = 0.2 (gray line), roll tilt perception is further biased, already from rotation onset onward. The model also predicts an illusory translation percept and a decay of rotation perception to non-zero values.

whereas the otoliths sense a change of the GIF in the roll plane. Only when the canal activity has dissipated, the sensory conflict is resolved and the otolith signals are reluctantly interpreted as due to tilt.

These centrifuge experiments suggest that a change in the GIF vector induced by linear acceleration may be centrally interpreted as a change in tilt. Can tilt also be interpreted as translation? A paradigm where this might occur is off-vertical axis rotation (OVAR), where subjects are rotated in yaw at a constant velocity about an axis that is tilted relative to the direction of gravity (Figure 3.2A). Due to the tilted axis, head orientation changes continuously with respect to gravity, as the body alternates between roll and pitch tilt. In a recent study (Vingerhoets et al., 2006), following up on earlier investigations by Denise et al. (1988) and Guedry (1974), we have shown that the initially veridical rotation percept during prolonged OVAR decays gradually (Figure 3.2B) and that a percept of circular head translation against the actual direction of movement emerges concurrently (Figure 3.2C,D). We found that the illusory translation percept matched the predictions of the canal-otolith interaction model fairly well, provided that a leaky integrator was included in the translation pathway (see Figure 3.1A).

Unless there are phase shifts between perceived tilt and actual tilt, the canal-otolith interaction model implies that when decomposition of the GIF vector errs toward overestimating translation, the tilt estimate will have an opposite bias. Thus, the canal-otolith interaction hypothesis predicts that the gradually developing illusory translation percept during OVAR (Figure 3.2D) must be accompanied by a gradually emerging underestimation of tilt. The present chapter tested this specific prediction quantitatively, using the OVAR stimulation paradigm. We also tested whether these experiments would support the extension of the canal-otolith interaction model with the idiotropic mechanism (**h** in Figure 3.1A) that has been proposed

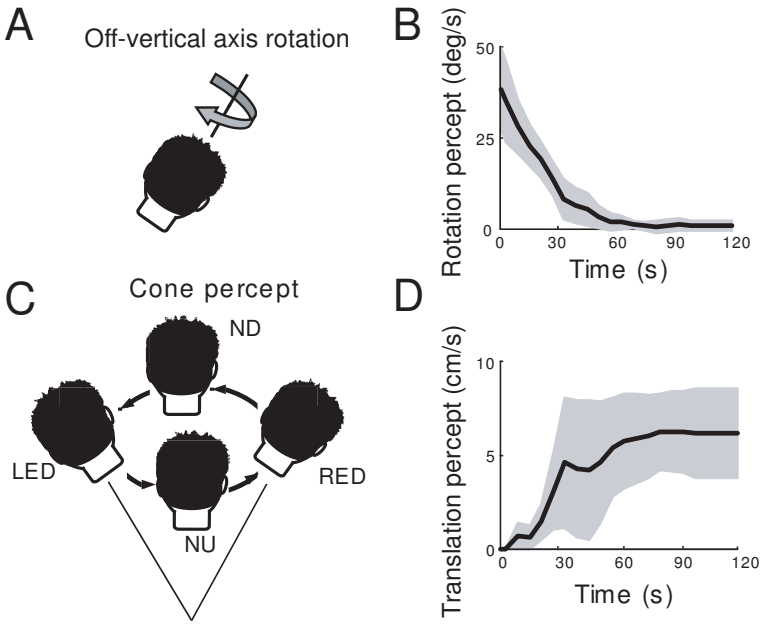

Figure 3.2 *Schematic summary of self-motion percept during OVAR. A: Subject is rotated clockwise in yaw, in darkness, about an axis that is tilted relative to gravity. B: Rotation percept gradually decays to near zero-values due to the high-pass characteristics of the canals. Mean response curve across subjects (±SD, gray zone) from Vingerhoets et al. (2006) for OVAR at 30°/s and 15°tilt. Note the contradiction with the model predictions shown in Figure 3.1D, where the rotation percept persists. C: Translational motion perceived by the subject after prolonged OVAR. Subjects feel their head describing a circular path while always facing the same direction in space. Together with the continuously changing perception of tilt, this induces a feeling of being translated along a cone, where the subject successively feels to be nose up (NU), right ear down (RED), nose down (ND) and left ear down (LED) etc. D: The percept of being translated along the cone emerges gradually, typically after an initial delay. Data (±SD) from Vingerhoets et al. (2006).*

on the basis of static tilt experiments (Mittelstaedt, 1983). In its original form, the model predicts that subjects in static roll-tilt conditions have correct percepts about the direction of gravity after a transient period (see black line in Figure 3.1C). However, many reports have shown that stationary subjects, tilted sideways in darkness, make systematic errors when adjusting a luminous line parallel to the perceived direction of gravity. At large tilt angles, the subjective visual vertical (SVV) deviates toward the long-body axis (Aubert or A-effect), as if tilt is underestimated, with errors amounting up to 35° when the body is tilted 120° (Kaptein and Van Gisbergen, 2004, 2005; Mittelstaedt, 1983, 1989; Schöne, 1964; Udo de Haes, 1970; Van

Beuzekom and Van Gisbergen, 2000). For small body tilts (<30°), these errors are generally much smaller and may even reverse sign (E-effect or Müller effect).

Most of these static tilt studies have suggested that the computation of the SVV depends heavily on the otoliths, whose signal in stationary conditions reflects the pull of gravity (Eggert, 1998; Mittelstaedt, 1983, 1989; Schöne, 1964). There is no reason to hold disambiguation errors responsible for the A-effect, since it has never been reported that stationary tilted subjects experience an illusory awareness of being translated. Instead, Mittelstaedt's original model (Mittelstaedt, 1983), which does not incorporate a solution for the ambiguity problem, explained the A-effect as the result of a bias signal, known as the idiotropic vector. This head-fixed vector was seen as a computational strategy to mitigate the effect of a putative inbalance in the otolith signal at small tilts, at the expense of large systematic errors at the rarely encountered large tilt angles. As in Mittelstaedt et al. (1989) and Zupan et al. (2002), we incorporated a head vector contribution in the scheme of Figure 3.1A, which extends the canal-otolith interaction model with a stage that can explain the static A-effects in verticality perception. Inspired by several studies (Dyde et al., 2006; Groen et al., 2002; Mittelstaedt, 1983; Zupan and Merfeld, 2005; Zupan et al., 2002), we modeled the subjective vertical as a weighted vector sum of the estimated direction of gravity and the direction of the long-body axis ($\tilde{\mathbf{g}} = \hat{\mathbf{g}} + w \cdot \mathbf{h}$, see Figure 3.1B). Parameter w is a tilt-independent variable, which represents the relative weights of these two vectors and can vary across subjects. Head vector $\mathbf{h}$ has virtually no effect on verticality perception when estimated head tilt is small.

The ability of the extended model to account for the static A-effect is illustrated in Figure 3.1C, showing both the actual roll-tilt angle and $\tilde{\mathbf{g}}$. The dashed line indicates a constant velocity roll rotation to a final tilt angle of 45°. With a moderate weight (w = 0.2) of head vector $\mathbf{h}$, the model replicates the well-known finding in the SVV literature that the roll tilt angle implied by $\tilde{\mathbf{g}}$ (gray line) is substantially smaller than the actual tilt angle (38° instead of 45°). This systematic error in the SVV, which has been confirmed experimentally from 2 to 90 s after rotation stop (Jaggi-Schwarz and Hess, 2003), cannot be reproduced by the original canal-otolith interaction model, lacking the bias signal (w = 0), as shown by the black line.

Predictions of the extended model for one of our OVAR experiments, are shown in Figure 3.1D. Perceived roll tilt, reflected in the SVV, demonstrates that tilt is increasingly underestimated as time during OVAR proceeds and that the head-referenced bias ($w \cdot \mathbf{h}$) induces an additional underestimation (gray line), right from rotation onset. Because the effect of head vector $\mathbf{h}$ depends on $\hat{\mathbf{g}}$, it is not entirely constant over time. The other panels illustrate that an illusory percept of translation develops slowly over time whereas rotation perception decays exponentially to non-zero values.

To test the SVV predictions of the extended model, we investigated whether the SVV in extreme roll tilt positions during OVAR indeed shows a gradually developing underestimation of tilt, superimposed on a tilt-related bias. To do so, we used three different combinations of tilt angle and rotation speed, testing how the time course of the SVV depends on these factors. We also assessed the SVV in a static tilt experiment, for comparison with the possible tilt-related error component in the dynamic data. Our results suggest that the canal-otolith interaction model can explain the SVV data during OVAR when extended by an idiotropic mechanism.

3.2 Methods

3.2.1 Subjects

Six subjects (five male, one female), aged between 25 and 62 years (mean ± SD: 33 ± 14 years), gave written informed consent to participate in the experiments. Four of them (JG, NK, RV and SP) also participated in our previous OVAR study (Vingerhoets et al., 2006). Four subjects (MV, NK, SP and TG) were totally naive regarding experimental goals. Subjects did not have any known visual, vestibular or other neurological disorders.

3.2.2 Setup

Subjects were seated in a motor-driven and computer-controlled vestibular chair. The apparatus consisted of three adjustable, nested frames that could be arranged to allow subject rotation about any axis in space. For the present experiments, the setup was configured to rotate subjects in yaw about an off-vertical axis. In the chair, subjects were secured with safety belts, hip and shoulder supports and Velcro straps around the feet. The head was firmly fixated in a natural upright position for looking straight ahead, using a padded adjustable helmet. The rotation axis of the chair was aligned with the center of the inter-aural axis, parallel to the long body axis. The right eye was patched to prevent double vision.

A uniformly illuminated line with an angular subtense of 22°was attached to the chair at 0.80 m in front of the subject. The line could be controlled by computer with an angular resolution of 0.5°. The rotation axis of the line, which was parallel to the subject's naso-occipital axis and intersected the subject's skull midway between the two eyes, was perpendicular to the rotation axis of the chair, so that the line could be rotated in the fronto-parallel plane. At the time when tests were taken, at each left ear down (LED) and right ear down (RED) position, this plane was perpendicular to the floor. The line was polarized by a bright dot at one end and served to determine the subjects' dynamic and static SVV.

3.2.3 Experimental paradigms

The subjective visual vertical was tested under both dynamic and static conditions, in two separate series of experiments. All experiments took place in complete darkness. Subjects were allowed to move their eyes freely at all times.

Dynamic SVV

In the dynamic experiments, subjects were rotated clockwise (seen from above) about the yaw axis which was tilted (15 or 45°) relative to the earth-vertical (i.e., off-vertical axis rotation, OVAR). After the subject was restrained, the chair was pitched backwards to the tilt angle chosen for the experiment and then rotated to the LED starting position. After 10 s of rest in that position, the chair was accelerated within 1 s to the constant velocity (30 or 50°/s) to be tested in the experiment, which was then maintained for 2 minutes.

To test the subjects' SVV at various points in time after rotation onset, we used an adaptive yes-no procedure. Each time during the run when the subject passed through the LED and RED phase, the luminous line in the fronto-parallel plane was flashed for 10 ms at a certain orientation specified by computer. Shortly after the flash, subjects used a toggle switch to indicate if the line deviated in CW or CCW direction from their perceived direction of the vertical. An adaptive staircase procedure used the set of responses collected in the series of trials from a given run to update the orientation of the line to be presented at the same test points in the next run (for further details see section *Adaptive-staircase procedure*). The purpose of this procedure was to adjust the orientation of the line in small steps, run after run, until it appeared earth-vertical to the subject.

Since subjects were tested in the LED and RED phase, where physical roll tilt was maximal (see Figure 3.2C), the interval between the sequential line flashes was 6 s for the 30°/s runs and 3.6 s for the 50°/s runs. Between runs, subjects were stationary in the nose up position for 90 s, with the room lights on, to allow reorientation. Subjects were tested for three combinations of tilt angle and rotation velocity: 45° tilt at 30°/s, 45° tilt at 50°/s and 15°tilt at 50°/s in separate sessions. We will refer to these conditions as the large-tilt & low-speed condition, the large-tilt & high-speed condition and the small-tilt & high-speed condition, respectively. Testing in each condition comprised 20 runs, subdivided in two experimental sessions of about 40 minutes each. Because of the potentially nauseous nature of the OVAR stimulus, the first experimental session of each subject tested the least provocative condition (45°tilt at 30°/s). Subjects never received feedback about their performance.

Static SVV

We used the static paradigm to examine the subjective vertical during static roll tilt. The subject was first pitched backward (15 or 45° relative to gravity) and then rotated by 90° at 20°/s about this off-vertical axis to either the LED or the RED position, in alternating runs. Once this stationary tilt position was reached, there was a 10 s waiting period before testing began. To determine the static SVV, we used the same yes-no design as in the dynamic experiment, except that testing in a given run was now limited to five consecutive flashes. Subsequently, the subject was rotated back to the nose up orientation for a 30 s rest period with the room lights on in order to allow reorientation. In two separate sessions, subjects were tested at the two different tilt angles (15° LED/RED and 45° LED/RED). Each session took about 45 minutes and comprised 15 runs.

3.2.4 Definition of angles

Since subjects were tested in the LED and the RED phase of rotation, the amount of physical head roll-tilt equaled the tilt angle of the rotation axis. Accordingly, head roll-tilt, denoted by ρ, was -15 or -45° for LED and +15 or +45° for RED. Response error, indicated by γ, was defined as the angular difference between the SVV and the true vertical (see inset Figure 3.3A). SVV deviations in clockwise direction (seen from behind the subject) were taken positive. Accordingly, an SVV setting biased in the direction of body tilt (A-effect) yields a positive γ value in the RED phase (inset Figure 3.3A) and a negative γ value in the LED phase. A bias in the opposite direction (E-effect) yields negative and positive γ values for the RED and LED phase, respectively.

3.2.5 Adaptive-staircase procedure

In both paradigms, we used a sequential set of adaptive staircases to determine the time course of the subject's SVV after the onset of OVAR stimulation. Each adaptive staircase in this set was designed to test the SVV repeatedly, across runs, at one particular point in time after OVAR onset. Each new run added a further test step to all staircases by presenting the luminous line at an orientation based on the response at that same point in time in the previous run. Thus, if the subject's response to the first line stimulus testing the SVV at time Tn was 'clockwise', the line testing the SVV at Tn in the next run would be presented at a more counterclockwise orientation (see definition of step size below), and so on, until the response to the Tn trial in a subsequent run reversed to 'counterclockwise'. Such a response reversal then started a series of adjustments in the opposite direction until the next response

reversal occurred. After many runs, the accumulated set of responses across all sequential runs invariably showed an adaptive staircase pattern that converged on the line orientation that the subject considered vertical at a particular point in time after rotation onset. The SVV was defined as the line orientation at which the response in repeated trials fluctuated between 'clockwise' and 'counterclockwise'. Applying this procedure of gradually completing a sequential set of independent staircase procedures allowed us to sample the dynamic evolution of the SVV in time intervals of a few seconds (6 s for 30°/s runs and 3.6 s for the 50°/s runs, see above). The staircase began with a 8° step size ± 1° scatter which was reduced to 4° ± 1° scatter after two reversals and further reduced to 2° step size ± 1° scatter after four reversals. In all subjects, the staircase results from the dynamic experiments yielded at least six reversals (typically eight to fourteen). In the static experiments, where only fifteen runs were performed, most staircases also yielded at least six reversals (typically seven to nine). The SVV was computed as the mean across the last six reversals.

To illustrate by example how the adaptive staircase procedure worked in practice, Figure 3.3A shows all line orientations presented in the RED phase trials in the first (denoted by open circles) and second (represented by filled boxes) OVAR run. For example, in the gray marked trial of the first run, the line was tilted -14° with respect to gravity and elicited a correct 'counterclockwise' response from the subject. Accordingly, the adaptive procedure adjusted line orientation in the second run to -7°. Figure 3.3B shows how line orientations late in the session bounced up and down between two limits marked by multiple response reversals. Also note the first step size reduction after the second reversal, which occurred in the fifth run, and the second step size reduction after the fourth reversal in the seventh run. Figure 3.3C shows all line orientations from panel B, as seen by the subject, to illustrate that in the first four runs the line orientation was repeatedly adjusted in the clockwise direction, while in the later runs it scattered around 7°.

3.2.6 Model simulations

Improved model parameters

We used Matlab 7.0 and Simulink 6.0 (The Mathworks) to simulate the canal-otolith interaction model outlined in Figure 3.1A. This scheme is based on the model proposed by Merfeld and Zupan (2002), but extended with a stage including a weighted head vector (**h**) (Mittelstaedt et al., 1989; Zupan et al., 2002). In model version C3, which emerged as optimal in Vingerhoets et al. (2006), the four internal model parameter values were $k_a = -4$, $k_f = 2\ s^{-1}$, $k_{f\omega} = 8\ s^{-1}$ and $k_\omega = 8$. In the previous study, we reported that this model version provided a good fit to the

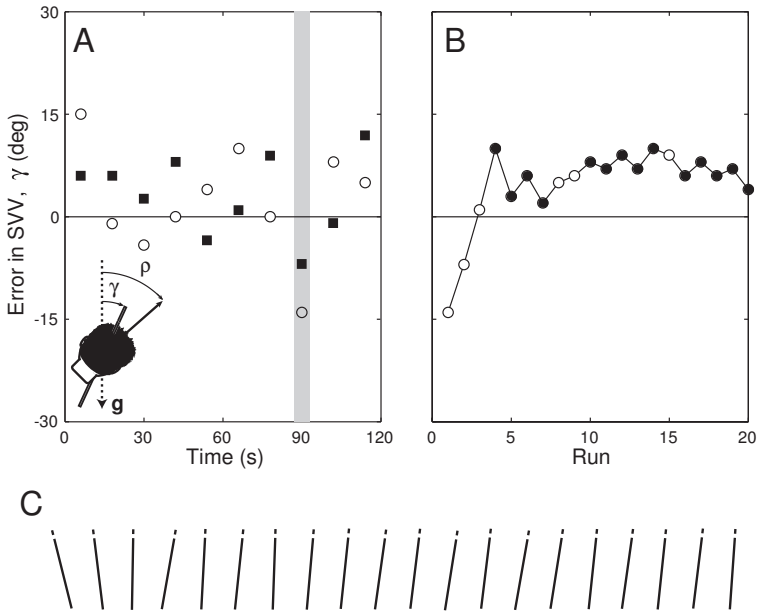

Figure 3.3 *Explanation of adaptive staircase procedure. A: Line orientations presented in subsequent trials in the RED phase of the first and second run of a session. Open circles: stimuli during sequential trials of first run; squares denote stimuli of second run. For the second run, all stimuli were adapted in the direction desired by the subject during the first run. In this example, the subject indicated that the first line in the first run deviated in clockwise direction from his subjective vertical. In trials 2, 3 and 4 of the first run the response was opposite: here the subject signaled that the line appeared counterclockwise with respect to his percept of verticality. Inset: Angular variables in the experiment. ρ: body tilt angle, equal to tilt angle of the rotation axis;* ***g****: direction of the physical vertical; γ: response error, taken as the angular separation between the true vertical (****g****) and the SVV. B: Adaptive staircase, showing changes in line orientation across runs for the eighth RED trial. The two stimuli in the gray bar in panel A correspond to the first two stimuli in panel B. Panel B further shows that this subject repeatedly indicated, in subsequent runs, that the line deviated in counterclockwise direction from his perceived direction of gravity but shifted to 'clockwise' response in the fourth run. Runs where the subject switched response, by reporting 'clockwise' while in the previous run the response was 'counterclockwise', or vice versa, are denoted as a response reversal (reversal for short) and are marked by filled circles. In this example of an adaptive staircase, a total of 14 reversals was obtained. The SVV was calculated as the mean of the last six reversals. C: Illustration of the same line orientations in world coordinates. The line was presented more and more clockwise in the first four runs. Final line orientations scatter around a 7° clockwise tilt position, signifying an A-effect of 7°.*

observed translation percepts during OVAR. However, in testing the model's performance, we overlooked one of its important features, namely the predicted phase lags. These can be quite substantial and should be taken into account in a proper model evaluation. In the present study, we therefore decided to recalculate the best fit parameters for all rotation and translation data of Vingerhoets et al. (2006) but now taking the phase shift into account. As in Vingerhoets et al. (2006) we first determined the best-fit time constant of the leaky integrator by minimizing the sum of squared errors, keeping the internal model parameters fixed at values published in Merfeld et al. (2005a). Accounting for the phase shift led to a longer time constant of the leaky integrator of 0.06 s. Subsequently, we searched within a limited parameter space (testing values of -0.5, -1, -2 ,-4 and -8 for k_a and 0.5, 1, 2, 4 and 8 for the other parameters) for the internal-model parameter set that yielded the smallest sum of squared errors. The parameters that provided the best description were $k_a = -4$, $k_f = 4\ \mathrm{s}^{-1}$, $k_{f\omega} = 8\ \mathrm{s}^{-1}$ and $k_\omega = 8$, which means that only parameter k_f was changed from 2 to 4 in comparison with model C3 from Vingerhoets et al. (2006). The corrected fit curves, showing only minute differences with the originals shown in Figure 2.15A,B of the previous chapter, match these data quite well. The revised parameter set was held fixed for all subjects, leaving only the weight of the head vector as a free parameter among individual subjects. We could not obtain a best-fit parameter set based on rotation, translation and tilt percepts in individual subjects, since not all subjects participated in both OVAR studies. We therefore determined the best-fit parameters across the group of subjects, since we wished to include data on all percepts.

Model predictions

The model prediction for the SVV was based on the vector sum of the orientation of gravity with respect to the head and a weighted head vector (i.e., $\tilde{\mathbf{g}} = \hat{\mathbf{g}} + w \cdot \mathbf{h}$). Vector $\mathbf{h}$ points downward along the main body axis with a magnitude of 1 G and parameter w denotes its weight (see Figure 3.1B). Since the SVV responses yielded only the directional error of $\tilde{\mathbf{g}}$, not its amplitude, we could only determine the relative weighting of the two vectors. Therefore, we fixed the gain of $\hat{\mathbf{g}}$ to unity and allowed w to vary freely across subjects. The model prediction for the SVV data was taken as SVV = atan($\tilde{g}_y/\tilde{g}_z$).

Model predictions for the SVV depend on OVAR conditions and the weight of the head vector. The left-hand column of Figure 3.4 shows the actual roll-tilt of the chair (solid line) and the predicted perceived roll tilt (dashed line), defined as atan($\hat{g}_y/\hat{g}_z$) . The model predicts a gradually worsening underestimation of tilt and a steadily increasing phase lag for all conditions. Both the underestimation of tilt and the phase lag are more pronounced for higher speeds. Measurements were

taken at the physical LED and RED positions, but because of the phase lag, there is a time shift with respect to the perceived LED and RED positions predicted by the model. This phase shift ($\Delta\phi$) is plotted in the insets in the right-hand panels, which show that phase shift increases exponentially in time and levels off at a value depending on rotation speed and tilt angle. The lag is not constant since it depends on the model's estimate of angular velocity ($\hat{\boldsymbol{\omega}}$), which declines slowly. In the model, angular velocity is determined using the canal signals, which dissipate during prolonged rotation with a given time constant. An internal feedback loop, which takes the angular difference between the GIF measured by the otoliths and estimated GIF as a measure for angular velocity, extends this time constant, but underestimation will ultimately ensue. Since the phase shift between $\hat{\mathbf{g}}$ and $\mathbf{g}$ depends on the cross product of $\hat{\boldsymbol{\omega}}$ and $\hat{\mathbf{g}}$, a time varying $\hat{\boldsymbol{\omega}}$ will lead to a time varying phase shift.

The predicted errors for LED and RED are indicated in the right-hand panels of Figure 3.4, showing predictions with ($w = 0.2$) and without ($w = 0$) head vector contribution. In the absence of a tilt-related bias ($w = 0$, thin line), the model, based on signal $\hat{\mathbf{g}}$, predicts relatively small errors in the large-tilt & low-speed condition. Predicted errors show an exponential increase to a substantially larger asymptotic value of about 10° in the large-tilt & high-speed condition and to 7° in the small-tilt & high-speed condition. Thus, predicted dynamic effects are more prominent for the high-speed conditions. As shown by thick lines, involvement of the head vector ($w = 0.2$) adds a bias that is already present at rotation onset. For the large tilt conditions this bias is about 8°, while for the small tilt condition it is limited to about 3°. Note that the effect of the head vector is largest at rotation onset and decreases slightly when the direction of $\hat{\mathbf{g}}$ approaches $\mathbf{h}$ later in the run.

Model evaluation

In the Results section we will compare the performance of three model versions. The first two model versions, one with and one without idioptropic mechanism, are outlined above and in Figure 3.4. A third version of the model, which is not discussed in Figure 3.4, is inspired by Mittelsteadt's original model (Mittelstaedt, 1983). This version assumes no dynamic disambiguation error, but only a constant bias from the idiotropic mechanism. The model versions were compared with actual data using the root mean squared error (RMSE), the variance-accounted for percentage (VAF) and the Bayesian Information Criterion (BIC). The RMSE is defined as the square root of the mean quadratic distance between the data points and the corresponding model prediction:

$$\mathrm{RMSE}_i = \sqrt{\frac{1}{N}\sum_n [\Psi(n) - \hat{\Psi}_i(n)]^2}$$

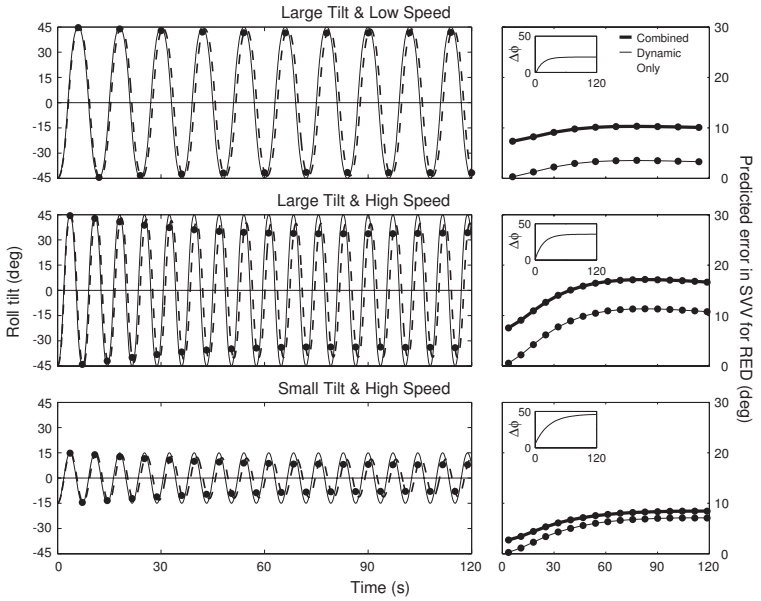

Figure 3.4 *Model predictions for tilt perception during OVAR. Parameter values:* $k_a = -4$, $k_f = 4\ s^{-1}$, $k_{f\omega} = 8\ s^{-1}$ *and* $k_\omega = 8$. *Left-hand panels plot physical roll-tilt (solid line) and simulated perceived roll-tilt (dashed line, defined as* $\text{atan}(\hat{g}_y/\hat{g}_z)$*) as a function of time for the dynamic only model. Measurements were taken when the subject was at RED and LED (filled circles). In all conditions predicted perceived roll-tilt shows a gradually increasing phase lag with respect to actual roll-tilt, reaching a maximum after about 60 s. In parallel, the amplitude of perceived roll-tilt decays gradually, reflecting a growing underestimation of tilt. Right-hand panels plot the predicted error in the SVV at RED position, defined as actual roll-tilt minus perceived roll-tilt. Sampled errors are shown connected by lines, both without (thin line, labeled Dynamic only) and with (w = 0.2, thick line, labeled Combined) head vector contribution (**h**). The head vector induces an offset in predicted SVV errors. When* $\hat{\mathbf{g}}$ *approaches* **h**, *the effect of the head vector becomes smaller, so that the effect exerted by* **h** *is not constant in time. The filter characteristics of the canals cause a slight decrease in perceived tilt after about 60 s for the two large tilt conditions. Insets in right-hand panels: phase shift (*$\Delta\phi$*, in degrees) is an exponential function of time after rotation onset. Asymptotic values: 24° for large-tilt & low-speed, 34° for large-tilt & high-speed and 41° for small-tilt & high-speed.*

where $\Psi(n)$ is data point n, $\hat{\Psi}_i(n)$ is the corresponding value estimated from model i and N is the number of data points. Accordingly, smaller RMSE values indicate a better fit. The VAF provides a normalized measure for how well the model predicts the variance of the data and is defined as:

$$\text{VAF}_i = (1 - [\text{var}(\Psi - \hat{\Psi}_i)/\text{var}(\Psi)]) \times 100$$

where Ψ is the data and $\hat{\Psi}_i$ is the model prediction from model i (Cullen et al., 1996; Green and Angelaki, 2003). A value closer to 100 indicates a better fit. The BIC, which provides a measure of the adequacy of the number of model parameters, is defined as:

$$\mathrm{BIC}_i = \log(\frac{1}{N}\sum_n [\Psi(n) - \hat{\Psi}_i(n)]^2) + (P/2)\log(N)/N$$

where P is the number of fit parameters (Green and Angelaki, 2003; Schwarz, 1978). A more appropriate model is characterized by a lower BIC value.

3.3 Results

We studied the sense of verticality during OVAR to test the extended canal-otolith interaction model presented in Figure 3.1A. The model predicts errors in the SVV, stemming from two different sources (Figure 3.4). First, the decay of rotational cues from the canals during prolonged OVAR causes misinterpretation of the otolith signals in the form of gradually worsening tilt underestimation. Second, the idiotropic mechanism (**h**) causes further tilt underestimation by biasing the subjective vertical towards the long-body axis, right from rotation onset onward, particularly at larger tilts. We will first report the SVV results in static conditions of 15° and 45° roll tilt to document the idiotropic effect. Subsequently, we present the data on the SVV during OVAR and test if errors from both origins can be identified.

3.3.1 Static SVV

Classical descriptions of the SVV in tilted subjects (Mittelstaedt, 1983; Schöne, 1964; Udo de Haes, 1970) report A-effects for large tilt angles and reduced A-effects or E-effects for small tilt angles. We saw the same trend in our static paradigm as illustrated in Figure 3.5, which shows a bar diagram of the response errors (γ) obtained at 45° tilt (panel A) and at 15° tilt (panel B). In this figure, positive errors refer to an A-effect and negative errors indicate an E-effect. If subjects had performed flawlessly, γ would be zero for all conditions. In the 45° tilt conditions, most subjects showed A-effects, often asymmetric for the LED and RED positions. In the 15° tilt condition, A-effects were smaller and E-effects became more prevalent. As might be expected from the literature, there were clear idiosyncratic differences in the error pattern expressed in the 15° and 45° conditions. Subject JG, for example, invariably showed an A-effect, which was smaller for 15° tilt than for 45° tilt. By contrast, subject TG, had robust E-effects in the 15° tilt condition that were even still noticeable at 45° tilt. Overall, the general pattern of errors during

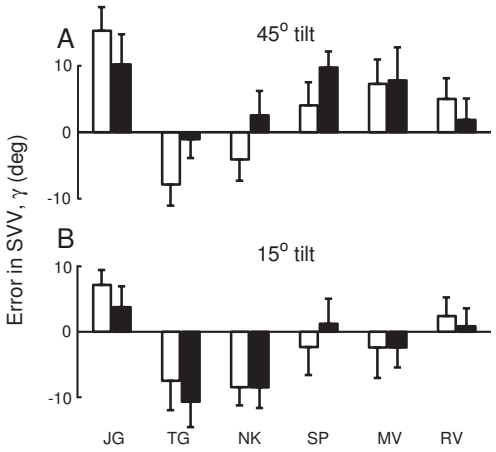

Figure 3.5 *Bar plot of mean SVV errors (±SD) during the static experiment. White bars: LED, Black bars: RED. Signs of SVV errors for LED were inverted for illustrative purposes. Positive errors denote an A-effect; negative errors indicate an E-effect. A: Errors in the static experiment at 45° tilt. Apart from NK and TG, all subjects show A-effects for both RED and LED. Mean error for LED 3.3°, mean error for RED 5.2°. B Errors in the static experiment at 15° tilt. A-effects became smaller or even reversed to E-effects, compared to the 45° tilt condition. Mean error for LED -1.8°, mean error for RED -2.6°.*

the static tilt conditions was quite consistent with the literature in that A-effects became smaller at smaller tilt angles and sometimes even reversed to E-effects. A two-way analysis of variance confirmed a significant effect of tilt angle on the SVV in each subject ($F(1,16) > 8.2$; $P \leq 0.01$ for each subject). In five out of six subjects, there was a significant effect of tilt direction (LED/RED) on the SVV settings ($F(1,16) > 8.7$; $P \leq 0.01$ for these five subjects), confirming the suggestion of response asymmetry in Figure 3.5.

3.3.2 Dynamic SVV

As mentioned earlier, the model (Figure 3.1A) predicts two types of errors during dynamic OVAR conditions: an offset that is most prominent in the large tilt conditions and a dynamic, time-dependent, component that is most pronounced in the high speed conditions (Figure 3.4). Figure 3.6 shows the time course of the SVV errors from subject MV. All three testing conditions caused tilt underestimation, expressed as positive errors for RED and as negative errors for LED. As in the static experiment, LED and RED responses were not precisely symmetric. Close inspection of the two large tilt conditions (Figure 3.6A,B) reveals that the response, in both LED and RED position, shows already an A-effect right at rotation onset, indicating a tilt-related bias. The high speed responses comply with the model (Figure 3.4) by showing substantial dynamic effects. In both panels, errors in the SVV increase exponentially with time to a steady-state value after about 60 s. As predicted, the dynamic component was more striking in the high speed conditions, while the bias was more obvious in the large tilt conditions. In summary, the data

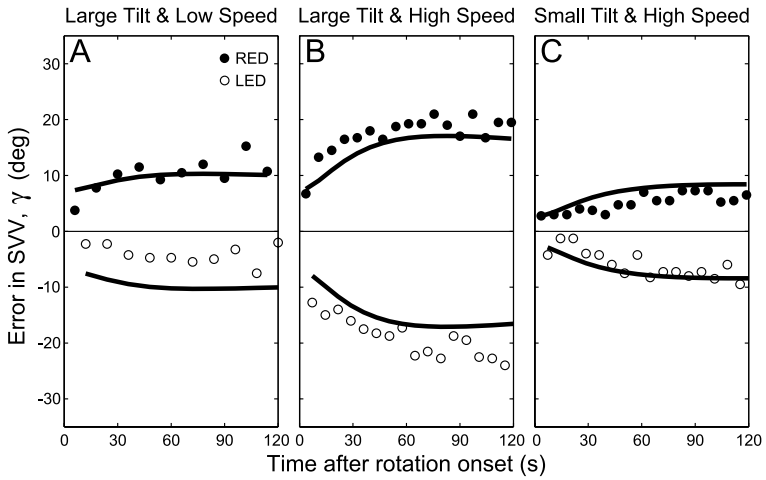

Figure 3.6 *Time course of errors in SVV during OVAR. Open circles: LED trial data; filled circles: RED trial data; solid line: model fit with w = 0.2. Data from subject MV. A: errors in the 30°/s and 45° tilt condition do not start at zero and show a slight increase as rotation continues. B: errors are already present at t = 0 in the 50°/s and 45° tilt condition; dynamic increase in tilt underestimation is about 15°. C: in the 50°/s and 15°tilt condition, errors are initially smaller but again show a slight increase with time.*

from this subject support the model predictions by showing a dynamic response error pattern that seems superimposed on a tilt-related offset. The bold lines in Figure 3.6 represent model predictions, to be discussed later in this section.

3.3.3 Relation between dynamic and static results

We observed that virtually all subjects already made systematic SVV errors at the onset of rotation. If this error has the same size as the static error shown in Figure 3.5, this would suggest the expression of a head bias in dynamic conditions, in line with the scheme in Figure 3.1A. To investigate this, in a lumped comparison across all subjects, we plotted the error observed in the static tilt paradigm (static SVV error) against the error in the first measurement after rotation onset in the dynamic paradigm (initial dynamic SVV error), at corresponding tilt angles. In this analysis, shown in Figure 3.7, we inverted the sign of the LED data to allow pooling with RED data.

A linear regression, which quantified the apparent relationship, revealed a significant correlation ($r = 0.76$; $p < 0.001$; $n = 36$), a slope not significantly different from unity (0.81 ± 0.12) and an intercept close to zero ($-2.4 \pm 1.0°$). This suggests that the errors occurring at OVAR onset, whether expressed as an A- or an E-effect,

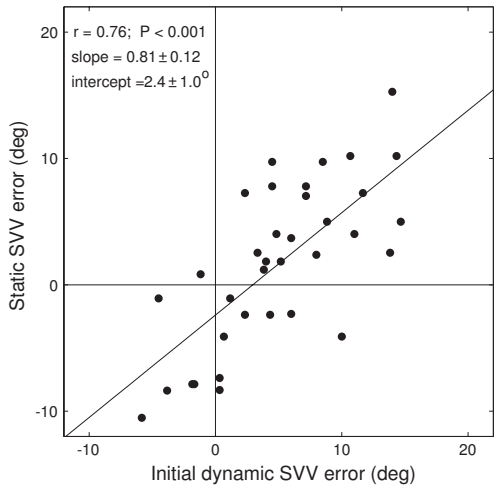

Figure 3.7 *Correlation between initial dynamic error and error in static experiment. Errors for the same tilt angle are plotted against each other.*

resemble those in corresponding static tilt conditions. In other words, the A and E-effects found in static conditions reflect a tilt-related mechanism that also comes into play when the same tilt angle is tested dynamically.

3.3.4 The dynamic component

In the previous section it was shown that the bias in the SVV in dynamic conditions is quite similar to the SVV in static tests at the same tilt angle. We will now explore if the remaining time-dependent part of the response can be explained by the canal-otolith interaction model ($w = 0$). To this end, we isolated the dynamic component by subtracting the static response from the total response in each subject and then pooled the result over subjects. Figure 3.8 shows that the population average (solid line) has a clear dynamic component, which is quite well matched by the predictions of the canal-otolith interaction model (dashed line). Both model and data show a weak dynamic effect in the large-tilt & low-speed condition that becomes more substantial for the small-tilt & high-speed condition and is most pronounced in the large-tilt & high-speed condition. Hence, for the pooled data, the time-dependent component of verticality judgments observed during OVAR may be regarded as a genuine manifestation of improper disambiguation of the otolith signal. The evaluation of the combined model on a more individual basis will be presented in the next section.

3.3.5 Model fits

The notion, that SVV errors during prolonged OVAR contain a static contribution, which can also be observed in stationary (non-moving) subjects, and a disambigua-

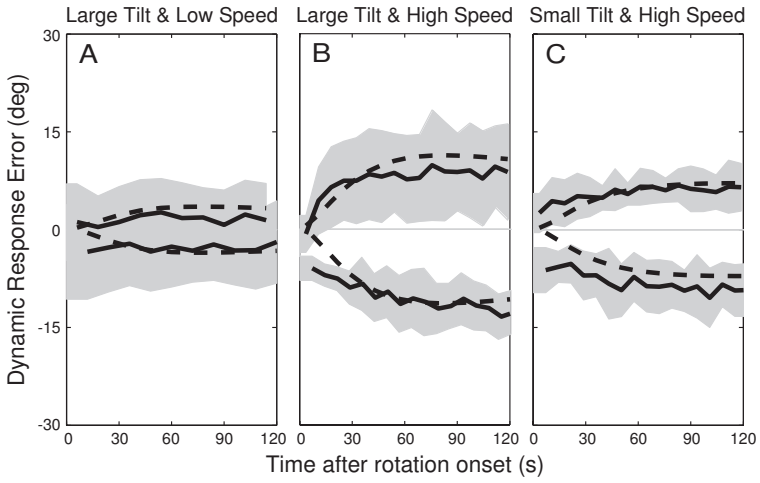

Figure 3.8 *Dynamic component of the SVV during OVAR. Solid lines: population average ± SD (gray zone). Dashed lines: model predictions with parameter values:* $k_a = -4$, $k_f = 4$ s^{-1}, $k_{f\omega} = 8$ s^{-1} *and* $k_\omega = 8$. *A: 30°/s and 45° tilt condition. B: 50°/s and 45° tilt condition. C: 50°/s and 15° tilt condition.*

tion contribution that depends on tilt angle and rotation speed, will now be tested further. To test the dependence of the SVV ($\tilde{\mathbf{g}}$) on these two factors quantitatively, we fitted parameter w in the extended model to the data from each subject separately:

$$\tilde{\mathbf{g}}(t) = \hat{\mathbf{g}}(t) + w \cdot \mathbf{h} \tag{3.1}$$

In this equation $\hat{\mathbf{g}}(t)$ is the internal representation of gravity, $\mathbf{h}$ is the head vector, and w represents the weight of the head vector, used as a free parameter. As an example, using $w = 0.2$, the thick lines in the right-hand column of Figure 3.4 (labeled Combined) illustrate predictions of this model . The panels clearly show the offset and the dynamic effect.

For comparison, we also computed the residual error between data and original model, without the idiotropic mechanism:

$$\tilde{\mathbf{g}}(t) = \hat{\mathbf{g}}(t) \tag{3.2}$$

In essence, this equation is identical to Equation 3.1 with $w = 0$. Figure 3.4 also shows predictions of this version (thin lines, labeled Dynamic only) where only the dynamic effect remains. Likewise, to assess whether the dynamic contribution is essential, we fitted a version with only the idiotropic mechanism:

$$\tilde{\mathbf{g}}(t) = \mathbf{g_0}(t) + w \cdot \mathbf{h} \tag{3.3}$$

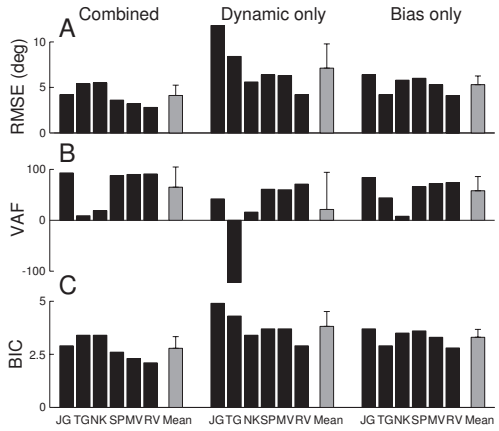

Figure 3.9 *Evaluation of three versions of extended model. Values pooled for LED and RED. A: RMSE values. B: VAF percentages. C: BIC values.*

In this equation $\mathbf{g_0}$ is the true direction of gravity represented in a head-fixed coordinate frame. This model version assumes no disambiguation errors, only the constant bias from Equation 3.1.

We obtained the error in the SVV, predicted by each of the three model versions, by taking the difference between actual roll-tilt and roll-tilt reflected by the SVV, computed as $\text{atan}(\tilde{g}_y/\tilde{g}_z)$. Fits were performed on all static and dynamic data simultaneously. From our experiments, we obtained a total of 20 static data points and 88 dynamic data points for each subject. In order to give equal weight to the static and dynamic data in our fit procedure, we extended the static data points with the mean of the five measurements such that the number of data points in the static condition matched the number of data points in the corresponding dynamic paradigm.

As a measure of how well each model version fitted the data, we used the root mean squared error (RMSE), the variance accounted-for percentage (VAF) and the Bayesian Information Criterion (BIC). To calculate the BIC we used $P = 1$ for the combined and bias only models and $P = 0$ for the dynamic only model. As explained in the Methods section, a model is preferable above a competing scheme if its RMSE and BIC values are smaller and the VAF percentage is higher. Figure 3.9A shows RMSE values for each model and each subject separately. The combined model (Equation 3.1) clearly outperformed the reduced versions specified by Equations 3.2 and 3.3, respectively, in 4 out of 6 subjects. As can be seen, depriving the model from the head vector contribution led to a consistent increase in RMSE (Combined versus Dynamic only). Leaving out the dynamic mechanism reflecting canal-otolith interaction (Combined versus Bias only) also caused a clear increase in RMSE, except in subject TG. The same conclusions can be drawn for the BIC and VAF values. Higher VAF percentages were found for the model that includes dynamic and bias effects (Combined) in all subjects, except TG. Simi-

larly, we found the lowest BIC values, indicating a better model, for the combined model in all subjects but TG. In addition to subject TG, who is clearly an outlier, one may note that the combined model is only marginally better in subject NK. All in all, the results show that the combined model is definitely better in 4 out of 6 subjects. A two-way analysis of variance with model (combined/bias only) and measurement phase (RED/LED) as factors confirmed that the differences in RMSE and BIC between the combined model and the bias-only model were significant ($F(1,20) > 10.9$; $P < 0.004$) whereas the differences in VAF were not significant ($F(1,20) < 0.45$; $P > 0.51$). In addition, there was no significant main effect of measurement phase, or a significant interaction, confirming that the model performed equally well for LED and RED data. We therefore conclude that the mean errors in the subjective visual vertical during OVAR, based on population data, reflect imperfect otolith disambiguation and a tilt-related bias.

Figure 3.10 presents fits of the extended model for the RED measurements in each subject, for each of the three dynamic conditions. Best fit lines for both LED and RED in one subject (MV) are shown in Figure 3.6. According to the combined model, we should observe two effects: a time-dependent increasing SVV error which is most pronounced in the high-speed conditions and an initial bias that is largest for the large tilt conditions. Although this is indeed the general picture arising from the data, individual fits may not always be convincing in all aspects. For example in the large-tilt & low-speed condition, the model correctly predicts no substantial dynamics, but the bias in the first collected SVV sample is not always matched correctly. Also, the temporal dynamics of the small-tilt & high-speed condition in the data is less convincing than in the model. On the other hand, for the large-tilt & high-speed condition both effects are clearly present in all subjects except TG. And while the intersubject differences in time course are not captured, the model generally gives a very reasonable account of the data. Together with the model analysis shown in Figure 3.9, this suggests that the combined scheme is currently the best model to describe our data. To fit the initial bias, all subjects required a weight (w) that was significantly different from zero (t-test, $P < 0.05$). As shown in the right hand margin of Figure 3.10, weights ranged from -0.18 to 0.49 with a mean value of 0.13 (SD: 0.23), indicating considerable intersubject variability. In two subjects, NK and TG, the fit assigned a negative weight to the head vector to account for the predominant E-effect in their data (see Figure 3.5).

As a final note, we investigated whether a substantially better fit could be obtained if the best-fit parameters of the internal model were only determined by the dynamic component of the present SVV data, rather than by the Vingerhoets et al. (2006) data. To this end, we searched for the best-fit parameters for the dynamic component of the SVV data. Importantly, this best-fit tilt-only parameter set yield-

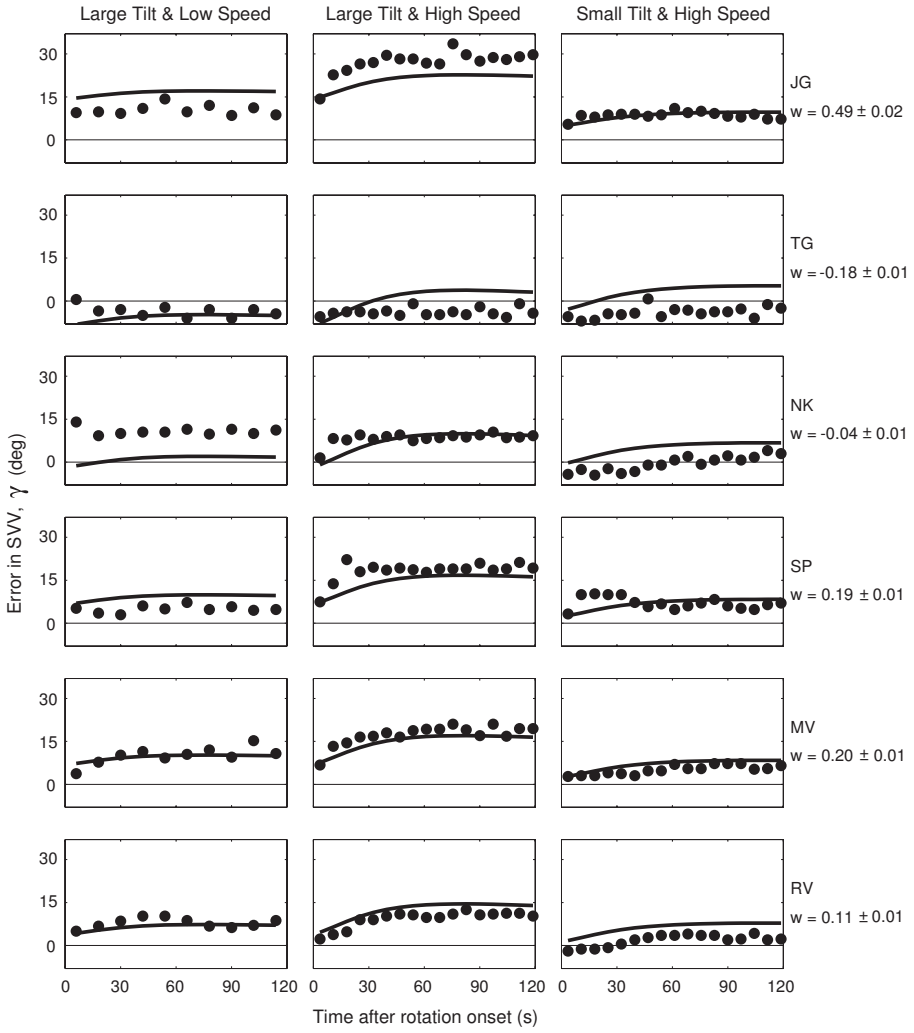

Figure 3.10 *Response errors and fits of combined version of extended model. Only RED data and fits are shown. Left: 45° tilt and 30°/s condition. All subjects display an underestimation of tilt with no clear trend over time, except for TG. Middle: 45° tilt and 50°/s condition. Underestimation of tilt increases with time. Right: 15° tilt and 50°/s condition. Initial underestimation of tilt is smaller than in the large tilt conditions. Tilt underestimation increases only slightly with time. Individual w values (±SD) are displayed on the right-hand side.*

ing values $k_a = -4$, $k_f = 2$ s^{-1}, $k_{f\omega} = 8$ s^{-1} and $k_\omega = 2$, provided no substantial fit improvement in the dynamic SVV component pooled across subjects and conditions as shown in Table 3.1. Moreover, as Table 3.1 further shows, this model was

Parameters based on:	Parameter values					Fit residuals (RMSE)	
	k_a	k_f	$k_{f\omega}$	k_ω	τ_{leaky}	Translation & rotation data (deg/s)	Dynamic SVV component
Rotation & translation data	-4	4	8	8	0.06	5.6	5.2
Dynamic SVV component	-4	2	8	2	0.06	8.2	5.1

Table 3.1 *Model performance with two different parameter sets. One parameter set was based on rotation and translation data from Vingerhoets et al. (2006), the other set was based on the dynamic SVV component from the present study. Models perform comparably on SVV data, but the adopted model performs best for translation and rotation data. RMSE values are averages across subjects and conditions. Dimensions:* k_f s^{-1}; $k_{f\omega}$ s^{-1} ; τ_{leaky}, *s; Parameters* k_a *and* k_ω *are dimensionless.*

clearly inferior for the translation and rotation data. On this basis, we conclude that the adopted parameter set, with $k_a = -4$, $k_f = 4$ s^{-1}, $k_{f\omega} = 8$ s^{-1} and $k_\omega = 8$, provides the best description for motion percepts during OVAR.

3.4 Discussion

In a previous study (Vingerhoets et al., 2006) we found that the illusory translation percepts during OVAR are consistent with predictions from an adapted version of the canal-otolith interaction model originally proposed by Merfeld and Zupan (2002). The present study was designed to test an extended version of this model (Figure 3.1A) by measuring verticality perception during prolonged OVAR. The extended model predicts a combination of two types of errors: a dynamic time-dependent error due to improper interpretation of the ambiguous otolith signal and a response bias related to tilt angle. To test this prediction, we implemented an adaptive staircase paradigm to assess the SVV both dynamically during OVAR and under static tilt conditions. In the dynamic experiments, the SVV showed an error pattern that typically started off from a non-zero value and then increased further toward a steady-state error after about 60 s. These dynamic results, in combination with the static results, confirm the predicted superposition of the two effects. We will first discuss our approach to quantify the time course of verticality perception. Next, we relate the two observed effects to previous investigations in the literature. Finally, we will consider a possible alternative modeling approach to the present data.

3.4.1 Methodological aspects

We tested verticality perception during OVAR using an adaptive psychophysical procedure to adjust a luminous line in iterative fashion until it appeared world vertical to the subject. Our staircase procedure has a clear advantage when compared to a continuous-tracking method. The latter was used by Keusch et al. (2004), who asked subjects to continuously align a luminous line with the direction of gravity while they were being rotated. With this approach, measurements at different tilt angles are clearly not independent and the time needed for the adjustment may affect the time course of the response. In the present study, these problems were avoided by applying a staircase procedure over runs in combination with a flashed line.

Anoter methodological aspect with relevance for the interpretation of our results concerns the fact that the subjective visual vertical is not necessarily a direct reflection of our percept of body orientation in space. Several investigations have shown that roll-tilted subjects may have a rather accurate estimate of body tilt but may yet show a large A-effect in their SVV settings (Kaptein and Van Gisbergen, 2004; Mast and Jarchow, 1996; Mittelstaedt, 1983). According to Mittelstaedt (1983) this apparent disparity is due to the tendency to use the body axis as a partial reference for verticality judgments in the context of the SVV task, but not in the perception of body tilt. A possible indication that body tilt percepts during OVAR may differ from SVV results comes from experiments from Denise et al. (1988), who asked subjects to verbally estimate the cone angle during OVAR. Denise and coworkers reported that subjects perceived a cone angle greater than the actual tilt angle. This is clearly in contrast with our SVV data which indicate a slight underestimate of body tilt. For more decisive conclusions, body tilt percepts would have to be tested more quantitatively, but an appropriate method to do this remains to be developed.

3.4.2 Evaluation of the combined model

We have demonstrated that the combined model, proposed in Figure 3.1A, provides the best fit to our data for the majority of our subjects. This finding suggests that both disambiguation errors and an idiotropic mechanism contribute to verticality perception during OVAR. These components, which thus far had not been studied in combination, will be discussed in the following section.

Tilt-related bias

It is well established that subjects, when tilted sideways in darkness, make systematic errors in judging visual verticality (Kaptein and Van Gisbergen, 2004, 2005;

Mittelstaedt, 1983; Schöne, 1964; Udo de Haes, 1970; Van Beuzekom and Van Gisbergen, 2000). Mittelstaedt (1983, 1989) has interpreted these errors as the manifestation of a neural strategy that effectively compensates for an unbalance in the number of hair cells on the utricule and the saccule. This strategy relies on an internal bias signal, called the idiotropic vector, which causes a tendency to align the visual line with the long body axis. In Mittelstaedt's scheme, the SVV is the vector sum of the gravity vector in normalized otolithic components and the tilt-independent, head-fixed idiotropic vector. As a result, the idiotropic vector limits the size of the SVV errors at small tilts, at the expense of larger errors (A-effects) at large tilt angles. We did not include the putative unbalance in the otoliths in our model and conceived the SVV as the vector sum of the estimated gravity vector in head-coordinates and a weighted vector pointing downwards along the body-axis, in line with the fact that gravity usually pulls in this direction (see Figure 3.1B). A similar approach was followed by others (Dyde et al., 2006; Groen et al., 2002; Zupan and Merfeld, 2005; Zupan et al., 2002). The average weight found in this study, w = 0.13, is quite comparable to the value of 0.2 observed by Dyde et al. (2006). Importantly, how the brain solves the ambiguity problem of the otoliths, which later became a topic of keen interest in the field (Angelaki et al., 1999, 2001; Merfeld and Zupan, 2002), is not considered in Mittelstaedt's original model. This scheme, widely used as an explanation for the A-effect in stationary tilt, is basically a static model with no provisions to account for the dynamic changes in the SVV that we found in the course of OVAR stimulation. On the other hand, it appears that canal-otolith interactions, which successfully account for the time course and the magnitude of the dynamic SVV component (see Figure 3.8), do not explain the occurrence of systematic errors in static tilt (Figure 3.1C). Our finding of a tilt-related effect in dynamic conditions supports the basic notion of a head bias as an additional element in the canal-otolith interaction model (Figure 3.1A).

The disambiguation process

As linear accelerometers, the otoliths sense gravito-inertial force (GIF), i.e. the vector sum of gravitational force and inertial force arising from linear acceleration. For reliable spatial orientation the brain must disambiguate the otolith signal into a tilt and a translation component. The canal-otolith interaction model suggests that these components are inversely linked which implies that an increase of one should lead to a decrease of the other (Merfeld et al., 2005a). Such inverse linkage has been demonstrated in monkey and human oculomotor studies (Haslwanter et al., 2000; Paige and Seidman, 1999; Wood, 2002).

Against this background, we wondered whether similar complementary trends can be discerned in the perceptual domain during OVAR stimulation. In a previ-

ous study (Vingerhoets et al., 2006) we quantified the time course of the illusory translation percept during OVAR. Simulations showed that this translation percept was described fairly well by the canal-otolith interaction model in Figure 3.1A. In the present study we found that the dynamic component of the verticality percept during OVAR also conformed with the model's predictions. In addition, in the previous study (Vingerhoets et al., 2006) we observed that the translation percept increased with rotation speed, and the present study showed a parallel trend for tilt underestimation. On this basis, we conclude that, overall, tilt and translation perception during OVAR are mutually coupled, consistent with the idea that canal-otolith interactions play an important role in motion perception during OVAR. That is not to say that there are no discrepancies between the time courses of these two perceptual variables. For example, our previous study (Vingerhoets et al., 2006) showed that the onset of the translation percept could be delayed by as much as 50 s, while the present SVV data never showed any sign of a delay. We cannot provide an explanation for this difference.

Another aspect of the disambiguation process concerns the possible occurrence of phase shifts. In an earlier OVAR study, Denise et al. (1988) reported that their subjects felt being in the nose-up position 0 to 50° before they actually reached this position, which indicates a perceptual phase lead. By contrast, as shown in Figure 3.4, the present canal-otolith interaction model predicts phase lags of about 24° in the large-tilt & low-speed condition, 34° in the large-tilt & high-speed condition and 41° in the small-tilt & high-speed condition. Preliminary results from three subjects in one of our testing conditions (large-tilt & high-speed), yielded no evidence for either a phase lag or lead. However, it would seem premature to dismiss Merfeld's model because it conflicts with Denise et al. (1988) and our preliminary data. Clearly, more work is necessary to establish conclusive evidence concerning the perceptual lags or leads during OVAR stimulation.

Further modeling aspects

We experimentally distinguished two contributions to the subjective visual vertical during OVAR. One contribution stems from a mechanism that generates tilt-dependent systematic errors, the other originates from the process of otolith disambiguation. The scheme in Figure 3.1A incorporates both effects. The model can also simulate the illusory translation percepts during OVAR if extended with a leaky integrator. Taken together, the model captures important aspects of the neural strategies that underlie orientation and motion perception during OVAR.

That being said, it cannot be denied that further improvements of the model would be needed. For example, the model would gain explanatory power if it could account for the simultaneous occurrence of E-effects at small tilt angles and A-

effects at large tilt angles. Also, it is not immediately clear how the model could explain the putative additive canal effects on the SVV during yaw rotation, observed by Pavlou et al. (2003). Nevertheless, in retrospect, the canal-otolith interaction model, first suggested about 15 years ago by Merfeld et al. (1993), has been of great value in understanding the central computations involved in vestibular signal processing. However, it has become clear that its original formulation cannot fully explain motion perception during OVAR. Previously we found that a leaky integrator had to be incorporated to obtain a more accurate explanation of the translation percepts. The present work prompted the addition of a head bias to improve the predictions of verticality percepts. These extensions, although technically sound, nevertheless raise the question of whether an alternative modeling approach could provide a more unified account of these central computations. For example, Bayesian frameworks have been successfully applied recently to explain performance in various perception and action domains (Ernst and Banks, 2002; Knill and Pouget, 2004; Körding and Wolpert, 2004; Niemeier et al., 2003; Stocker and Simoncelli, 2006; Weiss et al., 2002). Bayesian models combine various sources of information to optimize performance in the context of optimal observer theory. A statistically optimal alternative for current canal-otolith interaction models has been proposed by Laurens and Droulez (2007). The basic idea is that the brain makes assumptions about the probability of various body motions and applies Bayesian inference to disambiguate the vestibular signals. An a priori assumption in their model entails that low rotation velocities and small accelerations are most probable in daily life.

A Bayesian alternative for the idiotropic vector concept was formulated by Eggert (1998). In his theory, the SVV computation is based on the otolith signal, which is corrupted by noise, and the *a priori* assumption that the body is usually upright. With certain assumptions about the otolith noise and the prior, Eggert's model yields predictions similar to those of the idiotropic vector model proposed by Mittelstaedt (1983). Whether these interesting developments can be combined into a general framework -allowing a unified explanation of the data observed in this study- remains a topic for further investigations.

Acknowledgements We thank H. Kleijnen, G. van Lingen, S. Martens and G. Windau for technical support. Dr. Dora Angelaki kindly provided illustrations of the canals and otoliths. We also acknowledge three anonymous referees for valuable suggestions for improvement of an earlier version of this manuscript. This work was supported by Radboud University Nijmegen (NICI and FNWI), by the Netherlands Organization for Scientific Research and by the Human Frontier Program.

Chapter 4

Body-tilt and verticality perception during multiple cycles of roll rotation

4.1 Introduction

In the present study we tested spatial orientation in humans during constant velocity roll rotation. We characterize this ability by two types of measures: judgments about visual line orientation in space (SVV) and estimates of body tilt (SBT). We start the Introduction with a brief review of important perceptual tests in the spatial-orientation domain.

Numerous studies have demonstrated that tilted subjects make systematic errors when asked to set a luminous line to the vertical in otherwise complete darkness (for review see Mittelstaedt, 1983). At large tilt angles, subjective visual vertical (SVV) settings in these studies deviated in the direction of body tilt (Aubert or A-effect), whereas tests at small tilt angles (< 30°) revealed almost veridical performance or small errors of opposite sign (Müller or E-effect) (Kaptein and Van Gisbergen, 2004, 2005; Mittelstaedt, 1983; Schöne, 1964; Udo de Haes, 1970; Van Beuzekom and Van Gisbergen, 2000). Recently, Kaptein and Van Gisbergen (2004, 2005) described an abrupt transition from A- to E-effects at large tilt angles. To explore the possibility that a deficiency of the vestibular system causes the A-effects, Mittelstaedt (1983) designed an experiment in which he asked subjects on a tilt table to actively assume a 90° roll tilt position in total darkness, and then, in that actively chosen position, to set a luminous line parallel to gravity.

Adapted from: Vingerhoets RAA, Medendorp WP, Van Gisbergen JAM (2008) *J. Neurophysiol.*, 99: 2264-2280

The results showed that almost all subjects were able to roll themselves very close to the intended 90° position. Yet, amazingly, the subsequently-obtained luminous line settings deviated up to 30° from true vertical. In a similar experiment, Mast and Jarchow (1996) confirmed these findings for the visual horizontal. Recently, Kaptein and Van Gisbergen (2004) further extended the dissociation between the SVV and SBT across the entire 360° tilt range. The general picture emerging from their results is that systematic errors in the SBT were much smaller than in the SVV and lacked the steep discontinuity found in the SVV at large tilts. Furthermore, the SBT responses showed hysteresis effects, depending on which direction of rotation was used to reach the tested tilt angle. The hysteresis was not seen in the SVV. Some studies have linked errors in the SVV to undercompensation for ocular counterroll (Pavlou et al., 2003; Wade and Curthoys, 1997). Such uncorrected eye torsion may be responsible for small overcompensation errors (E-effects) at tilts below 60°, but works in the wrong direction to account for the undercompensation errors (A-effects) that are found at larger tilts.

Compared with the extensive literature on verticality perception during static roll tilt, studies on the SVV and SBT under dynamic conditions are scarce. Several studies have tested roll-tilt perception during sinusoidal roll tilt (Merfeld et al., 2005a,b; Park et al., 2006; Wright and Glasauer, 2006). Others have tested verticality perception during earth-horizontal (Mittelstaedt et al., 1989) and earth-vertical yaw rotation (Pavlou et al., 2003) or at intermediate tilt angles (Vingerhoets et al., 2007; Wood et al., 2007). Keusch et al. (2004) undertook a dynamic roll-tilt study in a limited tilt range using constant-velocity and constant-acceleration rotation and reported that error patterns depend on the rotation profile. All these studies have suggested that signals from the semicircular canals are an important factor in verticality perception. To further test this idea, we now, for the first time, compare measurements on body-tilt perception and visual verticality perception during three cycles of roll rotation at a constant rotation speed of 30°/s. Assuming that the time constant for the units innervating the canals in humans is approximately equal to the 5.7 s time constant found in monkeys (Fernandez and Goldberg, 1971), we estimate that during constant velocity roll-rotation at 30°/s, the canal signal has decayed by more than 80% after one cycle (12 s). However, it should be noted that it is possible that the velocity storage mechanism sustains the roll-velocity percept.

To estimate the potential effect of deteriorating canal signals, we shall now discuss the challenges facing the brain when it has to judge visual orientations in space and briefly consider the putative role of the canals in that process. Determining the orientation of a visual line with respect to the direction of gravity when one is tilted requires integration of retinal information and eye orientation in space. Thus, for ideal performance, the brain must know the orientation of the eyes in the head

and the orientation of the head in space. In the absence of visual cues, information about head orientation in space is mainly supplied by the vestibular system, which has otoliths for the detection of inertial acceleration and tilt and uses semicircular canals to sense rotations. Since the otoliths, as linear accelerometers, sense the sum of inertial and gravitational accelerations (known as gravito-inertial force, GIF), they cannot distinguish tilt and translation without further processing (Angelaki and Dickman, 2000; Fernández and Goldberg, 1976; Loë et al., 1973). Recent studies have argued that the brain uses the canal signal to solve this problem (Angelaki et al., 1999; Glasauer, 1992; Glasauer and Merfeld, 1997; Merfeld, 1995a; Merfeld and Zupan, 2002; Yakusheva et al., 2007; Zupan et al., 2002). Put simply, the brain interprets a change in the otolith signal as a result of tilt if the otolith signal is consistent with rotation signaled by the canals and as due to translation otherwise. Several human studies have shown that the canal-otolith interaction hypothesis provides a fair description of human perception during various motion paradigms such as centrifugation, combined tilt and translation and post-rotational tilt (Merfeld et al., 2005a,b; Merfeld and Zupan, 2002; Merfeld et al., 2001).

Recently, we showed that the canal-otolith interaction model proposed by Merfeld and Zupan (2002) could also explain human translation and tilt percepts during OVAR, once the model was extended by the additional processing stages (leaky integrator and bias mechanism) shown in Figure 4.11A (for detail see Vingerhoets et al., 2006, 2007). The core of this extended model has three output variables coding internal representations (denoted by hat symbols) of the direction of gravity in a head-centric frame ($\hat{\mathbf{g}}$), of head acceleration assigned to translation ($\hat{\mathbf{a}}$) and of angular head rotation velocity ($\hat{\omega}$). During OVAR, involving rotation about a tilted yaw axis, an illusory percept of translation gradually develops after rotation onset. This percept could be simulated by the model, when a leaky integrator was included in the translation pathway (Vingerhoets et al., 2006). Visual verticality percepts during OVAR were also accounted for by the model Vingerhoets et al. (2007), provided that signal ($\hat{\mathbf{g}}$) was combined with an egocentric bias ($\mathbf{b}$), with a weighting factor w, that effectively pulls the SVV toward the long-body axis (Fig 4.1B). As our model (Figure 4.1A) suggests that the egocentric bias works out similarly under static and dynamic conditions, the first objective of the present study is to explore whether errors in the SVV under dynamic conditions are comparable to those under static conditions. Our second aim is to investigate whether the dissociation of SVV and SBT performance, observed under static conditions, can be generalized to roll rotation under dynamic conditions. The working hypothesis to be tested, made explicit in Figure 4.1A, holds that both tasks share the same source signal ($\hat{\mathbf{g}}$) but that they differ in that the bias mechanism is only involved in the SVV task. As several studies have emphasized the importance of the canal signal in verticality perception,

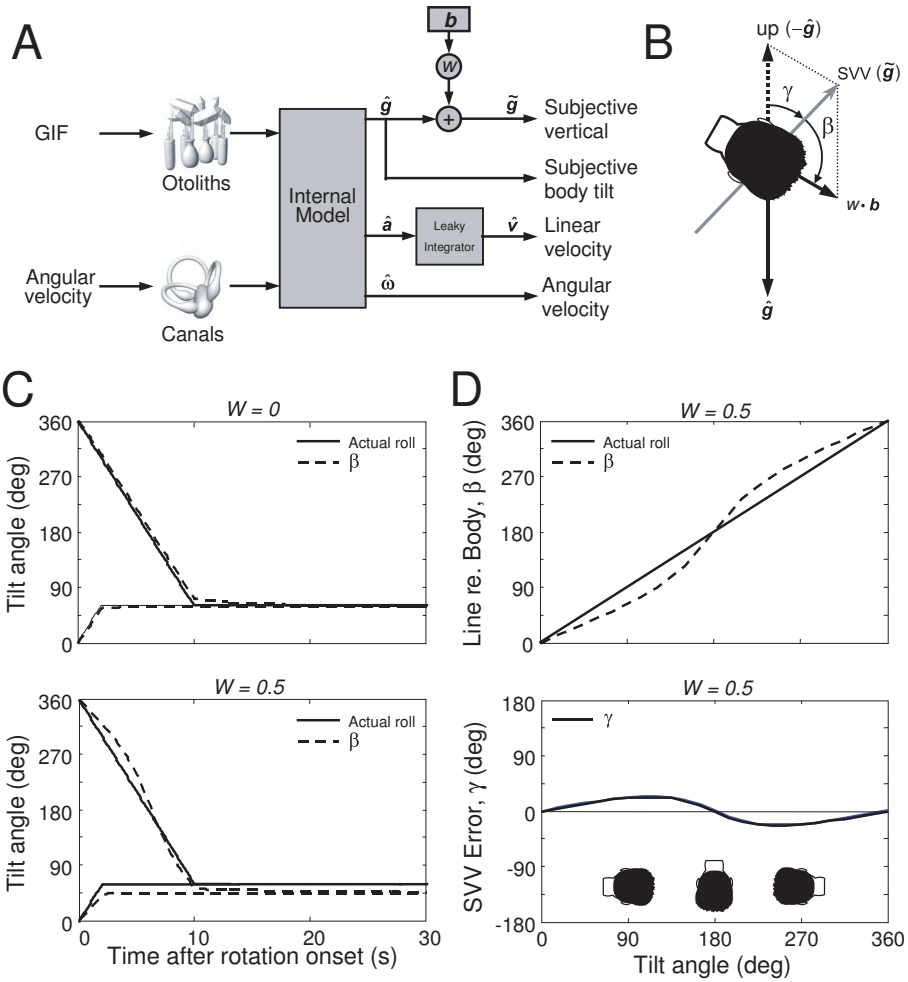
A
b
W
GIF
Otoliths
Internal Model
Subjective vertical
Subjective body tilt
Leaky Integrator
Linear velocity
Angular velocity
Angular velocity
Canals
B
up (−ĝ)
SVV (g̃)
γ
β
w • b
ĝ
C
W = 0
Actual roll
β
Tilt angle (deg)
W = 0.5
Time after rotation onset (s)
D
W = 0.5
Line re. Body, β (deg)
W = 0.5
γ
SVV Error, γ (deg)
Tilt angle (deg)

← **Figure 4.1** *A: Canal-otolith interaction model with egocentric bias mechanism. Otoliths detect gravito-inertial force (GIF), the sum of inertial acceleration and gravitational acceleration, while the canals integrate angular acceleration to angular velocity. Based on canal signals, otolith signals, internal models of the sensors, and inbuilt laws of physics, the model provides estimates of the internal representation of gravity ($\hat{\mathbf{g}}$), the internal representation of linear acceleration ($\hat{\mathbf{a}}$) and the internal representation of angular velocity ($\hat{\boldsymbol{\omega}}$). The internal representation of gravity ($\hat{\mathbf{g}}$) drives the percept of subjective body tilt (SBT) directly. SVV ($\tilde{\mathbf{g}}$) is calculated as a weighted sum of subjective zenith (-$\hat{\mathbf{g}}$) and an egocentric bias ($\mathbf{b}$) that pulls the estimate of verticality toward the long body-axis. B: Internal representation of the upward direction (-$\hat{\mathbf{g}}$) is weighted with an egocentric bias vector ($\mathbf{b}$) to calculate the subjective visual vertical ($\tilde{\mathbf{g}}$) .i.e., $\tilde{\mathbf{g}} = -\hat{\mathbf{g}} + w \cdot \mathbf{b}$. β denotes the angle between the SVV and the long-body axis and γ represents the angular error in the SVV. C: Model predictions for angle β when a subject is rotated at 30°/s to an absolute tilt angle of 60° directly by CW rotation or by a detour CCW rotation. Internal-model parameters: $k_a = -4$, $k_f = 4\ s^{-1}$, $k_{f\omega} = 8\ s^{-1}$ and $k_\omega = 8$. Top panel: without egocentric bias ($w = 0$) β progressively lags behind as rotation continues, but quickly catches up after rotation has stopped. Bottom panel: egocentric bias ($w = 0.5$) introduces an additional systematic error that persists after rotation stop. The bias pulls the estimate toward upright, i.e. to 360° for tilt angles > 180° and to 0° for tilts < 180°. D: Model prediction for a static SVV experiment where a subject is tested across the whole 0-360° tilt range. Top panel: actual roll and angle β. Angle γ is biased toward upright. Bottom panel: Error in SVV. Model predicts A-effects denoted by positive errors in the range 0 to 180° and negative errors for the range 180 to 360°.*

the final goal of the present study is to test how well the brain can maintain the internal representation of gravity ($\hat{\mathbf{g}}$) during prolonged roll rotation in the dark despite the decay of the canal signals. To facilitate the interpretation of the data, we now evaluate the predictions of our canal-otolith interaction model (Figure 4.1A) for verticality perception during both static and dynamic roll tilt experiments.

4.1.1 Model predictions

Veridical performance in the SVV test requires that β, which is the angle between the long-body axis and the SVV (see Figure 4.1B), equals the actual roll-tilt angle (ρ). Due to the decay of the canal signals, the model predicts that the computation of $\hat{\mathbf{g}}$ lags behind, which causes a difference in the SVV depending on whether the tested tilt angle was reached via a clockwise (CW) or counterclockwise (CCW) rotation. Figure 4.1C, upper panel, plots β for a classical stationary experiment where the subject is rotated from upright to 60° roll tilt, using a direct CW rotation, and for a detour CCW rotation to the same final tilt angle, both in the absence of the bias effect ($w = 0$). Note that, in this special case without bias, the SBT predictions (not shown) would be identical. In both simulations, the SVV lags behind the actual roll tilt. This leaves a small difference between CW and CCW rotation directly

after rotation stop which vanishes quickly. Thus, when testing the static SVV is delayed until some 30 s after rotation stopped, a common procedure also adopted in our static experiments, any trace of the lag in $\hat{\mathbf{g}}$ has disappeared. For comparison, the bottom panel of Figure 4.1C shows the simulation for the SVV with an egocentric bias weight of 0.5. Again, the small difference between CW and CCW rotation disappears within a few seconds after rotation stop, but the A-effect introduced by the egocentric bias remains. Figure 4.1D summarizes the predicted outcome of a static SVV experiment for the entire 0 to 360° tilt range. The top panel shows angle β, whereas the bottom panel shows the error in the SVV, denoted γ (defined as in Figure 4.1B). The egocentric bias causes undercompensation for tilt, leading to positive SVV errors for rightward absolute tilt angles and negative errors for leftward absolute tilt angles. So, in summary, these simulations imply that systematic errors in static SVV experiments reflect biasing effects rather than sluggishness of the disambiguation mechanism. Since the bias mechanism does not affect the SBT, the model predicts no systematic errors in the body-tilt percept under static testing conditions.

The model makes interesting predictions about the dynamic spatial orientation percepts during rotation. For a bias weight (w) of 0.5, Figure 4.2A presents simulations of the four output variables during three complete consecutive cycles of CW rotation (i.e., 1080°) at a speed of 30°/s. Note, first of all, that the SVV, reflected in β, shows the superposition of two error components: the cyclical effect of the egocentric bias and a phase delay reflecting the accumulating effect of signal $\hat{\mathbf{g}}$ progressively lagging behind actual roll-tilt. The subjective body tilt (SBT) in the second panel only shows the phase delay. As a direct corollary of these lag-related errors in the SBT, the model further predicts a translation percept ($\hat{v_y}, \hat{v_z}$) that has no basis in the actual pure-rotation stimulus ($v_y = v_z = 0$). A final prediction is that the percept of roll rotation ($\hat{\omega_z}$) decays slowly from an initial value close to veridical (30°/s) down to a steady state value of about 20°/s. Panel B, which shows the perceived head trajectory predicted by the model, will be discussed later (see Discussion).

In this study we leave the predicted translation and angular velocity percepts aside and concentrate on testing the model's SBT and SVV predictions. How the combination of the phase lag in $\hat{\mathbf{g}}$ and the bias mechanism ($w = 0.5$) affects the dynamic SVV can be seen in Figure 4.2C where the dashed lines show β simulations during CW and CCW rotation. Comparison with the actual tilt angle (solid line) reveals cyclical deviations in the form of a waxing and waning A-effect, caused by the head bias, in all three cycles of rotation. Close inspection of Figure 4.2C discloses a gradually increasing phase delay in β, leveling off at about 15°, which adds an additional source of errors in the SVV. Figure 4.2D demonstrates how these

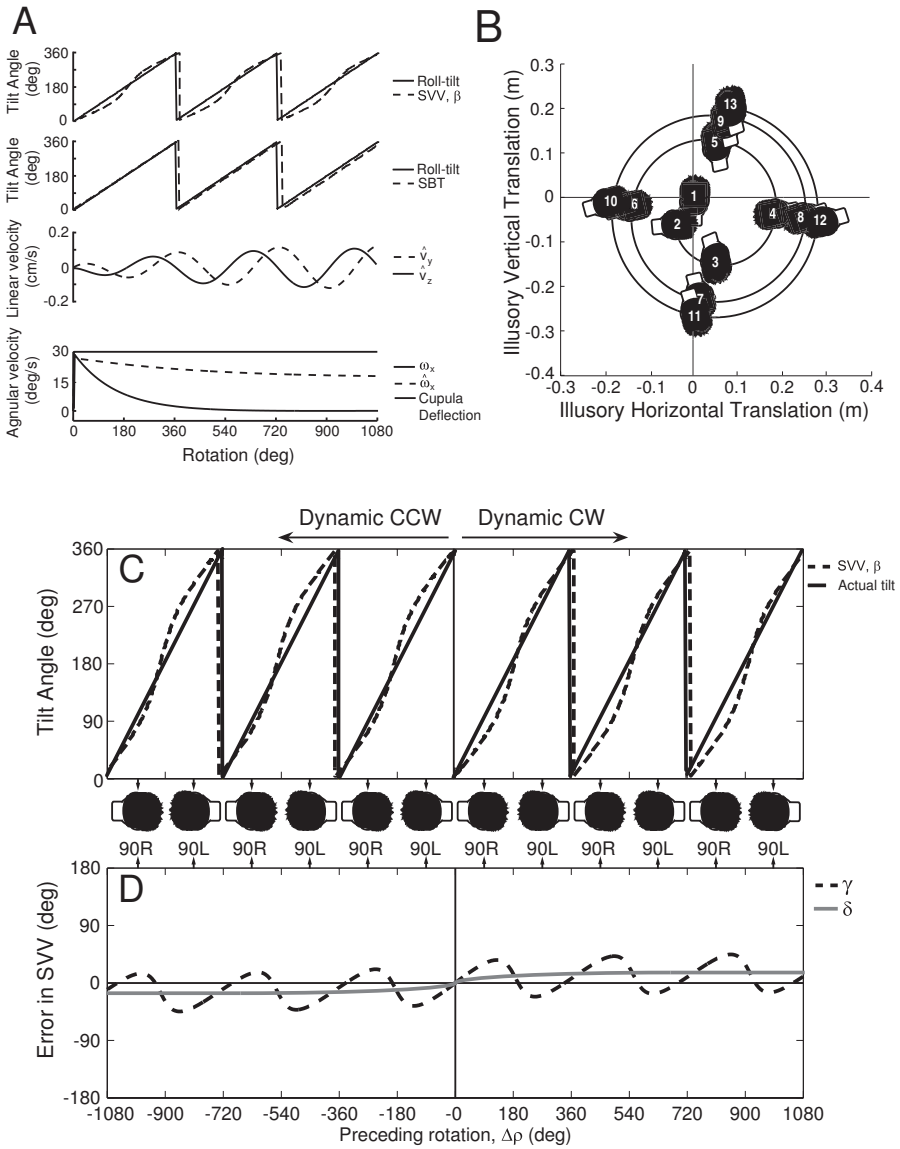
A
Tilt Angle (deg)
360
180
0
Roll-tilt
SVV, β
Tilt Angle (deg)
360
180
0
Roll-tilt
SBT
Linear velocity (cm/s)
0.2
0
-0.2
Agnular velocity (deg/s)
30
15
0
Cupula Deflection
0 180 360 540 720 900 1080
Rotation (deg)
B
Illusory Vertical Translation (m)
0.3 0.2 0.1 0 -0.1 -0.2 -0.3 -0.4
-0.3 -0.2 -0.1 0 0.1 0.2 0.3 0.4
Illusory Horizontal Translation (m)
13
9
5
10
6
1
2
4
8
12
3
7
11
Dynamic CCW
Dynamic CW
C
Tilt Angle (deg)
360
270
180
90
0
SVV, β
Actual tilt
90R 90L 90R 90L 90R 90L 90R 90L 90R 90L 90R 90L
D
Error in SVV (deg)
180
90
0
-90
-180
γ
δ
-1080 -900 -720 -540 -360 -180 -0 180 360 540 720 900 1080
Preceding rotation, Δρ (deg)

← **Figure 4.2** *Model predictions for three cycles of constant velocity roll-rotation. A: Top graph: systematic errors in β caused by the combined effects of the egocentric bias mechanism and the phase lag. Second graph: errors in the percept of body tilt (SBT) due to the phase lag. Third graph: as a result of the phase lag, the model predicts an illusory translation percept in the horizontal plane ($\hat{v}_y$) and in the vertical plane ($\hat{v}_z$). Bottom graph: Actual angular velocity is 30°/s in roll (ω_x). Cupula deflection decays completely. By contrast, due to internal feedback loops in the internal model, the sense of roll-rotation ($\hat{\omega}_x$) decays more slowly and settles at a steady-state value of about 20°/s. B: Schematic summary of predicted self-motion percept during constant velocity roll rotation. Perceived head orientation is shown every 3 s. Model predicts a feeling of spiraling outward into an orbit while simultaneously rotating about the roll-axis. Perceived head orientation is not upright after three complete cycles of rotation (head 13), due to the phase delay. C: SVV model predictions for three complete cycles of roll rotation. Angle β lags behind actual roll tilt and is biased toward upright due to the egocentric bias. D: Error in SVV (γ) consists of two contributions. Egocentric bias causes a periodical error pattern in the SVV. Phase delay causes a positive offset for CW rotation and a negative offset for CCW rotation. Error in SBT (δ) is not influenced by the bias mechanism and only reflects errors due to the phase delay.*

effects work out in the SVV error (γ). The bias mechanism induces a periodical error, superimposed on an exponentially rising offset due to the gradually increasing phase lag. As shown, the phase lag leads to a negative and a positive offset for CCW and CW rotations, respectively. For comparison, the solid line in this panel shows the predicted errors in the dynamic SBT (δ), which reflect the phase lag.

To test if verticality perception during continuous roll-rotation can be described by the extended canal-otolith interaction model (Figure 4.1A), we measured the SBT and SVV in subjects during three consecutive cycles of roll rotation at 30°/s. We examined if the predicted A-effects in dynamic conditions would actually occur and whether their magnitude would reflect the same egocentric bias as in static control experiments. In addition, we tested whether the dissociation between the SBT and SVV generalizes to dynamic roll-tilts. Finally, we explored whether our results support the model prediction that otolith disambiguation becomes imperfect, in the form of a phase lag, when canal signals are dissipating. Our results show enlarged A-effects under dynamic conditions, suggesting enhanced egocentric-bias effects. We found no gradual deterioration of SVV performance with time, suggesting that otolith-disambiguation errors were small despite the gradual decay of canal signals. The dynamic SBT, which showed no clear evidence of the predicted accumulating phase lag either, lacked the large systematic errors observed in the SVV task, indicating a clear dissociation of performance in the two tasks.

4.2 Methods

4.2.1 Subjects

Six subjects (four male, two female) aged between 21 and 63 years (mean ± SD: 31 ± 16 years) gave written informed consent to participate in this study. All subjects were free of any known neurological, vestibular or ocular disorders. All participants except JG were naive with respect to the purpose of the experiments. Before the actual experiment began, subjects were carefully instructed about the task and got a few practice runs. They never received feedback about their performance.

4.2.2 Experimental setup

The subject was seated in a computer-controlled vestibular chair that was configured for rotation about the roll axis. The head, positioned at the rotation center, was restrained in a natural upright position using a padded helmet. The torso was secured with seat belts and adjustable shoulder and hip supports. To ensure a broad distribution of tilt-induced forces over the entire torso, subjects wore a padded breast-shoulder-plate under the seat-belt straps. The legs and feet were fixated with Velcro straps and a foot rest. Subjects did not wear earplugs and auditory cues were not masked.

In all experiments, roll rotation started from the upright position and alternated regularly between CW and CCW. The chair rotated with a constant velocity of 30°/s, using peak accelerations and decelerations of 50°/s^2 during the start and stop phase. During rotation, the SVV was tested using a uniformly illuminated line (angular subtense: 20°) that was mounted on the vestibular chair at approximately 90 cm in front of the subject. The line, polarized by a bright dot at one end, was controlled by computer with an angular resolution of 0.5°. Its rotation axis coincided with the cyclopean eye of the subject and the rotation axis of the vestibular chair, so that the line rotated in the fronto-parallel plane.

4.2.3 Paradigms

The subjective visual vertical (SVV) was tested under both static and dynamic tilt conditions in two separate series of experiments. SVV testing in all experiments relied on verbal scaling of flashed-line orientations in space as used before (Kaptein and Van Gisbergen, 2005; Van Beuzekom et al., 2001). This verbal scaling method was adopted because the method of adjustment was too slow for dynamic conditions. Also, an adaptive staircase method in which the orientation of the luminous line is adjusted in small steps, in consecutive runs, in the direction indicated by the subject (Vingerhoets et al., 2007), did not suffice because of the bistable percepts

that occurred under dynamic conditions (see Results). From five subjects we also collected subjective body tilt (SBT) estimates under the same dynamic conditions, for comparison with the SVV data. All experiments took place in complete darkness. Vision was always binocular and subjects were allowed to move their eyes freely.

Static SVV paradigm

In the static experiment, subjects were rotated CW or CCW about their roll axis to a final tilt angle between 0 and 360°, which was chosen randomly at 15°intervals. Once the final tilt position was reached, there was a 30 s waiting period before testing began to allow dissipation of rotational signals.

The verbal-scaling procedure was implemented as follows. After the waiting period, the polarized line was flashed briefly for 2 ms at 2 s intervals. The subject estimated the orientation of ten sequentially flashed lines in Earth-centric coordinates, using a clock scale. For example, when the subject judged the line as earth-horizontal, with the dot on the right, the response was "15 minutes past (the hour)". Generally, responses were made with an attempted precision of 0.5 - 1 min. To present visual line orientations across the whole 0-360° range for each tilt angle, we divided this range into ten equal segments and drew a random line orientation from each segment without replacement. Presenting the chosen line orientations in random order forced subjects to make independent judgments and prevented repeating previous responses. The verbal responses were written down and recorded digitally to allow checking afterwards. Occasional failures to respond caused a total of about 2% of missing data.

After 10 verbal responses, the subject was rotated back to the upright position to remain there for 30 s with the room lights on until the next trial began. It took two sessions of about 45 minutes to collect the data from all 49 static CW and CCW tilt angles along the 360° tilt range.

Dynamic SVV paradigm

The dynamic experiment tested the subjective visual vertical during constant velocity roll rotation. Starting from upright, the subject was rotated 1140° CW or CCW, i.e., 3 consecutive cycles (1080°) and an additional 60° to leave the subject at least 2 s to respond in each experimental run, so that data for 1080° tilt could be collected. At regular intervals during the 38 s run, the subject had to estimate line orientations using a clock scale (see Static SVV paradigm). As in the static experiment, the line orientations for a given tilt angle were presented randomly but equally spaced around the clock. The SVV was tested at 15° intervals along the

entire 0 - 1080° tilt range. In different runs, the first flashed line was presented at either 0, 15, 30 or 45° tilt and subsequently every 60°, to ensure that ultimately all 15°intervals were covered, while still leaving the subject 2 s to respond before the next stimulus appeared. The subject was instructed to estimate the angle of the flashed line in earth coordinates at the time when it was presented. After the run was completed, the subject was rotated back to upright and was given 30 s for re-orientation, with the room lights on. In most subjects it took 5 sessions of about 45 minutes to collect the data of the dynamic SVV paradigm.

To illustrate that the verbal scaling method provides consistent and reliable data in both static and dynamic experiments, Figures 4.3A,B present the verbal estimates of the line's orientation in space as a function of its actual spatial orientation for one tilt angle (240°). Accordingly, the dashed line with unity slope represents ideal performance. Considerable A-effects, expressed as positive y-intercepts of the regression line, occurred both statically and dynamically. All data points scatter along the regression line with a slope very close to one, which means that the A-effect does not depend on the orientation of the probe line relative to earth-coordinates or relative to the subject. This indicates that visual space for a tilted subject is rotated but not distorted. The analysis corroborates previous findings by Van Beuzekom et al. (2001) under static conditions and demonstrates that this conclusion generalizes to dynamic conditions. To allow a lumped analysis across all tilt angles, we subtracted the average A-effect from the data points for each tested tilt angle and then pooled all data as shown in panel C and D for this subject. Again, these panels indicate no systematic distortion in the verbal reports depending on the orientation of the probe line relative to subject or earth. Finally, the fit lines from all subjects, shown in panel E and F, demonstrate that this description holds for all subjects, both statically and dynamically.

Dynamic SBT paradigm

In this paradigm we tested perceived body tilt during three consecutive cycles of roll rotation. As in the dynamic SVV paradigm, rotation started from upright and alternated between 1140° CW and 1140° CCW. No luminous line was presented in this paradigm. Instead, a small LED, which was located straight ahead of the subject, on the rotation axis, first flashed randomly between 0 and 3 s after rotation start and subsequently randomly after each 3-5 s. The flashes prompted the subject to report perceived body tilt at the time of the flash, using a clock scale, as if the body were the minute hand (Van Beuzekom and Van Gisbergen, 2000). Subjects were not informed about the rotation speed to prevent that they used timing as a cue for their orientation. The verbal responses were written down by the experimenter and recorded digitally to allow checking afterwards. Five of the subjects

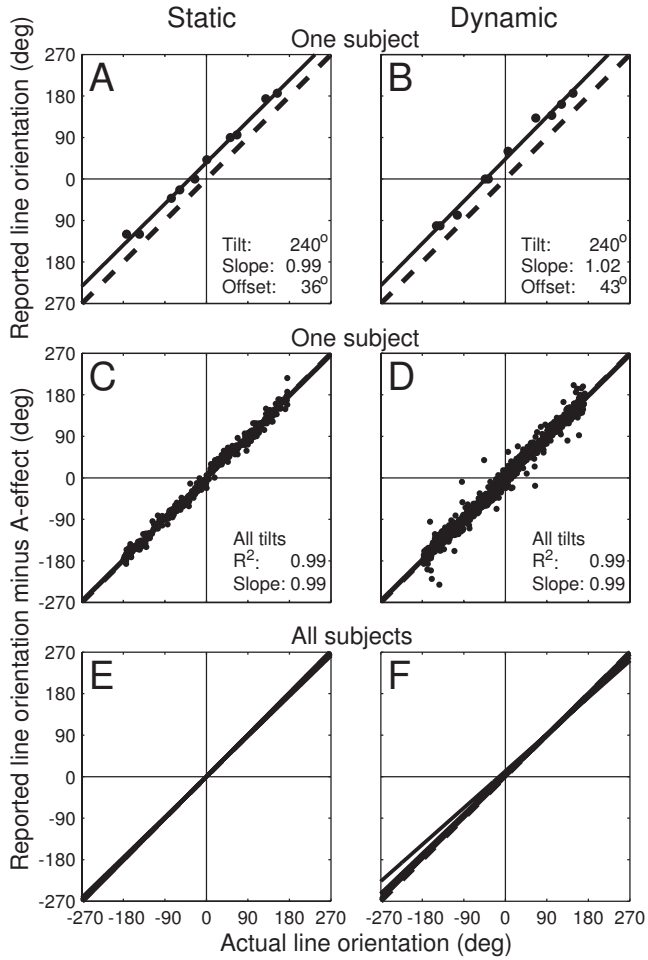

Figure 4.3 *Visual line orientation judgments, obtained using verbal scaling, as function of actual line orientation in world. A,B: Verbal reports for 240° roll tilt C,D: Verbal reports minus average error pooled across all tilt angles for A-cluster. Based on 364 data points for static and 1161 for dynamic. E,F: Fit lines from all subjects for pooled verbal reports.*

that participated in the SVV task also took part in this paradigm. It took 4 to 5 sessions of about 45 minutes to collect all data from each subject.

4.2.4 Data analysis

Definition of angles

In the Results section, responses have been plotted against the total amount of preceding rotation ($\Delta\rho$) which ranges from -1080 to 1080° in the dynamic experiment and from -360 to 360° in the static experiment. CW rotations (seen from behind the subject) ran from 0 to 1080° whereas CCW rotations started at 0 and ended at -1080°. In addition to this notation, we also use "absolute tilt" to denote the deviation from upright on a 0-180 ° scale. All figures showing tilt-dependent responses have been doubly-labeled with both $\Delta\rho$ and absolute tilt scales, where 90R and 90L indicate 90° right-ear down and 90° left-ear down, respectively. We use ρ to denote angular head position on a scale from 0 to 360°. For example, the head position shown in Figure 4.4A (ρ = 120°), could have been reached by $\Delta\rho$ = -960, -600, -240, 120, 480 or 840°.

Response error (γ) in the flashed-line experiments, a measure for the angular error in the visual verticality percept, was defined as the difference between the actual orientation of the line in space and the corresponding verbal estimate (Figure 4.4A). Errors in CW direction, seen from behind the subject, were taken positive. Accordingly, A-effects yield positive and negative γ values for rightward and leftward absolute tilt, respectively. To convey other aspects of subject performance, it is more appropriate to use parameter β, defined as the angle between the SVV and the subject's long-body axis (Figure 4.1B). Response parameters β and γ are linked by $\beta = \rho - \gamma$. Perfect task execution requires $\beta = \rho$.

Response errors in the SBT task, indicated by δ, were defined as the angular difference between actual and reported body-tilt (see Fig 4.4B). Errors in clockwise direction, seen from behind the subject, were taken positive for easy comparison of SVV and SBT errors. If errors in the SVV were simply caused by errors in the SBT, the two error profiles would be similar.

Cluster analysis

As the Results section will show, we observed two distinct SVV response clusters at large tilt angles that we denote as A- and E-cluster, in accordance with Kaptein and Van Gisbergen (2005). To partition the data points into two clusters, we used an algorithm that searches for two cluster centroids which minimize the sum of point-to-cluster-centroid distances, as implemented in the function "kmeans" (Matlab 7.0 Statistics Toolbox, The Mathworks). To increase the robustness of the cluster analysis we temporarily reduced the complete data set which actually consists of multiple clusters to only two clusters by pooling data from different cycles as well as from different rotation directions (CW and CCW) and then collapsing them

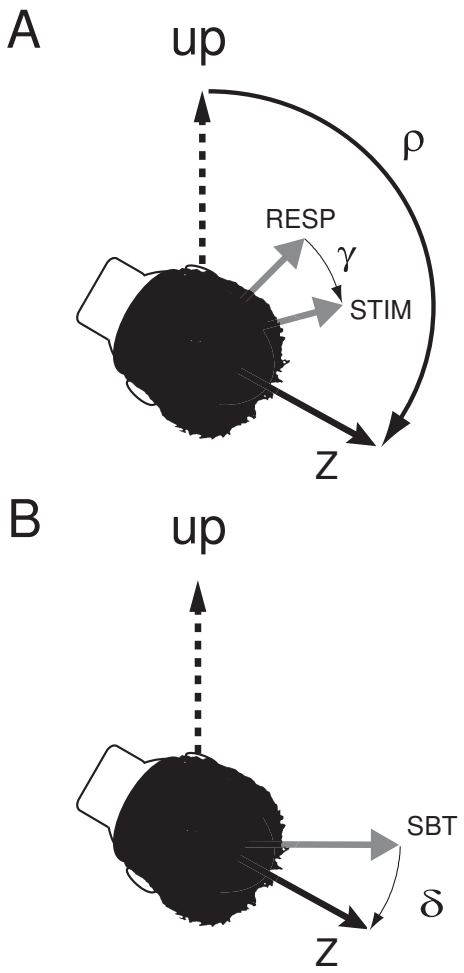

Figure 4.4 *Definition of angles with subject in rear view. Tilt position (ρ) is 120° in both panels. A: Error in SVV (γ in deg) is defined as actual line orientation (STIM) minus estimated line orientation (RESP). B: Response error in the subjective body tilt paradigm (δ) is defined as actual (Z) minus reported tilt angle (SBT). The example shows tilt underestimation.*

onto the 0 to 180° range. Note that this was only an intermediate step in which each data point was labeled and then returned to its original position. In subject SB, we were able to separate the clusters under static conditions using the kmeans routine but the responses in the dynamic experiment could not be separated in this manner. In this case, we defined all data points closer to the diagonal $y = x$ as the A-cluster (open circles in Figures 4.5-4.7) and data points closer to $y = x - 180$ as the E-cluster (filled circles in Figures 4.5-4.7). These A and E-clusters in Figures 4.5-4.7 will be discussed in more detail in the Results section.

4.2.5 Model simulations

Model simulations were run to find the bias weights (w_E for E-cluster, w_A for A-cluster) that provided the best fits to the data. For this purpose, we used Matlab 7.0 and Simulink 6.0 (The Mathworks) to simulate the canal-otolith interaction model outlined in Figure 4.1A. This scheme was used previously in Vingerhoets et al. (2007) to describe verticality perception during off-vertical axis rotation (OVAR). The core of the scheme, the internal model, was originally proposed by Merfeld and Zupan (2002). Simulations were performed using the same internal model parameters $k_a = -4\ s^{-1}$, $k_f = 4\ s^{-1}$, $k_{f\omega} = 8$ and $k_\omega = 8$ that were found to be optimal in Vingerhoets et al. (2007).

In the simulations, angle β was calculated as $\beta = \text{atan}(\tilde{g}_y/\tilde{g}_z)$, where $\tilde{\mathbf{g}}$ denotes the vector sum of the subjective zenith ($-\hat{\mathbf{g}}$) and the weighted bias vector (i.e., $\tilde{\mathbf{g}} = -\hat{\mathbf{g}} + w \cdot \mathbf{b}$, see Figure 4.1B). The predicted error in the SVV was calculated as $\gamma = \rho - \beta$. The predicted error in the SBT (δ) was obtained using $w = 0$ in the same equations.

4.3 Results

We first measured the accuracy of the subjective visual vertical (SVV) at static tilt angles separated by 15° intervals along the entire 0-360° range. These data served as a baseline for comparison with the dynamic SVV at the same tilt angles in each of three consecutive cycles of roll rotation. We also collected subjective body tilt (SBT) estimates under the same dynamic conditions, to explore if errors in visual verticality perception can be attributed to errors in tilt perception.

4.3.1 Overview of main findings

Response measures

To introduce our results, Figure 4.5 plots both compensation angle β and response error γ during static and dynamic tilt in subject SV. Although our verbal scaling method is less precise than classical adjustment methods, we obtained firm results with a clearly delineated pattern of responses. In the case of flawless performance, all data in panels A and B would fall along the solid lines. The static experiment (Figure 4.5A) shows systematic errors in the ranges 90 - 135° and 225 - 270°, which have been highlighted in a γ plot (Figure 4.5C). The present pattern of systematic errors shows striking similarities with findings in Kaptein and Van Gisbergen (2004, 2005). To begin with, at small tilt angles (≤ 30°), performance is nearly flawless, on average, but for large tilt angles A-effects up to 45° may be noticed.

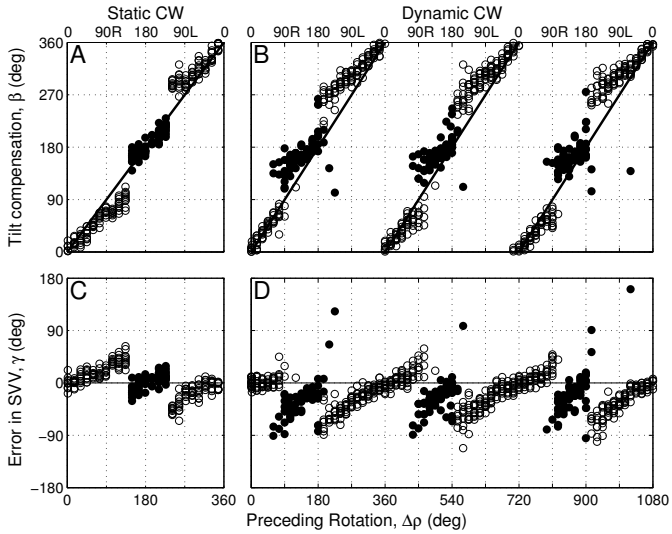

Figure 4.5 *Static and dynamic SVV results from subject SV. Data from CW rotation. Different symbols show the result of the cluster analysis. A: Angle β (Figure 4.1B) in static experiment. Ideal behavior requires β = ρ (solid line). A-cluster (open circles) responses are biased toward upright (0 and 360°); E-cluster (filled circles) responses are biased toward 180°. B Angle β in dynamic experiment. Initially β = ρ, later there are A-effects and E-effects. C: SVV errors in static experiment. Near the inverted position (150 - 225°) E-effects occur. The remaining tilt range shows A-effects. D: SVV errors dynamic experiment. In the first 90°errors are rather small. Subsequently, errors show a repeating pattern of A- and E-effects in successive cycles.*

Upon entering the tilt region near upside down (135 - 225°), the A-effect does not show the smooth decay back to zero reported in classical descriptions (Schöne, 1964; Udo de Haes, 1970). Instead, we see an abrupt transition from A-effects to E-effects as reported by Kaptein and Van Gisbergen (2004, 2005). These large-tilt responses were denoted E-effects because they deviate away from the median head-body plane, just as in the E-effects sometimes seen at small tilt angles. In the dynamic experiment (Figure 4.5B, D) results are qualitatively similar. Note that β (panel B) follows a repeating pattern in the three sequential cycles, returning close to actual tilt around upright ($\Delta\rho$ = 0°, 360°, 720°, 1080°) and developing systematic errors in the form of A and E-effects at large tilt angles. Panel D shows how this tilt-dependent deviation from ideal performance ($\beta \neq \rho$) causes a periodic error pattern with zero crossings near upright. In the following sections we describe and analyze the data from all subjects.

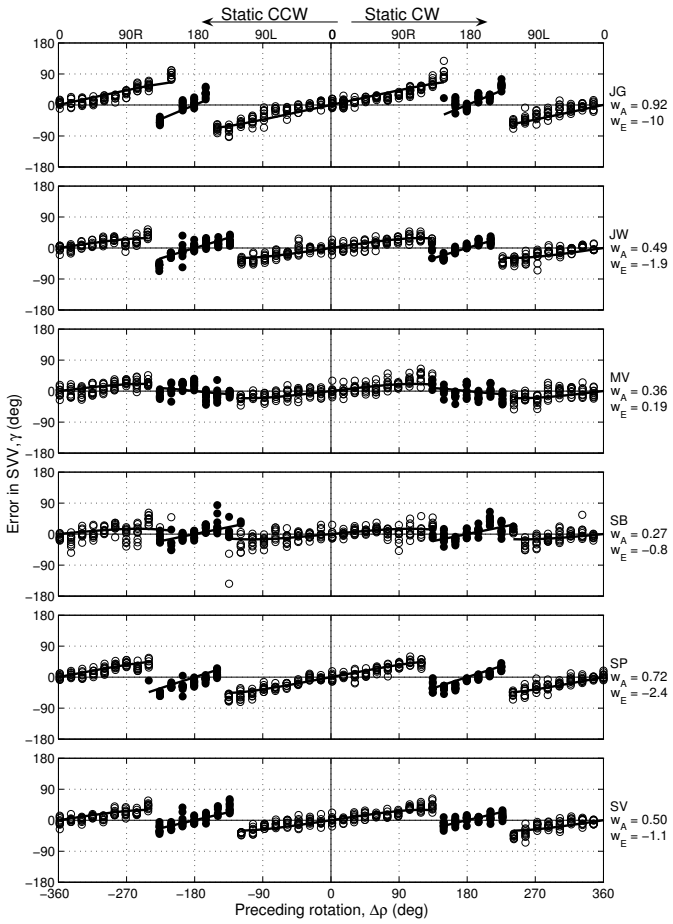

Figure 4.6 *Static SVV error profiles from all subjects. In this and following figures the horizontal axis is doubly labeled. The bottom scale denotes the amount of rotation imposed on the subject. The labeling on top denotes absolute tilt angle, the deviation from upright. CW responses should be read from the center to the right; CCW responses from the center to the left. Open circles, which extend up to about 150° absolute tilt, show a gradually increasing A-effect that can be fitted quite well with a positive weight of the egocentric bias in the model. Filled circles at the near inverted positions show a clear E-effect, which can be described by a negative weight of the egocentric bias. Note that in static conditions 270° CW is essentially the same vestibular stimulus as -90° CCW, with similar responses. Solid lines: model fits.*

Static SVV

Our complete static data set (Figure 4.6) shows a similar pattern of A- and E-effects in different tilt ranges, for both CW and CCW rotation, in all subjects. The fit line

through the data will be discussed later (see section "Calculating bias weigths"). All subjects demonstrated A-effects that increased steadily for tilt angles up to about 135°. Beyond this range, five out of six subjects showed an abrupt transition from A-effects to E-effects with again a sudden return to A-effects around 225°. This A-E dichotomy was less clear in subject MV. The strong impression of two distinct response modes was confirmed by cluster analysis (kmeans, see Methods), which yielded clearly delineated A-effect (open circles) and E-effect (filled circles) clusters in all subjects. This analysis established that the A-response mode prevailed for tilt angles up to about 135° and that the E-effect mode was dominant for tilt angles near upside down. Note the sharp demarcation between A and E cluster in most subjects, with no clear sign of bimodal responses. The latter finding may be related to the fact that all data points at a given tilt angle were obtained in a single trial. Kaptein and Van Gisbergen (2005) found that subjects seldom switch response mode within one trial.

Qualitatively, CW and CCW error patterns look quite similar. Indeed, a repeated-measures two-way analysis of variance on the A-cluster data showed no significant main effect of the preceding rotation direction ($F(1,5) = 0.58$, $P = 0.48$) and no significant interaction between tilt angle and rotation direction ($F(16,80) = 0.003$, $P = 1$).

Dynamic SVV

To allow a direct side-by-side comparison of static and dynamic results, Figure 4.7 presents CW data from the static experiment and from the first cycle of the corresponding dynamic experiment. The response patterns, both showing a steadily increasing A-effect with tilt angle, and an E-effect in the near upside down region, look qualitatively similar. However, closer inspection reveals clear quantitative differences. First, several subjects show larger A-effects in the dynamic experiment. This difference is very marked in subject SB, who shows only limited errors in the static condition but makes errors up to 180° in the dynamic paradigm. The smooth increase of dynamic errors with tilt angle in SB and JG suggests that the responses at 180° are not simply line-polarity misjudgments. Instead, these large errors indicate that these subjects, when in the A-response mode, misperceived lines directed toward the floor of the lab as pointing upward. In qualitative terms, this effect can be explained as follows. Under dynamic conditions, the bias in these subjects becomes so strong that their evaluation of the line is almost equivalent to performing the task in body coordinates, with hardly any effect of the degree of body tilt. As long as body tilt is small or modest, the direction of gravity is still almost aligned with the body axis so that the body-associated bias is not so obvious. However, this leads to errors of 180° in the extreme case that the two references (gravity, body)

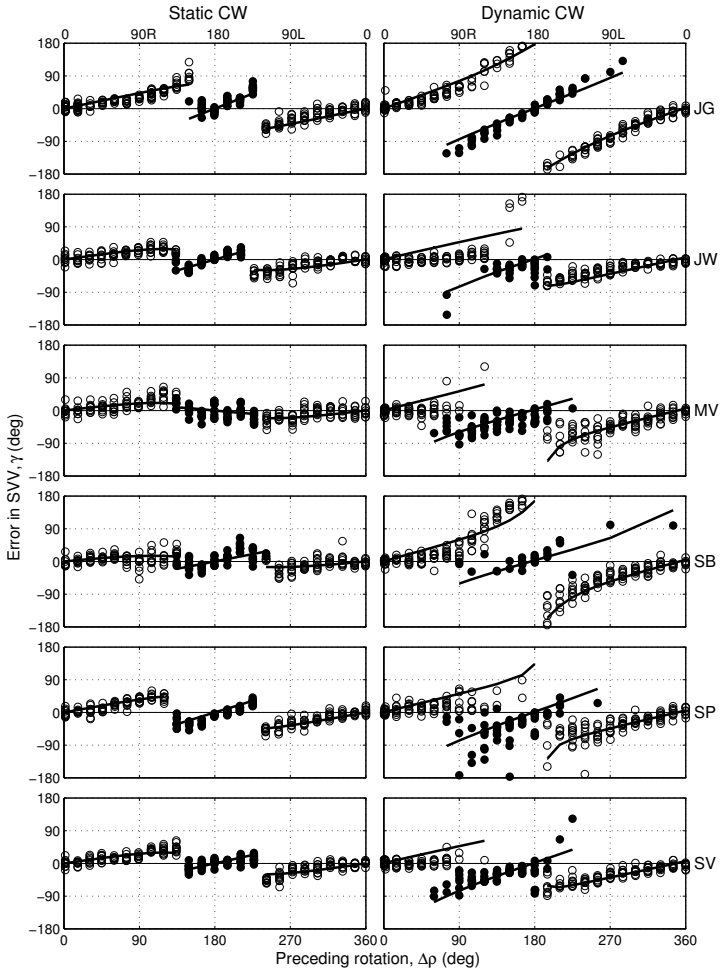

Figure 4.7 *Comparison of static and dynamic results. Left column: Errors in static subjects, tested after CW rotation. Right column: Errors in the first dynamic CW cycle. In both paradigms there is a clear A-effect that dominates in the range of absolute tilt angles up to about 135°. Errors in the A-cluster are generally larger in the dynamic paradigm. At large absolute tilts, a response of the E-type emerges. In the dynamic paradigm the tilt range of E-type responses is larger and shifted to the left. Static responses are mostly unimodal at a given tilt angle; dynamic responses at near inverted tilt are often bimodal (A and E). Solid lines: model fits.*

are in opposition. A further noticeable difference is that there is less inter-subject variability in the static paradigm. For example, subjects JG and SV show similar

error profiles in the static paradigm, but quite different patterns in the dynamic paradigm. Another clear difference between the static and dynamic results concerns the E-cluster. In the static paradigm, the E-cluster is approximately symmetric around 180°, between 120 and 240°, but in the dynamic paradigm it has shifted to smaller tilt angles, between 90 and 195° in most subjects. A similar asymmetry in the tilt range with E-responses can be seen in CCW responses (see Figure 4.8). A final outstanding difference highlighted by Figure 4.8 is that the relatively sharp boundaries between A- and E-clusters in static results disappear under dynamic conditions. In the dynamic paradigm, the A and E-clusters occupy overlapping tilt ranges so that the response distribution becomes bimodal. That two responses modes may coexist at certain large tilt angles has been reported earlier by Kaptein and Van Gisbergen (2005). We cannot exclude that this difference has its origin in the testing method. Subjects were statically tested 10 times within a single run, but dynamic data at a given tilt angle were collected in separate runs.

What is the effect of prolonged rotation on the SVV in later cycles? Recall that the canal-otolith interaction model (Figure 4.1A) cannot fully sustain the tilt signal, due to the decay of canal signals (see Figure 4.2C), causing the predicted dynamic SVV to be different in the first, second and third rotation cycle (Figure 4.2D). The actual data from all three cycles for both CW and CCW rotations, shown in Figure 4.8, rather indicate a roughly repeating pattern of A and E-clusters for all subjects, without clear signs of a phase shift. For a quantitative analysis of the phase-lag issue see section "Analysis of phase shifts". The A-clusters are centered around the upright positions, while E-cluster responses dominate around the inverted tilt positions. However, note that the E-cluster is shifted to smaller tilt angles, as we already observed in Figure 4.7.

Close scrutiny of the initial part of the first cycle, up to 90°, reveals smaller errors than in the corresponding tilt ranges in subsequent cycles, but the responses during the second and third cycle are virtually identical. We tested this onset effect by pooling CW and CCW data and comparing responses from the tilt range 0 - 90R in the first, second and third cycle in a two-way ANOVA with tilt angle and cycle as factors. We found no significant interaction ($F(12, 105) = 0.99$; $P = 0.46$) but a significant main effect of both tilt angle ($F(6, 105) = 35.15$; $P < 0.01$) and cycle ($F(2, 105) = 4.88$; $P < 0.01$). Tukey's post-hoc test revealed that these errors in the second and third cycle of rotation were not significantly different but both were significantly larger than those in the same range of the first cycle of rotation, confirming the existence of a clear onset effect.

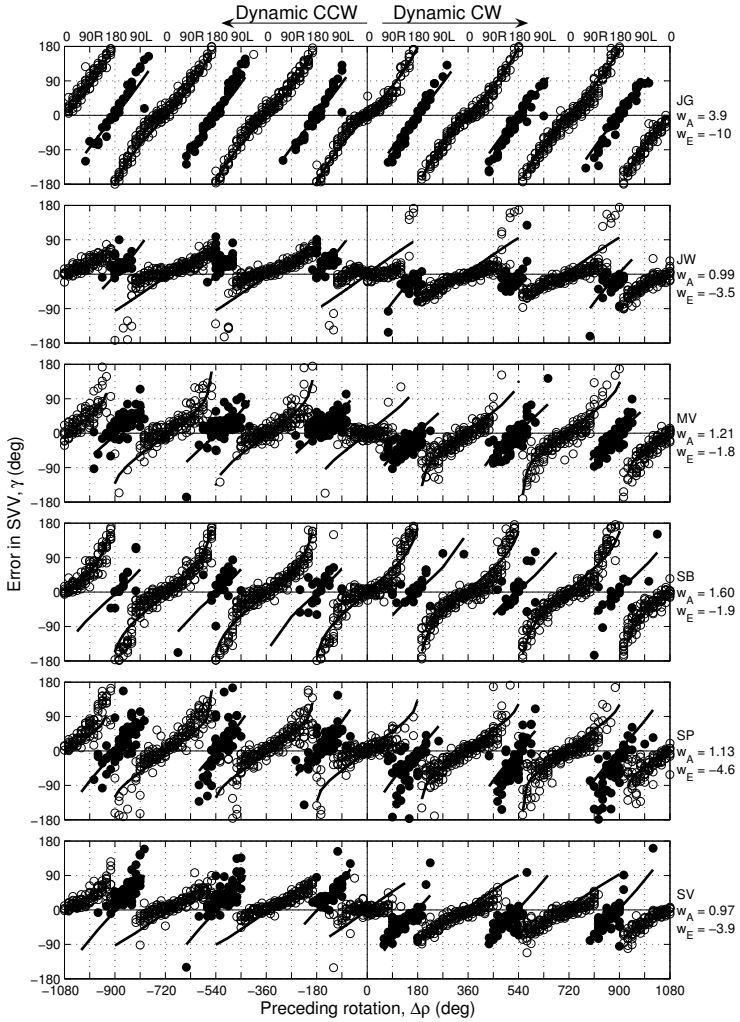

Figure 4.8 *Error profiles of the dynamic SVV in all subjects. Although errors just after rotation onset appear smaller than in later cycles, there is a repeating response pattern across sequential cycles. Solid lines: model fits to dynamic A-clusters have bias weights that are larger than in static conditions (compare with Figure 4.5). Fitting E-clusters requires negative bias weights. Note that E-clusters in CW and CCW are shifted in opposite directions, indicating a clear phase shift.*

Dynamic SBT

In a final experiment, we tested subjects in the subjective body tilt (SBT) paradigm, where they verbally reported their current body tilt estimate on a clock scale, when

prompted by a LED flash (see Methods). Figure 4.9 plots the difference (δ, see Figure 4.4B) between the absolute tilt angle and the estimated tilt angle for all five tested subjects. Mean errors are much smaller than in the dynamic SVV paradigm, showing no convincing overall resemblance with the tilt-related pattern of errors in the SVV task (Figure 4.8). To investigate this further, we calculated correlations between SVV errors, separately for the A and E-cluster, and the SBT data. The correlation was only significant in subject SP, indicating a clear dissociation of performance in the two spatial orientation tasks at the population level.

Most subjects tend to show tilt overestimation in the first 90° after rotation onset (positive errors for CCW and negative errors for CW). This impression was confirmed by a two-way ANOVA with tilt angle and cycle as factors, which revealed a significant main effect of rotation cycle ($F(2, 105) = 14.06$; $P < 0.01$). Tukey's post-hoc test showed that SBT errors in the selected tilt range (0 to 90R) in the second and third cycle of rotation were not significantly different but were different from those in the same range in the first cycle of rotation, by showing underestimation. In this sense, the onset effect observed in the SVV data has a parallel in the SBT data. From the perspective of the model, the fact that an onset effect showed up in both the dynamic SVV and SBT data may indicate that it is already present in signal $\hat{\mathbf{g}}$, but its origin remains unclear. One could speculate that it was caused by activation of the vertical semicircular canals (Jaggi-Schwarz and Hess, 2003; Jaggi-Schwarz et al., 2003; Keusch et al., 2004; Pavlou et al., 2003) or that a computational delay, which is not in the model, is involved (see Discussion, section "Disambiguation process").

In some subjects (e.g., SP), the error pattern in the SBT looks periodic. To analyze this in more detail, we averaged the data in bins of 15° and pooled across subjects. This yielded a pattern that was roughly similar for CW and CCW rotation as shown in Figure 4.10. For both rotation directions, the error in SBT starts at a negative value, which indicates overestimation of tilt and corresponds to the onset effect described above. Subsequently the error reverses sign and increases, but resets at 360° tilt. Then the error increases again in the next cycle and returns to zero at 720° tilt. Also the third cycle shows this characteristic, suggesting that subjects develop a slight phase lag during each cycle, that resets at upright. This is reminiscent of results from Kaptein and Van Gisbergen (2004). The reset at upright deviates from the model prediction of steadily increasing errors previously shown in Figure 4.2D and replicated here, and may reflect factors not included in the model such as somatosensory cues.

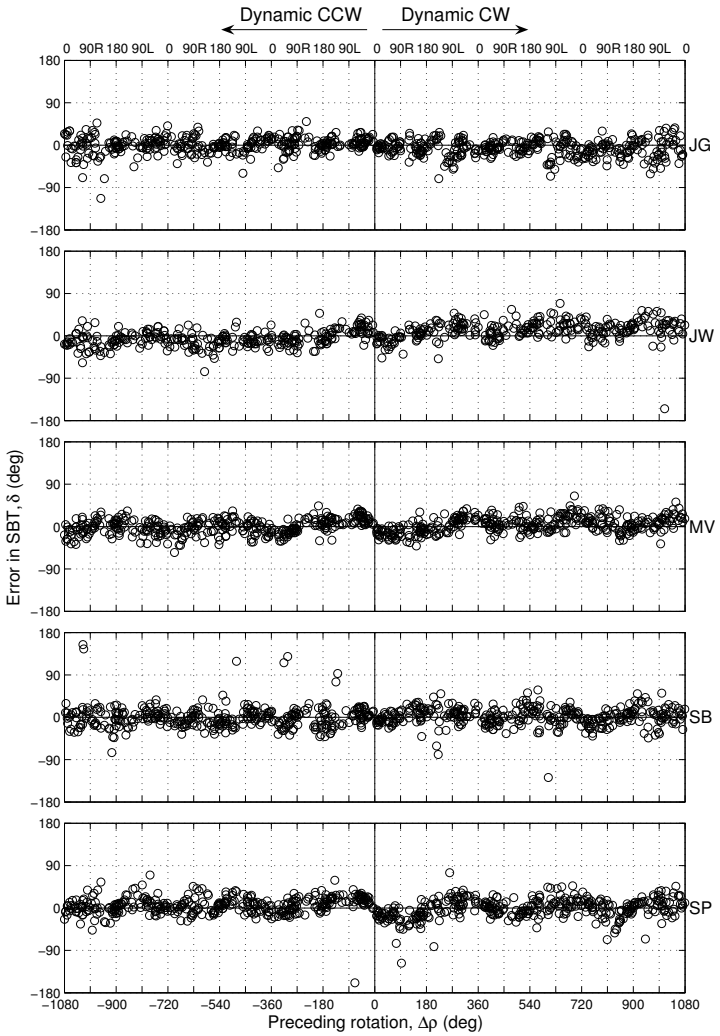

Figure 4.9 *Dynamic SBT task. Systematic errors are generally small and there are no indications of a tilt-dependent pattern of errors as in the SVV.*

4.3.2 Calculating bias weights

Static fits

We used the extended canal-otolith interaction model shown in Figure 4.1A to fit the weight of the egocentric bias separately to the A- and E-cluster data from each subject. The fit, indicated by the solid lines in Figure 4.6, was made on CW and

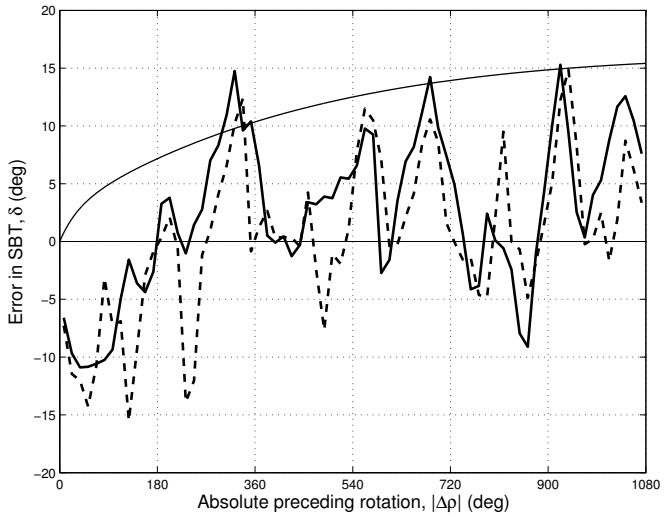

Figure 4.10 *Errors in dynamic SBT task averaged and pooled across subjects. Error patterns for CW (thick line) and CCW (dashed line) are similar. Both patterns start with an negative offset and then increase up to 10°. After one cycle, errors reset and then gradually increase again. Same pattern in the third cycle. Model prediction (thin line) shows a steadily increasing underestimation error. Sign of CCW errors was inverted to allow comparison with CW data.*

CCW data simultaneously. Overall, the fits capture the A-effects quite well, except that in some subjects (JG and SV) the slope of the model fit is somewhat too steep at small tilt angles and slightly too small for larger tilt angles. The figure also shows that the separate fit of the model to the E-cluster provides a good description of this response mode. The best fit bias weights for the A and E-cluster are indicated at the right-hand side of the figure. Table 4.1 also lists the individual weight values together with RMSE and R^2 values of the fits. For the A-cluster, individual bias weights range from 0.27 to 0.92 (mean ± SD: 0.54 ± 0.24) indicating that the estimated direction of gravity is on average about twice as important in the SVV computation as the egocentric bias. RMSE values range from 10.1 to 18.4°(mean ± SD: $13.0 \pm 3.0°$) corresponding to a modest 2-3 minutes on the clockscale. The E-cluster fits yielded negative weights except in subject MV. Since the bias vector is defined as pointing in the direction of the head, a negative amplitude of this vector means effectively that it is pointing in the direction of the feet. A negative bias weight for the E-cluster therefore indicates that these responses are biased toward the upward pointing feet (see Kaptein and Van Gisbergen, 2005, for further

Subject	Static A-cluster			Static E-cluster		
	w_A	RMSE (deg)	R^2	w_E	RMSE (deg)	R^2
JG	0.92 ± 0.02	13.4	0.87	-10	16.0	0.69
JW	0.49 ± 0.01	11.2	0.75	-1.9 ± 0.4	13.4	0.67
MV	0.36 ± 0.02	14.0	0.51	0.19 ± 0.04	17.4	0.10
SB	0.27 ± 0.02	18.4	0.25	-0.8 ± 0.2	18.4	0.38
SP	0.72 ± 0.02	10.1	0.88	-2.4 ± 0.5	14.3	0.57
SV	0.50 ± 0.02	11.1	0.76	-1.1 ± 0.2	12.2	0.60

Table 4.1 *Individual weights of the egocentric bias and RMSE and R^2 values for the static SVV fits. Fit parameter w_E was bounded at -10 because decreasing it further did not improve the fit.*

details). Individual bias weights for this cluster range from -10 to 0.19 (mean ± SD: -2.67 ± 3.70). Since the fit parameter was constrained to remain within -10 to +10, the bias weight of subject JG is at the boundary, but the respective RMSE value is comparable to the others. For all subjects except MV, the absolute value of the bias weight is larger for the E-cluster, indicating that the egocentric frame becomes more dominant in this tilt range. RMSE values for the E-cluster range from 12.2 to 18.4° (mean ± SD: 15.4 ± 2.4°), comparable to those of the A-cluster.

Dynamic fits

Figure 4.7, showing both static and dynamic data, demonstrates that the model can also be tuned to fit the dynamic data. However, to describe the larger A-effects under dynamic conditions, the egocentric bias had to be increased compared to the static fits. With this increased bias weight, the model can even account for the errors up to 180° seen in subjects JG and SB. In the other subjects, the fit to the A-cluster in the range 0 to 180° overestimates the errors that were actually observed. This effect occurs because the fit is based on data from all three cycles and errors in the first 90° are somewhat smaller than those in later cycles, as we confirmed statistically above. Apart from this, Figure 4.8 shows that the overall fit provides a fair description of the dynamic data. Except for the onset effect in the first 90°, the A- and E-cluster pattern repeats itself in successive cycles. Note that there are no clear signs of an upward trend for CW rotation and a downward trend for CCW rotation corresponding to the phase lag predicted by the model (see Figure 4.2D). A more thorough analysis of the phase-lag issue follows in the next section.

The best-fit bias weights are listed on the right-hand side of the figure (see also Table 4.2). The dynamic bias weights in both clusters exceed the static val-

	Static A-cluster			Static E-cluster		
Subject	w_A	RMSE (deg)	R^2	w_E	RMSE (deg)	R^2
JG	3.9 ± 0.2	17.5	0.96	-10	20.4	0.89
JW	0.99 ± 0.01	29.9	0.29	-3.5 ± 1.2	28.1	-0.16
MV	1.21 ± 0.02	24.9	0.70	-1.8 ± 0.1	23.9	0.43
SB	1.60 ± 0.04	24.9	0.89	-1.9 ± 0.4	33.9	0.41
SP	1.13 ± 0.02	29.5	0.72	-4.6 ± 1.7	38.8	0.39
SV	0.97 ± 0.02	25.4	0.31	-3.9 ± 0.6	25.9	0.41

Table 4.2 *Individual weights of the egocentric bias and RMSE and R^2 values for the dynamic SVV fits. Fit parameter w_E was bounded at -10 because decreasing it further did not improve the fit.*

ues in all subjects. Individual bias weights range from 0.97 to 3.9 (mean ± SD: 1.63 ± 1.12) for the A-cluster and from -10 to -1.8 (mean ± SD: -4.27 ± 3.02) for the E-cluster. These larger dynamic bias weights suggest that the body-axis is more dominant as a partial reference for verticality judgments than in static tilts. A possible explanation for this phenomenon will be presented in the section "A Bayesian perspective on the bias effect" in the Discussion. Table 4.2 shows that RMSE values are approximately twice as large as in the static paradigm, which is mainly due to the increased scatter in the responses. As indicated by the comparable R^2 values, the average error pattern is still fitted quite well. Thus, the analysis shows that the model in Figure 4.1A can account quite well for both the static and dynamic SVV data, if we allow different egocentric biases for these two conditions as well as for the A- and E-cluster.

To test whether the egocentric bias mechanism only affects the SVV, without influencing the SBT estimates (see Introduction), we also fitted the bias weights to the dynamic SBT data. This resulted in bias weights ranging from -0.02 to 0.2 (mean ± SD: 0.05 ± 0.09) with only the bias weight in subject SB significantly different from zero. These results support the notion that the egocentric bias mechanism is not part of the body-tilt estimation pathway.

4.3.3 Analysis of phase shifts

As mentioned in the Introduction, several studies have suggested that canal signals are crucial to discriminate tilt and translation from the inherently ambiguous otolith signal. Along this line, the canal-otolith interaction model (Figure 4.1A) implies that when the canal signal decays, the brain has problems keeping track of the direction of gravity, which leads to a phase delay in the tilt percept that can best be

seen at the zero crossings of the simulation in Figure 4.2C. To test whether the data actually show this phase shift, we examined the SVV estimates near the upright positions ($\Delta\rho = \pm 360°, \pm 720°$). If there is in fact no phase shift, one expects SVV estimates to be aligned with the long-body axis ($\beta = 0$) when the subject is upright ($\rho = 0$), independent of the subject's bias weight. On this basis, we estimated the phase shifts by determining at which tilt angle β equals 0, on average. The top row of Figure 4.11 plots the β zero crossings predicted by the model for two different bias weights. The intersecting dashed and solid lines in the panels show that the predicted phase delay does not depend on the bias weight assumed in the simulation. Initially, as rotation starts, the model predicts no phase delay as illustrated by the 0° panel in the center. However, after one cycle of CW rotation (360°), the β zero crossing predicted by the model occurs when the actual tilt angle is about 10° (i.e. when $\Delta\rho = 370°$), indicating a phase delay of approximately 10°. After two complete cycles of rotation (720°), the predicted phase delay has further increased to about 15°. In similar fashion, the two left-hand panels in the top row illustrate the phase delay for CCW rotations. The second row of Figure 4.11 shows all SVV estimates from subject JW for absolute tilt angles between -45° and 45° together with the linear fit based on the data points in this tilt range. The shifts in actual β zero crossings are obviously very small. If anything, the fit lines appear shifted rightward for CCW zero crossings and leftward for CW rotations, thereby contradicting the model prediction. Fit lines from all subjects, shown in the bottom row, support the conclusion that there is no clear evidence for a phase lag.

This lack of evidence for a substantial phase shift in the A-cluster, contrasts with Figure 4.7 where we observed that the E-cluster range was shifted to smaller tilt angles under dynamic conditions as compared to static conditions. The E-cluster starts approximately at 135° and ends at about 225° under static conditions, while dynamically the E-cluster lies roughly between 90 and 195°, which is a shift of about 30-45°. Possible explanations of this observation will be explored in the Discussion (see section "Disambiguation process").

Finally, to investigate the possibility of a phase lag in the SBT results, we plotted the model prediction for δ superimposed on the pooled data in Figure 4.10. The model predicts a monotonically increasing phase lag over the course of the three rotation cycles. Clearly, the data do not match this prediction in all aspects. First of all, it seems as if the data show a vertical shift of about 10° with respect to the model prediction. In addition, while the phase tends to increase with rotation angle, the data also show phase resets around the upright positions, which are not predicted by the model. In the Discussion we will elaborate on possible underlying mechanisms of these observations.

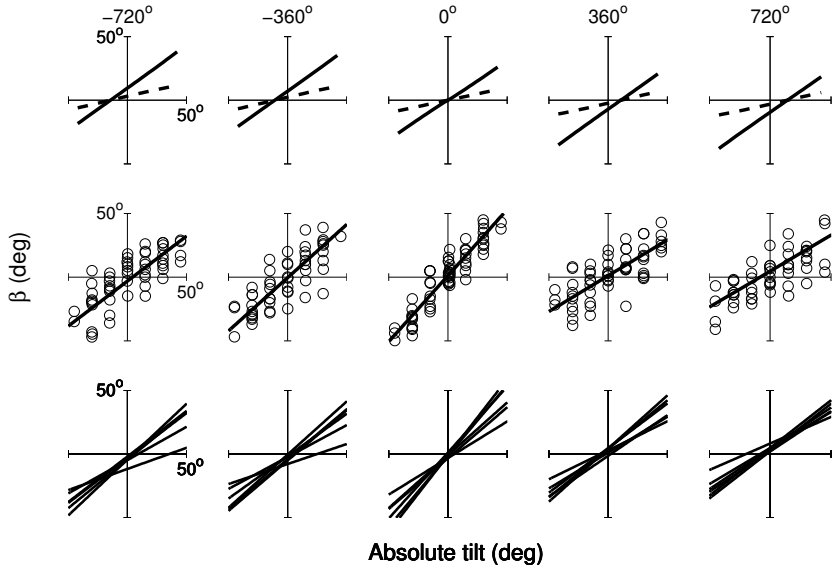

Figure 4.11 *Analysis of phase shifts in dynamic SVV data. Top row: Model predictions of β zero-crossings for an egocentric bias of 0.5 (solid line) and 3.5 (dashed line). Model predicts a phase lag that increases with preceding rotation time. For CW rotation β equals zero at 10° after the first zero crossing (Δρ = 370°) and 15° after the second zero crossing (Δρ = 735°). For CCW rotation the effect is symmetric: β = 0 when the absolute tilt angle is -10° (Δρ = −370°) or -15°(Δρ = −735°). Middle row: Angle β and fit lines for subject JW around zero-crossings. Bottom row: Fit lines from all subjects. Zero-crossings are not shifted in the predicted direction.*

4.4 Discussion

4.4.1 Research questions and main findings

We studied the accuracy of two distinct spatial orientation percepts - the SVV and the SBT - during three cycles of continuous roll rotation. For comparison, we also collected static SVV measurements. Model simulations (Figures 4.1 and 4.2) led us to expect the following results. 1) A cyclical pattern of gradually waxing and waning A-effects in the SVV task, linked to the egocentric bias. Since the bias mechanism was assumed to be static, the model predicts a similar pattern for dynamic and static roll tilts. 2) Since the bias mechanism is only engaged in the SVV computation, the model predicts that these effects have no parallel in the SBT data. 3) A gradually increasing phase lag in both SVV and SBT percepts, caused by

imperfections of the disambiguation stage when the canal signal decays.

The first model prediction was not borne out by the data: while our SVV findings bear obvious signs of the operation of a mechanism that biases visual verticality percepts to the long-body axis, it is all too clear that the notion of a fixed bias is untenable. The fact that subjects showed larger A-effects in the dynamic experiments than in the static experiments shows that the bias effect can vary, depending on circumstances. A possible interpretation of this finding will be discussed below (see section "A Bayesian perspective on the bias effect"). The emergence of the E-cluster at large tilts, both in the dynamic and static experiments, presents a further challenge. The interpretation of this phenomenon as a shift in the egocentric reference frame at near-inverse tilts (Kaptein and Van Gisbergen, 2004, 2005) will be subject of discussion in the next section.

Comparison of the two dynamic data sets revealed that the second model prediction was closer to the mark. Strong signs of egocentric biasing in the SVV were virtually lacking in the SBT judgments. This remarkable difference in performance lends support to the notion that these percepts reflect different processing of a shared tilt signal (see Figure 4.1A). Finally, neither the SVV findings (Figure 4.11), nor the SBT data (Figure 4.10) showed clear evidence of an accumulating phase delay in the course of prolonged rotation. This finding, suggesting that disambiguation errors were small in the present conditions, will be discussed later (see section "Disambiguation process").

4.4.2 Tilt-related bias

Using the egocentric bias mechanism in combination with the canal-otolith interaction model (Figure 4.1A), we simulated the SVV during static and dynamic roll tilt. In its simplest form, with a single bias weight, the model predicts that the error in the SVV gradually increases up to absolute tilts of about 135° and then gradually decays back to zero at 180° tilt under static conditions (Figure 4.1D). However, our data clearly contradicted the model prediction by showing an abrupt switch from A to E-effects at large tilt angles. To account both for A-effects for tilt angles up to about 135° and E-effects at large tilt angles, we had to adopt different weight values (w) with opposite sign. The fact that fitting the E-cluster requires a switch to a negative bias weight implies that the egocentric bias, normally directed toward the head, can flip to the feet. Kaptein and Van Gisbergen (2005) have suggested that the switch may reflect a shift to a more cognitive strategy. These authors reported that while subjects had a vivid percept of the visual upright at small tilts, such a strong awareness of visual space was lacking at large tilt angles. Nevertheless, at these extreme tilts a feeling of being tilted at a very large tilt angle, induced by strong somatosensory cues, is unmistakable, prompting an SVV setting close

to the upward-pointing feet. When we analyzed data from single runs, we found that in some runs subjects only provided A-responses, suggesting that they were in the the normal low-level mode throughout the whole run and did not switch to the supposedly more cognitive E-response mode.

We observed that different bias strengths were necessary to account for the A- and E-clusters in the static data. In addition, these bias weights had to be increased to fit the larger errors in the dynamic paradigm. The latter finding is a contrast with our OVAR study (Vingerhoets et al., 2007) where we found an almost one-to-one relation between static and dynamic A-effects. Moreover, the weights found in the present study, both statically (mean ± SD: 0.54 ± 0.24) and dynamically (mean ± SD: 1.63 ± 1.12), are substantially larger than those observed during the OVAR paradigm (mean ± SD: 0.20 ± 0.15). This may be due to the fact that we tested a more complete tilt range in the present study, as opposed to only two tilt angles in Vingerhoets et al. (2007). But, as we discuss below, this difference could also be an indication that the brain processes yaw and roll rotation cues differently, as suggested by Klier et al. (2006).

4.4.3 A Bayesian perspective on the bias effect

So far we sidestepped the problem of which mechanism may cause the SVV to be a compromise between the true direction of gravity and an egocentric reference frame, using the egocentric bias vector to quantify the effect. This pragmatic approach has been adopted before in various studies (Dyde et al., 2006; Groen et al., 2002; Haslwanter et al., 2000; Zupan and Merfeld, 2005; Zupan et al., 2002). However, an important question relates to the origin of this bias. Mittelstaedt (1983, 1999, 1986) proposed that the egocentric bias serves to correct for putative systematic errors in the tilt signal caused by unequal numbers of hair cells in the saccule and the utricle. However, this interpretation would require further assumptions to explain the results of the present SBT experiments, in which the dynamic tilt estimates from our subjects were quite good, by comparison, with no signs of major systematic errors. Earlier static studies (Bortolami et al., 2006a,b; Kaptein and Van Gisbergen, 2004; Mast and Jarchow, 1996; Van Beuzekom and Van Gisbergen, 2000) have also demonstrated that body-tilt estimates show only modest deviations from true body tilt. Furthermore, Mittelstaedt's notion that the idiotropic vector is a fixed idiosyncratic constant contrasts with our finding that the dynamic results indicate an increased egocentric-bias weight.

We are now faced with a peculiar situation. Under dynamic conditions, the SBT, which can be seen as a reflection of the internal representation of gravity, seems quite accurate. Yet, in a different task, large errors in the SVV point to an egocentric bias mechanism. Ironically, it would therefore appear as if an almost

veridical internal representation of gravity is spoilt by an egocentric bias. How can this make sense? A way out of this conundrum may come from an alternative modeling approach that reinterprets the egocentric bias in terms of a tilt prior in a Bayesian observer model (Eggert, 1998; MacNeilage et al., 2007). In this guise, the bias mechanism becomes an element in an optimal strategy to handle noisy tilt signals. The basic idea is that when there is no sensory tilt signal, the brain makes a conservative a priori assumption that the head is usually upright. This a priori assumption can then be overruled by sensory evidence. In case of weak evidence the brain still relies mostly on the prior belief. However when the sensory signal becomes more reliable, the brain will assign more weight to information from the sensors. The result of the combination of prior information and sensory information is that the final percept is very stable when the prior and the sensory information are compatible, in this case for tilt angles close to upright. This is useful when the brain has to combine the relatively noisy tilt information with the very precise retinal information about line orientation. As these small tilt angles occur most often, this would be a smart strategy to optimize performance during daily life. The downside of this computational strategy is that it goes at the expense of systematic errors at large tilt angles that occur only rarely in everyday life.

But why then is the prior only used for the SVV and not for body tilt estimation? A speculative explanation is that precision is more important for the visual system than accuracy, for reasons of visual stability. Thus to allow a stable percept of the visual world, noise in the tilt signal is reduced by combining it with a prior. For the percept of body tilt it is probably less important to be precise and more useful to be accurate and therefore the prior does not take part in this process. This hypothesis is in line with remarkable findings by Mast and Jarchow (1996), who showed that body tilt adjustments to a 90° horizontal position, in the dark, are more noisy than SVV settings at the same tilt angle.

From a Bayesian perspective, the larger systematic errors in the SVV for the dynamic paradigm can be explained by a noisier tilt signal under these conditions, for example as a result of a lack of integration time. According to Bayes' rule, a noisier tilt signal leads to more weight of the prior and thus to a final estimate that will be biased more toward upright. Hence, a noisier tilt signal leads to a stronger bias. In addition, it is conceivable that the physiological internal model is less reliable in seldom experienced orientations (e.g. upside down) thus leading to more weight for the prior and a larger bias. This is consistent with our finding that the bias weights of the E-cluster were larger than the bias weights of the A-cluster. It remains a topic for further study to see if this Bayesian approach is a realistic modeling perspective.

4.4.4 Disambiguation process

Since gravitational and inertial acceleration forces are physically indistinguishable, the otolith signal is ambiguous (Angelaki and Dickman, 2000; Fernández and Goldberg, 1976; Loë et al., 1973). Thus, to mediate reliable spatial orientation, neural strategies must exist to solve the inverse problem of determining which combination of tilt and translation has led to a given otolith signal. Here we evaluated the canal-otolith interaction hypothesis as one such strategy proposed in the literature. This hypothesis, implemented in the model shown in Figure 4.1A, suggests that the brain uses internal models that incorporate canal signals to solve the ambiguity problem. But even when canal cues dissipate, for example, during prolonged rotation in the dark, this model predicts that humans are still able to retain a reasonable internal representation of the direction of gravity. The model achieves this by comparing the measured GIF and the estimated GIF and using this angular difference as an additional estimate of roll rotation. As a consequence, the decay of the canal signal only results in a phase shift of the internal representation of gravity with respect to the actual direction of gravity. According to the model and the parameters we have chosen, this phase shift does not exceed 15° for the present stimulus conditions.

If our model, suggesting that $\hat{\mathbf{g}}$ is the source signal for SVV and SBT, is correct, both should have an accumulating phase shift. However, in the present stimulus conditions, neither SVV nor SBT showed clear signs of a monotonically increasing phase shift. To conclude that otolith disambiguation was almost perfect under the present experimental conditions, would be a marked contrast with our earlier OVAR studies (Vingerhoets et al., 2006, 2007) where, in line with the model predictions, illusory translation and tilt underestimation occurred as a result of imperfect otolith disambiguation. The question is how this discrepancy can be explained. The model is quite consistent in predicting a similar phase delay for both OVAR and roll rotation. In addition, the predicted cone illusion during OVAR has a parallel during roll rotation, as illustrated in Figure 4.2B. During roll rotation, the model predicts a feeling of spiraling outward into an orbit with a roughly 0.3 m radius. It would seem that such an effect should be quite noticeable to the subject, but we have no evidence that this percept occurs. As this illusory translation percept is well established during off-vertical axis yaw rotation, but is questionable during roll, the possibility should be considered that the brain processes body motions in roll and in yaw differently. A similar suggestion was made in the spatial updating study of Klier et al. (2006), who found different degrees of updating for yaw and roll rotations. Updating performance after whole body yaw movements, even when the rotation axis was perpendicular to gravity, showed larger errors and was not facilitated by gravity in the same way as roll updating. Klier et al. (2006) as well

as Bockisch et al. (2005) suggested that this may be linked to the fact that yaw rotation is usually parallel to gravity and therefore stimulates the otoliths to a much lesser extent than roll head movements. Thus, the fact that canal and otolith signals are rarely coupled for yaw rotations might have resulted in a system that is not well developed for these situations.

In line with other studies reporting a mismatch for the phase response in model predictions and data (Glasauer, 1995; Park et al., 2006), we think that it would be premature to discard the entire model structure, solely on the absence of phase shifts. First of all, the phase lag of 15° is a relatively small effect to look for via verbal reports during dynamic stimulation. Furthermore, while the A-cluster had no significant phase shift, there was an intriguing shift in the E-cluster range under dynamic conditions. Inevitably, the computation of the responses in the dynamic condition, which requires combining retinal and tilt information, must be subject to a delay after the presentation of the visual stimulus. Subjects were instructed to report the spatial orientation of the line at the time when it was presented, but the computational delay may present a problem. If they are actually computing the orientation of the line a second later, their tilt angle will have changed 30° in the interval, which is the approximate amount of the shift in the E-cluster. Thus, responses plotted at a body tilt of 90° would actually correspond to a body tilt of 120°. In other words, a computational delay would be expressed as a phase advance in the data. Since the phase shift in the A-cluster, tested at 0° tilt was almost negligible, it is clear that a fixed computational delay, identical for both clusters and all tilt angles, cannot explain our data. At this point one can either simply reject the hypothesis, or accept the possibility that the computational delay for the A-mode was shorter. We feel that this admittedly speculative assumption is actually not entirely unreasonable, for three reasons. A smaller computational delay in the A-mode, in the order of 500 msec, would help to explain why the maximum 15° phase delay predicted by the model (see Figure 4.2C) was not actually found. Furthermore, a longer computational delay in the E-mode would fit in with earlier suggestions that its responses are more cognitive (Kaptein and Van Gisbergen, 2005). Finally, as the computational delay leads to a phase advance or, in other words, overestimation of tilt, a delay in the order of about 300 ms may also explain why the SBT data is shifted approximately 10°downward compared to the model prediction (see Figure 4.10).

In summary, we conclude that errors in visual verticality perception under dynamic conditions are not caused by errors in body-tilt estimation, that the egocentric-bias mechanism becomes stronger during constant-velocity roll rotation and that disambiguation of the otolith signal shows no major errors, despite the decay of canal signals.

Acknowledgements We acknowledge Hans Kleijnen, Ger van Lingen, Stijn Martens and Günter Windau for excellent technical support. We had many helpful discussions with Ronald Kaptein about the design of the experiment. Sanne Vaarhorst, Sam Bruijs and Maarten van der Heijden helped running the experiments. This work was supported by Radboud University Nijmegen (NICI and FNWI). Further support came from grants of the Netherlands Organisation for Scientific Research and the Human Frontier Science Program awarded to W.P. Medendorp.

Chapter 5

Fusion of optic and vestibular tilt cues in visual verticality perception

5.1 Introduction

In this chapter, we investigate how the orientation of a peripheral visual frame and lateral body-tilt signals affect the subjective visual vertical (SVV) and test whether two alternative models can account for the data. The literature contains numerous reports on the effects of each of these factors in isolation, but combined studies, particularly those with a modeling background, are very rare. To provide a survey of the important concepts, we first review current knowledge about visual frame effects on the SVV in upright observers, then discuss previous SVV studies in tilted observers in the absence of a visual frame and conclude by reviewing previous work on the interaction of frame and body-tilt signals.

Natural scenes have an overrepresentation of world-horizontal and vertical orientations (Coppola et al., 1998; Van der Schaaf and Van Hateren, 1996) and typically contain polarity cues indicating which direction is up. Strong effects of a rich panoramic stimulus have been found in experiments where subjects in upright position adjusted a luminous line to the perceived direction of gravity while viewing a tilted furnished room (Asch and Witkin, 1948a; Howard and Childerson, 1994). But also in more impoverished stimulus conditions, for example when using a simple square frame devoid of obvious polarity cues, average verticality settings clearly deviate in the direction of the tilted frame (Witkin and Asch, 1948). This phe-

Adapted from: Vingerhoets RAA, De Vrijer M, Van Gisbergen JAM, Medendorp WP (2008) *J. Neurophysiol.*, submitted

nomenon, known as the rod-and-frame effect, has been confirmed by many other studies (see Beh et al., 1971; Cian et al., 2001; DiLorenzo and Rock, 1982; Dyde and Milner, 2002; Ebenholtz, 1977; Ebenholtz and Benzschawel, 1977; Spinelli et al., 1991; Wenderoth and Beh, 1977; Zoccolotti et al., 1992). Spinelli et al. (1991) found a cyclical modulation of the SVV when the orientation of the frame was varied across a 90° range. The recent finding by Li and Matin (2005a,b) that even a single peripheral line can be as effective as a complete square, with the same 90° periodicity, indicates that the square configuration is not crucial. In this context, the cyclical modulation of the SVV seems to suggest that a single line or a frame is an ambiguous indicator of four potential up directions: two corresponding to its orientation and two perpendicular to it. Matin and Li (1995) suggested that these effects stem from a rather primitive global vision system that interprets an anisotropic orientation distribution in the visual field as an ambiguous body tilt signal that combines with the nonvisual tilt cues provided by the vestibular system to determine the SVV.

Before discussing the nature of this visuo-vestibular fusion process in more detail, we first provide some background about the peculiarities of the SVV in roll-tilted observers, in the absence of panoramic visual stimuli. At large tilt angles, the orientation of a luminous test line is misperceived, even without a frame. This was first described by Aubert (1861), and ever since, this phenomenon has been extensively investigated. Numerous experiments, testing the ability of roll-tilted subjects to adjust a luminous line to the perceived direction of gravity in an otherwise dark room have found a consistent pattern of tilt undercompensation at tilts beyond $\tilde{6}0°$, known as the Aubert or A-effect, while at smaller tilts the opposite effect (E-effect) may occur (Kaptein and Van Gisbergen, 2004, 2005; Mittelstaedt, 1983; Schöne, 1964; Udo de Haes, 1970; Van Beuzekom and Van Gisbergen, 2000). A widely-accepted explanation for the A-effect at large tilts holds that the SVV reflects a compromise between the direction indicated by the tilt sensors and an egocentric reference. Models incorporating this concept have taken two different forms. Mittelstaedt (1983) proposed that the A-effect is linked to a so-called idiotropic vector, an internal bias signal expressing the tendency to assume that the subjective vertical is aligned with the head axis. In this model, the SVV setting is a compromise between the tilt signal of the otoliths and the idiotropic vector. Recently, an alternative model using Bayesian signal processing has been formulated (De Vrijer et al., 2008; Eggert, 1998), in which the SVV depends on the statistical properties of the various signals that are involved. More specifically, this model incorporates a priori information, that body-tilt is usually small, in the form of a prior probability distribution centered around zero. Furthermore, the sensory tilt signal in the model is assumed to be noisy and the outcome of the Bayesian estimator is an optimal

compromise based on the mean and the width of the sensory signals and the prior distribution (De Vrijer et al., 2008; Eggert, 1998; MacNeilage et al., 2007).

Given the topic of this chapter, a crucial question is how the effects of a visual frame combine with those of body tilt in the perception of visual verticality. Several studies have shown that the frame effect becomes more pronounced when the observer is tilted (Asch and Witkin, 1948b; Bischof, 1974; Bischof and Scheerer, 1970; Corbett and Enns, 2006; Dyde et al., 2006). Bischof and Scheerer (1970) studied the combined effect of body tilt and visual frame tilt by testing the effect of a slowly rotating parallel-stripe pattern on the SVV settings, at various roll-tilt angles of the observer. The stripe pattern acted as an attractor when its orientation deviated slightly from the subjective vertical. Further rotation of the pattern gradually reduced the attraction effect until a new attraction effect emerged around 90°. Bischof and Scheerer suggested that the lines thus provide a fourfold ambiguous indicator of which way is up, an interpretation that got later support from Li and Matin (2005a,b).

Mittelstaedt (1986) studied the effect of a visual frame on the SVV in subjects tilted 90° in roll. He found that a visual frame with a polarization direction aligned with the SVV does not affect the setting of a small luminous line, whereas other visual frame orientations clearly modulate the SVV. To account for these observations, later confirmed by Eggert (1998), Mittelstaedt (1986, 1988) extended his original model (Mittelstaedt, 1983) by conceiving the SVV as a weighted sum of the otolith signal, the idiotropic vector and an additional vector that points in the upward direction defined by the visual frame of reference. In this chapter, we will refer to this extended model as the Mittelstaedt model. Following this account in Bayesian terms, we have extended the model proposed by De Vrijer et al. (2008) for the SVV in dark-tilted subjects with an additional stage to incorporate head-tilt cues derived from visual-frame information in a statistically-optimal fashion (see Methods for full description of both models). We will refer to this model as the Bayesian model.

In the present study, we put both models to the test by investigating the effect of a visual frame, consisting of a single peripheral visual line, on the SVV at three different body-tilt angles (0, 60 and 120°). These tilt angles were combined with a broad range of visual frame angles (-90 to 90° in steps of 10°) to determine the frame SVV. For comparison, we also determined the SVV in complete darkness (dark SVV). In the experiment, subjects were rotated in complete darkness to the tilt angle chosen for testing, where they were then shown the visual frame line. Subsequently, after a short viewing period, they adjusted a short luminous test line parallel to the perceived direction of gravity. Consistent with both models, our results show a 90° periodic modulation on the frame SVV, which increases when the

body is tilted away from upright. Our data also confirm that visual frames aligned with or perpendicular to the dark SVV do not affect the frame SVV. Although the two models cannot capture all aspects of the data, we conclude that they provide valuable insights into the centrally weighted fusion of visual, vestibular and egocentric signals in human spatial orientation.

5.2 Methods

5.2.1 Subjects

Six subjects (four male, two female) aged between 23 and 64 years (mean ± SD: 32 ± 16 years) gave informed consent to participate in this study. All subjects were free of any known vestibular disorder and had normal or corrected to normal vision. All participants except two (JG and MV) were naive with respect to the purpose of the experiments. Before the experiment began, subjects were carefully instructed about the task and were given a few practice runs. They never received feedback about their performance. Vision was always binocular.

5.2.2 Setup

The subject was seated in a computer-controlled vestibular chair with nested gimbals that was configured to rotate subjects about their roll axis. The subject's head, positioned at the rotation center, was restrained in a natural upright position relative to the torso using a padded helmet. The torso was secured with seat belts and adjustable shoulder and hip supports. The legs and feet were fixated with Velcro straps and a foot rest.

The SVV was tested using a uniformly-illuminated line with an angular subtense of 20° mounted on the vestibular chair at approximately 90 cm, straight ahead in front of the subject. The SVV test line was polarized by a bright dot at one end and could be controlled by computer with an angular resolution of 0.5°. The rotation axis of the test line coincided with the cyclopean eye of the subject and the rotation axis of the chair, so that it rotated in the fronto-parallel plane. The observer adjusted the orientation of the test line with a joystick to indicate the SVV, both in the presence and in the absence of a visual frame stimulus. We will refer to the SVV determined in otherwise complete darkness as the "dark SVV" whereas the SVV in the presence of the frame line will be denoted as "frame SVV".

The visual frame stimulus was a line (to be denoted as "frame line") with an angular subtense of 108° whose center was located at 54° eccentricity. The frame line could be rotated in the fronto-parallel plane about an axis that coincided with the rotation axis of the SVV test line. It was presented at orientations ranging from

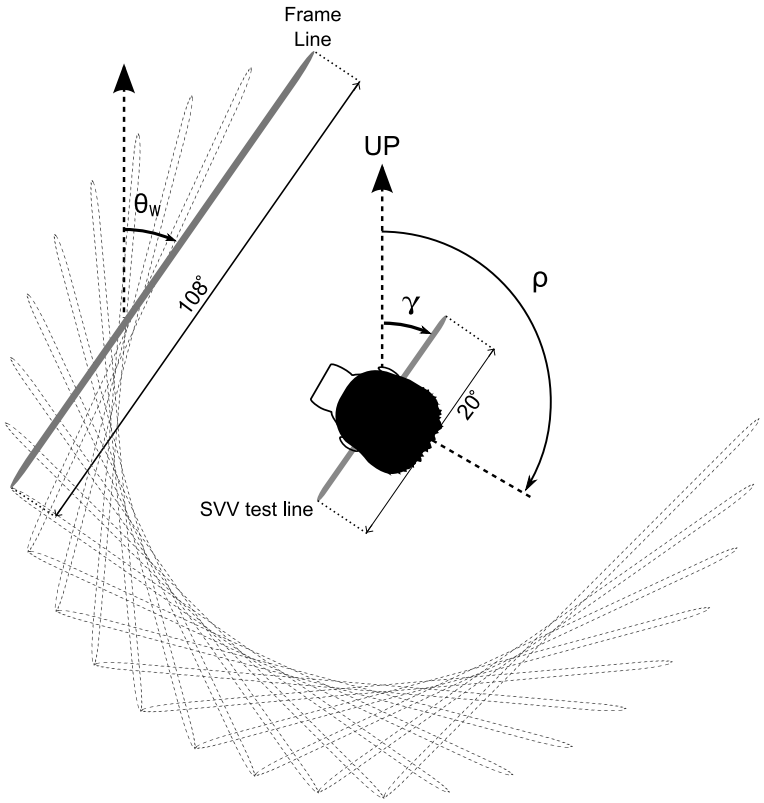

Figure 5.1 *Illustration of visual line stimuli. All 18 orientations of the frame line, which was 108° long. Frame-line orientation in world coordinates is denoted by θ_w. Angular subtense of the SVV test line was 20°. No other contours were visible (completely dark room). Error in SVV (γ in deg) is defined as the angular difference between the final orientation of the SVV test line and the direction of gravity. Angles ρ and γ are defined as positive in CW direction, seen from behind the subject. Body-tilt angle (ρ) shown here is 120°.*

-90 to 90° relative to the dark SVV at 10° intervals, yielding a total of 18 different frame line orientations (see Figure 5.1). An orientation of 0° denoted that the frame line was parallel to the dark SVV. When the frame line was oriented at 90 or -90°, it was perpendicular to the dark SVV. Subjects were instructed that the frame line could have any orientation in space and thus provided no reliable clue as to the direction of gravity.

5.2.3 SVV experiment

In each run, the initially upright subject was rotated clockwise (seen from behind) about the roll axis to the tilt angle chosen for testing (0, 60 or 120°). The chair rotated with a constant velocity of 30°/s, using a peak acceleration and deceleration of about $50°/s^2$. Once the desired tilt position was reached, there was a 30 s waiting period before SVV testing began to allow rotational signals to subside. Subsequently, the test line was presented in a random orientation and the subject adjusted its orientation parallel to the perceived direction of gravity with the dot pointing upward in space. After the subject completed the adjustment, a new test line appeared at a random orientation. The time available for each adjustment was 15 s. After five consecutive adjustments the subject was returned back to upright to remain there for 45 s with the room lights on to allow reorientation.

Each session of about 45 min started by testing the dark SVV. This was done extensively in the first session (three measurements for each tilt angle) and only once in later (2^{nd}-4^{th}) sessions. Runs testing the frame SVV differed in two aspects from the dark SVV runs. First, when testing the frame SVV, the frame line was lit from the moment of arriving at the final tilt position until the end of the run, whereas the dark SVV was tested in complete darkness. Second, when the frame SVV was tested, subjects also gave a verbal estimate of the frame line orientation in the world using a clockscale, before the actual SVV adjustment task started.

5.2.4 Data analysis

Response error (γ) was defined as the difference between the true direction of gravity and the SVV setting of the subject (see Figure 5.1). Errors (γ) in CW direction, seen from behind the subject, were taken positive. Accordingly, A-effects yielded positive γ values and E-effects yielded negative γ values.

5.2.5 Model simulations

As we shall see in the Results section, both the degree of body tilt and the orientation of the frame line affected the visual verticality percept. Mittelstaedt (1988, 1986) proposed a model to account for both effects. In the following we first provide an outline of this model and then describe an alternative Bayesian framework recently proposed by De Vrijer et al. (2008), here extended with an additional stage for visual frame processing.

Mittelstaedt's model

Mittelstaedt (1986, 1988) proposed a framework (Figure 5.2) incorporating the effects of the estimated direction of gravity, the idiotropic vector and visual panoramic cues on the percept of verticality. As explained in the Introduction, the idiotropic vector represents the tendency to assume that the SVV is aligned with the long-body axis. Figure 5.2A illustrates the idea behind the model in schematic fashion. The direction of gravity sensed by the otoliths (**G**), the idiotropic vector (**M**) and the direction of visual panoramic cues (**P**) are modeled by vectors with lengths proportional to their relative weights. The internal representation of gravity is represented by an upward pointing unit vector. The idiotropic vector, pointing along the long-body axis, has a weight that can vary across subjects to account for differences in the size of the A-effect in the dark SVV. In the simple case that the visual frame is a highly polarized visual scene, its effect can be modeled by a single vector **P**, pointing in the polarization direction of the visual scene. In this special case, the model determines the percept of verticality by adding vectors **G**, **M** and **P**, as shown in Figure 5.2A. In the following, we translate this graphical account into mathematical terms to allow for the handling of more ambiguous visual frames, like a single line.

Mittelstaedt (1986, 1988) defined vectors **G**, **M** and **P** in a head-fixed coordinate system in which the x-axis is aligned with the naso-occipital axis, the y-axis corresponds to the interaural axis and the z-axis is the vertical axis. The three vectors can then be written as: $\mathbf{G} = (0, \sin\rho, \cos\rho)$, $\mathbf{M} = (0, 0, M)$ and $\mathbf{P} = (0, V\sin\theta_r, V\cos\theta_r)$, where gravity is normalized: $|\mathbf{G}| = 1$, ρ is the tilt angle of the body and M is the length of the idiotropic vector. For simplicity, we ignore ocular torsion so that the angle between the upward direction of the visual scene and the head's z-axis equals the orientation of the visual scene on the retina, denoted by θ_r. The luminous line, serving as an indicator of the SVV, is also conceived as a vector: $\mathbf{L} = (0, \sin\beta, \cos\beta)$, in which β is the angle between body and SVV. When the observer rotates indicator **L** until it is aligned with **G**, this is equivalent to reducing the cross-product between **L** and **G** to zero, which yields:

$$\sin\beta \cdot \cos\rho - \cos\beta \cdot \sin\rho = 0 \tag{5.1}$$

Including the notion that the SVV setting is a compromise between the actual tilt signal of the otoliths and the idiotropic vector yields:

$$\sin\beta(\cos\rho + M) - \cos\beta \cdot \sin\rho = 0 \tag{5.2}$$

which represents the classical scheme (Mittelstaedt, 1983) for conditions with-

out additional visual cues. To add the effect of panoramic cues, indicated by vector **P**, to the equation we can write:

$$\sin\beta(\cos\rho + M + V\cos\theta_r) - \cos\beta(\sin\rho + V\sin\theta_r) = 0 \tag{5.3}$$

Before we can apply the model to our testing conditions, it should be realized that **P** has four ambiguous polarization directions in the case of a single frame line. In contrast to a rich panoramic scene, the frame line yields the same effect when rotated by 90 or 180° (Li and Matin, 2005a,b). To incorporate this 90° periodicity-effect of the frame line, the following equation can be derived (see Appendix):

$$\sin\beta(\cos\rho + M) - \cos\beta\sin\rho + V_4\sin 4(\beta - \theta_r) = 0 \tag{5.4}$$

In this equation, the third term represents the visual frame effect, with V_4 denoting the length of the vector that represents the four effective orientations of the visual frame. The factor 4 in this term expresses the four-fold periodicity across 360°, corresponding to the four polarization directions associated with the frame stimulus. When the subject adjusts β so that the cross product reduces to zero, the resulting SVV can be regarded as the vector sum of **G** and **M** and the **P** vector closest to their resultant.

Model predictions of the frame SVV (solid line) in Figure 5.2B show that the error pattern for upright is 90° periodic with a first positive peak around 27° and a first negative peak at -27°. Note that, due to factor $(\beta - \theta_r)$, the predicted error pattern deviates from a symmetric sine wave. The horizontal dashed line, indicating the error in the dark SVV, shows that the model predicts a flawless dark SVV for upright. Since the dark SVV can be regarded as the orientation that is perceived as vertical, we also indicated it as a vertical dashed line in the plot to illustrate the orientation at which the frame line is aligned with the dark SVV. For the tilted conditions, the periodic error pattern is superimposed on a constant bias representing the A-effect in the dark SVV, caused by the idiotropic vector (**M**). Furthermore, the error pattern is shifted to the right and thus no longer symmetric around the vertical axis through the origin (y-axis). This shift reflects the model prediction that a frame line aligned with the vector sum of **M** and **G** (i.e. the dark SVV) has no effect on the verticality percept which means that the error pattern now becomes symmetric around the orientation parallel to the dark SVV indicated by dashed lines. Finally, the panels express the model prediction that the effect of the frame line increases slightly with tilt angle, as indicated by the larger peak-to-trough distance in the body-tilt conditions.

In testing the quality of this model, the best-fit parameters M and V_4 were found by minimizing the sum-of-squared-errors, with the constraint that only positive V_4 values were allowed.

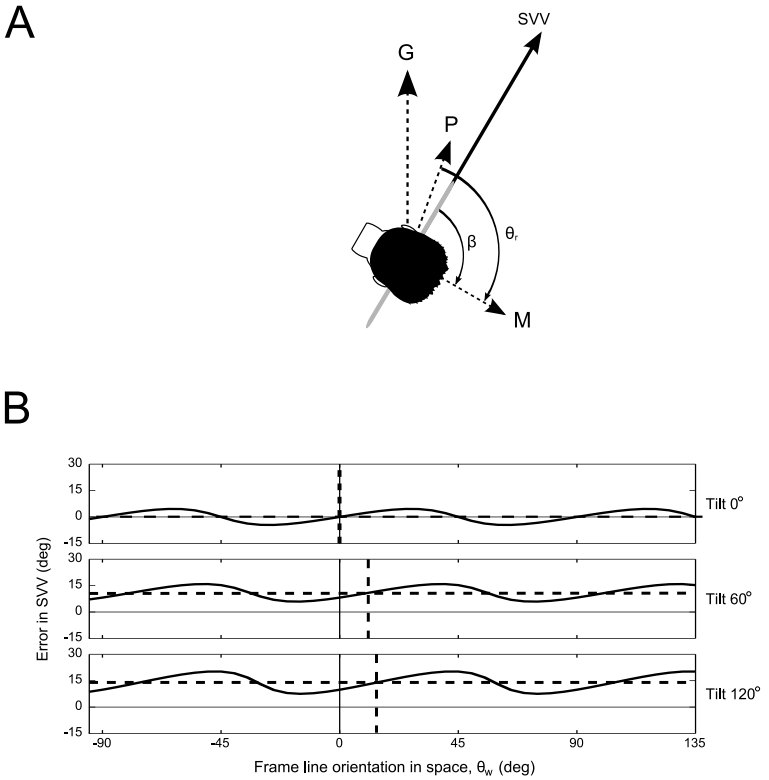

Figure 5.2 *Mittelstaedt's model. A: Graphical representation of the subjective visual vertical (SVV) as the resultant of the sensed gravity vector (**G**), the idiotropic vector (**M**) and the up-direction implied by the visual panorama (**P**). B: Model predictions of Mittelstaedt's model with $M = 0.25$ and $V_4 = 0.1$. Solid line: frame SVV predictions. Horizontal dashed line: sign and magnitude of predicted error in dark SVV. Vertical dashed line: predicted orientation of the dark SVV in space. Note that the error pattern is 90° periodic. For the tilted conditions the model predicts A-effects (positive bias).*

Bayesian model

De Vrijer et al. (2008) recently described a Bayesian approach to simulate the dark SVV in tilted observers. In the model, computation of the dark SVV is based on the head tilt signal, which is assumed to be veridical but corrupted by noise, and an *a priori* assumption that the head is usually upright. We extended this model with an additional stage for the processing of visual-frame cues, as shown in Figure 5.3. The inputs to the extended model are head orientation in space (ρ) and the retinal orientations of the SVV test line (ϕ_r) and the visual frame line (θ_r). The crucial signal in the model is β, the central tilt signal that ultimately transforms retinal

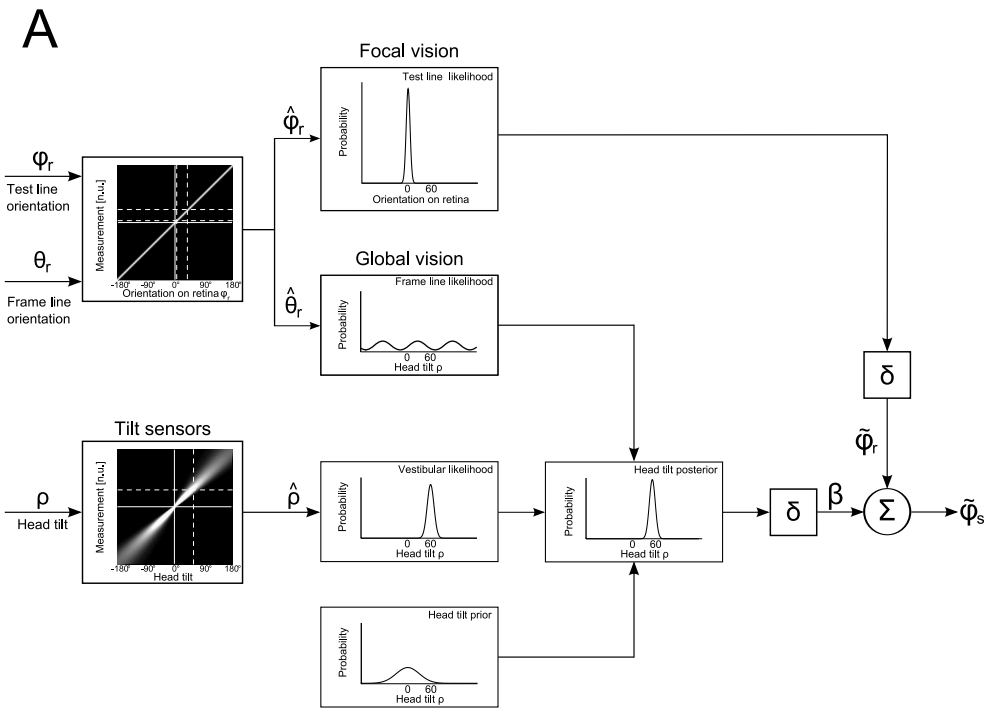
A
Focal vision
Test line likelihood
Probability
Orientation on retina
Global vision
Frame line likelihood
Head tilt ρ
Test line orientation
Frame line orientation
Measurement [n.u.]
Orientation on retina φr
Tilt sensors
Head tilt
Vestibular likelihood
Head tilt posterior
Head tilt prior
δ
β
Σ

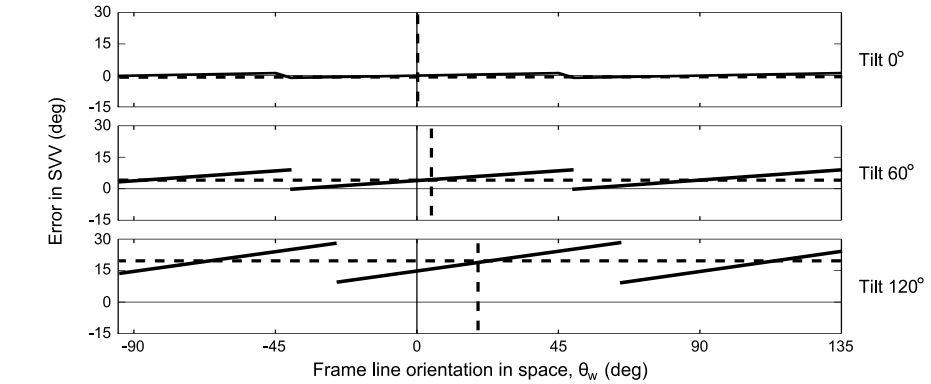
B
Error in SVV (deg)
Tilt 0°
Tilt 60°
Tilt 120°
Frame line orientation in space, θw (deg)

← **Figure 5.3** *Bayesian model. A: Sensory signals coding head tilt and line orientation are represented by probability distributions. The focal vision system provides an unbiased visual signal $\hat{\phi}_r$ of the luminous test line. The observer selects the orientation $\tilde{\phi}_r$ with maximum probability (decision rule, δ). The global vision box represents the inbuilt assumption that natural visual contour distributions are peaked at orientations parallel and perpendicular to gravity, by showing maxima at 90° intervals in the frame likelihood. Head tilt signal (vestibular likelihood) is combined with prior information and the frame likelihood using Bayes' rule to obtain the posterior probability distribution. A decision rule δ is used to select the compensatory tilt angle β with maximum posterior probability (MAP). The world-centered orientation of the visual stimulus $\tilde{\phi}_s$ is obtained by a linear combination of the compensatory tilt signal and the visual orientation of the test line, $\beta + \tilde{\phi}_r$. It is assumed that subjects adjust the test line such that $\tilde{\phi}_s = 0$. B: Predictions of the frame SVV using $\sigma_p = 13°$, $\sigma_f = 10°$, $a_0 = 1.5°$, $a_1 = 0.035$. Format as in Figure 5.2B. Effect of frame line, which is very small for upright, becomes larger in tilted conditions. Error pattern shows discontinuities which are not predicted by the Mittelstaedt model (Figure 5.2)*

signals to spatial coordinates. Since the model is designed to combine noisy signals in an optimal fashion, it deals with probability distributions instead of deterministic signals.

Body-tilt signal and prior. We first describe how the model works in the absence of visual panoramic cues. Following De Vrijer et al. (2008), we assume that signal $\hat{\rho}$, provided by extraretinal head-tilt sensors, like the otoliths, has a linear but noisy relation with input angle ρ. As a result, a given tilt angle ρ yields a distribution of signals, as indicated by the vertical dashed line in the bottom left panel in Figure 5.3A. The brain must solve the inverse problem of determining which tilt angle caused the given sensory signal, as indicated by the horizontal dashed line. Because of the noise in the system, there is no unique solution and a statistical approach is required. The Bayesian scheme applies knowledge of the forward ρ to $\hat{\rho}$ relationship to compute the probability that any particular tilt angle produced the incoming sensory signal. The result of this computation, the vestibular likelihood function $P(\hat{\rho}|\rho)$ which comprises all non-retinal tilt signals, is based exclusively on the sensory evidence $\hat{\rho}$ and is modeled by a Gaussian centered at ρ with standard deviation σ_{tilt}. To obtain a statistically optimal tilt estimate, the Bayesian model also takes into account prior knowledge, which is expressed by the prior $P(\rho)$, a Gaussian with standard deviation σ_p centered on zero head tilt, to account for the fact that small head tilts are most common. For a particular tilt angle, the combination of sensory evidence and prior knowledge yields the posterior probability $P(\rho|\hat{\rho})$ distribution according to Bayes' rule: $P(\rho|\hat{\rho}) = k \cdot P(\hat{\rho}|\rho)P(\rho)$, where k is a constant that serves to normalize the posterior distribution. The location of the peak of the posterior distribution $P(\rho|\hat{\rho})$ is denoted by β and lies in between the peaks

of the prior and the vestibular likelihood (see Carandini, 2006). Compensatory tilt signal β is defined by the relative widths of the prior and the likelihood following De Vrijer et al. (2008):

$$\beta(\rho) = \frac{\sigma_{\mathrm{p}}^2}{\sigma_{\mathrm{p}}^2 + \sigma_{\mathrm{tilt}}^2} \cdot \rho \tag{5.5}$$

To account for the nonlinear increase of the A-effect with tilt angle, the model assumes that the noise in the tilt signal (σ_{tilt}) increases linearly with tilt angle:

$$\sigma_{\mathrm{tilt}}(\rho) = a_0 + a_1|\rho| \tag{5.6}$$

In addition, we made the assumption that the visual noise is independent of line orientation on the retina.

The visual frame stage. To adapt the model to the present testing conditions, it was extended with a stage for the processing of visual panoramic cues. The scheme proposes that a frame line affects the SVV by serving as a visual cue for head tilt, along with the non-visual tilt signal (Howard, 1982). Thus, to incorporate the frame signal in the computation of β, Bayes' rule must be extended with the frame likelihood governed by the frame angle θ_r. Ignoring eye torsion, we can calculate the posterior probability as:

$$P(\rho|\hat{\rho}, \hat{\theta}_r) = k \cdot P(\hat{\rho}|\rho)P(\hat{\theta}_r|\rho)P(\rho) \tag{5.7}$$

where $P(\hat{\theta}_r|\rho)$ represents the frame likelihood.

Since, the polarization direction indicated by a single line is ambiguous, yielding the same effect if rotated by 90 or 180° (Li and Matin, 2005a,b), we conceived the effect of the frame line as an angular distribution with four equally probable cardinal directions (Figure 5.3A, left column, middle panel). The associated frame likelihood function is a circular distribution with one peak at the presented line angle and other peaks at 90° intervals (middle column, middle panel). In other words, each frame line leads to an ambiguous head tilt estimate where four possibilities stand out as most likely. The strength of the frame cue is reflected by the sharpness of the four peaks and the modulation depth in the frame likelihood function. In case of a visual frame with only randomly oriented lines, the angular distribution would be a perfect circle and the frame likelihood function would become entirely flat indicating that, based on the visual frame information, all head tilts are equally likely.

To express the four-fold periodic influence of the frame line, we represented the frame likelihood by a combination of four Gaussian distributions with one peak at the frame line orientation and the other peaks at 90° intervals (see Figure 5.3A):

$$P(\hat{\theta}_r|\rho) = \sum_{n=0}^{3} \frac{1}{\sqrt{2\pi\sigma_f^2}} e^{-(\hat{\theta}_r-\rho-n\cdot 90)^2/(2\sigma_f^2)} \tag{5.8}$$

While technically sound, using Equation 8 makes it impossible to find an analytical expression for β similar to equation 5.5. We therefore calculated the prior, the frame likelihood and the vestibular likelihood numerically using MATLAB (MATLAB 7.0, The Mathworks) and simply multiplied them to obtain the posterior distribution. As a last step, we took the tilt angle with the highest probability, i.e. the maximum a posteriori (MAP), as the final model prediction of the head tilt signal. The orientation of the test line in space, $\hat{\phi}_s$, is obtained by combining the compensatory tilt signal β with the perceived orientation of the test line $\hat{\phi}_r$.

Figure 5.3B, depicting model predictions obtained with the parameter values $\sigma_p = 13°$, $\sigma_f = 10°$, $a_0 = 1.5°$, $a_1 = 0.035$ (close to fit results in the Results section), shows that the predicted effect of the frame line is very small for upright. However, more clearly than in the Mittelstaedt model, the effect becomes more manifest for the tilted conditions. In these conditions, the frame effect is superimposed on a constant bias induced by the prior. Note that the predicted error pattern shows sharp transitions that are not seen in the predictions of the Mittelstaedt model. To understand their occurrence, recall that the posterior function describing the best estimate of head tilt reflects the product of three probability curves: the prior, the vestibular likelihood and the frame likelihood. At each simulated body-tilt angle, the prior and the vestibular likelihood are fixed and the traces show the effect of presenting the frame line at various orientations. Two special cases are easy to understand. First, when observer and frame line are aligned vertically, the frame SVV and the dark SVV are identical. Second, in a tilted body position the dark SVV is a compromise between the prior and the vestibular likelihood. When the frame line is aligned with the dark SVV, the peaks coincide so that the frame has no effect. For other frame tilts, the four-peak frame likelihood can shift the SVV in either direction, depending on the precise location of the peaks with respect to the prior and the vestibular likelihood. Interestingly, when two peaks of the frame likelihood are almost at the same distance from the peak of the product of the prior and the vestibular likelihood, the posterior distribution can become bimodal. The two peaks will be equally high in case that the frame line is tilted exactly 45° with respect to the dark SVV. However, around this bistable position, one peak is higher and taking the MAP yields a final estimate of β. Only a small change in frame line orientation is sufficient to favor the other peak, resulting in a jump in the β estimate when the MAP is taken. These jumps cause the discontinuities shown in Figure 5.3B.

This model was fitted to the data with the least-squares method using the routine fmincon (MATLAB 7.0, The Mathworks). Since leaving all four parameters

free for each subject caused overfitting, parameters σ_p, σ_f and the increase of the noise in the tilt signal (a_1, see Equation 5.6) were fitted at the population level, whereas the offset of the tilt-signal noise (a_0) was allowed to vary freely among our subjects. Fitting parameter a_0 at the population level and a_1 individually did not yield different conclusions and will not be discussed further.

5.3 Results

The goal of the present study was to investigate how tilt cues provided by a visual frame and by the vestibular system contribute to the SVV. We first assessed the effect of frame line orientation on the SVV at three different roll tilt angles and then explored whether these data could be fitted by the two models described in the Methods section.

5.3.1 Overview of main findings

To introduce our results, Figure 5.4 plots frame SVV errors in subject SP as a function of frame-line orientation in space, for each body-tilt angle. As in the model predictions (Figures 5.2B and 5.3B), the horizontal dashed line denotes sign and magnitude of the error in the dark SVV, with positive errors indicating an A-effect and negative errors indicating an E-effect. The vertical dashed line represents the orientation of the dark SVV in space. For upright, the dashed lines almost coincide with the y and x-axis, indicating that the dark SVV is almost flawless. In this subject, the dark SVV showed a small A-effect at 60° tilt and a more pronounced A-effect at 120° tilt, which is consistent with previous reports (Kaptein and Van Gisbergen, 2004, 2005; Schöne, 1964; Udo de Haes, 1970; Van Beuzekom and Van Gisbergen, 2000).

Judged from the vertical distance of the data points to the horizontal dashed lines, which represents the induced changes with respect to the dark SVV, the frame effect depends on two factors: the orientation of the frame line and the degree of body tilt. There was only a modest 90° periodical SVV modulation with the subject in upright position, but a more robust frame effect emerged at 60 and 120° body tilt. Note that frame lines parallel to the dark SVV (see vertical dashed line), and those perpendicular to it, yield a frame SVV equal to the dark SVV. The effect of other frame-line orientations, in the tilted conditions, shows a vertical asymmetry. Unlike the situation in upright, the periodical response pattern has a downward bias. To illustrate: in the 60° tilt panel, varying the frame orientation has a stronger capacity to elicit E-effects than to increase the A-effect seen in the dark SVV. Similarly,

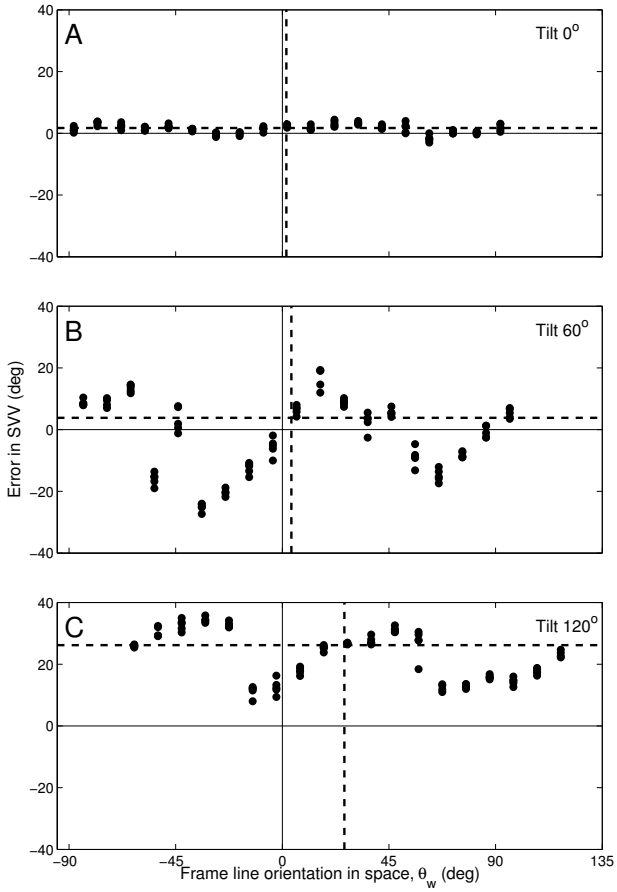

Figure 5.4 *Frame SVV in subject SP. Ideal performance requires that all data (filled circles) fall along the x-axis. Horizontal dashed line: sign and magnitude of error in dark SVV. Vertical dashed line: orientation of the dark SVV in space. A: 0° tilt. Effect of frame line is a modulation of only a few degrees. Small positive errors occur for frame line orientations from -90 to 45° and 0 to 45°. B: 60° tilt. Frame SVV depends on the orientation of the frame line, showing two positive and two negative peaks. Error is negative on average (E-effect) and ranges from about -25 to approximately +20°. C: 120° tilt. Pattern is shifted to the right and upward compared to panel B. Error in SVV is positive on average (A-effect) and ranges from about -10 to approximately +40°.*

in the 120° condition, the maximum decrease in the A-effect clearly exceeds the maximum increase induced by other frame orientations.

The complete data set from all subjects (Figure 5.5) shows common features along with intersubject differences. First, the dark SVV (dashed lines) is almost flawless for upright, but shows small A-effects in some subjects (JG, MV and SP) and E-effects in others (FW and JK) at 60° tilt. At 120° tilt, all subjects have a clear A-effect of at least 20° in their dark SVV. In all subjects, the effect of the frame line is only small for upright but becomes more pronounced in the tilted positions. At these tilt angles, the frame line modulates the SVV with an approximate periodicity of 90°, as in Li and Matin (2005a). In line with the observations in Figure 5.4, the complete data set also illustrates the downward shift in the tilted conditions (60 and 120° tilt), with more data points below the horizontal dashed line than above. This indicates that varying the frame orientation mostly tends to decrease A-effects and to increase E-effects. Finally, it should be noted that the error pattern for the largest tilt condition shows steep discontinuities in several subjects (FW, JG, PB and SP).

5.3.2 Detailed analysis of frame effect

To quantify our data in a first-order approximation, using a descriptive approach like Li and Matin (2005a), we fitted the following sinusoid to our frame SVV data for each subject and condition separately:

$$\mathrm{SVV} = F \cdot \sin(\alpha[\theta_w - \Delta\Phi]) + F_0 \tag{5.9}$$

In this equation F represents the amplitude of the modulation caused by varying the orientation of the frame line in space (θ_w, see Figure 1), α reflects its periodicity, $\Delta\Phi$ denotes the phase shift and F_0 is the vertical offset of the sinusoid. The solid lines in Figure 5.5 represent the fits. Fit parameters and statistical results are summarized in Table 5.1. As can be seen, the fits provide a reasonable description of the strength of the frame effect ($0.13 < R^2 < 0.72$). In line with Li and Matin (2005a) we found that parameter α was generally close to 4 (mean ± SD: 4.2 ± 0.4) thus providing evidence for a 90° periodicity. The magnitude of the frame effect, expressed in fit parameter F, will be discussed in more detail in the next section. Table 5.1 further shows that parameter F_0 is typically smaller than the dark SVV in the 60 and 120° tilt condition, confirming the impression of a downward shift of the frame SVV curve with respect to the dark SVV. Finally, if the frame SVV curve would be a sine wave relative to the dark SVV orientation, parameter $\Delta\Phi$ would be equal to the dark SVV. However, if the frame SVV curve would more resemble a cosine, $\Delta\Phi$ would equal the dark SVV minus 22.5° (a quarter period). Table 5.1 demonstrates that $\Delta\Phi$ is generally smaller than the dark SVV for the tilted conditions, but not by as much as 22.5°. We will further explore the shape of the error pattern in relation to the dark SVV in a later section ("Frames improve large tilt SVV").

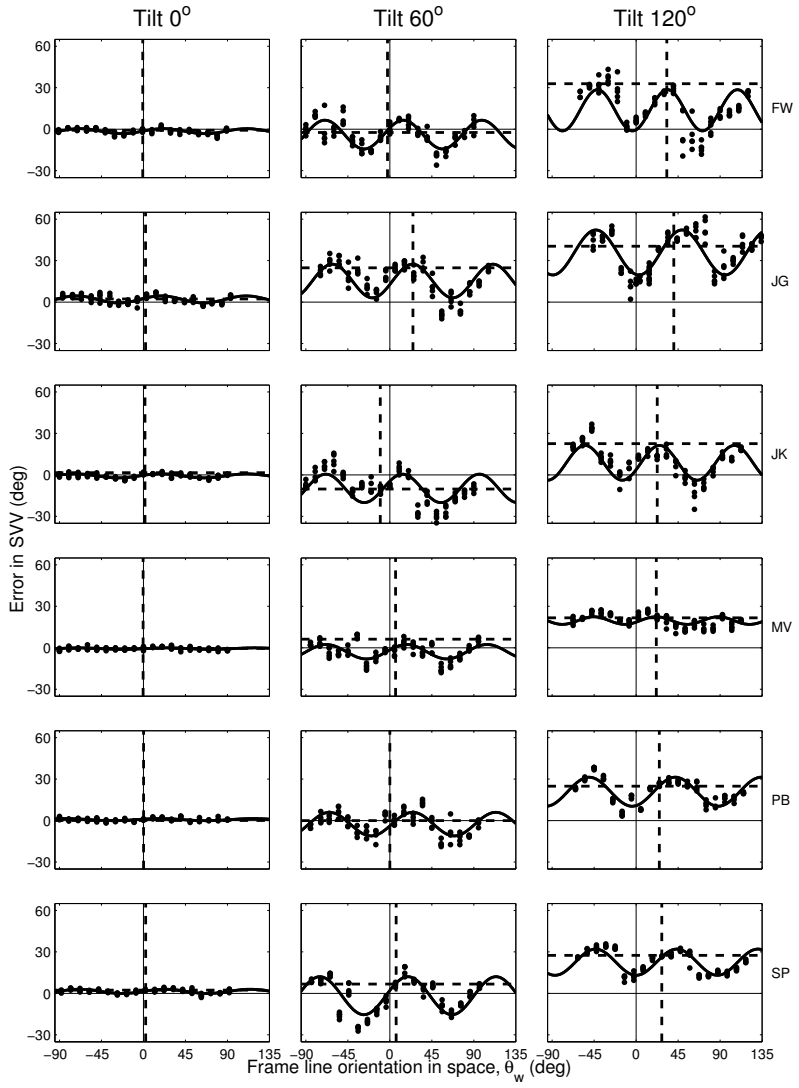

Figure 5.5 *Results from all subjects. Format as in Figure 5.4. Solid lines: sinusoidal fits (see Eqn. 5.9). Left column: 0° tilt. Effect of frame line is small in all subjects. Middle column: 60° tilt. On top of the small offset in the SVV, there is a clear modulation due to the frame line. Right column: 120° tilt. Errors in SVV show a positive bias and a strong modulation due to the orientation of the frame, except in subject MV.*

Body Tilt (deg)	Subject	Dark SVV (deg)	F (deg)	α $(\text{deg})^{-1}$	$\Delta\Phi$ (deg)	F_0 (deg)	R^2	RMSE (deg)
0°	FW	-0.8	1.8 ± 0.2	4.0 ± 0.1	-1 ± 1	-1.4 ± 0.1	0.46	1.3
	JG	2.3	2.6 ± 0.3	3.9 ± 0.1	-4 ± 2	2.0 ± 0.2	0.42	2.1
	JK	1.6	1.5 ± 0.2	3.9 ± 0.1	-4 ± 2	-0.7 ± 0.1	0.43	1.2
	MV	-0.4	0.5 ± 0.2	3.8 ± 0.3	2 ± 4	-0.6 ± 0.1	0.13	1.0
	PB	0.1	0.7 ± 0.1	3.6 ± 0.2	-8 ± 3	0.7 ± 0.1	0.23	1.0
	SP	2.3	1.5 ± 0.2	3.9 ± 0.1	0 ± 1	1.4 ± 0.1	0.51	1.0
60°	FW	-2.4	10.4 ± 0.9	4.3 ± 0.1	-7 ± 1	-3.9 ± 0.6	0.61	5.7
	JG	24.8	12 ± 1	4.2 ± 0.1	3 ± 1	15.1 ± 0.8	0.55	7.7
	JK	-10.2	10 ± 1	4.4 ± 0.1	-7 ± 2	-9.8 ± 0.9	0.40	8.7
	MV	6.2	5.2 ± 0.8	4.2 ± 0.2	-4 ± 2	-2.9 ± 0.6	0.30	5.5
	PB	0.0	8.5 ± 0.9	4.0 ± 0.1	2 ± 1	-2.6 ± 0.6	0.53	5.6
	SP	6.8	14 ± 1	3.8 ± 0.1	-4 ± 1	-1.7 ± 0.7	0.66	6.8
120°	FW	32.9	15 ± 2	4.8 ± 0.1	15 ± 1	14 ± 1	0.49	10.7
	JG	40.4	16 ± 1	3.9 ± 0.1	26 ± 1	35.9 ± 0.9	0.67	8.3
	JK	22.6	12 ± 1	4.5 ± 0.1	5 ± 1	8.7 ± 0.7	0.62	7.0
	MV	21.7	2.7 ± 0.6	5.4 ± 0.2	5 ± 2	19.7 ± 0.4	0.18	4.0
	PB	24.9	10.5 ± 0.7	3.9 ± 0.1	18 ± 1	20.9 ± 0.5	0.72	4.5
	SP	27.5	9.5 ± 0.7	4.1 ± 0.1	22 ± 1	22.6 ± 0.5	0.69	4.4

Table 5.1 *Sinusoidal fits to the frame SVV using* $SVV = F \cdot \sin(\alpha[\theta_w - \Delta\Phi]) + F_0$ *. Parameter* F *is larger in tilted conditions,* α *is close to 4 for all conditions.* $\Delta\Phi$ *and* F_0 *are generally smaller than the dark SVV value, which is shown for comparison.*

Effect of body tilt

We used parameter F as a measure for the magnitude of the frame effect. Consistent with the picture in Figure 5.5, the frame effect was clearly larger in tilted subjects. Figure 5.6 shows how the effect depends on tilt angle. We found a consistent increase from 0° to 60° tilt in all subjects, but when the tilt angle was further increased to 120°, the effect remained roughly constant, with a slight increase in four subjects and some decrease in the other two (MV and SP). A paired t-test confirmed that the difference between the 0° and 60° tilt condition was significant ($P < 0.001$), while the difference across subjects between 60° and 120° tilt was not significant ($P = 0.56$). These findings are roughly in line with previous findings in a slightly different paradigm (Bischof and Scheerer, 1970). These authors observed that the modulating effect of the visual orientation stimulus increased steeply from 0° to 60° tilt, to remain roughly constant up to 120°, followed by a decay at still larger tilt angles.

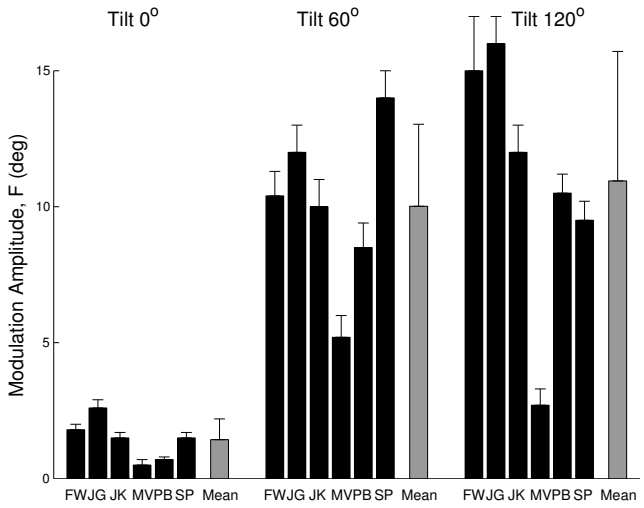

Figure 5.6 *Bar plot of amplitude (F) of fitted sinusoid (Eqn. 5.9) at the three tilted conditions. Amplitude is small for upright and larger for tilted subjects.*

Frame line parallel to dark SVV has no effect

Previous findings in the literature Mittelstaedt (1986, 1988) suggest that the frame line has no effect when it is aligned with the dark SVV. This observation is confirmed by Figure 5.5 which shows that, in almost all subjects and tilt conditions, the frame SVV is close to the intersection of the dashed lines indicating the dark SVV. To test this further, Figure 5.7 shows a scatter plot of the dark SVV against the frame SVV when the frame line was aligned with the dark SVV. A linear regression revealed a significant correlation ($r = 0.97; P < 0.001; n = 18$), a slope that differed not significantly from unity (0.96 ± 0.06) and an intercept not significantly different from zero (-1 ± 1). This confirms that a frame line parallel to the dark SVV does not change the visual verticality percept.

Frame line orientation is misperceived at large body tilt

As explained in Methods, subjects estimated the perceived orientation of the frame line on a clock scale before the SVV adjustment task began. The panels in Figure 5.8 present the verbal orientation estimates from subject FW as a function of the actual orientation in space, for each body-tilt angle separately. The solid lines denote a linear fit through the data. All data points scatter along the regression line with a slope close to one, which means that the accuracy of the estimate does not

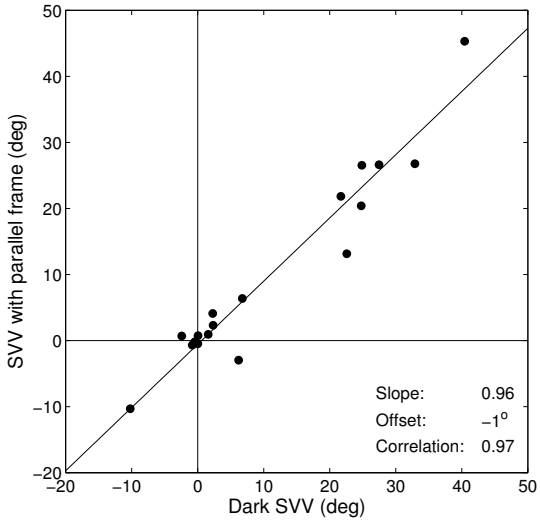

Figure 5.7 *Correlation of errors in the dark SVV and SVV errors when frame line is parallel to the dark SVV. The correlation is significant ($r = 0.97; P < 0.001; n = 18$); the slope is not significantly different from unity (0.96 ± 0.06) and the intercept not significantly different from zero (-1 ± 1).*

depend systematically on the orientation of the frame line. The intercept in the 120° tilt condition, which clearly deviates from zero, denotes a systematic error (A-effect) in the perceived orientation. This analysis was done for all subjects and the resulting intercepts were compared with their dark SVV obtained using the test line. A two-way ANOVA showed a significant main effect of tilt angle ($P < 0.001$), but revealed no significant interaction ($P = 0.47$) nor a difference between the dark SVV and the intercept ($P = 0.59$). This analysis suggests that visual space in a tilted observer is rotated but not distorted, as shown earlier for a short luminous line in chapter 3 and by Van Beuzekom et al. (2001). The present analysis indicates that the visual frame used in our study is subject to the same A-effect (or E-effect) as a short luminous line.

Frames improve large tilt SVV

Since the peripheral frame line is also subject to the A-effect or E-effect (see Figure 5.8), it will look off-vertical to the tilted observer when it is in fact presented world-vertical. We wondered whether, despite this complication, a world-vertical frame line would still improve spatial vision by reducing the systematic errors in

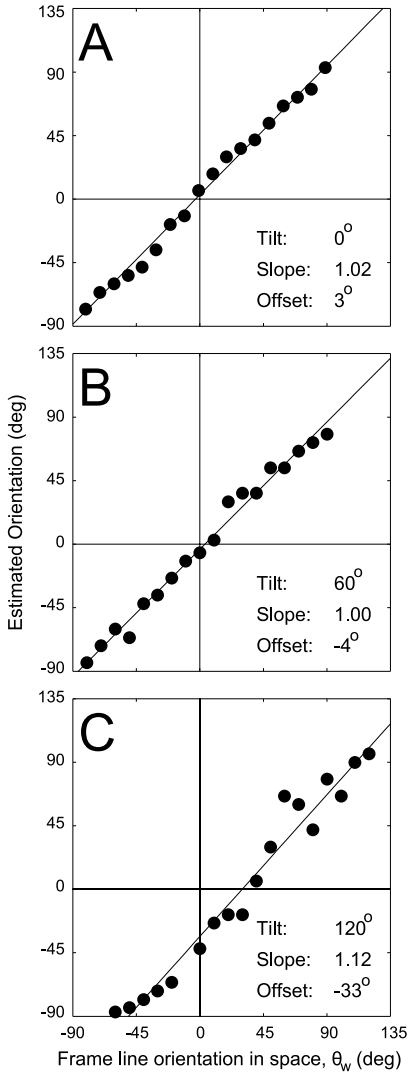

Figure 5.8 *Estimated frame line orientations obtained using verbal scaling, as a function of frame line orientation in space. Clockscale estimates were converted into degrees. A-effects cause underestimation of line orientation leading to a negative intercept. Filled circles: verbal reports. Solid lines: Linear fits. A: 0° tilt. B: 60° tilt. C: 120° tilt.*

the SVV. To explore this, Figure 5.9 plots the population average of the frame SVV error pattern (solid line) and the population average of the dark SVV (white line), each with the standard error of the mean (gray band). For upright the average error is small for all frame line orientations, so there is no clear improvement for a world-vertical frame. In both tilted conditions the frame SVV is more accurate when the frame line is world vertical. For 60° tilt, the improvement was rather small and not significant (paired t-test, $P = 0.23$). At 120° tilt, however, the effect of the world-vertical frame line was stronger and significant (paired t-test, $P = 0.025$). The fourfold periodicity of the frame line effect suggests that a world-horizontal frame

line (dotted line) will also bring improvement to the SVV, but again this effect was only significant at 120° tilt (paired t-test, $P < 0.001$).

The average response curves for the tilted conditions further corroborate the impression of a downward shift in Figure 5.5. For 60° tilt, the mean response curve is shifted downward and has negative peaks reflecting increased E-effects. Furthermore, the frame SVV at 120° tilt seems to be improved by a broad range of visual frame cues around the spatially veridical orientation, whereas the frame line almost never deteriorates performance. These data indicate that, when there is a clear error in the dark SVV, performance can be enhanced by presenting optic frame cues.

Symmetry relation of frame effect is tilt dependent

As we have shown (see Figure 5.7), a frame line parallel to the dark SVV yields a frame SVV virtually identical to the dark SVV. Is the change in the frame SVV for different frame orientations symmetric around the dark SVV? If so, we could characterize the pattern of errors by an odd function, just like a sine, such that frame lines with a more rightward orientation than the dark SVV pull the frame SVV to the right, while frame lines with a more leftward orientation pull the frame SVV to the left. To investigate the symmetry relation, Figure 5.10 shows the difference between the frame SVV and the dark SVV as a function of frame line orientation relative to the dark SVV. Positive y-values represent an increased A-effect and negative values indicate decreased A-effects or increased E-effects. All three data panels, representing the three tilt conditions, confirm the earlier conclusion that a frame line aligned with the dark SVV has no effect. For the zero tilt condition, the mean response to frame lines deviating from this neutral orientation shows a weak modulation resembling an odd function, indicating that frame lines on either side of the dark SVV can induce equal and opposite effects. This picture has changed in the largest tilt condition (120°), where the symmetry in the error curve is best described by an even function, like a cosine wave. This symmetry relation indicates that frame lines to the right or to the left of the dark SVV pull the frame SVV in the same direction and decrease the A-effect. In summary, the error pattern evolves from a description by an odd function at upright to the specification by an even function at 120° tilt.

5.3.3 Model fits

Although the sinusoid fits (Eqn. 5.9) yielded a reasonable first-order account of the characteristics in the data, they served only a descriptive purpose and do not provide a conceptual explanation of the present observations. With the latter objective in mind, we have described two conceptual frameworks in the Methods section,

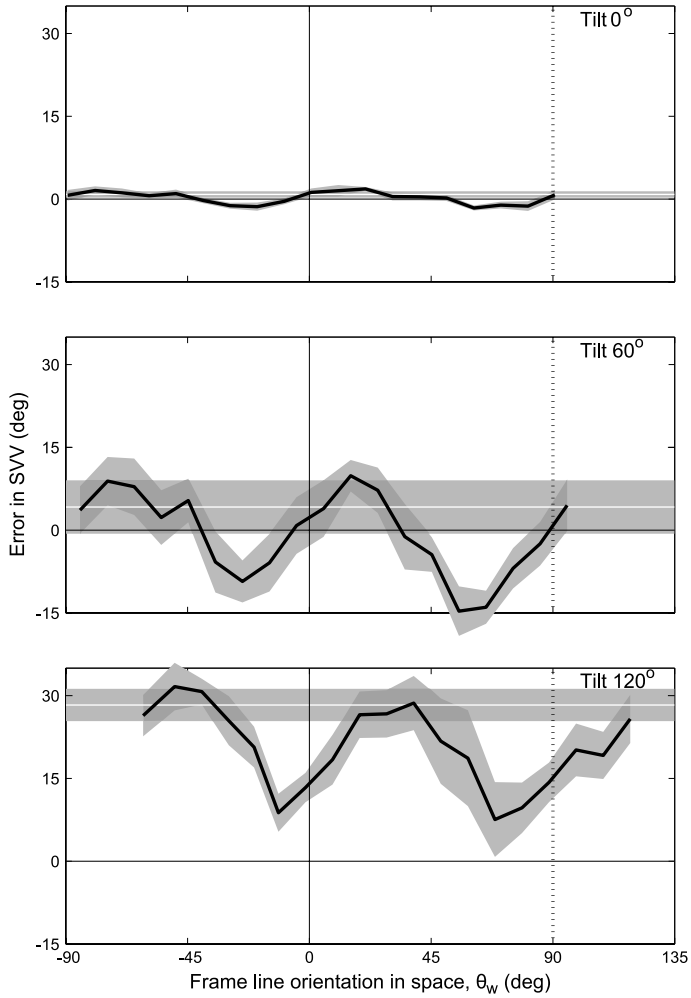

Figure 5.9 *Population average of frame effect and dark SVV. Gray bands: SE. For upright the frame effect is small. The frame effect is larger in 60° and 120° tilted subjects. At 60° tilt, the frame can induce larger E-effects; at 120° tilt the frame reduces the A-effects.*

whose explanatory power will now be tested. In short, the model developed by Mittelstaedt proposes that the visual verticality percept is constructed by adding the vectors representing the effects of gravity, the idiotropic vector and a visual panoramic cue in a weighted fashion. The alternative scheme, the Bayesian model, takes a different perspective on information processing in the present conditions. It assumes that sensory information is noisy and ambiguous and accounts for this by means of probability distributions. It also incorporates prior knowledge that our

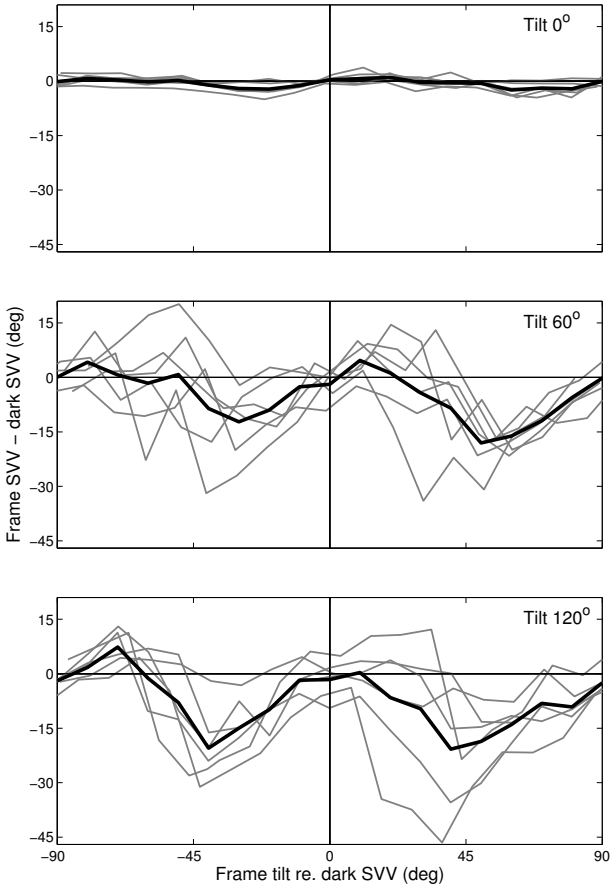

Figure 5.10 *Population average (bold lines) of difference between frame SVV and dark SVV, superimposed on data from single subjects (gray lines). In all panels, the origin denotes a frame line orientation parallel to the dark SVV and a frame SVV equal to the dark SVV. Population average shows a transition from an odd function at upright to a downward shifted even function at 120° tilt.*

head is normally upright and then computes the statistically optimal estimate of body tilt using Bayes' rule.

Subject	M	V_4	R^2	RMSE (deg)
FW	0.14	0.11	0.22	11.8
JG	0.52	0.17	0.71	9.3
JK	0.01	0.12	0.17	11.1
MV	0.21	0.03	0.27	9.5
PB	0.24	0.12	0.35	10.1
SP	0.26	0.11	0.31	11.3

Table 5.2 *Fit parameters (dimensionless) and RMSE and R^2 values for the Mittelstaedt model fits.*

Mittelstaedt model

Figure 5.11 (gray lines) presents fits of Mittelsteadt's model to the observed frame SVV error patterns. The model predicts two effects: a positive constant error (A-effect) that increases with tilt angle, due the idiotropic vector, and a periodic modulation that depends on the orientation of the visual frame line. This is indeed the general picture arising from the data. For example, the model predicts no systematic error and only small effects of the frame line in upright subjects. In the tilted conditions, the model is generally capable of matching the increased size of the modulation. Yet, the individual fits are not always convincing. For example, the constant offsets are not fitted well in some subjects. The reason is that several subjects show substantial E-effects at 60° tilt, which cannot be reproduced by the model. Across tilt conditions, the model's R^2 scores range from to 0.17 to 0.71 (mean ± SD: 0.34 ± 0.19) as listed in Table 5.2. This table also shows that the weight of the idiotropic vector ranges from 0.01 to 0.52 (mean ± SD: 0.23 ± 0.17) across subjects. The effect of this parameter is best understood by comparing subjects JK ($M = 0.01$) and JG ($M = 0.52$) at 120° tilt. Whereas the fit for JK is almost symmetric around the x-axis, the fit curve of JG for this condition shows a substantial vertical offset of about 30°. Fit parameter V_4 represents the effect of the frame line. Its value, which ranges from 0.03 to 0.17 (mean ± SD: 0.11 ± 0.05), highlights the difference between subjects that depend heavily (e.g., JG) or only slightly (e.g., MV) on the visual frame.

Bayesian model

To prevent overfitting (see Methods), we only allowed noise parameter a_0 to vary among subjects, while the remaining three parameters (σ_p, σ_f and a_1) were determined as a best-fit value across subjects. The fit results are shown in Figure 5.11 (black lines). Table 5.3 shows the fit values for σ_p, σ_f and a_1, corresponding to

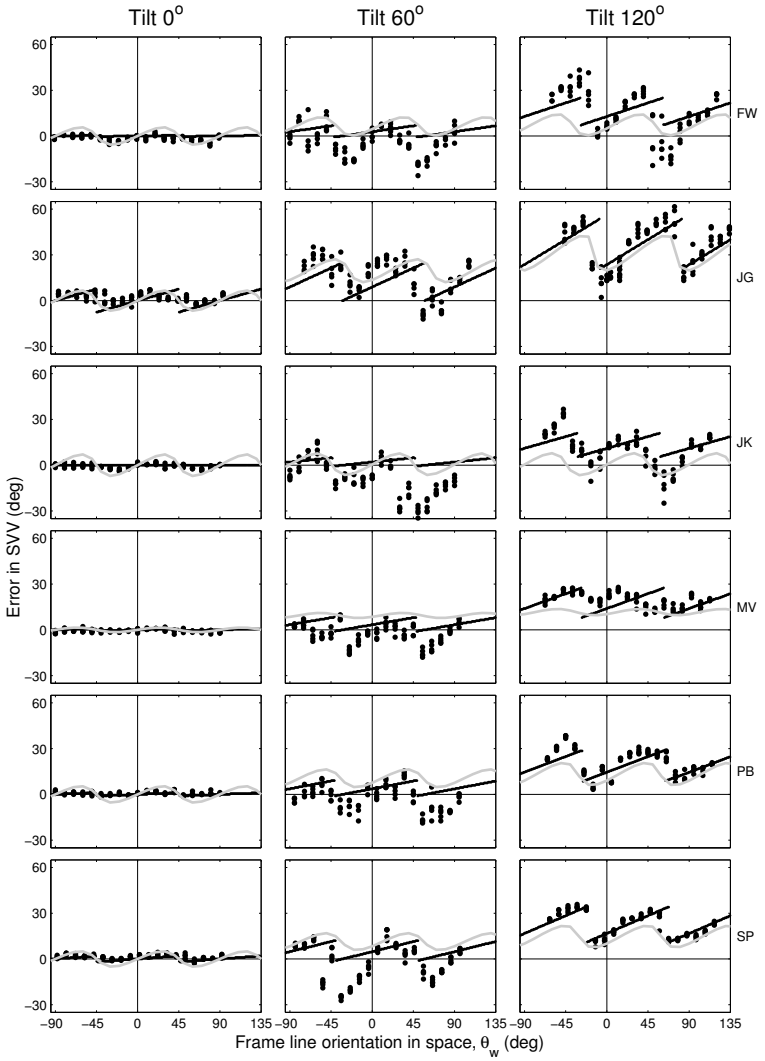

Figure 5.11 *Model fits to frame SVV data. Individual fits of the Mittelstaedt model (gray lines) and the Bayesian model (solid lines). Both models can fit the fourfold periodicity. Mittelstaedt model fits are smooth functions, Bayesian model fits show discontinuities.*

13°, 9.5° and 0.035, respectively. The positive value for parameter a_1 indicates that the noise in the tilt signal must increase with tilt angle if the model is to explain the data. Parameter a_0, which represents the noise level when the subject is upright, ranges from 0.4° to 4.5° (mean ± SD: 1.8° ± 1.5°). The Bayesian model combines

Subject	σ_p (deg)	σ_f (deg)	a_0 (deg)	a_1	R^2	RMSE (deg)
FW			0.9		0.43	10.0
JG			4.5		0.72	9.3
JK			0.4		0.23	10.8
	13	9.5		0.035		
MV			1.3		0.66	6.5
PB			1.5		0.72	6.5
SP			2.1		0.67	7.8

Table 5.3 *Fit parameters and RMSE and R^2 values for the Bayesian model fits.*

the vestibular likelihood, the frame likelihood and the prior distribution to obtain the posterior distribution. We assumed that the Bayesian observer uses the peak of the posterior as the best estimate of head tilt (maximum-a-posteriori, MAP). Since parameter a_1 is positive, the tilt noise increases with tilt angle so that the vestibular likelihood becomes less peaked and broader. As a result, the prior and the frame likelihood are weighted more heavily, causing the constant offset (A-effect) and the frame effect to increase with tilt angle, as shown in all model fits. Along the same lines, when parameter a_0 is larger in a particular subject, the vestibular likelihood is already broader at upright and again the frame likelihood and the prior have more weight. This is exemplified by subject JG, who has the largest a_0 value and thus a relatively noisy vestibular tilt signal. Consequently, this subject shows the largest bias, induced by the prior, and the strongest visual frame effect, induced by the frame likelihood. For all subjects, fit lines and data match best for 0 and 120° tilt, as in the Mittelstaedt model. For upright, modulations are very small, while at 120° tilt they are very pronounced with sometimes abrupt transitions. The model fits these sharp transitions quite accurately in subjects FW, JG, PB and SP. However, this model also has difficulties in accounting for the 60° tilt data, which is mainly due to its inability to simulate the E-effects regularly found at this tilt angle. Yet, everything being taken into account, the Bayesian model provides a better fit to the data than Mittelstaedt's vector model, as illustrated by the higher R^2 values in each individual subject, ranging from 0.23 to 0.72 (mean ± SD: 0.57 ± 0.20). In addition, the individual RMSE values based on the Bayesian fits, shown in Table 5.3, are lower than the corresponding values of the Mittelstaedt model fit.

5.4 Discussion

5.4.1 Main findings and relation to earlier studies

We studied the interaction between the effects of body tilt and a visual frame line on the subjective visual vertical (SVV) at three different tilt angles using a broad range of visual frame orientations. For comparison, we also collected SVV settings in full darkness. In line with earlier reports on the SVV (Kaptein and Van Gisbergen, 2004, 2005; Schöne, 1964; Udo de Haes, 1970; Van Beuzekom and Van Gisbergen, 2000), we found that the dark SVV was almost flawless in upright subjects, showed small A-effects or even E-effects at 60° tilt and large A-effects at 120° tilt. With regard to the frame SVV we made the following observations.

First, we observed that frame lines aligned with or perpendicular to the dark SVV had no effect on the perception of verticality. This result is consistent with data obtained in tilted subjects by Mittelstaedt (1986) and by Eggert (1998).

Second, we found that the frame line acted as an attractor for small deviations from the dark SVV, whereas frame line tilts beyond 45° and up to 90° relative to the dark SVV repelled the frame SVV. At a frame tilt of 90° there was no effect. Thus, a single frame line modulates the SVV in a cyclical fashion with a 90° period as if indicating two potential up directions corresponding to its orientation and two perpendicular to it. This 90° periodicity is in agreement with results from Bischof (1974), Bischof and Scheerer (1970) and Eggert (1998), who tested the effect of a stripe pattern on the visual verticality percept of roll tilted subjects. In addition, this four-fold periodicity was also observed by Li and Matin (2005a), who tested the SVV in upright observers using a single frame line. The observation by Bischof (1974) that the axis perpendicular to a parallel stripe pattern has a less strong attracting effect than the main axis was not seen in our data.

Our third finding was that the effect of the frame line became substantially larger in tilted subjects, while retaining the 90° periodicity. The larger frame effect in tilted subjects has also been reported earlier in studies using smaller tilt angles than the present study (Asch and Witkin, 1948b; Corbett and Enns, 2006). This finding is also consistent with reports by Bischof and Scheerer (1970) and Bischof (1974) showing that the effect of the stripe pattern increased with body tilts up to 60°, then leveled off and decreased again beyond tilts of 120°.

Finally, we found that the frame line in tilted conditions usually led to a reduction of the A-effect. At 60° tilt, this trend took the form of E-effects in some subjects. We further established that the symmetry relation of the frame SVV pattern changed from a sine function at upright to a cosine-like function at 120° tilt. As far as we know, this effect has not been reported in the earlier literature. Furthermore, we made the novel observation of steep discontinuities in the frame SVV

error pattern in several subjects in the 60 and 120° tilt condition.

We will now discuss these observations in terms of the two spatial orientation models put central in this study.

5.4.2 Modeling aspects

Optic-vestibular interactions subserving spatial vision

The vestibular sensors that are involved in spatial orientation have some limitations. For example, the otoliths cannot discriminate inertial forces caused by tilt or translation and the semicircular canals work as a high-pass filter and thus cannot sense low-frequent rotations. It has therefore been proposed that the brain combines information from various sensory modalities to obtain optimal estimates of the motion variables (Droulez and Darlot, 1989; Glasauer and Merfeld, 1997; Merfeld et al., 1993; Vingerhoets et al., 2006, 2007; Zupan et al., 2002). While these studies have been mainly concerned with vestibular interactions, our present study focuses on the visual-vestibular interactions. That optic flow information can be used to complement the head angular velocity signal of the canals was shown by Dichgans and colleagues (1972). They reported that upright subjects, viewing a large visual pattern rotating about the roll body-axis, felt as if they were moving continuously in the opposite direction and that the visual vertical could deviate by as much as 15° from true vertical.

Likewise, optostatic cues can complement the head tilt signals of the otoliths and thus affect the tilt percept. This effect is exploited in amusement parks where tilted houses are used to impose a percept of body tilt in actually upright observers. That even simpler visual orientation cues such as a square frame or even a large single visual line can affect the verticality percept, probably has an ecological basis. Natural scenes contain an overrepresentation of world-horizontal and world-vertical orientations (Coppola et al., 1998; Van der Schaaf and Van Hateren, 1996). The brain can use this information, inferring that the optostatic cues most likely represent world-horizontal or world-vertical orientations. Accordingly, when asked to set a line parallel to the direction of gravity, the setting will deviate in the direction indicated by the visual frame. How this notion is implemented in the two models tested in the present study will be discussed next.

Optic-vestibular sensor fusion in the Mittelstaedt and the Bayesian model

Mittelstaedt (1986, 1988) extended his model to incorporate the effect of visual frame cues on the SVV. In his model, the frame SVV is a weighted sum of three factors: the direction of gravity, the idiotropic vector and the upward direction indicated by the visual scene. Mittelstaedt tested this model only in 90° tilted subjects.

In the present study we extended the test conditions to three different tilt angles: 0, 60 en 120°. Along with Mittelstaedt's idiotropic vector model, we also explored a so-called Bayesian model. Bayesian frameworks have successfully been applied to explain performance in various perception and action domains (Ernst and Banks, 2002; Knill and Pouget, 2004; Niemeier et al., 2003; Stocker and Simoncelli, 2006; Weiss et al., 2002). These models combine various sources of information, to optimize performance in the context of optimal observer theory. A Bayesian reinterpretation of the idiotropic vector concept was first formulated by Eggert (1998) and tested in modified form by De Vrijer et al. (2008). In our Bayesian model, the perception of verticality is based on the vestibular tilt signal, which is assumed to be veridical but corrupted by noise, an a priori assumption that the body is usually upright, and a four-peak frame likelihood representing an inbuilt assumption that natural visual contour distributions have peaks at orientations that are parallel and perpendicular to gravity.

Both models have much in common. In the Mittelstaedt model the A-effect is explained by the idiotropic vector that represents the tendency of tilted subjects to include the long-body axis as a reference for the direction of gravity. In the Bayesian model, the A-effect is the result of including prior knowledge that one is most likely to be upright. While the formulation is different, the idiotropic vector and the prior are closely related. For example, their effect is quite similar as both models would predict that in zero-gravity subjects align the SVV with the long body axis. Moreover, Eggert (1998) has shown that with certain assumptions, his Bayesian scheme can yield identical results as the Mittelstaedt (1983) model. In addition, the visual frame stages of both models are also quite similar, by relying on a feed-forward structure where the vestibular and the visual signal are combined in a relatively simple way. The basic idea can best be understood at upright. In this situation, the **G** and **M** vector in the Mittelstaedt model are aligned and consequently changing the **P** vector has not much effect. Likewise, in the Bayesian model the peaks of the vestibular likelihood and the prior coincide, leading to a limited influence of the frame likelihood. Along this line, it is interesting to recall that the frame effect is larger in the tilted conditions (see Figure 5.6), suggesting that the brain assigns relatively more weight to the visual information when tilted. Both models can replicate this effect.

The difference between both models originates mainly in the underlying assumptions. Mittelstaedt (1983) proposed that the egocentric bias serves to correct for putative systematic errors in the tilt signal caused by unequal numbers of hair cells in the saccule and the utricle. Note that we followed Mittelstaedt (1986) by not including this putative unbalance, simply conceiving the SVV as a weighted sum of the gravity vector, the idiotropic vector and the visual panorama vector. In the

Bayesian scheme the prior is an element in an optimal strategy to handle noisy tilt signals. The result of the combination of prior information and sensory information is that the final percept is very stable when the prior and the sensory information are compatible, in this case for tilt angles close to upright. This is useful when the brain has to combine the relatively noisy tilt information with the very precise retinal information on line orientation. As these small tilt angles occur most often, this would be a smart strategy to optimize performance in daily life. The downside of this computational strategy is that it goes at the expense of systematic errors at large tilt angles that occur only rarely.

Both models performed well in explaining the increase of the frame effect with tilt angle and both replicated the four-fold periodicity in our data. The prediction of both models that a frame line aligned with the dark SVV has no effect was also borne out by the data. From a statistical perspective, the Bayesian model performed somewhat better than the Mittelstaedt model, with an average R^2 value of 0.57 (SD: 0.20) versus 0.34 (SD: 0.19). Considering that the Bayesian model required fewer free parameters than the Mittelstaedt model (9 vs 12), a case can therefore be made in favor of the Bayesian scheme. That is not to say that it always provided the best fit, as demonstrated in Figure 5.11. At any rate, both models which commonly suggest that verticality perception is based on visual, vestibular and egocentric references, provide an inspiring background to guide further investigation of the optic vestibular signal fusion underlying visual verticality perception.

Possible model refinements

To our knowledge, this study is the first that qualitatively compares model predictions and frame effect data at three different tilt angles. Although the models performed relatively well, a few reservations should be made. The models could not explain all the idiosyncracies of the data (see Figure 5.11). Moreover, the models have severe difficulties in explaining the changing symmetry relations in the error pattern (see Figure 5.10). We do not know whether this may relate to our experimental testing procedure, e.g. only using clockwise tilt angles, or to our measurement of the dark SVV which was only established at the beginning of each experiment. We cannot rule out that the dark SVV has changed during the course of the experiment, which could explain both the vertical and the horizontal asymmetry in our data (Figure 5.10). For a more decisive conclusion on model performance, measurements at a broader range of tilt angles and keeping track of the dark SVV will be required in future work.

In the models, we assumed that the orientation of the frame line and the SVV test line are perceived without any systematic bias related to ocular counterroll that occurs during head tilt (Bockisch and Haslwanter, 2001; Miller 2nd and Graybiel,

1971). Wade and Curthoys (1997) found that ocular counterroll has an effect on the interpretation of the orientation of visual stimuli, which could possibly help to explain the E-effects that we observed at 60° tilt. A further refinement of the models could be made by adding a provision for ocular counterroll.

An interesting implication from the Bayesian approach is the possibility of bistable response modes. The reason for this bistability is related to the four-peak frame likelihood. The final estimate of tilt-compensation signal β is taken as the maximum of the posterior distribution which is constructed by multiplying the prior, the vestibular likelihood and the frame likelihood. When two peaks of the frame likelihood are at about the same distance from the peak of the product of the prior and the vestibular likelihood, the posterior distribution has two peaks, representing two possible response types. Bistable responses have been reported earlier in the visual literature in slant perception (Van Ee et al., 2003) but also in the SVV in chapter 3 and by Kaptein and Van Gisbergen (2005). The latter authors reported that subjects usually do not switch response mode within a single trial, which could explain why we did not find bimodal response distributions in the present study. The predicted bistablity suggests a possibility to distinguish between the two models in future work.

5.5 Appendix

5.5.1 Mittelstaedt model

As outlined in the Methods section, Mittelstaedt (1986, 1988) proposed that the effect of visual cues, the idiotropic vector and gravity on the SVV can modeled by representing these cues as vectors: $\mathbf{G} = (0, \sin\rho, \cos\rho)$, $\mathbf{M} = (0, 0, M)$ and $\mathbf{P} = (0, V\sin\theta_r, V\cos\theta_r)$. The luminous line that serves as indicator of the SVV is also conceived as a vector: $\mathbf{L} = (0, \sin\beta, \cos\beta)$.

These definitions of $\mathbf{P}$ and $\mathbf{L}$ only hold when both the visual scene and the indicator are uniquely polarized in one direction. The visual-frame lines used in our experiment, however, have the same influence on the verticality percept when they are rotated by 180° or 90° (see Li and Matin, 2005a,b) and thus may elicit effects that are functions of multiples of θ_r. To account for this fact, $\mathbf{L}$ and $\mathbf{P}$ can be extended as follows:

$\mathbf{L} = (0, \sum_n L_n \sin(n\beta), \sum_n L_n \cos(n\beta))$ and $\mathbf{P} = (0, \sum_n P_n \sin(n\theta_r), \sum_n P_n \cos(n\theta_r))$.

In the model, the observer rotates the indicator $\mathbf{L}$, until the following cross-product equals zero:

$$\mathbf{L} \times (\mathbf{G} + \mathbf{M} + \mathbf{P}) = \mathbf{L} \times (\mathbf{G} + \mathbf{M}) + \mathbf{L} \times \mathbf{P} = 0 \tag{5.10}$$

Further specification of the first term, denoted as gravito-idiotropic term, yields:

$$\sum_n L_n \sin(n\beta) \cdot (G\cos\rho + M) - \sum_n L_n \cos(n\beta) \cdot G\sin\rho \tag{5.11}$$

Similarly, specifying the second term gives:

$$\sum_n L_n P_n \sin(n\beta) \cdot \cos(n\theta_r) - \sum_n L_n P_n \cos(n\beta) \cdot \sin(n\theta_r) \tag{5.12}$$

which can be simplified to:

$$\sum_n L_n P_n \sin(n(\beta - \theta_r)) \tag{5.13}$$

In Mittelstaedt's model, gravity is normalized ($G = 1$) and it is assumed that only the first order term of the gravito-idiotropic contribution adds to the complete equation that determines the SVV:

$$\sin\beta \cdot (\cos\rho + M) - \cos\beta\sin\rho + \sum_n V_n \sin(n(\beta - \theta_r)) = 0 \tag{5.14}$$

with $V_n = \frac{P_n L_n}{L_1}$. In line with the findings from Li and Matin (2005a,b) we found a four-fold periodicity, which implies that components V_1, V_2 and V_3 of our simple frame stimulus did not contribute significantly to our fits. In the present testing conditions, Equation 5.14 can therefore be simplified to:

$$\sin\beta \cdot (\cos\rho + M) - \cos\beta\sin\rho + V_4 \sin 4(\beta - \theta_r) = 0 \tag{5.15}$$

Acknowledgements We thank Hans Kleijnen, Ger van Lingen, Stijn Martens and Günter Windau for technical support. This work was supported by Radboud University Nijmegen (NICI and FNWI). Further support came from grants of the Netherlands Organisation for Scientific Research and the Human Frontier Science Program awarded to W.P. Medendorp.

Bibliography

Angelaki DE and Dickman JD. Spatiotemporal processing of linear acceleration: primary afferent and central vestibular neuron responses. *J Neurophysiol* 84: 2113–2132, 2000.

Angelaki DE and Hess BJ. Three-dimensional organization of otolith-ocular reflexes in rhesus monkeys. I. Linear acceleration responses during off-vertical axis rotation. *J Neurophysiol* 75: 2405–2424, 1996a.

Angelaki DE and Hess BJ. Three-dimensional organization of otolith-ocular reflexes in rhesus monkeys. II. Inertial detection of angular velocity. *J Neurophysiol* 75: 2425–2440, 1996b.

Angelaki DE, McHenry MQ, Dickman JD, Newlands SD, and Hess BJM. Computation of intertial motion: Neural strategies to resolve ambiguous otolith information. *J Neurosci* 19: 316–327, 1999.

Angelaki DE, Wei M, and Merfeld DM. Vestibular discrimination of gravity and translational acceleration. *Ann N Y Acad Sci* 942: 114–127, 2001.

Asch SE and Witkin HA. Studies in space orientation. I. Perception of the upright with displaced visual fields. *J Exp Psychol* 38: 325–337, 1948a.

Asch SE and Witkin HA. Studies in space orientation. II. Perception of the upright with displaced visual fields and with the body tilted. *J Exp Psychol* 38: 455–477, 1948b.

Aubert H. Eine scheinbare bedeutende Drehung von Objecten bei Neigung des Kopfes nach rechts oder links. *Virchows Arch* 20: 381–393, 1861.

Beh HC, Wenderoth PM, and Purcell AT. The angular function of the rod-and-frame illusion. *Percept Psychophys* 9: 353–355, 1971.

Bischof N. Optic-vestibular orientation to the vertical. In: *Handbook of sensory physiology, Vol IV. Vestibular system, Part 2. Psychophysics, applied aspects and*

general interpretations, edited by Kornhuber H. Berlin-New York: Springer-Verlag, 1974, p. 155–190.

Bischof N and Scheerer E. Systems analysis of optic-vestibular interaction in the perception of verticality. *Psychol Forsch* 34: 99–181, 1970.

Bockisch CJ and Haslwanter T. Three-dimensional eye position during static roll and pitch in humans. *Vision Res* 41: 2127–2137, 2001.

Bockisch CJ, Straumann D, and Haslwanter T. Human 3-D aVOR with and without otolith stimulation. *Exp Brain Res* 161: 358–367, 2005.

Bortolami SB, Pierobon A, Dizio P, and Lackner JR. Localization of the subjective vertical during roll, pitch and recumbent yaw body tilt. *Exp Brain Res* 173: 364–373, 2006a.

Bortolami SB, Rocca S, Daros S, Dizio P, and Lackner JR. Mechanisms of human static spatial orientation. *Exp Brain Res* 173: 612–622, 2006b.

Bos JE and Bles W. Theoretical considerations on canal-otolith interaction and an observer model. *Biol Cybern* 86: 191–207, 2002.

Brown JH. Magnitude estimation of angular velocity during passive rotation. *J Exp Psychol* 72: 169–172, 1966.

Carandini M. Measuring the brain's assumptions. *Nat Neurosci* 9: 468–470, 2006.

Cian C, Raphel C, and Barraud PA. The role of cognitive factors in the rod-and-frame effect. *Perception* 30: 1427–1438, 2001.

Clark B and Graybiel A. Factors contributing to the delay in the perception of the oculogravic illusion. *Am J Psychol* 79: 377–388, 1966.

Coppola DM, Purves HR, McCoy AN, and Purves D. The distribution of oriented contours in the real world. *Proc Natl Acad Sci USA* 95: 4002–4006, 1998.

Corbett JE and Enns JT. Observer pitch and roll influence: the rod and frame illusion. *Psychon Bull Rev* 13: 160–165, 2006.

Cullen KE, Rey CG, Guitton D, and Galiana HL. The use of system identification techniques in the analysis of oculomotor burst neuron spike train dynamics. *J Comput Neurosci* 3: 347–368, 1996.

Curthoys IS. The delay of the oculogravic illusion. *Brain Res Bull* 40: 407–412, 1996.

Darlot C, Denise P, Droulez J, Cohen B, and Berthoz A. Eye movements induced by off vertical axis rotation (OVAR) at small angles of tilt. *Exp Brain Res* 73: 91–105, 1988.

De Vrijer M, Medendorp WP, and Van Gisbergen JAM. Shared computational mechanism for tilt compensation accounts for biased verticality percepts in motion and pattern vision. *J Neurophysiol* 99: 915–930, 2008.

Denise P, Darlot C, Droulez J, Cohen B, and Berthoz A. Motion perceptions induced by off-vertical axis rotation (OVAR) at small angles of tilt. *Exp Brain Res* 73: 106–114, 1988.

Dichgans J, Held R, Young LR, and Brandt T. Moving visual scenes influence the apparent direction of gravity. *Science* 178: 1217–1219, 1972.

DiLorenzo JR and Rock I. The rod-and-frame effect as a function of the righting of the frame. *J Exp Psychol Hum Percept Perform* 8: 536–546, 1982.

Droulez J and Darlot C. The geometric and dynamic implications of the coherence constraints in three-dimensional sensorimotor interactions. In: *Attention and Performance XIII*, edited by Jeannerod M. New York: Erlebaum, 1989, p. 495–526.

Dyde RT, Jenkin MR, and Harris LR. The subjective vertical and the perceptual upright. *Exp Brain Res* 173: 612–622, 2006.

Dyde RT and Milner AD. Two illusions of perceived orientation: one fools all of the people some of the time; the other fools all of the people all of the time. *Exp Brain Res* 144: 518–527, 2002.

Ebenholtz SM. Determinants of the rod-and-frame effect: the role of retinal size. *Percept Psychophys* 22: 531–538, 1977.

Ebenholtz SM and Benzschawel TL. The rod-and-frame effect and induced head tilt as a function of observation distance. *Percept Psychophys* 22: 491–496, 1977.

Eggert T. *Der Einfluss orientierter Texturen auf die subjektive Vertikale und seine systemtheoretische Analyse* (Ph.D. thesis). Munich, Germany: Munich Technical University, 1998.

Ehrenstein WH and Ehrenstein A. Psychophysical methods. In: *Modern techniques in neuroscience research*, edited by Windhorst U and Johansson H. Berlin: Springer-Verlag, 1999, p. 1211–1241.

Ernst MO and Banks MS. Humans integrate visual and haptic information in a statistically optimal fashion. *Nature* 415: 429–433, 2002.

Fernandez C and Goldberg J. Physiology of peripheral neurons innervating semicircular canals of the squirrel monkey: II. Response to sinusoidal stimulation and dynamics of peripheral vestibular system. *J Neurophysiol* 34: 661–675, 1971.

Fernández C and Goldberg JM. Physiology of peripheral neurons innervating otolith organs of the squirrel monkey. I. Response to static tilts and to long-duration centrifugal force. *J Neurophysiol* 39(5): 970–984, 1976.

Fisher SK, Ciuffreda KJ, Tannen B, and Super P. Stability of tonic vergence. *Invest Ophthalmol Vis Sci* 29: 1577–1581, 1988.

Fitzpatrick RC and Day BL. Probing the human vestibular system with galvanic stimulation. *J Appl Physiol* 96: 2301–2316, 2004.

Freeman TC. Transducer models of head-centred motion perception. *Vision Res* 41: 2741–2755, 2001.

Furman JM, Schor RH, and Schumann TL. Off-vertical axis rotation: a test of the otolith ocular reflex. *Ann Otol Rhinol Laryngol* 101: 643–650, 1992.

Glasauer S. Interaction of semicircular canals and otoliths in the processing structure of the subjective zenith. *Ann N Y Acad Sci* 656: 847–849, 1992.

Glasauer S. Linear acceleration perception: frequency dependence of the hilltop illusion. *Acta Otolaryngol Suppl* 520: 37–40, 1995.

Glasauer S and Merfeld DM. Modeling three dimensional vestibular responses during complex motion stimulation. In: *Three-Dimensional Kinematics of Eye, Head and Limb Movement*, edited by Fetter M, Misslich H, Tweed D, and Haslwanter T. Amsterdam: Harwood Academic, 1997, p. 387–398.

Goldberg J and Fernandez C. Physiology of peripheral neurons innervating semicircular canals of the squirrel monkey: I. Resting discharge and response to constant angular accelerations. *J Neurophysiol* 34: 635–660, 1971.

Graybiel A and Brown R. The delay in visual reorientation following exposure to a change in direction of resultant force on a human centrifuge. *J Gen Psychol* 45: 143–150, 1951.

Green AM and Angelaki DE. Resolution of sensory ambiguities for gaze stabilization requires a second neural integrator. *J Neurosci* 23: 9265–9275, 2003.

Green DM and Swets JA. *Signal Detection Theory and Psychophysics*. New York: Wiley, 1966.

Groen EL, Jenkin HL, and Howard IP. Perception of self-tilt in a true and illusory vertical plane. *Perception* 31: 1477–1490, 2002.

Guedry FE. Psychophysics of vestibular sensation. In: *Handbook of sensory physiology, Vol IV. Vestibular system, Part2. Psychophysics, applied aspects and general interpretations*, edited by Kornhuber HH. Berlin-New York: Springer-Verlag, 1974, p. 3–154.

Haslwanter T, Jaeger R, Mayr S, and Fetter M. Three-dimensional eye-movement responses to off-vertical axis rotations in humans. *Exp Brain Res* 134: 96–106, 2000.

Hess BJ and Angelaki DE. Inertial processing of vestibulo-ocular signals. *Ann NY Acad Sci* 871: 148–161, 1999.

Howard IP. *Human visual orientation*. New York: Wiley, 1982.

Howard IP and Childerson L. The contribution of motion, the visual frame, and visual polarity to sensations of body tilt. *Perception* 23: 753–762, 1994.

Israel I, Chapuis N, Glasauer S, Charade O, and Berthoz A. Estimation of passive horizontal linear whole-body displacement in humans. *J Neurophysiol* 70: 1270–1273, 1993.

Israel I, Chapuis N, Glasauer S, Charade O, and Berthoz A. Spatial memory and path integration studied by self-driven passive linear displacement. I. Basic properties. *J Neurophysiol* 77: 3180–3192, 1997.

Jaggi-Schwarz K and Hess BJM. Influence of dynamic tilts on the perception of earth-vertical. *Exp Brain Res* 149: 340–350, 2003.

Jaggi-Schwarz K, Ortega M, and Hess BJM. Reciprocal error behaviour in estimated body position and subjective visual vertical. *Exp Brain Res* 150: 122–125, 2003.

Kaptein RG and Van Gisbergen JAM. Interpretation of a discontinuity in the sense of verticality at large body tilt. *J Neurophysiol* 91: 2205–2214, 2004.

Kaptein RG and Van Gisbergen JAM. Nature of the transition between two modes of external space perception in tilted subjects. *J Neurophysiol* 93: 3356–3369, 2005.

Keusch S, Hess BJ, and Jaggi-Schwarz K. Direction specific error patterns during continuous tracking of the subjective visual vertical. *Exp Brain Res* 155: 283–290, 2004.

Klein SA. Measuring, estimating and understanding the psychometric function: a commentary. *Percept Psychophys* 63: 1421–1455, 2001.

Klier EM, Hess BJ, and Angelaki DE. Differences in the accuracy of human visuospatial memory after yaw and roll rotations. *J Neurophysiol* 95: 2692–2697, 2006.

Knill DC and Pouget A. The Bayesian brain: the role of uncertainty in neural coding and computation. *Trends Neurosci* 27: 712–719, 2004.

Körding KP and Wolpert DM. Bayesian integration in sensorimotor learning. *Nature* 426: 244–247, 2004.

Kushiro K, Dai M, Kunin M, Yakushin SB, Cohen B, and Raphan T. Compensatory and orienting eye movements induced by off-vertical axis rotation (OVAR) in monkeys. *J Neurophysiol* 88: 2445–2462, 2002.

Lackner JR and Graybiel A. Postural illusions experienced during Z-axis recumbent rotation and their dependence upon somatosensory stimulation of the body surface. *Aviat Space Environ Med* 49: 484–488, 1978a.

Lackner JR and Graybiel A. Some influences of touch and pressure cues on human spatial orientation. *Aviat Space Environ Med* 49: 798–804, 1978b.

Laurens J and Droulez J. Bayesian processing of vestibular information. *Biol Cybern* 96: 389–405, 2007.

Li W and Matin L. The rod-and-frame effect: the whole is less than the sum of its parts. *Perception* 34: 699–716, 2005a.

Li W and Matin L. Visually perceived vertical (VPV): induced changes in orientation by 1-line and 2-line roll-tilted and pitched visual fields. *Vision Res* 45: 2037–2057, 2005b.

Loë PR, Tomko DL, and Werner G. The neural signal of angular head position in primary afferent vestibular nerve axons. *J Physiol* 230: 29–50, 1973.

MacNeilage PR, Banks MS, Berger DR, and Bülthoff HH. A Bayesian model of the disambiguation of gravitoinertial force by visual cues. *Exp Brain Res* 179: 263–290, 2007.

Mast F and Jarchow T. Perceived body position and the visual horizontal. *Brain Res Bull* 40: 393–398, 1996.

Matin L and Li W. Multimodal basis for egocentric spatial localization and orientation. *J Vestib Res* 5: 499–518, 1995.

Mayne R. A systems concept of the vestibular organs. In: *Handbook of sensory physiology, Vol IV/2. Vestibular system, Part 2. Psychophysics, applied aspects and general interpretations*, edited by Kornhuber H. Berlin-New York: Springer-Verlag, 1974, p. 493–580.

Medendorp WP, Tweed DB, and Crawford JD. Motion parallax is computed in the updating of human spatial memory. *J Neurosci* 23: 8135–8142, 2003.

Medendorp WP, Van Gisbergen JAM, and Gielen CC. Human gaze stabilisation during active head translations. *J Neurophysiol* 87: 295–304, 2002.

Medendorp WP, Van Gisbergen JAM, Van Pelt S, and Gielen CC. Context compensation in the vestibuloocular reflex during active head rotations. *J Neurophysiol* 84: 2904–2917, 2000.

Merfeld DM. Modeling human vestibular responses during eccentric rotation and off vertical axis rotation. *Acta Otolaryngol* 520: 354–359, 1995a.

Merfeld DM. Modeling the vestibulo-ocular reflex of the squirrel monkey during eccentric rotation and roll tilt. *Exp Brain Res* 106: 123–134, 1995b.

Merfeld DM, Park S, C Gianna-Poulin FOB, and Wood S. Vestibular perception and action employ qualitatively different mechanisms: I. Frequency response of VOR and perceptual responses during translation and tilt. *J Neurophysiol* 94: 186–198, 2005a.

Merfeld DM, Park S, Gianna-Poulin C, Black FO, and Wood S. Vestibular perception and action employ qualitatively different mechanisms. II VOR and perceptual responses during combined tilt and translation. *J Neurophysiol* 94: 199–205, 2005b.

Merfeld DM, Young LR, Oman CM, and Shelhamer MJ. A multidimensional model of the effect of gravity on the spatial orientation of the monkey. *J Vestib Res* 3: 141–161, 1993.

Merfeld DM, Zupan L, and Peterka RJ. Humans use internal models to estimate gravity and linear acceleration. *Nature* 398: 615–618, 1999.

Merfeld DM and Zupan LH. Neural processing of gravito-inertial cues in humans. III. Modeling tilt and translation responses. *J Neurophysiol* 87: 819–833, 2002.

Merfeld DM, Zupan LH, and Gifford CA. Neural processing of gravito-inertial cues in humans. II. Influence of the semicircular canals during eccentric rotation. *J Neurophysiol* 2001.

Miller 2nd EF and Graybiel A. Effect of gravitoinertial force on ocular counterrolling. *J Appl Physiol* 31: 697–700, 1971.

Mittelstaedt H. A new solution to the problem of the subjective vertical. *Naturwissenschaften* 70: 272–281, 1983.

Mittelstaedt H. The subjective vertical as a function of visual and extraretinal cues. *Acta Psychol* 63: 63–85, 1986.

Mittelstaedt H. The information processing structure of the subjective vertical. A cybernetic bridge between its psychophysics and its neurobiology. In: *Processing structures for perception and action*, edited by Marko H, Hauske G, and Struppler A. Weinheim: Verlag Chemie, 1988, p. 217–263.

Mittelstaedt H. The role of the pitched-up orientation of the otoliths in two recent models of the subjective vertical. *Biol Cybern* 61: 405–416, 1989.

Mittelstaedt H. The role of the otoliths in perception of the vertical and in path integration. *Ann N Y Acad Sci* 871: 334–344, 1999.

Mittelstaedt H, Glasauer S, Gralla G, and Mittelstaedt ML. How to explain a constant subjective vertical at constant high speed rotation about an earth-horizontal axis. *Acta Otolaryngol Suppl* 468: 295–299, 1989.

Niemeier M, Crawford JD, and Tweed DB. Optimal transsaccadic integration explains distorted spatial perception. *Nature* 422: 76–80, 2003.

Okada T, E G, Shallo-Hoffmann J, and Bronstein AM. Vestibular perception of angular velocity in normal subjects and in patients with congenital nystagmus. *Brain* 122: 1293–1303, 1999.

Paige GD and Seidman SH. Characteristics of the VOR in response to linear acceleration. *Ann N Y Acad Sci* 871: 123–135, 1999.

Paige GD and Tomko DL. Eye movement responses to linear head motion in the squirrel monkey. I. Basic characteristics. *J Neurophysiol* 65: 1170–1182, 1991.

Park S, Gianna-Poulin C, Black FO, Wood S, and Merfeld DM. Roll rotation cues influence roll tilt perception assayed using a somatosensory technique. *J Neurophysiol* 96: 486–491, 2006.

Pavlou M, Wijnberg N, Faldon ME, and Bronstein AM. Effect of semicircular canal stimulation on the perception of the visual vertical. *J Neurophysiol* 90: 622–630, 2003.

Raphan T and Cohen B. Velocity storage and the ocular response to multidimensional vestibular stimuli. In: *Reviews of Oculomotor Research. I Adaptive Mechanisms in Gaze Control: Facts and Theories*, edited by Berthoz A and Melvill-Jones G. Amsterdam: Elsevier, 1985, p. 123–143.

Raphan T, Matsuo V, and Cohen B. Velocity storage in the vestibulo-ocular reflex arc (VOR). *Exp Brain Res* 35: 229–248, 1979.

Schöne H. On the role of gravity in human spatial orientation. *Aerospace Medicine* 35: 764–772, 1964.

Schwarz G. Estimating the dimensions of a model. *Ann Statist* 6: 461–464, 1978.

Seidman SH, Telford L, and Paige GD. Tilt perception during dynamic linear acceleration. *Exp Brain Res* 119: 307–314, 1998.

Spinelli D, Antonucci G, Goodenough D, Pizzamiglio L, and Zoccolotti P. Psychophysiological mechanisms underlying the rod-and-frame illusion. In: *Field dependence - independence: cognitive style across the life span*, edited by Wapner S and Demick J. Hillsdale, NJ: Lawrence Erlbaum Associates, 1991, p. 37–60.

Stocker AA and Simoncelli EP. Noise characteristics and prior expectations in human visual speed perception. *Nat Neurosci* 9: 578–585, 2006.

Telford L, Seidman SH, and Paige GD. Dynamics of squirrel monkey linear vestibuloocular reflex and interactions with fixation distance. *J Neurophysiol* 78: 1775–1790, 1997.

Telford L, Seidman SH, and Paige GD. Canal-otolith interactions in the squirell monkey vestibulo-ocular reflex and the influence of fixation distance. *Exp Brain Res* 118: 115–125, 1998.

Turano KA and Massof RW. Nonlinear contribution of eye velocity to motion perception. *Vision Res* 41: 385–395, 2001.

Udo de Haes HA. Stability of apparent vertical and ocular countertorsion as a function of lateral tilt. *Percept Psychophys* 8: 137–142, 1970.

Van Beuzekom AD, Medendorp WP, and Van Gisbergen JAM. The subjective vertical and the sense of self orientation during active body tilt. *Vision Res* 41: 3229–3242, 2001.

Van Beuzekom AD and Van Gisbergen JAM. Properties of the internal representation of gravity inferred from spatial-direction and body-tilt estimates. *J Neurophysiol* 84: 11–27, 2000.

Van der Schaaf A and Van Hateren JH. Modeling the power spectra of natural images: statistics and information. *Vision Res* 36: 2759–2770, 1996.

Van Ee R, Adams WJ, and Mamassian P. Bayesian modeling of cue interaction: bistability in stereoscopic slant perception. *J Opt Soc Am A Opt Image Sci Vis* 20: 1398–1406, 2003.

Vingerhoets RAA, Medendorp WP, and Van Gisbergen JAM. Time course and magnitude of illusory translation perception during off-vertical axis rotation. *J Neurophysiol* 95: 1571–1587, 2006.

Vingerhoets RAA, Van Gisbergen JAM, and Medendorp WP. Verticality perception during off-vertical axis rotation. *J Neurophysiol* 97: 3256–3268, 2007.

Wade SW and Curthoys IS. The effect of ocular torsional position on perception of the roll-tilt of visual stimuli. *Vision Res* 37: 1071–1078, 1997.

Weiss Y, Simoncelli EP, and Adelson EH. Motion illusions as optimal percepts. *Nat Neurosci* 5: 598–604, 2002.

Wenderoth P and Beh H. Component analysis of orientation illusions. *Perception* 6: 57–75, 1977.

Wertheim AH. Motion perception during self-motion: the direct versus inferential controversy revisited. *Behav Brain Sci* 17: 293–355, 1994.

Wichmann FA and Hill NJ. The psychometric function: I. Fitting, sampling and goodness of fit. *Percept Psychophys* 63: 1293–1313, 2001.

Witkin HA and Asch SE. Studies in space orientation: IV further experiments on perception of the upright with displaced visual fields. *J Exp Psychol* 38: 762–782, 1948.

Wood S, Reschke MF, Sarmiento LA, and Clement G. Tilt and translation motion perception during off-vertical axis rotation. *Exp Brain Res* 182: 365–377, 2007.

Wood SJ. Human otolith-ocular reflexes during off-vertical axis rotation: effect of frequency on tilt-translation ambiguity and motion sickness. *Neurosci Lett* 323: 41–44, 2002.

Wright WG and Glasauer S. Subjective somatosensory vertical during dynamic tilt is dependent on task, inertial condition, and multisensory concordance. *Exp Brain Res* 172: 310–321, 2006.

Yakusheva TA, Shaikh AG, Green AM, Blazquez PM, Dickman JD, and Angelaki DE. Purkinje cells in posterior cerebellar vermis encode motion in an inertial reference frame. *Neuron* 54: 973–985, 2007.

Young LR. Perception of the body in space: mechanisms. In: *Handbook of Physiology. The Nervous System. Sensory Processes.*, edited by Geiger SR. Bethesda: American Physiological Society, 1984, p. 1023–1066.

Zoccolotti P, Antonucci G, Goodenough DR, Pizzamiglio L, and Spinelli D. The role of frame size on vertical and horizontal observers in the rod-and-frame illusion. *Acta Psychol* 79: 171–187, 1992.

Zupan LH and Merfeld DM. An internal model of head kinematics predicts the influence of head orientation on reflexive eye movements. *J Neural Eng* 2: S180–S197, 2005.

Zupan LH, Merfeld DM, and Darlot C. Using sensory weighting to model the influence of canal, otolith and visual cues on spatial orientation and eye movements. *Biol Cybern* 86: 209–230, 2002.

Zupan LH, Peterka RJ, and Merfeld DM. Neural processing of gravito-inertial cues in humans. I. Influence of the semicircular canals following post-rotatory tilt. *J Neurophysiol* 84: 2001–2015, 2000.

Summary

This thesis describes the results of a research project that focused on how visual and vestibular signals are used by the human brain to maintain spatial orientation and visual stability. Given the limitations of the vestibular sensors in terms of bandwidth and precision, outlined in chapter 1, achieving this is far from trivial. Existing spatial orientation models have specified in some detail how the brain could cope with these imperfections when it comes to reconstructing three crucial variables: angular rotation of the body in space, body-tilt with respect to gravity and linear translation of the body. Our objective was to collect extensive quantitative data sets in various static and dynamic conditions, for comparison with the model predictions. In chapters two and three we quantified the selfmotion and verticality percept of human subjects that were rotated in yaw about an off-vertical axis (OVAR). The perceptual data were compared with two spatial orientation models: the frequency segregation hypothesis and the canal-otolith interaction model. In the fourth chapter, we tested whether an extended version of the canal-otolith interaction model could account for the verticality percept during three cycles of constant velocity rotation. In the final chapter, we investigated how the presence of a tilted visual frame influences the verticality percept of roll-tilted human observers and compared the results with two subjective visual vertical models.

Chapter 2

Human spatial orientation relies on vision, somatosensory cues and signals from the semicircular canals and the otoliths. The canals measure rotation, while the otoliths are linear accelerometers, sensitive to tilt and translation. To disambiguate the otolith signal, two main hypotheses have been proposed: frequency segregation and canal-otolith interaction. So far these models were based mainly on oculomotor behavior. In this study we investigated their applicability to human self-motion perception. Six subjects were rotated in yaw about an off-vertical axis at various speeds and tilt angles, in darkness. During the rotation, subjects indicated at regular intervals whether a briefly presented dot moved faster or slower than their perceived

self-motion. Based on such responses, we determined the time course of the self-motion percept and characterized its steady-state by a psychometric function. The psychophysical results were consistent with anecdotal reports. All subjects initially sensed rotation, but then gradually developed a percept of being translated along a cone. The rotation percept could be described by a decaying exponential with a time constant of about 20 s. Translation percept magnitude typically followed a delayed increasing exponential with delays up to 50 s and a time constant of about 15 s. The asymptotic magnitude of perceived translation increased with rotation speed and tilt angle, but never exceeded 14 cm/s. These results were most consistent with predictions of the canal-otolith interaction model, but required parameter values that differed from the original proposal. We conclude that canal-otolith interaction is an important governing principle for self-motion perception that can be deployed flexibly, dependent on stimulus conditions.

Chapter 3

During prolonged rotation about a tilted yaw axis, often referred to as off-vertical axis rotation (OVAR), a percept of being translated along a conical path slowly emerges as the sense of rotation subsides. Recently, we found that these perceptual changes are consistent with a canal-otolith interaction model that attributes the illusory translation percept to improper interpretation of the ambiguous otolith signals. The model further predicts that the illusory translation percept must be accompanied by slowly worsening tilt underestimates. Here, we tested this prediction in six subjects by measuring the time course of the subjective visual vertical (SVV) during OVAR stimulation at three different tilt-rotation speed combinations, in complete darkness. Throughout the two minute run, at each left-ear-down and right-ear-down position, the subject indicated whether a briefly flashed line deviated clockwise or counterclockwise from vertical to determine the SVV with an adaptive staircase procedure. Typically, SVV errors indicating tilt underestimation were already present at rotation onset and then increased exponentially to an asymptotic value, reached at about 60 s after rotation onset. The initial error in the SVV was highly correlated to the response error in a static tilt control experiment. The subsequent increase in error depended on both rotation speed and OVAR tilt angle, in a manner predicted by the canal-otolith interaction model. We conclude that verticality misjudgments during OVAR reflect a dynamic component linked to canal-otolith interaction, superimposed on a tilt-related component that is also expressed under stationary conditions.

Chapter 4

To assess the effects of degrading canal cues for dynamic spatial orientation in human observers, we tested how judgments about visual-line orientation in space (subjective visual vertical task, SVV) and estimates of instantaneous body tilt (subjective body-tilt task, SBT) develop in the course of three cycles of constant-velocity roll rotation. These abilities were tested across the entire tilt range, in separate experiments. For comparison, we also obtained SVV data during static roll tilt. We found that, as tilt increased, dynamic SVV responses became strongly biased toward the head pole of the body axis (A-effect), as if body tilt was underestimated. However, upon entering the range of near-inverse tilts, SVV responses adopted a bimodal pattern, alternating between A-effects (biased toward head-pole) and E-effects (biased toward feet-pole). Apart from an onset effect, this tilt-dependent pattern of systematic SVV errors repeated itself in subsequent rotation cycles, with little sign of worsening performance. Static SVV responses were qualitatively similar, but showed smaller A-effects. By contrast, dynamic SBT errors were small and unimodal, indicating that errors in visual-verticality estimates were not caused by errors in body-tilt estimation. We discuss these results in terms of predictions from a canal-otolith interaction model, extended with a leaky integrator and an egocentric bias mechanism. We conclude that the egocentric-bias mechanism becomes more manifest during constant velocity roll-rotation and that perceptual errors due to incorrect disambiguation of the otolith signal are small, despite the decay of canal signals.

Chapter 5

We investigated the effect of visual and body-tilt cues on the subjective-visual vertical (SVV) in six human observers at roll tilts of 0, 60 and 120°. Subjects adjusted a small luminous-test line parallel to the perceived direction of gravity, in the presence of a large peripheral visual-frame line. These settings, referred to as the frame SVV, were compared to the SVV in complete darkness (dark SVV). We found the frame SVV to be virtually identical to the dark SVV for frame lines parallel or orthogonal to the dark SVV. Away from these neutral positions, the frame induced a small 90° periodic SVV-modulation in upright observers, which became quite pronounced when subjects were tilted. For upright, where the dark SVV was almost flawless, the frame SVV showed errors in either direction, following a roughly symmetrical pattern. By contrast, at 120° tilt, where the dark SVV invariably showed tilt under-compensation (A-effect), the frame effect became asymmetrical, with a stronger tendency to improve than to worsen performance. We tested whether our

findings could be explained by two spatial orientation models: Mittelstaedt's idiotropic model and a Bayesian scheme with a stage for the processing of optic cues. Both models show a 90° periodic frame effect that becomes stronger in tilt and explain why frame lines parallel or perpendicular to the dark SVV are ineffective. The performance of these models suggests that verticality perception is based on a centrally weighted fusion of visual, vestibular and egocentric references.

Samenvatting

Gewoonlijk hebben we een correct beeld van hoe ons lichaam in de ruimte staat, welke kant we op bewegen en van de oriëntatie en positie van objecten om ons heen. De centrale vraag in dit proefschrift is hoe ons brein in staat is om dit beeld te construeren en te behouden ondanks dat we zelf continu bewegen en objecten om ons heen zich ook kunnen verplaatsen. Onderzocht is welke zintuigen hierin een rol spelen en wat voor berekeningen de hersenen daarbij moeten uitvoeren. Een heel belangrijk zintuig in dit verband is het visueel systeem. Echter, ook in het donker kan een mens zich nog vrij goed oriënteren, waaruit blijkt dat het brein niet alleen afhankelijk is van het visueel systeem. Het heeft namelijk naast visuele informatie ook beschikking over signalen van het vestibulaire systeem. Dit bestaat uit twee onderdelen: de halfcirkelvormige kanalen en de otolieten. De kanalen meten rotaties en de otolieten meten zowel de zwaartekracht als krachten die ontstaan door lineaire versnellingen. Het signaal van de otolieten is dus ambigu: alleen op basis van dit signaal weet het centraal zenuwstelsel niet of we kantelen (reoriëntatie ten opzichte van de zwaartekracht) of versnellen. Echter, in de praktijk verwarren we deze twee bewegingen zelden, waaruit blijkt dat de hersenen een oplossing hebben voor dit ambiguïteitsprobleem.

Om te onderzoeken welke computationele strategieën hieraan ten grondslag kunnen liggen hebben we in de hoofdstukken twee en drie een experimentele stimulus gebruikt waarvan bekend is dat deze bij proefpersonen illusoire translatiegevoelens opwekt. In het experiment werden proefpersonen gedraaid om hun lengteas met een constante snelheid. Voor een draaias parallel aan de zwaartekracht verdwijnt het draaipercept, maar wanneer de as schuin staat ten opzichte van de richting van de zwaartekracht verdwijnt niet alleen het rotatiepercept, maar ontstaat er geleidelijk ook een translatiepercept. Een hypothese is dat dit veroorzaakt wordt doordat de hersenen de otolietstimulatie ten gevolge van de veranderende oriëntatie ten opzichte van de zwaartekracht foutief interpreteren als veroorzaakt door centripetale versnelling ten gevolge van een cirkelbeweging van het hoofd. Tijdens de experimenten is zowel het translatie- als het kantelgevoel van de proefpersonen gekwantificeerd en vergeleken met voorspellingen van twee mogelijke strategieën

die gebruikt kunnen worden om het dubbelzinnige otolietsignaal te interpreteren.

De eerste strategie, de frequentiescheidings-hypothese, veronderstelt dat de otolietsignalen in een neuraal circuit gescheiden worden in een hoogfrequent deel en een laagfrequent deel. Het hoogfrequente deel wordt dan geïnterpreteerd als ontstaan door lineaire versnelling, omdat versnellingen meestal kortdurend van aard zijn, terwijl het laagfrequente deel wordt gezien als het gevolg van kanteling omdat zwaartekracht constant is van richting en grootte. De tweede theorie, de kanaal-otoliet interactie hypothese, stelt dat het centraal zenuwstelsel kanaalsignalen gebruikt om het otolietsignaal te disambigueren. Namelijk, wanneer een verandering in het otolietsignaal gepaard gaat met een congruent kanaalsignaal wordt het otolietsignaal toegeschreven aan kanteling, en in andere gevallen wordt het gezien als het gevolg van lineaire versnelling.

In het vierde hoofdstuk hebben we het kanaal-otoliet interactiemodel getest in een experiment waarin proefpersonen drie complete zijdelingse rotaties ondergingen met constante snelheid in complete duisternis. Omdat kanaalsignalen verdwijnen bij rotaties op constante snelheid zou men verwachten dat het ontbinden van het dubbelzinnige otolietsignaal mis gaat onder deze omstandigheden. We hebben dit onderzocht door te meten hoe goed mensen zijn in het schatten van de oriëntatie van hun eigen lichaam en de oriëntatie van een lichtgevende lijn.

Zoals eerder gezegd is visuele informatie ook belangrijk voor ruimtelijke oriëntatie. Om te onderzoeken hoeveel gewicht het brein geeft aan visuele informatie en vestibulaire informatie is in hoofdstuk vijf onderzocht wat proefpersonen als verticaal beoordelen wanneer ze gekanteld zijn in het donker en er in het perifere gezichtsveld een lichtgevende lijn aanwezig is die geen informatie geeft over de richting van de zwaartekracht. De volgende paragrafen beschrijven in het kort de resultaten en de conclusies van elk hoofdstuk.

Hoofdstuk 2

De mens gebruikt informatie van het visueel systeem, van het somatosensorisch systeem, van de halfcirkelvormige kanalen en van de otolieten om zichzelf te oriënteren in de ruimte. De kanalen meten rotaties en de otolieten zijn accelerometers die gevoelig zijn voor kanteling en versnelling. Er zijn twee alternatieve hypotheses voorgesteld over hoe de hersenen het dubbelzinnige otolietsignaal ontrafelen: frequentiescheiding en kanaal-otoliet interactie. Deze hypotheses zijn vooral ontwikkeld en getest voor oogbewegingsstudies, maar in dit hoofdstuk onderzoeken we hun toepasbaarheid op perceptie van zelfbeweging. Zes proefpersonen werden op verschillende snelheden om hun lengteas gedraaid, terwijl deze as onder verschillende hoeken gekanteld was. Op regelmatige tijdstippen tijdens de rotatie

gaven proefpersonen aan of een kort aangeboden visuele stimulus sneller of langzamer bewoog dan zijzelf. Op basis van de antwoorden van de proefpersonen hebben we het tijdsverloop van het bewegingspercept bepaald. Ook is met behulp van een psychometrische functie het uiteindelijke stabiele zelfbewegingspercept gekarakteriseerd. De verkregen resultaten waren consistent met beschrijvingen van de proefpersonen. In het begin voelden alle proefpersonen zich om hun as draaien, maar vervolgens ontstond het gevoel dat ze met hun lichaam een kegel beschreven. Het rotatiepercept kon beschreven worden met een afvallende e-macht met een tijdsconstante van ongeveer 20 s. De grootte van het translatiepercept volgde een vertraagde stijgende e-macht met vertragingen tot 50 s en tijdsconstantes van ongeveer 15 s. De asymptoot van de grootte van het translatiepercept nam toe met rotatiesnelheid en kantelhoek, maar was nooit groter dan 14 cm/s. Deze resultaten waren het meest in overeenstemming met voorspellingen van het kanaal-otoliet interactie model, zij het met andere waarden voor de modelparameters dan gesuggereerd door eerdere studies. Wij concluderen daarom dat kanaal-otoliet interactie een flexibel mechanisme is dat een belangrijke rol speelt tijdens perceptie van zelfbeweging.

Hoofdstuk 3

Tijdens yaw rotaties om een gekantelde as, bekend als off-vertical axis rotation (OVAR), ontstaat bij proefpersonen het gevoel dat ze een translatiebeweging maken waarbij hun lichaam een kegel beschrijft, terwijl het percept van rotatie langzaam uitdooft. In hoofdstuk twee is gevonden dat het tijdsverloop van dit percept het meest overeenkomt met voorspellingen van een kanaal-otoliet interactie model, waarin het illusoire translatiepercept wordt geweten aan een verkeerde interpretatie van het dubbelzinnige otolietsignaal. Het model voorspelt tevens dat het ontstaan van het translatiegevoel gekoppeld is aan een langzaam verminderend kantelpercept. In dit hoofdstuk is deze voorspelling getest voor zes proefpersonen door het tijdsverloop van de subjectieve visuele verticaal (SVV) te meten tijdens OVAR voor drie verschillende kantelhoek-rotatiesnelheid combinaties in volledige duisternis. Telkens wanneer de proefpersoon in de uiterste zijwaartse kantelpositie (linkeroor beneden of rechteroor beneden) was, gaf deze aan of een kort geflitste lijn naar links of rechts afweek ten opzichte van de richting van de zwaartekracht. Op deze manier werd de SVV bepaald met een adaptieve staircasemethode op verschillede tijdspunten gedurende de rotatie van twee minuten. In het algemeen maakten de proefpersonen al direct na het begin van de rotatie fouten in de SVV. Deze fouten hadden het karakter van ondercompensatie voor kanteling en namen toe tot een asymptotische waarde die bereikt werd op ongeveer 60 seconden na het starten van de rotatie. De initiële fout in de SVV was sterk gecorreleerd met de fout in de SVV

in een statisch controle-experiment. De toename in de fout hing af van rotatiesnelheid en kantelhoek op een manier die overeenkwam met voorspellingen van het kanaal-otoliet interactie model. We concluderen daarom dat verticaliteitsschattingen tijdens OVAR een dynamische component bevatten die samenhangt met kanaal-otoliet interactie, met daarnaast een kantelhoek-gerelateerde component die ook tot uiting komt onder statische condities.

Hoofdstuk 4

Om de effecten van afnemende kanaalsignalen op dynamische spatiële oriëntatie te onderzoeken bij de mens, hebben we getest hoe beoordelingen van visuele lijn oriëntaties (subjectieve visuele verticaal taak, SVV) en schattingen van instantane lichaamsstand (subjective body tilt, SBT) zich ontwikkelen gedurende drie complete zijdelingse rotaties op constante snelheid. Deze twee aspecten werden getest over het hele kantelbereik (0-360°) in aparte experimenten. Ter vergelijking hebben we ook SVV metingen verricht tijdens statische kanteling. We vonden dat wanneer de kanteling toenam, de dynamische SVV steeds sterker afweek in de richting van de lichaamsas, alsof de kantelhoek werd onderschat door de proefpersoon. Echter, voor kantelhoeken dichtbij 180° vonden we twee typen responsies: A-effecten (afwijkingen richting het hoofd) en E-effecten (afwijkingen richting de voeten). Afgezien van een opstart effect herhaalde dit hoekafhankelijke patroon van systematische SVV fouten zich in opeenvolgende rotatiecycli, zonder duidelijke verslechtering. De statische metingen vertoonden een vergelijkbaar patroon, maar met kleinere A-effecten. De fouten in de schattingen van lichaamsstand daarentegen, waren klein en kenden geen onderverdeling in twee typen, wat erop duidt dat de fouten in de visuele verticaalschatting niet simpelweg veroorzaakt worden door een foutief kantelpercept. Deze resultaten zijn vergeleken met voorspellingen van een kanaal-otoliet interactiemodel, dat was uitgebreid met een lekke integrator en een mechanisme dat de SVV richting de lichaamsas trekt. We concluderen dat het aantrekkende mechanisme sterker wordt tijdens zijdelingse rotaties op constante snelheid en dat fouten ten gevolge van foutieve ontbinding van het dubbelzinnige otolietsignaal klein zijn ondanks het feit dat het kanaalsignaal uitdooft.

Hoofdstuk 5

In dit hoofdstuk hebben we het effect van visuele contouren en lichaamskanteling op de subjectieve visuele verticaal (SVV) onderzocht bij zes proefpersonen tijdens kantelingen van 0, 60 en 120 graden. De proefpersonen kregen de opdracht om een kleine lichtgevende lijn recht voor hen parallel aan de richting van de

zwaartekracht te zetten in aanwezigheid van een lange lichtgevende framelijn in het perifere gezichtsveld. Deze instellingen, frame SVV genoemd, werden vergeleken met de SVV in volledige duisternis (donker SVV). We vonden dat de frame SVV vrijwel identiek was aan de donker SVV voor framelijnen parallel aan of loodrecht op de donker SVV. Voor andere frameoriëntaties zorgde het frame voor een kleine, 90 graden periodieke modulatie bij proefpersonen in de rechtop positie, terwijl dit effect duidelijk sterker werd voor gekantelde proefpersonen. Voor rechtop was de donker SVV vrijwel foutloos en zorgde het frame zowel voor afwijkingen naar links als naar rechts volgens een symmetrisch patroon. Echter, als de proefpersoon 120 graden gekanteld was, vertoonde de donker SVV zonder uitzondering aanwijzingen voor onderschatting van de kantelhoek (A-effect), en was het frame-effect asymmetrisch met vaak een verbeterend effect en zelden een verslechterend effect. We hebben onderzocht of onze bevindingen verklaard kunnen worden met twee verschillende modellen: Mittelstaedt's idiotropische vector model en een Bayesiaans model met een extra sectie voor de verwerking van optische signalen. Simulaties van beide modellen vertonen een 90 graden periodiek frame effect dat groter wordt met kantelhoek en beide modellen voorspellen dat framelijnen parallel aan of loodrecht op de donker SVV geen effect hebben op de frame SVV. Deze modelfits suggereren dus dat perceptie van verticaliteit gebaseerd is op een centraal gewogen fusie van visuele, vestibulaire en lichaamsgebonden signalen.

Publications

Articles

Vingerhoets R.A.A., Medendorp W.P., Van Gisbergen J.A.M. Time course and magnitude of illusory translation perception during off-vertical axis rotation *J. Neurophysiol.* 95:1571-1587, 2006

Vingerhoets R.A.A., Van Gisbergen J.A.M., Medendorp W.P. Verticality perception during off-vertical axis rotation *J. Neurophysiol.* 97:3256-3268, 2007

Vingerhoets R.A.A., Medendorp W.P., Van Gisbergen J.A.M. Body-tilt and verticality perception during multiple cycles of roll rotation *J. Neurophysiol.* 99:2264-2280, 2008

Vingerhoets R.A.A., Van Gisbergen J.A.M., Medendorp W.P. Fusion of visual and vestibular tilt cues in the perception of visual vertical *under revision*

Abstracts

Van Gisbergen J.A.M., Kaptein R.G., Vingerhoets R.A.A. The dynamic subjective visual vertical during roll rotation. Program No. 268.6 Abstract Viewer/Itinerary Planner. *Washington, DC: Society for Neuroscience,*2003

Vingerhoets R.A.A., Medendorp W.P., Gielen S, Van Gisbergen J.A.M. Self-motion perception during off-vertical axis yaw rotation. Program No. 168.2 Abstract Viewer/Itinerary planner. *Washington, DC: Society for Neuroscience,* 2005

Vingerhoets R.A.A., Van Gisbergen J.A.M., Medendorp W.P. Perceptual correlate of otolith ambiguity: Time course of subjective vertical during off-vertical

axis rotation. Program No. 244.2 Abstract Viewer/Itinerary planner. *Atlanta, GA: Society for Neuroscience,* 2006

Vingerhoets R.A.A., Medendorp W.P., Van Gisbergen J.A.M. Verticality perception during body rotation in roll. Program No. 399.14 Abstract Viewer/Itinerary planner. *San Diego, CA: Society for Neuroscience,* 2007

Medendorp W.P., Vingerhoets R.A.A., De Vrijer M., Van Gisbergen J.A.M. The role of visual and vestibular tilt cues in human verticality perception *Barany meeting, Kyoto* 2008

Dankwoord

Dit proefschrift was er nooit gekomen zonder de hulp van mijn begeleiders Jan en Pieter. Jan, je ideeënrijkdom en jouw scherpte als proefpersoon tijdens de vele experimenten of als corrector als je mijn manuscript voor de zoveelste keer las, hebben dit proefschrift zeker naar een hoger niveau gebracht. Pieter, fysiek zat je iets verder weg, maar je betrokkenheid was er zeker niet minder om. Ook jouw kritische blik heeft dit proefschrift duidelijk verbeterd en met je vindingrijkheid wist je me altijd weer vooruit te helpen als ik het gevoel had vastgelopen te zijn. Onmisbaar was ook de technische ondersteuning: Günter, Ger, Hans en Stijn, hoe had ik ooit mijn experimenten kunnen voltooien zonder jullie? Stan, als promotor stond je meer aan de zijlijn, maar als het nodig was kon ik bij je aankloppen. Ook wil ik jou bedanken voor de prettige sfeer op en de goede organisatie van de afdeling. Hiervoor ook dank aan Judith, Margriet en Annet.

Nog belangrijker voor de goede sfeer was echter de aanwezigheid van een groot aantal fijne collega's. Ronald, eerst als stagebegeleider en later als kamergenoot leerde je me de beginselen van 'de stoel', Matlab en C. Dit is een goede basis geweest voor dit proefschrift. Maaike, we hebben elkaar vaak geholpen met experimenten, Matlab, voorbereiden van werkcolleges en het ontcijferen van correcties. Ook hadden we vele gezellige gesprekken over zaken buiten de wetenschap zoals klimmen, hardlopen, vakanties en muziek. Bedankt voor al je hulp en gezelligheid als kamergenote en leuk dat je mijn paranimf wilt zijn. Ook Bart, Denise, Joke, Joris, Joyce, Kees, Magteld, Marc, Marjan, Martijn, Noël, Onno, Peter, Rob, Sigrid, Tom en alle andere collega's door de jaren heen wil ik bedanken voor interesse, leuke en nuttige gesprekken, potjes dart, vrijdagmiddagbiertjes, juniorlunches, de carréloop, filmavonden, thee en koekjes. Door jullie heb ik nooit spijt gehad dat ik na mijn stage bij de afdeling biofysica ben blijven hangen. Daarnaast waren er nog de collega's op afstand: Stan, Sabine en Jurrian. Veel dank voor de gezelligheid tijdens de gezamelijke leesclub en conferenties.

Iris, Judith, Sam, Sanne en Maarten, hoewel ik soms misschien een andere indruk heb gegeven, hebben jullie me tijdens jullie stages veel werk uit handen genomen. Ik ben dankbaar voor jullie inzet, die waardevolle en zelfs gepubliceerde data heeft opgeleverd. Natuurlijk wil ik ook de vele proefpersonen niet onvermeld laten. Mijn experimenten bestonden vaak uit vele sessies en met name de inmiddels beruchte OVAR experimenten stelden jullie vrijwilligheid zwaar op de proef.

Het leven is meer dan een promotieonderzoek alleen, gelukkig kon ik rekenen op vriendschap, afleiding en gezelligheid van de "Tilburg-groep", klimmers, huisgenoten, voetballers en oud-studiegenoten. Onder hen ook mijn andere paranimf Arjan: we begonnen tegelijk met natuurkunde en bijna gelijk met een promotieproject. Het was altijd prettig om met jou de voor- en tegenspoed van het AIO-bestaan te bespreken. Bedankt dat je mijn paranimf wilt zijn.

Niet alleen tijdens de afgelopen jaren, maar ook daarvoor was er altijd de steun, het vertrouwen en de interesse van mijn ouders. Wat mij betreft zijn jullie de beste ouders die een kind zich kan wensen. Bregje en Meike, jullie hebben het zwaar met zo'n nerd als broer, maar toch hebben we het altijd gezellig samen. Tot slot, lieve Thamar, bedankt voor je optimisme op de momenten dat ik dat zelf even miste, maar vooral voor de heel fijne tijd die we tot nu toe hebben gehad. Ik vertrouw erop dat de tijd die komen gaat minstens zo mooi wordt.

Mei 2008
Rens Vingerhoets

Curriculum vitae

Op 23 december 1979 ben ik geboren in Tilburg. In deze mooie stad ging ik naar de Jeanne d'Arc basisschool en vervolgens naar het Pauluslyceum waar ik mijn VWO eindexamen cum laude haalde in 1998. Ik was erg geïnteresseerd in de exacte vakken en startte meteen na de zomer met de studie Natuurkunde in Nijmegen. Tijdens deze studie ontstond de interesse voor onderwerpen op het grensvlak van de biologie en natuurkunde. Een afstudeerstage in die richting vond ik bij de vakgroep Medische Fysica en Biofysica. Op deze afdeling deed ik onderzoek naar het waarnemen van visuele orientaties tijdens kantelingen. In november 2003 haalde ik mijn doctoraal examen natuurkunde en begon ik mijn promotieonderzoek bij dezelfde vakgroep Medische Fysica en Biofysica. Het boekje wat nu voor u ligt is het resultaat van dit onderzoek. Sinds december 2007 werk ik als klinisch fysicus in opleiding bij de afdeling radiotherapie van het UMC Utrecht.